

Solar influence on stratosphere-troposphere
dynamical coupling.

Isla Ruth Simpson

THESIS SUBMITTED FOR THE DEGREE OF
DOCTOR OF PHILOSOPHY OF THE UNIVERSITY OF LONDON
AND FOR THE
DIPLOMA OF IMPERIAL COLLEGE

June 27, 2009

*Space and Atmospheric Physics Group, The Blackett Laboratory, Imperial
College, London SW7 2BW, UK*

ABSTRACT

In recent years it has become apparent that changes in the stratosphere could have an impact on tropospheric circulation but the exact mechanisms involved in the coupling between the stratosphere and troposphere remain uncertain. Understanding these mechanisms is potentially important for many climate forcings, such as the 11-year solar cycle, volcanic eruptions, greenhouse gas emissions and ozone depletion/recovery.

Previous studies have suggested that heating or cooling of the lower stratosphere can result in latitudinal displacements of the tropospheric mid-latitude jets. This study focusses on the mechanisms involved in producing such a response. The primary aim of these experiments is to determine a possible mechanism whereby the tropospheric response to changing solar activity could be produced. The results are therefore presented in this context but the mechanism could apply to any forcing that results in a temperature perturbation of the lower stratosphere.

Spin-up ensemble experiments of a simplified General Circulation Model have been used to examine the chain of causality whereby perturbations in lower stratospheric temperature influence the tropospheric circulation. The results demonstrate the importance of altered eddy momentum fluxes around the tropopause in driving meridional circulation changes which transmit the response to lower levels. An important feedback is also found which involves changes in meridional wind shear across the jet latitude, altering eddy propagation and thus eddy momentum fluxes in the troposphere. It is found that the vertical temperature gradient around the tropopause and its latitudinal extent are important in determining the direction of displacement of the mid-latitude jet.

The impact of different tropospheric states on the response is then examined. Zonally asymmetric boundary conditions are introduced in the form of topography and a quadrupole change in tropospheric temperature and the effect of varying tropospheric jet structure is also investigated.

ACKNOWLEDGEMENTS

I would like to thank first and foremost my supervisor Prof Jo Haigh for all the help and advice and opportunities that she has given me throughout my PhD and for always managing to find the time to discuss my work. I would also like to thank Dr Mike Blackburn for all his help in the running of the model and the interpretation of the results and Dr Sarah Sparrow for many useful discussions and for providing some of the data presented in this thesis.

I am also very grateful to Dr Fenwick Cooper for providing some of the data for the long model runs of Chapter 5 and for making the long runs of Chapter 6 possible.

Finally I would like to thank all the friends and colleagues in SPAT for making my time at Imperial so enjoyable, for all the pub outings and coffee breaks. In particular I would like to thank Clare Heaviside, my office mate for the last three and a half years for all her wise advice and for making the time in the office so enjoyable and Payal Mehta for all the fun times and inspirational messenger conversations. Last but not least I would like to thank my parents for their continued support.

SYMBOLS

- a Radius of the earth (6.371e6 m)
 c zonal phase speed (ms^{-1})
 c_p Specific heat capacity of dry air at constant pressure ($1005 \text{ JK}^{-1}\text{kg}^{-1}$)
 f coriolis parameter = $2\Omega\sin\phi$
 $\mathcal{F}^{(\lambda)}$ zonal component of friction
 $\mathcal{F}^{(\phi)}$ meridional component of friction
 g acceleration due to gravity (9.8 ms^{-2})
 H density scale height (8km)
 k dimensionless zonal wavenumber
 k_f boundary layer frictional damping coefficient = $1/\text{frictional timescale}$
 k_T temperature relaxation coefficient = $1/\text{temperature relaxation timescale}$
 $K = \sqrt{k^2 + l^2 + m^2}$ Total wavenumber
 l meridional wavenumber
 m vertical wavenumber
 n^2 refractive index squared
 N buoyancy frequency
 p Pressure (hPa)
 p_s Surface pressure
 Q diabatic heating
 q potential vorticity
 \bar{q}_ϕ meridional gradient of potential vorticity ($\text{s}^{-1}\text{rad}^{-1}$)
 R Gas constant ($287\text{JKg}^{-1}\text{K}^{-1}$)
 t time
 T_{ref} Newtonian relaxation temperature profile
 u zonal wind (ms^{-1})

-
- v meridional wind (ms^{-1})
 \bar{v}^* TEM meridional wind
 w vertical velocity (ms^{-1})
 \bar{w}^* TEM vertical velocity
 x longitude (m)
 y latitude (m)
 z height = $-H \ln(p/p_s)$
 ζ_g geostrophic vorticity
 θ Potential temperature
 $\kappa = R/c_p \sim 2/7$
 λ Longitude ($^\circ$)
 ρ_o basic state density profile (a function of z only)
 ρ density
 $\sigma = p/p_s$
 ϕ Latitude ($^\circ$)
 Φ Geopotential height
 ψ stream function
 Ω angular velocity of the Earth $\sim 7.29e - 5s^{-1}$

CONTENTS

<i>Abstract</i>	1
<i>Acknowledgements</i>	3
<i>Symbols</i>	4
<i>1. Solar variability and the climate.</i>	20
1.1 Introduction to solar variability	21
1.2 The solar signal in the stratosphere	24
1.2.1 The low latitude stratosphere	25
1.2.2 The polar stratosphere	29
1.3 The solar signal in the troposphere	31
1.4 Possible mechanisms for a solar influence on tropospheric climate.	36
<i>2. Stratosphere-Troposphere coupling.</i>	39
2.1 Stratosphere-troposphere coupling in observations	39
2.2 Mechanisms of stratosphere-troposphere coupling	42
2.2.1 Direct mechanisms	42
2.2.2 Indirect mechanisms	46
2.3 The tropospheric response to heating perturbations in the stratospheres of simplified GCM's	51
<i>3. The model experiments and diagnostics</i>	54
3.1 The simplified General Circulation Model (sGCM)	54
3.2 The Experiments	60

3.2.1	Stratospheric heating experiments	60
3.2.2	Zonally asymmetric boundary conditions	63
3.2.3	Varying tropospheric baroclinicity	68
3.3	Diagnostics	70
3.3.1	The vertically integrated momentum budget	72
3.3.2	Stationary and transient eddies	73
3.3.3	The Transformed Eulerian Mean and Eliassen-Palm flux	74
3.3.4	The quasi-geostrophic index of refraction	76
3.3.5	Significance testing	78
4.	<i>Stratospheric heating experiments</i>	80
4.1	The equilibrium response to E5, U5 and P10 stratospheric heating	80
4.2	Spin-up ensemble results for the E5 experiment	83
4.2.1	The importance of changing eddy momentum fluxes	86
4.2.2	Comparison with a zonally symmetric model	95
4.2.3	Diagnosing the cause of the altered eddy momentum fluxes	98
4.3	Comparison with the U5 and P10 experiments	116
4.4	Discussion and Conclusion	123
5.	<i>Zonally asymmetric boundary conditions</i>	131
5.1	The control run simulations	133
5.1.1	The Q control run	133
5.1.2	The R control run	137
5.2	Issues with accurately determining the magnitude of response.	140
5.3	50000 day integrations of the Q and R experiments	145
5.3.1	Decorrelation timescales	148
5.4	Discussion and conclusions	151
6.	<i>The effect of varying tropospheric jet structure</i>	154
6.1	The control run tropospheres	155

6.2	The equilibrated response to stratospheric heating.	160
6.2.1	The E5 response.	161
6.2.2	The P5 response	166
6.3	Why the difference in magnitude of the tropospheric response?	168
6.3.1	Control run variability	170
6.3.2	TR2 and TR4 E5 spin-ups	182
6.3.3	Eddy feedback in the equilibrated situation.	186
6.4	Discussion and Conclusion	188
7.	<i>Conclusions and Future Work</i>	193
7.1	Conclusions	194
7.1.1	The mechanism	194
7.1.2	The effect of zonal asymmetries	197
7.1.3	The effect of varying tropospheric jet structure	199
7.2	Future work	202
	<i>Appendix</i>	205
	References	228

LIST OF FIGURES

1.1	The extended PMOD composite of total solar irradiance from 1976. Figure taken from the PMOD website (www.pmodwrc.ch).	22
1.2	Difference in spectral solar irradiance between solar maximum and solar minimum. (Top) percentage change, (Bottom) change in units of energy. Figure taken from Fröhlich & Lean (2004).	23
1.3	Difference between solar maximum and solar minimum of annually averaged zonal mean (a) temperature (K) and (b) zonal wind (ms^{-1}) from regression analysis of ERA-40 data. This figure is the corrected version of (a) Fig. 2 and (b) Fig. 3 of Crooks & Gray (2005) (Tom Frame, personal communication).	26
1.4	Annual mean zonally averaged temperature difference (K) between solar max and solar min from regression analysis of 1968 - 1998 NCEP data (Figure taken from Labitzke <i>et al.</i> (2002)).	27
1.5	Schematic of a possible mechanism for the production of the increased temperature in the tropical lower stratosphere in response to the solar cycle. (a) Enhanced solar heating in the upper stratosphere at solar maximum results in a strengthening of the polar night jet which acts to deflect planetary waves away from the subtropics (dashed arrow). This creates an anomalous divergence of wave activity which then weakens the B-D circulation (arrows in (b)). The anomalous descent in equatorial latitudes results in adiabatic warming of the lower stratosphere (Kodera, 2003).	28

1.6	Annually averaged zonal mean temperature response to the 11 year cycle. Shaded areas are not statistically significant at the 95% level. From Haigh (2003).	33
1.7	(Top) zonal mean zonal wind averaged over DJF, (bottom) change in zonal mean zonal wind between solar maximum and solar minimum in DJF. Solid contours = westerly winds, dashed contours = easterly winds. From Haigh & Blackburn (2006).	35
3.1	(a) Newtonian relaxation temperature profile for the control run climatology, (b) as (a) but potential temperature, (c) control run zonal mean temperature and (d) control run potential temperature for a 10 000 day control run average.	56
3.2	(a) Control run zonal mean zonal wind (ms^{-1}), (b) Control run stream function of the mean meridional circulation (10^{10}kgs^{-1}), (c) northward horizontal eddy momentum flux (ms^{-1}) ²	58
3.3	Kinetic energy spectrum of the control run as a function of dimensionless zonal wavenumber. Vertically integrated kinetic energy per unit area is shown.	59
3.4	Change in relaxation temperature profile (Experiment - Control) for the (a) E5, (b) U5 and (c) P10 heating experiments.	62
3.5	T_{ref} for the Q experiments: (a) Anomaly from original Held-Suarez forcing (3.5) at the surface, (b) surface T_{ref} , (c) meridional cross section of the anomaly from Held-Suarez at 90° longitude, (d) as (c) but for 270° longitude.	65
3.6	(a) Topographic height in metres (b) Cross section of topographic height through 0° longitude.	67
3.7	Meridional cross section of the perturbation to the original Held-Suarez relaxation temperature profile to produce experiments TR1(a), TR2(b), TR4(c), TR5(d).	68

-
- 4.1 (LHS) zonal mean temperature, (RHS) zonal mean zonal wind. The top panel shows the control run values (contour intervals: 10K and 2ms^{-1}) and the lower three panels show the difference between the equilibrium run and the control run for the E5, U5 and P10 experiments (contour intervals: 0.3K and 0.5ms^{-1}). 82
- 4.2 Evolution of zonal mean fields for the E5 experiment. (Top panel) control run values. (Bottom panel) equilibrium E5 - C. (Middle panels) difference between the 10 day averages of the spin-up and the equivalent 10 days of the control run for days 0 to 9 and 20 to 29. (LHS) Temperature (K), (Middle) Zonal wind (ms^{-1}), (RHS) Stream function of the mean meridional circulation (Top = 10^{10} kgs^{-1} , Middle = 10^8 kgs^{-1} , Bottom = 10^9 kgs^{-1}). Dashed contours are negative. Note the different contour intervals between panels. 85
- 4.3 As Fig. 4.2 but for (a) $\overline{u'v'}$ and (b) E-P flux scaled as in Edmon *et al.* (1980) for the E5 experiment. Note the different scale of the E-P flux vectors and the different contour intervals between plots. 88
- 4.4 (Top panel) 11-day running means of the change in each of the terms in Eq. 4.2 along with their sum and the difference in \bar{u} from the control run (hemf = 2nd term in Eq. 4.2), averaged from the top of the model to 700hPa. (Middle panel) 11-day running means of $f\bar{v}$ anomaly vertically integrated from 0 to 700hPa and from 700hPa to the surface. (Bottom panel) as top panel but averaged over 700hPa to the surface. (a) average over 34 to 37° latitude, (b) averaged over 54 to 57° latitude. . . 90

-
- 4.5 Vertically integrated momentum budget. (Top panel) control run, (Bottom panel) difference between the vertically integrated momentum budget of the equilibrium E5 run and the control run and (Middle panels) difference between the vertically integrated momentum budget for days 0 to 9 and 20 to 29 of the E5 run and the vertically integrated momentum budget for the equivalent 10 day chunks of the control run. 93
- 4.6 (Top panel) difference in E-P flux divergence between days 20 to 29 of the E5 spin-up and the equivalent days of the control run. (Bottom panel) as top panel but for $f\bar{v}^*$. Contour interval = $2e^{-6} \text{ ms}^{-2}$ 94
- 4.7 Response of the zonally symmetric model to E5 heating for days 0 to 9 and days 20 to 29 of the spin-up. Differences relative to day zero of the spin-up are shown. (a) zonal mean temperature, (b) zonal mean zonal wind and (c) stream function of the mean meridional circulation (10^8 kgs^{-1}). 96
- 4.8 Equilibrium response to E5 heating for the zonally symmetric response (a) Zonal mean temperature, (b) Zonal mean zonal wind and (c) stream function of the mean meridional circulation (10^9 kgs^{-1}). 97
- 4.9 Potential vorticity (anomaly from the zonal mean) at the 568hPa level averaged between 40° and 50° latitude. Contour interval = 0.02PVU, Threshold for large PV regions = 0.02PVU. Crosses = points of maximum PV, Solid lines = best fitting lines through the crosses for each PV track. 100
- 4.10 Distribution of phasespeeds (a) using a threshold PV value of 0.02 PVU and (b) using a threshold PV value of 0.05PVU. Percentage of phase speed tracks in 1ms^{-1} bins is shown. Vertical line shows the mean phase speed. 102

4.11	Distribution of phase speeds calculated from PV (anomalies from the zonal mean) averaged between 40 and 50° latitude using a PV threshold value of 0.03. Percentage of tracks with phase speeds in 1ms^{-1} bins is shown for (a)286hPa, (b)400hPa, (c)568hPa and (d)784hPa.	103
4.12	(a)-(c): Phase speed distributions for days 0 to 9, 20 to 29 and 40 to 49 of the spin-up. (d)-(e): difference in the phase speed distributions for the E5 and U5 spin-ups from the control run for days 0 to 9, 20 to 29 and 40 to 49.	104
4.13	Phase speed distributions for the equilibrium E5 and U5 runs and the control run. RHS = difference in the phase speed distributions between the equilibrium E5 and U5 runs and the control run.	105
4.14	(a) change in n^2 (contours) and scaled E-P flux (arrows) for days 0 to 9 of the E5 spin-up, (b) change in $\bar{q}_\phi/a(\bar{u}-c)$ using the change in \bar{q}_ϕ for the spin-up and \bar{u} from the control run and (c) change in $\bar{q}_\phi/a(\bar{u}-c)$ using the change in \bar{u} from the spin-up and \bar{q}_ϕ from the control run. Contours have been blanked out in regions where $c > u$. Note: values in the middle and bottom panels have been scaled by a^2 to make them non-dimensional for comparison with total n^2 . The E-P flux anomalies are the same in all panels.	108
4.15	Change in individual components of \bar{q}_ϕ ($10^{-6}\text{s}^{-1}\text{rad}^{-1}$). (a) change in \bar{q}_ϕ , (b) meridional curvature, (c) change in third term of \bar{q}_ϕ due to altered \bar{u} , (d) change in third term of \bar{q}_ϕ due to altered $\bar{\theta}$	111

4.16	(a) The full change in vertical E-P flux during days 0 to 9 of the spin-up. (b) The change in vertical E-P flux as calculated using Eq. 3.29 i.e. omitting the ageostrophic terms, (c) as (b) but using control run horizontal eddy heat flux and spin-up vertical temperature gradient for the calculation of F_z , (d) as (c) but using spin-up horizontal eddy heat flux and control run vertical temperature gradient in the calculation of F_z	113
4.17	As Fig. 4.14 but for days 40 to 49.	114
4.18	Difference between days 0 to 9 of the spin-up and the control run for (a) U5 \bar{T} , (b) P10 \bar{T} , (c) U5 \bar{q}_ϕ ($10^{-6}\text{s}^{-1}\text{rad}^{-1}$), (d) P10 \bar{q}_ϕ ($10^{-6}\text{s}^{-1}\text{rad}^{-1}$), (e) U5 E-P flux, (f) P10 E-P flux, (g) U5 $\overline{u'v'}$ and (h) P10 $\overline{u'v'}$	117
4.19	Difference between days 20 to 29 of the spin-up and the equivalent control run values for (a) U5 $\overline{u'v'}$, (b) P10 $\overline{u'v'}$, (c) U5 $\bar{\psi}$ (10^8kgs^{-1}), (d) P10 $\bar{\psi}$, (e) U5 \bar{u} and (f) P10 \bar{u}	119
4.20	Difference between days 40 to 49 and the equivalent 10 days of the control run for (a) U5 \bar{u} , (b) P10 \bar{u} , (c) U5 E-P flux and n^2 , (d) P10 E-P flux and n^2 , (e) U5 $\overline{u'v'}$ and (f) P10 $\overline{u'v'}$	122
4.21	Summary of the mechanism proposed for the production of tropospheric circulation changes in response to stratospheric heating perturbations.	125
5.1	(a) Q control run surface temperature (K), (b) difference in surface temperature between the Q control run and the C control run, (c) as (a) but for zonal wind (ms^{-1}) at the 286hPa level, (d) as (b) but for the zonal wind (ms^{-1}) at the 286hPa level.	135
5.2	Transient eddy fields for the average of the Q control run. (a) transient poleward eddy heat flux (Kms^{-1}) on the 784hPa level, (b) transient eddy kinetic energy (m^2s^{-2}) on the 286hPa level and (c) transient poleward eddy momentum flux (m^2s^{-2}) on the 286hPa level.	136

5.3	(a) Control run zonal wind (ms^{-1}) on the 240hPa level and (b) control run temperature (K) on the 967hPa level. Orographic height is overplotted in Red.	138
5.4	(a) Control run transient horizontal eddy heat flux (Kms^{-1}) on the 784hPa level, (b) control run transient eddy kinetic energy (m^2s^{-2}) on the 286hPa level and (c) control run transient horizontal eddy momentum flux (m^2s^{-2}) on the 286hPa level. Topographic height is overplotted in Red.	139
5.5	Difference in zonal mean zonal wind (ms^{-1}) between E5 and Control for (a) the 10000day runs with topography and (b) the 5000 day runs with a quadrupole perturbation to T_{ref} . . .	141
5.6	Difference between SH and NH of the Q response to E5 stratospheric heating. Grey regions are not statistically significantly different from zero at the 95% level	142
5.7	Daily zonal mean zonal wind anomalies from the time mean (ms^{-1}) on the 286hPa level for (a) the Q control run, (b) the QE5 run and (c) the difference between QE5 and Q.	144
5.8	Difference in zonal mean zonal wind between E5 and Control for (a) time mean excluding anomalous days and (b) anomalous days. Anomalous days are considered to be between days 1000 and 1700 in the NH and days 2700 and 3000 in the SH. .	145
5.9	(a) and (c) the 50000 day mean response to E5 stratospheric heating for the Q and R runs respectively. (b) and (d) the 95% confidence interval of the mean response to E5 heating for the Q and R runs respectively.	146
5.10	5000 day mean \bar{u} anomaly (E5 - C) at 286hPa and 54 deg latitude (crosses) and 37deg latitude (asterisks) for each hemisphere and each ensemble member of the Q and R runs. Mean values and 95% confidence intervals are shown along side. . . .	148

5.11	Decorrelation timescale for each ensemble member of the NH and SH of the R control run and the two hemispheres combined of the Q run. Ensemble mean and 95% confidence interval are shown alongside. (These values have been calculated by S.Sparrow).	149
6.1	Control run (top) zonal mean temperature (K), (middle) horizontal eddy heat flux (Km s^{-1}) and (bottom) stream function of the mean meridional circulation (10^{10}kgs^{-1}) for the ensemble means of (column 1) TR1, (column 2) TR2, (column 3) TR3, (column 4) TR4 and (column 5) TR5.	157
6.2	As Fig. 6.1 but for (top) E-P flux, (middle) horizontal eddy momentum flux (m^2s^{-2}) and (bottom) zonal wind (ms^{-1}). . .	158
6.3	E5 - C for (top) Temperature (K), (middle) zonal wind (ms^{-1}) and (bottom) stream function of the mean meridional circulation (10^9kgs^{-1}) for (left to right) ensemble mean of TR1 to TR5.	162
6.4	As Fig. 6.3 but for (top) E-P flux, (middle) horizontal eddy momentum flux and (bottom) horizontal eddy heat flux. . . .	163
6.5	Mean anomaly over all latitudes and pressures for each ensemble member (+’s) of each experiment. Ensemble mean and 95% confidence intervals are shown alongside.	164
6.6	(Left) zonal wind (ms^{-1}) and (Right) temperature (K) response to P5 stratospheric heating for the ensemble means of TR1 to TR5 from top to bottom.	167
6.7	Mean magnitude of zonal wind anomaly over all latitudes and pressures for each individual ensemble member of each experiment (+’s). The ensemble means and 95% confidence intervals are shown alongside.	168

-
- 6.8 (LHS) Time series of the zonal wind anomaly from the time mean of the control run on the 286hPa level of one ensemble member. (RHS) One-point correlation maps of the zonal mean zonal wind anomaly as a function of latitude for the ensemble mean. Top to Bottom = TR1 to TR5. 171
- 6.9 Zonal mean zonal wind anomaly from the time mean for days 2100 to 2300 of the control run simulation of one ensemble member of (a) TR5 and (b) TR2. (c) and (d) show the corresponding horizontal eddy momentum flux anomalies from the time mean. 172
- 6.10 e-folding/decorrelation timescale of the autocorrelation of the first EOF of variability in the zonal mean zonal wind for each ensemble member of each troposphere (+’s). Ensemble mean and 95% confidence interval are shown alongside. Decorrelation timescales calculated by Sarah Sparrow. 173
- 6.11 (LHS) meridional PV gradient on the 286hPa level for TR1 (top) to TR5 (bottom). (RHS) solid lines - refractive index, dashed=zonal wind on the 286hPa level scaled by a factor of 10. 176
- 6.12 Wave breaking latitude distribution of the ensemble means (50000 days) of the (left) Control, (middle) E5 and (right) E5 - Control, for each troposphere (top to bottom) TR1 to TR5. . 179
- 6.13 Horizontal eddy momentum flux anomaly for days 0 to 9 of (a) the TR2 spin-up and (b) the TR4 spin-up. 183
- 6.14 Spin-up evolution for the E5 response in TR2 and TR4 (a) mean $|\bar{u}|$ anomaly between 196hPa and the surface, (b) mean $|\bar{T}|$ anomaly from 0 to 200hPa, (c) correlation between anomalies in horizontal eddy momentum flux convergence and zonal wind between 196hPa and the surface and (d) as (c) but with 11-day smoothing. 184

-
- 6.15 (LHS) E5 equilibrium response, colours = zonal wind, contours = eddy momentum flux convergence, (solid = convergence, dashed = divergence), (RHS) as LHS but for the P5 response. Top to Bottom = TR1 to TR5. 187
- 6.16 (a) mean magnitude of zonal wind anomaly vs correlation between $\overline{u'v'}$ convergence and zonal wind anomaly at all latitudes and pressures for the E5 runs, (b) as (a) but for each of the individual ensemble members of the E5 experiments. (c) and (d) are as (a) and (b) but for P5. 188
- 7.1 Mean magnitude of zonal wind anomaly over all latitudes and pressures versus control run decorrelation timescale for the ensemble means of each E5 stratospheric heating experiment. 95% confidence intervals are also shown. 200

LIST OF TABLES

2.1	Summary of possible mechanisms that could be involved in stratosphere-troposphere coupling.	43
3.1	Summary of stratospheric heating experiments.	60
3.2	Summary of model runs with zonally asymmetric boundary conditions.	64
3.3	Summary of experiments with different tropospheric reference states.	69
6.1	Summary of the differences in tropospheric jet structure in going from TR1 to TR5.	160

1. SOLAR VARIABILITY AND THE CLIMATE.

Throughout history there have been accounts of various aspects of the climate changing with solar activity. Dating as far back as 400BC when the Greek astronomer, Meton noticed that at times when more sunspots appeared on the Sun the weather seemed to be wetter (Hoyt & Schatten, 1997) and perhaps more famously, William Herschel (Herschel, 1801) noticing a correlation between the number of sunspots and the price of wheat. Due to the large amount of variability present in the Earth's climate and the large number of forcing factors that influence it, it is difficult to determine whether such observations are indeed manifestations of a real link between solar activity and climate or chance correlations in a climate that is so variable.

In recent times, methods have been developed to look at the relationship between solar activity and the climate in the past. This involves the use of proxy records such as the growth of tree rings and the rate of production of cosmogenic isotopes estimated from ice cores (e.g. Bond *et al.* (2001) and references therein). But, it is only in the last few decades with the introduction of satellite monitoring of the Earth's atmosphere and solar irradiance that a quantitative measure of the influence that solar activity has on the climate has been obtained. It has now been shown that there are statistically significant correlations between various aspects of the Earth's climate and solar activity and knowledge on the subject has come a long way. However, as yet the exact mechanisms involved remain uncertain and there is still controversy as to the magnitude of the Sun's influence.

An example of this has been demonstrated in the attribution of the observed global warming over the last decades. Some have suggested that a large fraction of the observed global warming over the later part of the 20th

century was due to a decrease in the flux of galactic cosmic rays, associated with a change in the strength of the magnetic field that emerges from the Sun (Svensmark, 2007)¹. This has been disputed (Lockwood & Fröhlich, 2007) and it is widely accepted that most of the warming over the later half of the 20th century can be attributed to anthropogenic forcing (Solomon *et al.*, 2007). However, this demonstrates the importance of understanding and quantifying the effects that natural forcings such as solar activity have on our climate.

In this chapter the observational and modelling evidence for a solar influence on climate will be discussed, along with possible mechanisms by which solar activity, particularly over the 11-year cycle, could influence the climate.

1.1 *Introduction to solar variability*

The radiative output and magnetic activity of the sun are far from being constant. They vary on a number of timescales ranging from minutes to hundreds of years. There can be very short timescale fluctuations caused by solar flares in which the total solar irradiance (TSI) can increase by up to $\sim 0.003\%$ (Fröhlich & Lean, 2004). But, perhaps more important, from a climate perspective, are the longer term changes. The sun undergoes cyclic variations of several different periods ranging from an 11-year solar cycle to the Gleissberg cycle of 80 to 90 years and the Seuss cycle of around 200 years (Ogurtsov *et al.*, 2002). As well as these cyclic variations there have been times of severely reduced solar activity such as the Maunder minimum, in the late 17th/early 18th century, in which very few sunspots were observed on the sun at all.

These longer term variations have been shown to have an influence on the climate using proxy records (e.g. Bond *et al.* (2001)). However, it is now possible to investigate the influence that the Sun has on the climate over shorter time-scales such as the 11-year solar cycle. Observations are now starting

¹ See also '*The great global warming swindle*', Channel 4, First aired 040307

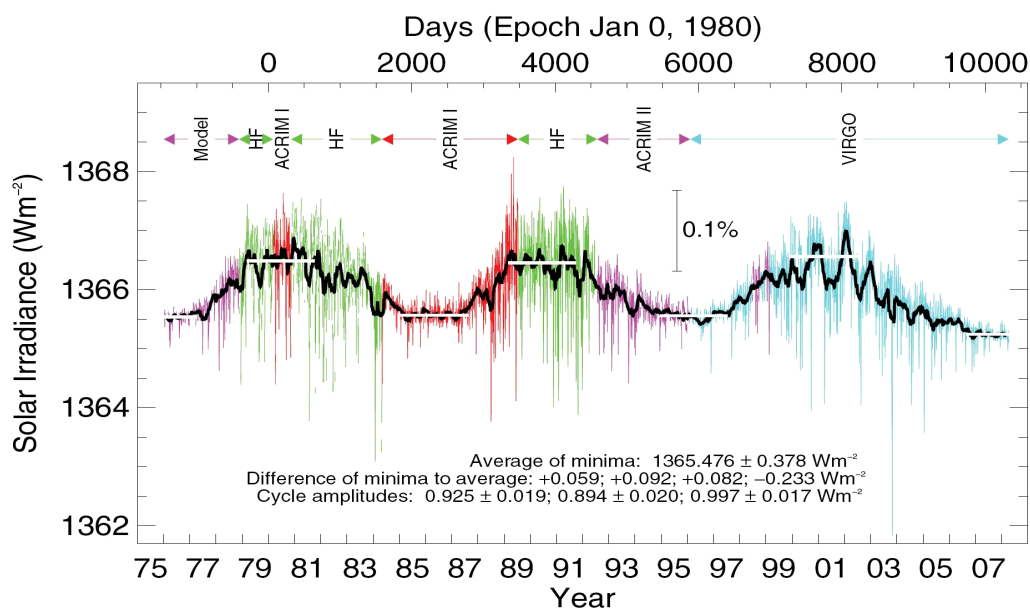


Fig. 1.1: The extended PMOD composite of total solar irradiance from 1976. Figure taken from the PMOD website (www.pmodwrc.ch).

to span a sufficient number of these cycles to demonstrate the changes in atmospheric circulation, temperature and chemistry that accompany them.

The 11-year cycle was first discovered by Heinrich Schwabe in 1843. It is associated with changes in the Sun's magnetic field. During solar maximum the magnetic activity is at its highest with there being significantly increased numbers of sunspots and events such as solar flares. During solar minimum the sun is much quieter and very few sunspots are observed. Along with this variation in magnetic activity there is a change in the radiative output of the Sun which is potentially of importance for climate. Although times of solar maximum are characterised by increased numbers of sunspots, which act to decrease the Sun's radiative output, its output actually increases. This is due to the presence of large numbers of faculae which are bright patches on the Sun's surface. A large proportion of the variation in TSI can be explained by the sum of the darkening due to sunspots and the brightening due to faculae. The overall result is typically an increase in TSI of $\sim 0.08\%$ from

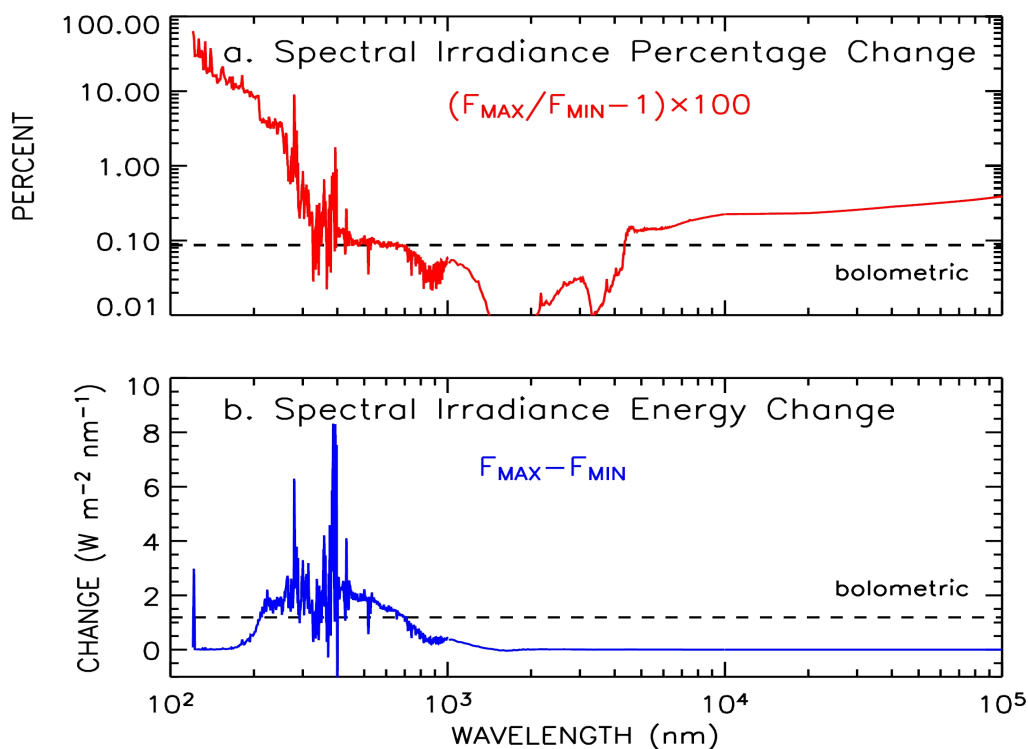


Fig. 1.2: Difference in spectral solar irradiance between solar maximum and solar minimum. (Top) percentage change, (Bottom) change in units of energy. Figure taken from Fröhlich & Lean (2004).

solar minimum to solar maximum (Fröhlich & Lean, 2004). This is illustrated in Fig. 1.1 which shows the PMOD composite: a composite of TSI measured from various different satellites. Details of the method of its construction can be found in (Fröhlich & Lean, 1998).

A change in TSI of less than 0.1% (or $1.4Wm^{-2}$) translates into a radiative forcing of around $0.25Wm^{-2}$ (Haigh, 2003). This is small when compared with other forcing, for example the estimated radiative forcing of $1.66Wm^{-2}$ due to the increase in atmospheric CO_2 since pre-industrial times (Forster *et al.*, 2007). However, the variations are not spectrally uniform and much larger changes are seen in some regions of the spectrum than others. This is demonstrated in Fig.1.2 (from Fröhlich & Lean (2004)) which shows the frac-

tional change in irradiance as a function of wavelength and also the change in irradiance in terms of energy. This shows a small fractional change in the visible and infrared part of the spectrum i.e. longer than around 400nm. However, at shorter wavelengths, there is a much larger fractional change with there being an order of magnitude difference in the change in the ultra-violet (UV) compared to the visible part of the spectrum. Around the 200nm region which is important for the production of ozone in the middle atmosphere there is an increase of the order $\sim 5\%$ at solar maximum compared to solar minimum (Lean *et al.*, 1997). However, due to the smaller amount of energy emitted by the sun in the UV region the difference in energy emitted between solar maximum and solar minimum is actually larger in the visible part of the spectrum.

To summarise the variations in solar irradiance that occur over the solar cycle: the change in TSI is small ($< 0.1\%$) but there is a much larger fractional change in the UV part of the spectrum compared to in the visible and infra-red regions.

1.2 *The solar signal in the stratosphere*

As the irradiance change over the 11-year solar cycle is not spectrally uniform, the direct radiative effect of the solar cycle on the atmosphere varies with altitude. UV radiation (~ 200 to 300nm) is primarily absorbed by ozone and molecular oxygen in the stratosphere whereas it is the visible and infrared radiation that reaches down into the troposphere. Therefore the much larger fractional change in UV irradiance as compared to in the visible and infrared implies that the solar cycle should have a greater influence on the stratosphere than the troposphere. A strong solar signal is now apparent in the stratosphere as a longer length of satellite data has become available. But, a complex structure has been revealed which depends not only on direct radiative heating but also changes in ozone concentration and dynamics as well as variations with season and a dependence/influence on the quasi-biennial

oscillation (QBO). Moreover, the inability of models to reproduce some of the observed structures has led to some uncertainty as to whether there are errors or aliasing in the extraction of solar signals from the observations or whether there are some processes that are not correctly represented in the models (Matthes *et al.*, 2003; Marsh & Garcia, 2007).

UV is not only absorbed by ozone in the stratosphere but it is also responsible for the photochemical production of it through the dissociation of molecular oxygen. Thus, changes in UV radiation not only affect the heating of the stratosphere directly but also alter ozone concentrations (Soukharev & Hood, 2006). This then feeds back onto the heating of the stratosphere as greater ozone concentrations result in increased absorption of UV. This important amplification through the absorption of UV by stratospheric ozone results in a highly non-linear atmospheric response and provides a potential mechanism for the amplification of the response to small irradiance changes (Haigh, 1994, 1996).

1.2.1 *The low latitude stratosphere*

In general observational studies tend to agree that the temperature signal over the solar cycle in the stratosphere in the tropics consists of a 3 cell pattern of variation with altitude (McCormack and Hood 1996, Hood 2004, Scaife 2000). These each suggest a large positive temperature correlation in the upper stratosphere which then decreases to either a low positive or in some studies a negative correlation at lower altitudes. This then increases to a positive response in the lower stratosphere. There are however discrepancies as to the magnitudes and locations of the various maxima and minima in the stratospheric temperature response. In an attempt to resolve these issues Crooks & Gray (2005) performed multiple regression analysis on the European centre for medium range weather forecasts reanalysis (ERA-40) dataset for two solar cycles from 1979 to 2001. It was suggested that the inconsistencies in the other studies may be due to not taking into account other forcing factors such as volcanic activity. So, in this study they have

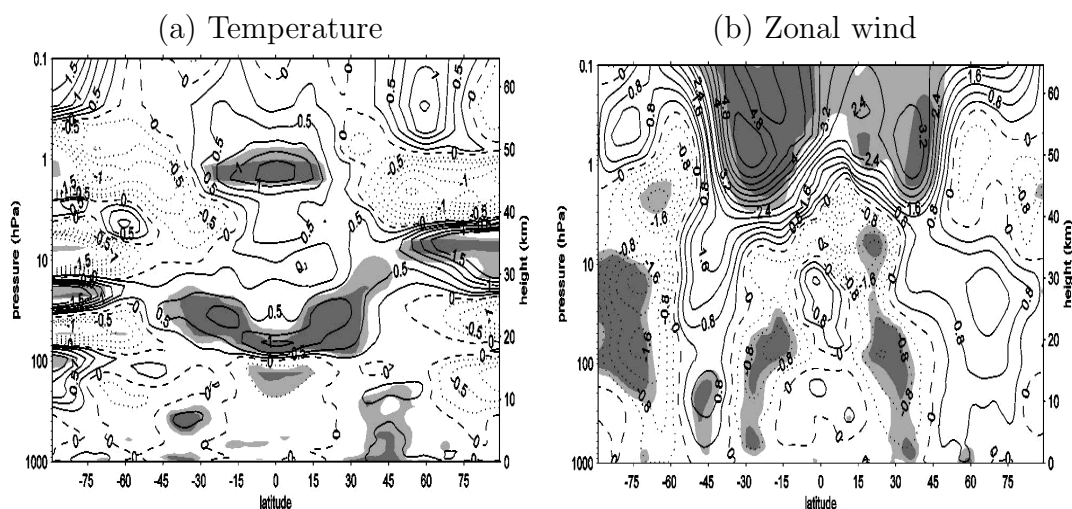


Fig. 1.3: Difference between solar maximum and solar minimum of annually averaged zonal mean (a) temperature (K) and (b) zonal wind (ms^{-1}) from regression analysis of ERA-40 data. This figure is the corrected version of (a) Fig. 2 and (b) Fig. 3 of Crooks & Gray (2005) (Tom Frame, personal communication).

taken great care in distinguishing between the solar response and that due to other forcing factors ². The resulting temperature response is shown in Fig. 1.3 (a) and the zonal wind response is shown in Fig. 1.3 (b). This shows that between about 20S and 20N the maximum temperature response occurs between about 40 and 50km, with an amplitude of about 1.2K. Below this there is a minimum in the temperature response but it remains positive. The temperature response then increases to another maximum in the lower stratosphere of about 1K.

Another study has been carried out by Labitzke *et al.* (2002) using the NCEP/NCAR reanalysis dataset from 1968-1998. The zonal mean temper-

² Since the publication by Crooks & Gray (2005) an error in the data used has been discovered. Rather than monthly mean values, the first day of each month was used in the original study. There is therefore a correction to the original results and here the corrected results are presented (Tom Frame, personal communication).

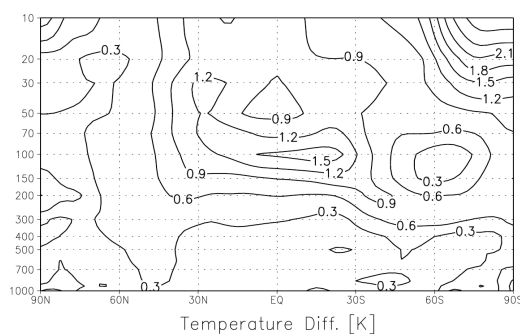


Fig. 1.4: Annual mean zonally averaged temperature difference (K) between solar max and solar min from regression analysis of 1968 - 1998 NCEP data (Figure taken from Labitzke et al. (2002)).

ature response to the 11-year solar cycle from this study is shown in Fig. 1.4. This dataset only goes up to 10hPa so the maximum in the upper stratosphere cannot be seen but this again shows an increase in temperature between solar maximum and solar minimum in the lower stratosphere. The largest temperature difference of about 1.5K is centred over the equatorial region between about 200 and 20hPa.

Although there are some discrepancies in the stratospheric temperature response between the various observational and reanalysis studies, they generally tend to agree that there is an increase in temperature in the upper stratosphere over the equatorial region of the order of 1 to 2K with a secondary maximum of the order of 1K increase in temperature of the equatorial lower stratosphere. Modelling studies have shown that this region of large positive temperature response in the upper stratosphere corresponds to the region of largest increase in shortwave heating (Matthes *et al.*, 2003). Thus, this upper stratospheric temperature response is likely to be due to increased absorption of UV by stratospheric ozone. However, the lower stratospheric maximum is most likely through a dynamical response rather than direct radiative heating.

One suggested pathway for the production of the equatorial lower strato-

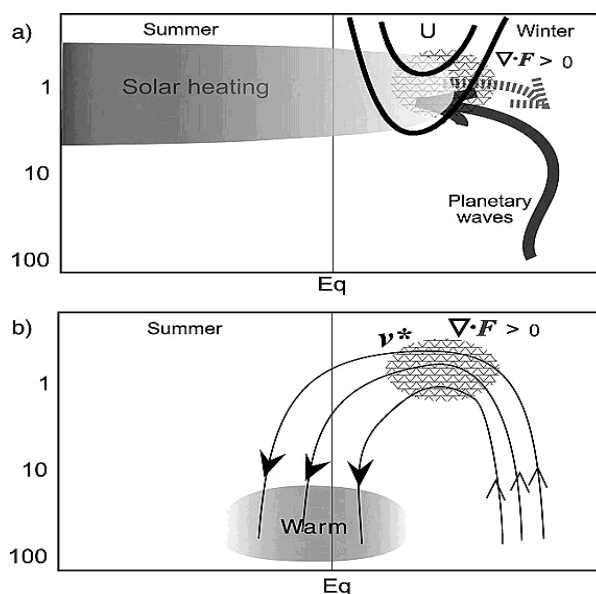


Fig. 1.5: Schematic of a possible mechanism for the production of the increased temperature in the tropical lower stratosphere in response to the solar cycle. (a) Enhanced solar heating in the upper stratosphere at solar maximum results in a strengthening of the polar night jet which acts to deflect planetary waves away from the subtropics (dashed arrow). This creates an anomalous divergence of wave activity which then weakens the B-D circulation (arrows in (b)). The anomalous descent in equatorial latitudes results in adiabatic warming of the lower stratosphere (Kodera, 2003).

spheric temperature increase is through a modification of the Brewer-Dobson (B-D) circulation (Kodera & Kuroda, 2002; Matthes *et al.*, 2006). This was first proposed by Kodera & Kuroda (2002) and is presented in a schematic form in Fig. 1.5. In the upper stratosphere of the winter hemisphere the large temperature gradient between low latitudes that are heated by solar radiation and the colder high latitudes results in a strong westerly jet known as the polar night jet. This is accompanied by a large scale meridional circulation from Equator to Pole that is driven by extratropical planetary wave

forcing, known as the B-D circulation (Andrews *et al.*, 1987).

The temperature anomaly produced in the equatorial upper stratosphere at solar maximum, as seen in Fig. 1.3 (a), enhances the equator to pole temperature gradient and thus strengthens the westerly polar night jet in the winter hemisphere through thermal wind adjustment (Fig. 1.3 (b)). Kodera & Kuroda (2002) have suggested that the stronger polar night jet acts to deflect planetary waves away from it which decreases the wave driving in the subtropics as depicted in the upper panel of Fig. 1.5. The effect of this is to weaken the B-D circulation and therefore produce anomalous downwelling and adiabatic warming over the tropical lower stratosphere in both the winter and summer hemispheres. This is a likely mechanism for the production of the tropical lower stratospheric temperature anomalies depicted in Figs. 1.3a and 1.4.

1.2.2 The polar stratosphere

Another pathway whereby the strong direct radiative response in the upper stratosphere can be transmitted to the lower stratosphere is through effects involving the stratospheric polar vortex. The strong polar vortex in the winter hemisphere stratosphere can break down in an event known as a Sudden Stratospheric Warming (SSW) where the polar stratospheric temperature can increase by a few tens of degrees (Limpasuvan *et al.*, 2004). These SSW's are initiated by planetary wave forcing in the upper stratosphere but the zonal wind and temperature anomalies associated with them are known to propagate down to the lower stratosphere (Baldwin & Dunkerton, 2001; Limpasuvan *et al.*, 2004). Thus, if the solar cycle influences planetary wave propagation it could also influence the lower stratosphere through this polar vortex pathway.

There is considerable evidence for such a mechanism. For example Kodera *et al.* (1990) have demonstrated that the solar signal in stratospheric zonal wind in the northern hemisphere (NH) appears as a poleward and downward propagating anomaly during winter, a result which has now been confirmed

by modelling studies (Matthes *et al.*, 2004). Towards the end of winter the stratospheric polar vortex breaks down due to the increased wave activity and decreased radiative forcing of the latitudinal temperature gradient. The stratosphere thus makes a transition from a radiatively controlled state to a dynamically controlled state and Kodera & Kuroda (2002) suggest that during solar maximum this radiatively controlled state is prolonged. This is intuitively what might be expected from the enhanced latitudinal temperature gradient due to increased shortwave heating in the upper stratosphere. The result is a jet in the upper stratosphere which is about 10ms^{-1} faster at solar maximum compared to solar minimum and a zonal wind anomaly which moves poleward and downward throughout the winter (Gray *et al.*, 2006).

An additional complication of the solar influence on the polar stratosphere is that it is observed to also depend on the sign of the zonal wind in the equatorial lower stratosphere (Labitzke, 1987, 2003; Labitzke & van Loon, 2000; van Loon & Labitzke, 2000). The QBO is an oscillation in the winds of the equatorial stratosphere between easterly and westerly with a period of around 2 years. The observational studies of Labitzke and van Loon have shown that there is a dependence of the solar signal in the polar lower stratosphere on the phase of the QBO. During the west phase of the QBO there is a positive correlation with the North polar temperature during winter. The opposite is seen at solar maximum during the easterly phase of the QBO. These correlations are a result of more major mid-winter warmings during solar max/QBO westerly and less major mid-winter warmings during solar max/QBO easterly. In other words at solar maximum, there is a reversal of the Holton-Tan effect which states that when the QBO is in its easterly phase there are more SSW's which is accompanied by a weaker polar vortex and warmer polar temperatures (Holton & Tan, 1980). The statistical significance of these results has been confirmed by other studies (Salby & Callaghan, 2004; Ruzmaikin & Feynman, 2002) and this observed relationship has now been reproduced in GCM runs with the equatorial winds

in the model relaxed toward observations (Matthes *et al.*, 2006). The success of these model runs in reproducing the observations was attributed to the improved zonal wind representation in the equatorial stratosphere.

Thus, it is clear that the stratospheric response to the solar cycle is a complex one involving dynamical processes and feedbacks with some of these processes not yet fully understood. Nevertheless, there are some clear solar signals found in the data and models. In this study we will be concerned with the heating of the equatorial lower stratosphere (Crooks & Gray, 2005; Labitzke *et al.*, 2002; Haigh, 2003) and rather than being concerned with how this is produced we shall be focussing on how this could impact on the tropospheric circulation.

1.3 *The solar signal in the troposphere*

As well as the significant effect of solar activity on the stratosphere, discussed above, changing solar activity has been shown to have an observable effect on tropospheric climate.

One of the most commonly cited occurrences of a solar influence on tropospheric climate is that of the Maunder Minimum (Eddy, 1976). This was a time of extremely low solar activity from the mid 17th century to the early 18th century when virtually no sunspots were observed on the Sun at all. During this time, Northern Europe and North America experienced extremely cold temperatures and consequently this period came to be known as 'The Little Ice Age'. This strong response appears to have been limited to this region with globally averaged temperature changes being small. This localised response has been attributed to the decrease in solar irradiance affecting sea surface temperatures which then shifted the North Atlantic Oscillation (NAO)/Arctic Oscillation (AO) into a low index state (Shindell *et al.*, 2001).

However, over the 11-year timescale variation of the solar cycle the oceans do not have time to fully respond due to their large heat capacity. Indeed

it is found that the solar cycle response in the oceans is limited to the top 100m (White *et al.*, 1997). It would therefore be expected that over shorter timescales such as the solar cycle, the climate should be less sensitive. This is not observed to be the case (Lean & Rind, 2001) and a solar signal is found in tropospheric climate which is non-uniform and larger than would be expected from the small change in direct radiative forcing of the troposphere.

In general, it is found that the globally averaged surface temperature is positively correlated with solar activity with an increase at solar maximum compared to solar minimum that is larger than expected from radiative forcing alone with no feedbacks (Douglass & Clader, 2002; Douglass *et al.*, 2004; Scafetta & West, 2005; Coughlin & Tung, 2004; Camp & Tung, 2007; Tung & Camp, 2008). Recently, using sophisticated statistical techniques where information about the spatial pattern of solar effects on surface temperature were used, Camp & Tung (2007) and Tung & Camp (2008) managed to obtain a global signal in surface temperature at greater than 95% significance level for the first time. Moreover, their results yielded a globally averaged temperature response of 0.2K which is considerably larger than previous estimates.

Thus, it is apparent that at solar maximum the globally averaged surface temperature increases and does so by an amount that is larger than expected without some sort of feedback process. However, looking at the spatial distribution of these temperature changes reveals a global pattern that is not at all spatially homogeneous. An example is shown in Fig. 1.6 which shows the annual averaged zonal mean temperature signal obtained from multiple linear regression of NCEP/NCAR reanalysis data (from Haigh (2003)). This demonstrates the statistically significant lower stratospheric temperature increase described in the previous section. But, now focussing on the tropospheric response, it can be seen that there is a statistically significant temperature response which consists of a banded increase in temperature of around 0.5K in mid-latitudes. This latitudinally banded temperature response is confirmed in other studies (Crooks & Gray, 2005; Lu *et al.*, 2007;

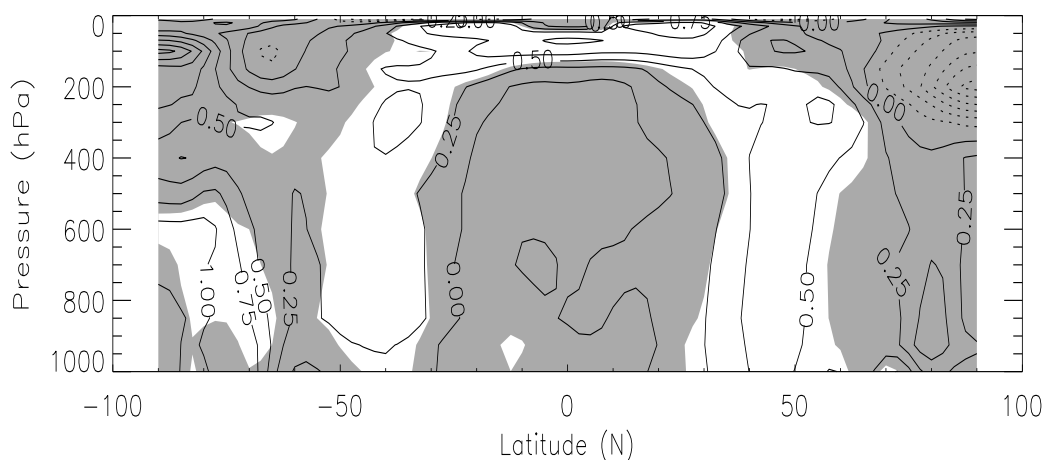


Fig. 1.6: Annually averaged zonal mean temperature response to the 11 year cycle. Shaded areas are not statistically significant at the 95% level. From Haigh (2003).

Gleisner & Thejll, 2003). This is a signal that is not just found in the winter hemisphere where the stratosphere is dynamically active nor is it just apparent in the northern hemisphere where planetary waves are prevalent.

The inhomogeneity of the tropospheric temperature signal is inconsistent with direct radiative forcing being the dominant effect. Rather it suggests that the tropospheric changes seen over the solar cycle are through a dynamical response. This is confirmed by the changes in tropospheric circulation that are observed over the solar cycle. Fig. 1.7 shows the change in zonal mean zonal wind between solar maximum and solar minimum, again from multiple linear regression of NCEP/NCAR reanalysis data (Haigh & Blackburn (2006)). The figure shows results averaged over December, January and February (DJF), but similar patterns are found in other seasons around the jet latitudes of those seasons. The top panel shows the zonal mean zonal wind for this season averaged from 1979 to 2002. The tropospheric circulation consists of strong westerly jets in mid-latitudes with maximum amplitude just below the tropopause. The lower panel then shows the solar signal. This consists of a weakened westerly wind on the equatorward side of

the jet of $\sim 1 \rightarrow 2 \text{ ms}^{-1}$ and a strengthened westerly wind on the poleward side of the jet of a similar magnitude, i.e. there is a poleward shift of the mid-latitude jets at solar maximum compared to solar minimum which is consistent with the temperature signal seen in Fig. 1.6 in terms of thermal wind balance. Analysis of vertical velocity data (Gleisner & Thejll, 2003) also suggests altered mean meridional circulation over the solar cycle with greater subsidence in mid-latitudes which is consistent with the increased temperature there through adiabatic warming.

This zonal mean response to the 11-year solar cycle is given further verification by GCM experiments using spectrally varying irradiance changes along with estimates of changes in ozone (Haigh, 1996, 1999; Shindell *et al.*, 1999; Larkin *et al.*, 2000). Haigh (1996, 1999) found a vertically banded structure in winds and temperatures for model experiments run in perpetual January mode. The most significant response was found in the summer hemisphere. Very similar patterns of response were found by Larkin *et al.* (2000) using a completely different model. Each of these model studies find that the zonal wind and temperature anomalies are associated with a weakening and broadening of the Hadley cell and a poleward shift of the Ferrell cells. The above data analysis and model experiments suggest the following as being the dominant changes in the zonal mean circulation of the troposphere over the solar cycle:

- Banded increase in temperature in mid-latitudes.
- Weakening and poleward shift of the mid-latitude jets.
- Weakening and expansion of the Hadley cells.
- Poleward shift of the Ferrell cells.

So far we have focussed only on the zonal mean response to solar activity, but clearly the atmosphere is not zonally symmetric, particularly in the northern hemisphere. Model results suggest that the temperature response in the NH winter is strongly dependent on longitude at all heights which suggests a

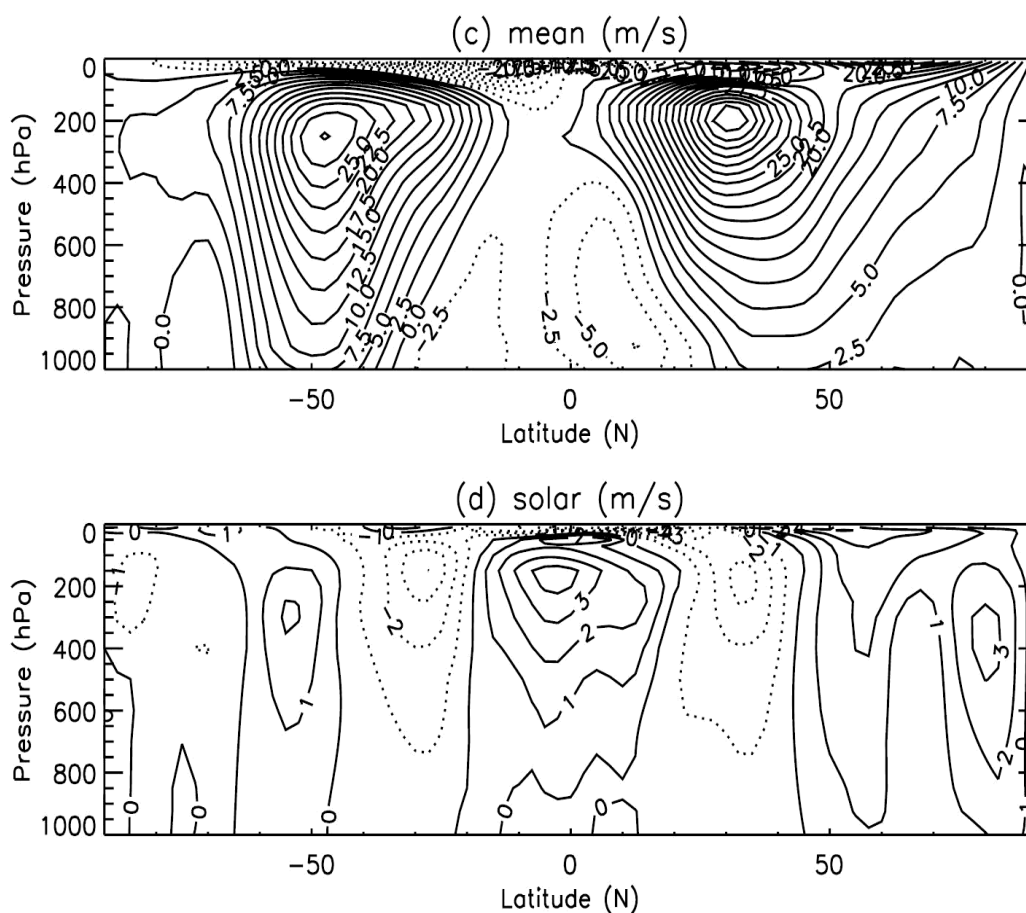


Fig. 1.7: (Top) zonal mean zonal wind averaged over DJF, (bottom) change in zonal mean zonal wind between solar maximum and solar minimum in DJF. Solid contours = westerly winds, dashed contours = easterly winds. From Haigh & Blackburn (2006).

modification of standing planetary waves (Schmidt & Brasseur, 2006). A result which is further confirmed by observational data (Berg *et al.*, 2007). Kodera (2003) has also showed that during times of lower solar activity the North Atlantic Oscillation (NAO) (a dominant mode of variability in the northern hemisphere) is confined to the Atlantic region whereas at times of higher solar activity it tends to spread out into a more annular pattern with a structure similar to that of the Arctic Oscillation (AO).

Now, with a greater length of observational data and more sophisticated GCMs some zonally varying aspects of the tropospheric response in the tropics are also beginning to be found and simulated. These seem to involve an intensification of circulation and precipitation regimes such as the monsoon (van Loon *et al.*, 2004; Kodera, 2004; Shindell *et al.*, 2006; Matthes *et al.*, 2006).

Thus, over the last few decades a picture of the tropospheric response to solar activity has been built up which involves not only a dynamical response which is visible in the zonal mean circulation but also a complicated zonally asymmetric structure involving an influence on internal modes of variability in the atmosphere. Moreover, an amplification mechanism is required to explain the magnitude of the observed tropospheric response. This study will focus on the mechanism responsible for the production of the zonal mean signal observed in re-analysis data and produced in GCM experiments.

1.4 Possible mechanisms for a solar influence on tropospheric climate.

The simplest mechanism whereby changes in solar activity can influence the troposphere is through the change in direct radiative forcing. However, over the 11-year cycle the change in direct radiative forcing on the troposphere is small and is unlikely to be able to explain the non-uniform response. Over longer timescales, such as during the Maunder Minimum (Shindell *et al.*, 2001) or the warming observed during the early 20th century (Meehl *et al.*, 2003), direct radiative forcing could play a role as the oceans have time to respond. Some evidence for this comes from the fact that on multi-decadal timescales the tropospheric temperature response appears to be larger in clear sky regions (Meehl *et al.*, 2003).

Nevertheless, on decadal timescales the oceans do not have time to fully respond. On such timescales direct radiative forcing is unlikely to be sufficient to produce the observed changes. Some other mechanism is required and this

is likely to involve some form of dynamical response given the non-uniformity of the temperature response and the presence of circulation changes.

One likely possibility, which is the focus of this investigation, is that the troposphere responds to the much larger changes that occur in the stratosphere (Hines, 1974; Bates, 1981). There is compelling evidence for such a mechanism from both observational and modelling results. Modelling studies have shown that the magnitude of the tropospheric response cannot be fully reproduced unless changes in stratospheric ozone are included (Haigh, 1994, 1996; Shindell *et al.*, 1999), implying that the changes in the troposphere are linked to the stratospheric response. This could be through changes in the polar stratosphere and through the temperature response that is observed in the equatorial stratosphere. Given that the zonal mean tropospheric response is apparent in both the NH and SH it is perhaps more likely that it is occurring through the tropical lower stratospheric heating. Any response to changes in the stratospheric polar vortex would be largely restricted to NH winter. It is the mechanism whereby this tropical lower stratospheric temperature increase could affect tropospheric circulation that is the focus of this study and the various mechanisms whereby the stratosphere can influence the troposphere will be elaborated upon in Chapter 2.

Further evidence for the increase in lower stratospheric temperature being important for the tropospheric response comes from analysis of the heat budget of the atmosphere and upper oceans to explain the decadal changes in tropical ocean temperature which lag solar irradiance variations by ~ 1 to 2 years (White *et al.*, 1997). White *et al.* (2003) and White (2006) found that surface radiative forcing by the 11-year cycle variability was insufficient to explain the changes in ocean diabatic heat storage. Moreover, they find that the heat that is lost from the troposphere to the oceans is balanced by heat that is advected downward from the lower stratosphere due to the mean circulation acting on the altered temperature gradient associated with the lower stratospheric warming.

Another completely separate mechanism that has been proposed for a

solar influence on tropospheric climate is through the effect that modulation of Galactic Cosmic Rays (GCR's) has on cloud cover. GCR's are high energy particles which bombard the Earth from outer space. The number of particles reaching the Earth is modulated by the interplanetary magnetic field which is stronger during times of higher solar activity. As a result there is a reduced incidence of GCR's during solar maximum. It is possible that this could influence cloud cover either through their direct effect on the production of cloud condensation nuclei or their effect on the atmospheric electric field (See e.g. Carslaw *et al.* (2002)).

Marsh & Svensmark (2000) advocated the former based on the high degree of correlation between GCR flux and low cloud cover between 1984 and 1991 found by Svensmark & FriisChristensen (1997). This theory has proved to be a controversial one and is still debated. Several problems with this mechanism have arisen. First and foremost, the time series' of GCR flux and cloud cover actually diverge after 1994 and the correlation is no longer apparent (Kristjansson & Kristiansen, 2000). Also, further studies using more reliable cloud data have found that the correlation is highest when the changes in cloud cover actually preceded the changes in GCR flux (Kristjansson *et al.*, 2002). Moreover, it is found that the correlation between TSI and cloud cover is equally high (Lockwood, 2002).

Kristjansson *et al.* (2004) proposed that the changes in the stratosphere affect tropospheric circulation such as to increase the temperature in the lower troposphere in the subtropics which in turn would affect static stability over the oceans and influence cloud cover. The solar activity/cloud cover correlations thus could also lend support to the stratospheric mechanism.

To conclude this section, there are several mechanisms by which solar variability can influence tropospheric climate. It is possible that a combination of all these is occurring but there is considerable evidence for a dynamical response to the larger signal in the stratosphere and it is this mechanism that is investigated in the following.

2. STRATOSPHERE-TROPOSPHERE COUPLING.

2.1 *Stratosphere-troposphere coupling in observations*

It has been known for a long time that the troposphere has a significant effect on the stratosphere, mainly through effects involving large scale atmospheric waves which propagate upward from the troposphere to the stratosphere affecting the circulation there. However, it is only recently that a coupling in the other direction has become apparent. In the last decade a great deal of research has been done into the effects that changes in the stratosphere might have on the troposphere and it is now widely accepted that there is a two-way dynamical coupling (Haynes, 2005; Shepherd, 2002). However, much work remains to be done to fully understand the mechanisms whereby the stratosphere influences the troposphere.

A coupling between the stratosphere and troposphere is now found in observational and modelling studies of the atmospheric response to various forcings. One area where it is of great importance to understand the influence the stratosphere can have on the troposphere is in the understanding of recent climate trends and the prediction of future climate change. Over the last few decades the stratosphere has undergone major changes. First with ozone depletion (Hartmann *et al.*, 2000) and now with ozone recovery (Eyring *et al.*, 2007) and increasing abundances of greenhouse gases (Santer *et al.*, 2003). Satellite observations over the last 3-4 decades have shown that, in general, there has been a cooling trend in the stratosphere (Ramaswamy *et al.*, 2001). Over this time the trends that have occurred in the stratospheric and tropospheric circulation appear to have been linked (Thompson & Solomon, 2002). It is therefore important to understand the mechanisms

whereby changes in the stratosphere influence the troposphere in order to understand and predict future changes in surface climate in response to anthropogenic forcings (Baldwin *et al.*, 2007).

As well as anthropogenic forcings there are many natural forcings that can potentially have an influence on tropospheric climate through a stratospheric pathway. One area that has been studied intensely is the tropospheric response to Sudden Stratospheric Warmings (SSW's) and variations in the stratospheric annular modes (e.g. Limpasuvan *et al.* (2004); Baldwin & Dunkerton (1999)). It is through this phenomenon that some of the first observational evidence for a stratospheric influence on the troposphere was found (Baldwin & Dunkerton, 2001). When the stratosphere undergoes a sudden warming event it is often accompanied by changes in the surface climate over the following 60 days. The warming of the polar stratosphere and associated weakening of the polar vortex appears first in the upper stratosphere and then propagates downward to the tropopause. Often this is then accompanied by altered tropospheric circulation patterns. The dynamical linkage in this case seems to occur through the annular modes of variability.

The annular modes are the leading modes of variability in the extratropical circulation (Thompson & Wallace, 2000). These modes are associated with fluctuations in the meridional pressure gradient in the extra-tropics and associated alteration of the zonal flow. In the stratosphere a high index state of the annular mode consists of a stronger meridional pressure/temperature gradient and stronger polar vortex. Similarly in the troposphere, variations in the annular modes are associated with altered sea level pressure (SLP) gradients and variations in position and strength of the tropospheric westerly jets (also known as the Arctic Oscillation (AO) in the Northern hemisphere). When there is a shift toward the higher index state of the stratospheric annular mode this is often accompanied by a higher index state of the tropospheric annular mode about 2 weeks later. Thus, often when there is an SSW and corresponding weakening of the stratospheric polar vortex in the NH there is a surface response of the form of a shift to the lower index state of the

AO. Over the Atlantic and Pacific regions this is manifest as a southward shift of the storm tracks. However, not every SSW event is associated with a change at the surface (Zhou *et al.*, 2002). There has also been some debate as to whether these observational results actually imply downward propagation from the stratosphere to the troposphere. Plumb & Semeniuk (2003) showed that similar structures to those found in the tropospheric response to SSW's could be produced by forcing at lower levels implying that there may actually be no downward propagation of information. A greater understanding of the processes whereby such variations in the stratospheric annular modes affect surface climate could be useful in weather prediction (Baldwin *et al.*, 2003).

In fact many of the suggested stratospheric changes that could influence the troposphere seem to do so through the annular modes of variability. For example, the aforementioned linkage in the stratospheric and tropospheric trends in response to ozone depletion and recovery appear to occur through the annular modes (Thompson & Solomon, 2002; Son *et al.*, 2008a). Also, with enhanced concentrations of greenhouse gases it is predicted that there will be a shift to the higher index state of the annular mode which could be associated with a cooling of the stratosphere (Lorenz & DeWeaver, 2007).

Volcanic eruptions can also influence the high latitude tropospheric circulation through the stratosphere. They inject large amounts of aerosol into the stratosphere which results in heating of the lower stratosphere at latitudes exposed to sunlight and so enhances the meridional temperature gradient and strengthens the stratospheric polar vortex. There is also an associated response in the surface climate in the form of a shift to higher index states of the annular modes (Hartmann *et al.*, 2000).

Another climate forcing where stratosphere-troposphere coupling is likely to be important is the focus of this study, that is the tropospheric response to varying solar activity. The results discussed in Chapter 1 suggest that some form of coupling between the stratosphere and troposphere plays an important role in transmitting the signal down into the troposphere and amplifying the effect. The tropospheric response consists of a poleward shift

of the mid-latitude jets (or a shift to the higher index state of the annular modes). This study will be focussing on how the changes in the stratosphere could produce this shift in tropospheric circulation. This chapter will therefore give an overview of the mechanisms that have been suggested for a coupling between the stratosphere and troposphere which can be of use in explaining the tropospheric response to changing solar activity as well as the surface response to each of the variations/forcings described above.

2.2 *Mechanisms of stratosphere-troposphere coupling*

The proposed mechanisms involved in stratosphere-troposphere coupling can be divided into two categories: direct and indirect. Direct mechanisms involve changes in the lower stratosphere directly influencing the circulation in the troposphere whereas the indirect mechanisms tend to involve changes in the stratospheric flow altering the propagation of waves from the troposphere (either large scale planetary waves or smaller scale baroclinic eddies) which then, through wave-mean flow interactions can result in altered tropospheric circulation. These mechanisms are summarised in table 2.1.

2.2.1 *Direct mechanisms*

The direct mechanisms are generally considered to be insufficient to account for the full tropospheric circulation response to stratospheric perturbations. This is due to the much larger proportion of mass that resides in the troposphere compared to the stratosphere. However, there is evidence for these direct mechanisms occurring, perhaps in combination with indirect mechanisms.

Mass redistribution involves an anomalous zonal forcing in the stratosphere resulting in a build up of mass in the polar cap which will in turn affect the surface pressure and thus geostrophically induce changes in the zonal wind at the surface. Baldwin & Dunkerton (1999) suggested that this mechanism could explain the correlation between SLP and lower strato-

Direct	Indirect
<ul style="list-style-type: none"> • Mass redistribution (Baldwin & Dunkerton, 1999; Sigmond <i>et al.</i>, 2003) • Downward control for zonal mean fields (Haynes <i>et al.</i>, 1991; Song & Robinson, 2004) • Potential Vorticity Inversion (Hartley <i>et al.</i>, 1998; Black & McDaniel, 2004; Ambaum & Hoskins, 2002) • Radiative processes (Grise <i>et al.</i>, 2009) 	<ul style="list-style-type: none"> • Planetary wave reflection (Hines, 1974; Perlwitz & Harnik, 2003; Kodera <i>et al.</i>, 2008) • Wave-mean flow interactions <ul style="list-style-type: none"> – Synoptic scale eddies (Kushner & Polvani, 2004; Song & Robinson, 2004; Haigh <i>et al.</i>, 2005) – Planetary waves (Boville, 1984; Kodera & Kuroda, 2002; Song & Robinson, 2004; Coughlin & Tung, 2005)

Tab. 2.1: Summary of possible mechanisms that could be involved in stratosphere-troposphere coupling.

spheric geopotential height that they find in their downward propagating AO signatures. An anomalous zonal forcing in the stratosphere would induce a meridional circulation. For example a westward zonal force in the NH would induce a poleward mean meridional circulation to try to balance it. The lower level return flow doesn't entirely balance the poleward flow due to friction (Haynes & Shepherd, 1989) resulting in an increase in mass at the pole. This

will therefore result in a change in meridional pressure gradient which will geostrophically induce a change in the zonal wind. The results of Sigmond *et al.* (2003) showed, using ECMWF re-analysis data, that in NH winters the zonal wind in the lower troposphere is indeed positively correlated with the strength of the equatorward meridional mass flux in the stratosphere.

Another direct mechanism is that of downward control. By this mechanism, a forcing can produce an acceleration in the zonal flow below through the meridional circulation that it induces. It was shown by Haynes *et al.* (1991) that a zonal force produces a response that is predominantly downward as follows.

Zonal mean quasi-geostrophic momentum balance in the Transformed Eulerian Mean (TEM) formulation and in the absence of friction is given by

$$\frac{\partial \bar{u}}{\partial t} - f \bar{v}^* = \bar{F} \quad (2.1)$$

(Andrews *et al.*, 1987) where \bar{F} is the zonal force per unit mass (due to wave breaking and other dissipative eddy processes), \bar{u} is the zonal mean zonal wind and \bar{v}^* is the meridional component of the TEM circulation. All other symbols have their usual meaning as given in the list of symbols. This can be combined with the mass continuity equation

$$\frac{1}{a \cos \phi} \frac{\partial}{\partial \phi} (\bar{v}^* \cos \phi) + \frac{1}{\rho_o} \frac{\partial}{\partial z} (\rho_o \bar{w}^*) = 0, \quad (2.2)$$

where $\rho_o = \exp(-z/H)$ and \bar{w}^* is the vertical component of the TEM circulation. Solving for \bar{w}^* in the steady state (i.e. $\partial u / \partial t = 0$) and in the presence of radiative damping it can be shown that, under the assumption that $\rho_o \bar{w}^* \rightarrow 0$, as $z \rightarrow \infty$

$$\bar{w}^* = -\frac{1}{a \rho_o \cos \phi} \frac{\partial}{\partial \phi} \left[\int_z^\infty \frac{\rho_o \bar{F} \cos \phi}{2 \Omega \sin \phi} dz' \right] \quad (2.3)$$

(Haynes *et al.*, 1991). This states that in the steady state, the circulation below some level z is controlled by the forcing \bar{F} above that level i.e. the influence of a forcing is solely downward in the steady state. This is the principle of downward control and it applies in the regions of the atmosphere

where the contours of constant angular momentum span the atmosphere in the vertical such as is the case in the extra-tropics. Haynes *et al.* (1991) also showed that even with time dependent forcing the response is predominantly downward if the timescales considered are longer than the radiative timescale. Through this mechanism, anomalous zonal flow in the stratosphere caused by, for example, anomalous wave forcing, will induce an anomalous meridional circulation which will stretch down in altitude and alter the zonal flow at lower levels through the coriolis force on the induced meridional circulation.

This principle was initially proposed in the context of the dynamics of the middle atmosphere but it is possible that forcing in the stratosphere could influence the troposphere through this mechanism. However, because of the much larger mass in the troposphere compared to the stratosphere, it is unlikely to be sufficient to explain the magnitude of the responses to the various forcings described above. But it is perhaps at work in conjunction with other mechanisms (Song & Robinson, 2004).

The downward control principle is a particular case for zonal mean fields. More generally, for 3D fields, the equivalent principle is that of potential vorticity inversion. The atmosphere is mostly in geostrophic and hydrostatic balance. Therefore, if any change occurs in the atmosphere (e.g. heating or wave forcing) then this will have a non-local effect as the atmosphere responds in order to maintain hydrostatic and geostrophic balance.

This can be illustrated using the quasi-geostrophic potential vorticity (PV):

$$q = \frac{1}{f_o} \nabla^2 \Phi + f + \frac{\partial}{\partial x} \frac{f_o}{\sigma} \frac{\partial \Phi}{\partial p} \quad (2.4)$$

where q is the PV, Φ is the geopotential height and all other symbols have their usual meaning as given in the list of symbols. This is a quantity that is only changed through diabatic or by frictional processes and from which the geopotential height and associated fields such as the zonal wind and temperature can be obtained. Clearly from equation 2.4, Φ is related to q by a second order differential operator so an anomaly in q implies changes in Φ that are non local and stretch out horizontally and vertically. The potential

vorticity thus illustrates how the geostrophic and hydrostatic adjustments in response to a diabatic or frictional process results in non local changes in geopotential height and thus temperature and wind structure of the atmosphere. A forcing which changes the stratospheric PV could therefore affect the circulation lower down. Both this mechanism and downward control suffer from the fact that the mass in the troposphere is much larger than that in the stratosphere. Nevertheless, several studies have shown that tropospheric changes can be produced in response to the PV anomalies associated with distortions of the stratospheric polar vortex (Hartley *et al.*, 1998; Ambaum & Hoskins, 2002; Black, 2002).

Until recently the mechanisms proposed for a stratospheric impact on the troposphere have largely been dynamical. Grise *et al.* (2009) have recently investigate the effect that radiative processes due to altered stratospheric temperatures and ozone can have on the troposphere. They investigated this for two cases: 1) the observed temperature trends in the SH over the last few decades and 2) the observed response to dynamical variability in NH winter. In both cases they find that the radiative effect of altered stratospheric temperatures on tropospheric temperatures is non-negligible. In the SH the radiative effect of stratospheric cooling can account for a significant proportion of the middle and upper tropospheric temperature trends. It cannot, however, account for the lower tropospheric temperature response and so it is likely that dynamics is also playing a role in the full response. So, they have shown that simply the altered radiative effect of a changing stratosphere can influence tropospheric temperature. This could then potentially have a further influence on tropospheric dynamics to produce the full response.

2.2.2 *Indirect mechanisms*

The indirect mechanisms that have been proposed involve atmospheric waves, either large scale planetary waves or smaller scale baroclinic eddies.

Large scale planetary waves (i.e. wavenumbers 1 and 2) are the only waves that are able to propagate high up into the stratosphere. They therefore pro-

vide a pathway by which changes that occur in the upper stratosphere can be transmitted downward. One way in which they could affect tropospheric circulation is through planetary wave reflection. Planetary waves generated in the troposphere propagate upward into the stratosphere. They could then be reflected back down into the troposphere where they would then interact with tropospheric waves and influence tropospheric circulation patterns. Thus, altered stratospheric circulation could alter the reflection of planetary waves thereby altering tropospheric circulation. There is now observational evidence for planetary wave reflection from the stratosphere having an influence on the troposphere during NH winter (Perlwitz & Harnik, 2003; Kodera *et al.*, 2008). Moreover, Perlwitz & Harnik (2004) have suggested that this provides a possible explanation for why the stratospheric circulation changes in the response to SSW's in the Baldwin and Dunkerton studies do not always propagate down to the surface. They suggest that there are two types of stratosphere-troposphere coupling depending on the dynamical state of the stratosphere and whether it is reflective or not. When the stratosphere is in a reflective state there is a strong coupling between the wavenumber 1 fields in the stratosphere and troposphere but there is no correlation between zonal mean fields. So, the years in which there is found to be a downward propagation of zonal mean annular mode signals are those in which the stratosphere is in a non-reflective state.

Another way in which large scale planetary waves can result in a coupling between the stratosphere and troposphere is through changes in their propagation and altered wave-mean flow interactions (Boville, 1984). Planetary waves propagate up into the stratosphere and, if they are not reflected, they are absorbed and deposit their momentum there. Altered stratospheric flow can alter the propagation of planetary waves and so alter where their momentum is being deposited and result in descent of zonal wind anomalies. Studies have shown that the downward propagation of zonal wind anomalies in the stratosphere associated with an altered polar vortex are due to interactions between planetary waves and the mean flow (Kodera *et al.*, 1990; Scott

& Polvani, 2004; Christiansen, 1999; Coughlin & Tung, 2005). The interaction between planetary waves and the mean flow could continue down into the troposphere. Indeed Perlwitz & Harnik (2004) have shown that when the stratosphere is in the state where wave-mean flow interactions are strong, the zonal mean variations associated with annular modes propagate downward.

Alternatively, wave-mean flow interactions could bring zonal wind changes down to the lower stratosphere which could then affect the structure of tropospheric planetary waves. This could explain the wavenumber 1 structure that is often associated with changes in the tropospheric NAM (Coughlin & Tung, 2005)

Thus, planetary wave propagation provides a promising mechanism for stratosphere - troposphere coupling in NH winter. But, it is unlikely to be able to explain coupling that is observed in other seasons, or coupling that is observed in the SH. Firstly, planetary waves can only propagate up into the stratosphere when the flow is westerly which is the case only in the winter hemisphere. Secondly, large scale planetary waves are produced by flow over large scale mountain ranges such as the Rockies or the Himalayas or through land-sea temperature contrasts. Planetary waves are therefore far more prevalent in the NH where there are more land surfaces and larger mountain ranges. Therefore, any mechanisms involving such waves will be far more effective in the northern hemisphere.

Hines (1974) and Bates (1981) proposed, long before the tropospheric response to solar activity was observed in satellite data, that a stratospheric influence on planetary wave propagation could result in a tropospheric response to changing solar activity. Such a mechanism is likely to have contributed to the tropospheric response found during northern hemisphere winter in modelling results (Haigh, 1996; Shindell *et al.*, 1999; Rind *et al.*, 2002; Matthes *et al.*, 2006). However, for instances of stratosphere-troposphere coupling that are observed in the southern hemisphere or in seasons other than winter, such as the zonal mean response to solar activity or the observed trends in the southern annular mode, another mechanism is required.

One such mechanism is through the effect that changes in the stratosphere can have on synoptic scale eddies. Eddies are produced by baroclinic instability that occurs in the strong meridional temperature gradient in mid-latitudes and so are present in both hemispheres. They are important in transferring heat and momentum and they are responsible for maintaining the strong westerly jet in the mid-latitude troposphere. It is therefore reasonable to expect that if any change in the lower stratosphere affects eddy propagation then this could influence the tropospheric circulation. Moreover, interaction between the eddies and the mean flow has been shown to be responsible for the increased persistence of the annular modes (Lorenz & Hartmann, 2001, 2003). Therefore it is also reasonable to expect that they might play a role in the annular mode signal that is apparent in response to many stratospheric forcings.

Many studies have now shown that tropospheric eddies are affected by various perturbations to the lower stratosphere and that they are important in producing the tropospheric response to such perturbations (Polvani & Kushner, 2002; Song & Robinson, 2004; Wittman *et al.*, 2004; Kushner & Polvani, 2004, 2006; Haigh *et al.*, 2005; Williams, 2006; Lorenz & DeWeaver, 2007). Many of these studies have investigated the effect of stratospheric temperature perturbations on the tropospheres of idealised GCM's and given the relevance of this to the present study they will be described in more detail in section 2.3.

Another example is the study of Wittman *et al.* (2007) which looked at the effect of increased stratospheric wind shear on baroclinic lifecycles. They found that increasing the vertical wind shear increased the saturation amplitude of the eddies which then resulted in an increased poleward displacement of the jet. They suggest that this process could account for the connection between the stratospheric and tropospheric NAM signals.

One other way in which the changes in the stratosphere could affect eddies is through alteration of the eddy phase speed. This was recently suggested by (Chen & Held, 2007) as a possible explanation for the recent poleward shift

of the SH westerly jet. They find that accompanying the poleward shift of the mid-latitude westerlies is an increased easterly phase speed of the eddies. Eddies break around the region known as the critical line which is where the eddy phase speed is equal to the zonal wind speed. Thus, if you have an altered phase speed there will be a change in the latitude of eddy breaking and so a change in the regions of convergence/divergence of momentum flux which will alter the zonal flow. They previously showed that this mechanism was responsible for the poleward shift of the jet in response to reduced surface friction in a simplified GCM and suggest that a similar mechanism may be at work here (Chen *et al.*, 2007). Altered zonal wind around the tropopause could change the eddy phase speed and induce a change in circulation. But, it remains to be seen whether changes around the tropopause are sufficient to alter eddy phase speeds and indeed whether the change in phasespeed accompanying the SH trend is a cause rather than an effect.

Finally, it is likely that altered eddy-mean flow interaction is happening in conjunction with other mechanisms. For example Song & Robinson (2004) have suggested a process which they call downward control with eddy feedback to explain the tropospheric response to torques applied to the stratosphere of their idealised GCM. By this mechanism, the applied torques induce a circulation response in the troposphere through downward control (Haynes *et al.*, 1991). This then affects tropospheric eddies which provides a feedback to amplify the response. However, Song & Robinson (2004) show that although this process is occurring in their model it does not give a complete description of the processes through which the stratosphere is influencing the troposphere.

There are, therefore, a number of mechanisms which could provide a coupling between the stratosphere and troposphere. It could be that each of these mechanisms plays a role depending on the type of forcing in the stratosphere. It is also likely that several mechanisms could be at work in conjunction with one another. In the context of the solar cycle, the small scale baroclinic eddy mechanism is a likely candidate given that the response

is not just restricted to the northern hemisphere or the winter hemisphere. Therefore, we will be focussing on the small scale baroclinic eddy mechanism. Specifically we will be investigating how it could be important in producing the tropospheric response to heating perturbations in the lower stratosphere.

2.3 *The tropospheric response to heating perturbations in the stratospheres of simplified GCM's*

Given the complexity of the atmosphere, it is useful to look at processes in simplified GCM's (sGCM's). In recent years several authors have investigated the effect of applying various different heating perturbations to the stratospheres of dry dynamical cores i.e. simplified GCM's that have a complete representation of dynamical processes but a highly parameterised representation of physical processes such as those involving moisture or radiation. In each of these experiments a significant tropospheric response is produced by heating/cooling the model stratosphere in some way (Kushner & Polvani, 2004, 2006; Polvani & Kushner, 2002; Williams, 2006; Haigh *et al.*, 2005; Lorenz & DeWeaver, 2007). As heating perturbations will be applied to the stratosphere of an sGCM in the following, some of the relevant results will be discussed here.

The work of Polvani and Kushner (Polvani & Kushner, 2002; Kushner & Polvani, 2004, 2006) has focussed on investigating the tropospheric response to the cooling of the polar stratosphere of an sGCM. Their model has good resolution in the stratosphere and therefore is capable of simulating the stratospheric polar vortex. They find that by cooling the polar stratosphere and thus strengthening the polar vortex, the tropospheric jet is shifted poleward by some 15° latitude. They demonstrate the importance of changing eddy momentum fluxes in producing the tropospheric response and furthermore it is found that the full response could not be produced without internal tropospheric eddy feedbacks.

There is now some debate as to the robustness of the magnitude of the

response as other experiments have found a much smaller shift of only around one fifth of the original magnitude (Gerber & Polvani, 2008; Chan & Plumb, 2009). The massive response found in the original experiments is thought to be due to their tropospheric circulation having been on the borderline of two different regimes: one in which the sub-tropical and eddy driven jets are well separated and the other in which they are not. Some recent experiments have now shown that the 15° shift is due to a transition between these two regimes (Gerber & Polvani, 2008). Under normal circumstances a much smaller response is produced. Nevertheless, the poleward shift of the jet in response to the stratospheric cooling is a robust response and their conclusions that it is the tropospheric eddy fluxes that are important remain valid.

Other studies have also looked at the effect of applying heating perturbations to the stratosphere of an sGCM but with a less well resolved stratosphere, such that any change in strength of the stratospheric polar vortex is not simulated. These too produce a tropospheric response which consists of a shift in position and strength of the tropospheric jets accompanied by altered synoptic scale eddy fluxes. The sign of which seems to depend on the sign and latitudinal distribution of the applied temperature perturbation.

For example Haigh *et al.* (2005) and Williams (2006) have shown that in response to a uniform increase in temperature of the stratosphere, and corresponding lowering of the tropopause, there is an equatorward shift of the mid-latitude jets. Analogously Lorenz & DeWeaver (2007) found a strengthening and poleward shift of the mid-latitude jets in response to a cooling of the stratosphere, such as is predicted in the response to increasing greenhouse gas concentrations. So, it appears that the sign of the tropospheric response depends on the sign of the temperature change in the stratosphere, or equivalently whether the tropopause is being raised or lowered. However, the tropospheric response also depends on the meridional distribution of the applied heating perturbation. Haigh *et al.* (2005) showed that if the stratosphere is heated preferentially at the equator then there is a poleward shift of the jet whereas if it is heated preferentially at the pole then there is an

equatorward shift of the jet. These results suggest that perhaps the change in meridional temperature gradient is important in determining the sign of the tropospheric changes.

Lorenz & DeWeaver (2007) performed some additional experiments to test whether the tropospheric response is most sensitive to changes in the height of the tropopause or changes in the meridional temperature gradient. They applied a heating perturbation of 20° latitude width and 150hPa height at various positions in the latitude-pressure plane. They find that, for example, when this heating is applied at low latitudes there is a dramatic change in the direction of the shift of the tropospheric jet as the heating perturbation is moved from below to above the tropopause. This suggests that it is the change in tropopause height that is important as each of these experiments have the same meridional temperature gradient but the sign of the tropopause height change is switched as the heating crosses the tropopause.

However, this is not the complete story as they also find a change in the sign of the tropospheric response as the heating moves meridionally, either above or below the tropopause.

The above experiments have demonstrated that in response to stratospheric heating perturbations there is a shift in the tropospheric circulation patterns which is accompanied by changes in synoptic scale eddy fluxes. Moreover, the response appears to depend not only on the sign of the heating perturbation but also on its meridional distribution. In the following we will attempt to resolve some of these issues as we investigate in more detail the mechanisms involved in producing the tropospheric response to perturbations in lower stratospheric temperature.

3. THE MODEL EXPERIMENTS AND DIAGNOSTICS

3.1 *The simplified General Circulation Model (sGCM)*

The sGCM used in the following experiments is the Reading IGCM2.2. It is a dry dynamical core that solves the primitive equations on a sphere formulated in terms of vorticity and divergence. This is done following the method of Hoskins & Simmons (1975) but with modification to include the angular momentum conserving vertical discretization of Simmons & Burridge (1981). However, this model uses sigma coordinates ($\sigma = p/p_s$) rather than the generalised vertical coordinates used by Simmons & Burridge (1981).

The primitive equations are solved using the spectral transform method (Orszag, 1970) with triangular truncation at wavenumber 42 which is roughly equivalent to a horizontal resolution of 2.8° by 2.8° . There are 15 levels in the vertical between the surface and $\sigma=0.0185$ with the level spacing chosen to give good resolution in the region of the tropopause which is important for investigations of the tropospheric response to stratospheric heating perturbations. The model levels are as follows: 18.5, 59.6, 106, 152, 197, 241, 287, 338, 400, 477, 569, 674, 784, 887 and 967 hPa.

While the model includes an accurate representation of large scale dynamical processes, it has a highly parameterised representation of physical processes. It is in this respect that the model is simplified. Instead of the detailed radiative, turbulence and moist parameterisations of a full GCM, there is simple forcing and dissipation as described by Held & Suarez (1994). Boundary layer friction is represented by Rayleigh damping of winds below

$\sigma = 0.7$ with a timescale of 1 day at the surface. Thus,

$$\frac{\partial(\bar{u}, \bar{v})}{\partial t} = \dots - k_f(\sigma)(\bar{u}, \bar{v}) \quad (3.1)$$

where ... represents the usual dynamical terms that act to accelerate the zonal wind (\bar{u}) or meridional wind (\bar{v}) and

$$k_f = k_o \max \left(0, \frac{\sigma - 0.7}{1 - 0.7} \right) \quad (3.2)$$

with $k_o = 1 \text{day}^{-1}$. The effect of sub-grid scale processes is parameterised by ∇^6 hyperdiffusion and at the model top the boundary condition is a reflective one i.e. $\dot{\sigma} = 0$. The climate is maintained by Newtonian relaxation of the temperature field to a zonally symmetric state i.e.

$$\frac{\partial T}{\partial t} = \dots - k_T(\phi, \sigma) [T - T_{ref}(\phi, p)] \quad (3.3)$$

where ... represents the usual dynamical terms which act to change the temperature. k_T is given by

$$k_T = k_a + (k_s - k_a) \max \left(0, \frac{\sigma - 0.7}{1 - 0.7} \right) \cos^2 \phi \quad (3.4)$$

where $k_a = 1/40 \text{ day}^{-1}$ and $k_s = 1/4 \text{ day}^{-1}$ such that the temperature is relaxed on a timescale of 40 days for $\sigma < 0.7$ (representing radiation and deep moist processes) reducing to 4 days at the equatorial surface (representing the planetary boundary layer). The Newtonian relaxation temperature profile T_{ref} is shown in Fig. 3.1a along with the equivalent plot for potential temperature (θ_{ref}) in Fig. 3.1b. As it is zonally symmetric, T_{ref} is a function of pressure (p) and latitude (ϕ) only and is given by

$$T_{ref}(\phi, p) = \max \left\{ (T_{tpeq} - \Delta T_{tp} \sin^2 \phi), \left[T_o - \Delta T_y \sin^2 \phi - (\Delta \theta_{eq} \cos^2 \phi + \Delta \theta_{pl} \sin^2 \phi) \log \left(\frac{p}{p_0} \right) \right] \left(\frac{p}{p_o} \right)^\kappa \right\}, \quad (3.5)$$

where p_o is the reference surface pressure ($= 1000 \text{hPa}$), T_{tpeq} is the equatorial tropopause temperature. ΔT_{tp} is the difference in temperature between

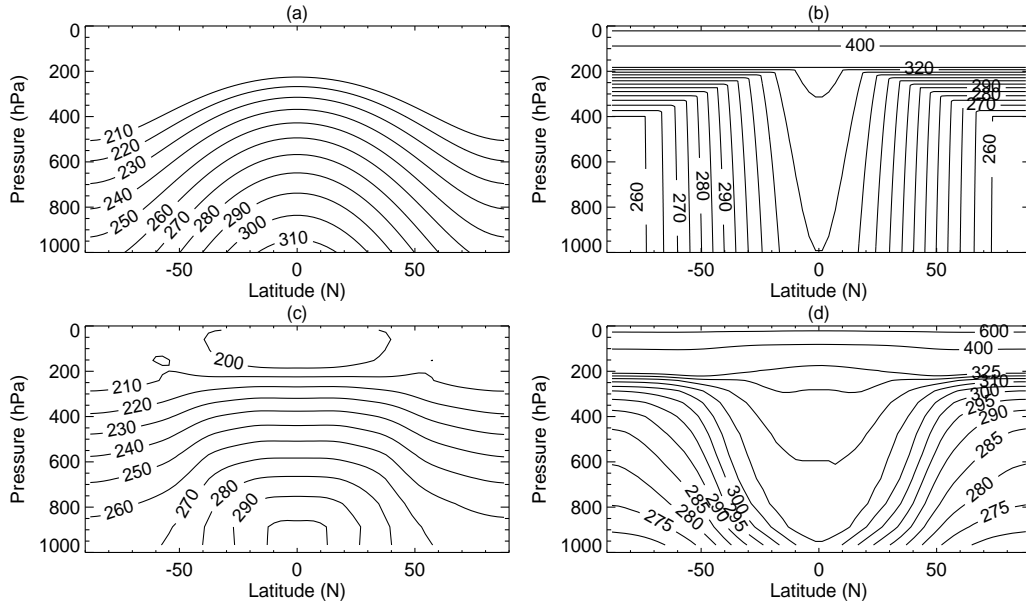


Fig. 3.1: (a) Newtonian relaxation temperature profile for the control run climatology, (b) as (a) but potential temperature, (c) control run zonal mean temperature and (d) control run potential temperature for a 10 000 day control run average.

the equatorial and polar tropopause. T_o is the surface temperature at the equator, ΔT_y is the difference between the equatorial and polar surface temperature and $\Delta\theta_{eq}$ and $\Delta\theta_{pl}$ are the increase in potential temperature with an increase in altitude of one pressure scale height at the equator and poles respectively. For the control run climatology, shown in Fig. 3.1, $T_o=315K$, $\Delta\theta_{eq} = 10K$ and $\Delta\theta_{pl}=0K$.

Thus, the relaxation temperature profile is isothermal in the stratosphere and has a negative latitudinal temperature gradient in the troposphere. There is some positive static stability in the tropics to limit gravitational instability. This decreases to zero at the poles as is demonstrated by the reduction in vertical gradient of θ_{ref} in going from equator to pole in Fig. 3.1.

When starting a simulation from rest a white noise perturbation is applied

to the surface pressure field in order to initiate baroclinic instability. The dynamical response of the model then results in a control run zonal mean temperature as shown in Figs. 3.1 (c) and (d). Values are shown for a 10000 day average after an initial spin-up period of 200 days. It can be seen that the model response to T_{ref} is to cause warming in mid-high latitudes and cooling at low latitudes such as to reduce the negative latitudinal temperature gradient in the troposphere. This also results in a higher static stability at mid-high latitudes than is present in T_{ref} . Moreover, it can be seen that the dynamical response of the model results in a temperature profile of the stratosphere that is no longer isothermal. The temperature is reduced at the equator compared to T_{ref} and enhanced at the poles resulting in a positive latitudinal temperature gradient in the stratosphere.

The dynamical response of the model to this simple forcing and dissipation results in a climatology that is close to that of the real atmosphere. Three of the key fields are shown in Fig. 3.2. The zonal mean zonal wind (\bar{u}) consists of a mid-latitude westerly jet in each hemisphere (centred around 45° latitude) in thermal wind balance with the latitudinal temperature gradient. These have a peak zonal wind speed of $\sim 30\text{ms}^{-1}$ just below the tropopause. The mean meridional circulation consists of a thermally direct Hadley cell extending to $\sim 30^\circ$ latitude. Poleward of this there is a thermally indirect Ferrell cell stretching to $\sim 60^\circ$ latitude. At higher latitudes there is a weaker thermally direct polar cell.

Another simplification of the model in its original configuration is that there is no orography. The surface boundary conditions are a spherical surface with no zonal asymmetries or topography so there is no forcing of large scale planetary waves. Planetary waves are therefore weak and eddy forced. This is in contrast to the real atmosphere where, in particular in the Northern hemisphere, mountain ranges and land-sea temperature contrasts force large planetary scale motions. We will, however, investigate the effect that introducing zonally asymmetric boundary conditions has on the model response.

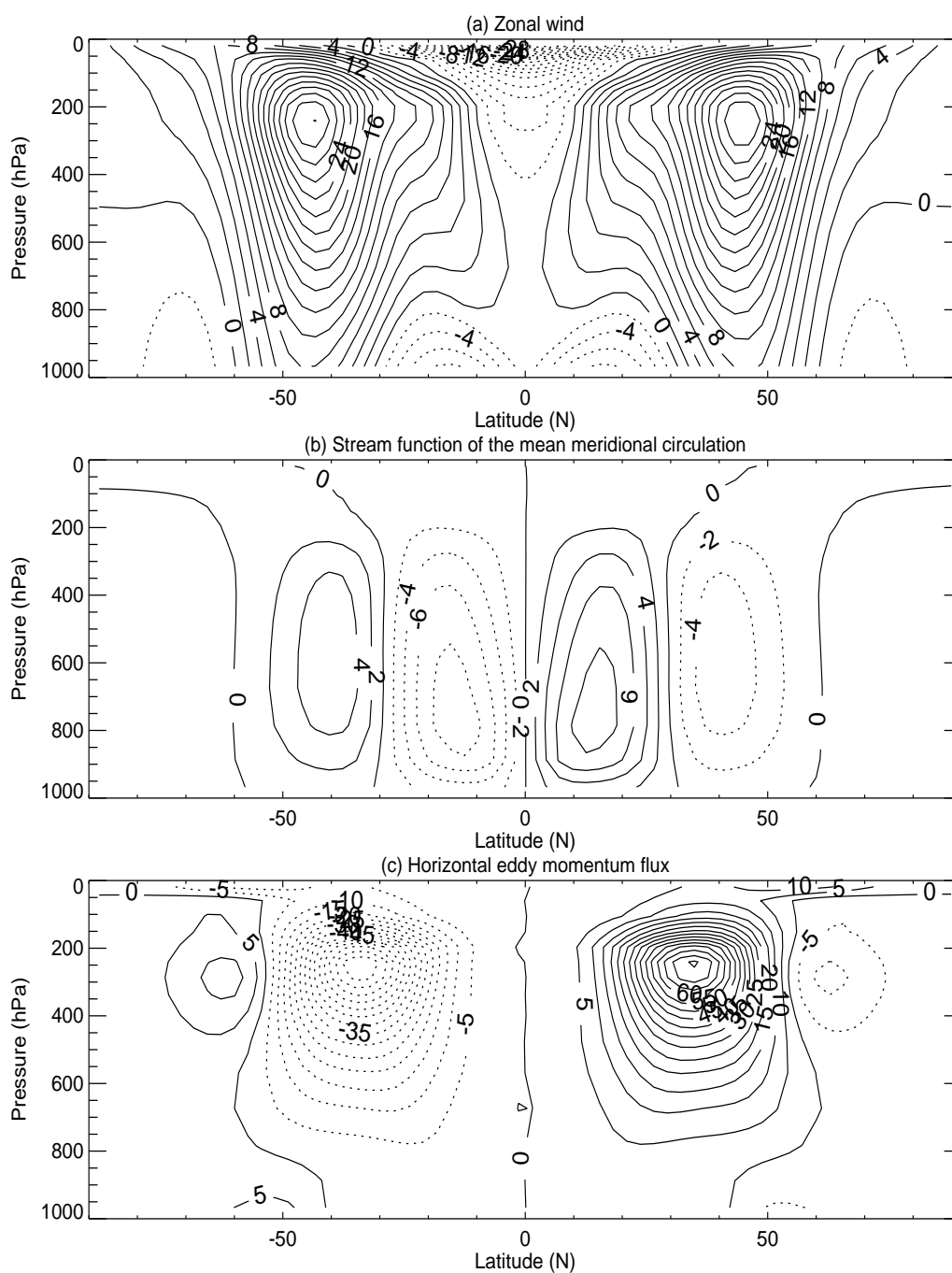


Fig. 3.2: (a) Control run zonal mean zonal wind (ms^{-1}), (b) Control run stream function of the mean meridional circulation (10^{10} kgs^{-1}), (c) northward horizontal eddy momentum flux ($\text{ms}^{-1})^2$.

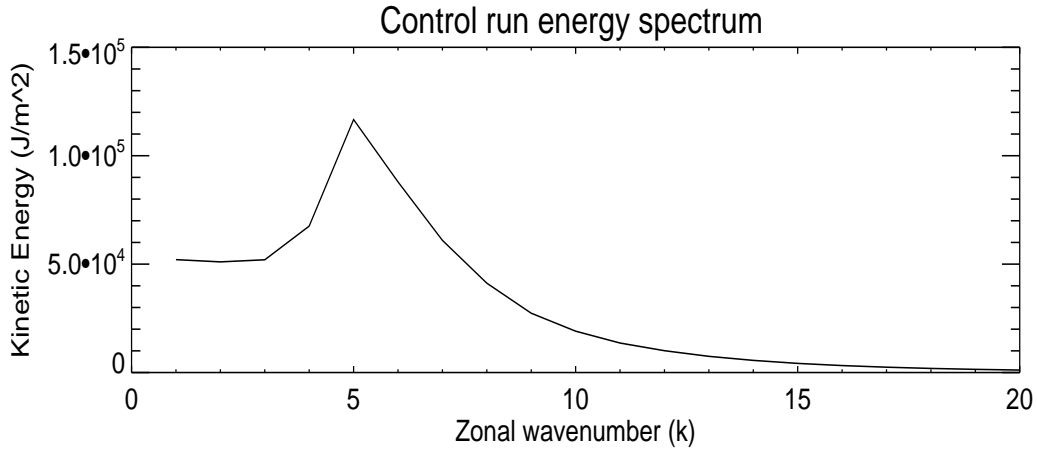


Fig. 3.3: Kinetic energy spectrum of the control run as a function of dimensionless zonal wavenumber. Vertically integrated kinetic energy per unit area is shown.

The kinetic energy spectrum of eddy motions in the model atmosphere as a function of dimensionless zonal wavenumber (k) is shown in Fig. 3.3. This shows the kinetic energy per unit area integrated over sigma levels. It can be seen that most of the eddy kinetic energy resides at synoptic scales with the peak in eddy kinetic energy occurring at zonal wavenumber $k=5$ and the most dominant wavenumbers in the kinetic energy spectrum range from 4 to 7. It can be seen that although there is no forcing of large scale planetary waves, there is some kinetic energy at wavenumbers 1 to 3 due to the upscale energy transfer from the dominant synoptic scales.

Thus, although this model has various simplifications it produces a fairly realistic climate. The simplifications in this GCM ensure that it is not computationally expensive and therefore allow it to be run for long integrations and allow it to be used for ensembles with a large number of members to ensure statistically significant results. Moreover, it allows dynamical mechanisms to be investigated in detail without the added complications of a full GCM. Simplified models such as these can be a very useful tool in investigating dynamical mechanisms which can then translate into more complicated,

realistic atmospheres.

This model will therefore be used in the following experiments to investigate the mechanisms involved in producing a tropospheric response to stratospheric heating perturbations.

3.2 The Experiments

The climate of the sGCM is maintained by Newtonian relaxation of the temperature field to the reference temperature $T_{ref}(\phi, p)$. It is therefore possible to apply heating perturbations to the model by simply changing the parameters that determine T_{ref} in equation 3.5. Here, the various experiments that have been performed with the sGCM are described. The main focus is the effect that stratospheric temperature perturbations have on the troposphere but the effect that changing various aspects of the model has on its response to stratospheric heating is also investigated.

3.2.1 Stratospheric heating experiments

The results of Haigh *et al.* (2005) (subsequently HBD05) demonstrated the equilibrium response to various heating perturbations applied to the strato-

Stratospheric heating experiments				
Name	Type	Length	T_{tpeq} (K)	ΔT_{tp} (K)
C	Control	2×10000 days	200	0
E5	Equilibrium	2×5000 days	205	5
	Spin-up	2×200×50 days	205	5
U5	Equilibrium	2×5000 days	205	0
	Spin-up	2×200×50 days	205	0
P10	Equilibrium	2×5000 days	200	-10
	Spin-up	2×200×50 days	200	-10

Tab. 3.1: Summary of stratospheric heating experiments.

sphere of the sGCM. In chapter 4, spin-up ensemble experiments of some of these heating perturbations are performed to further investigate the mechanisms involved in transmitting the response of the applied heating perturbation to the troposphere below. Three different heating perturbation experiments have been performed by changing the equatorial tropopause temperature (T_{tpeq}) and the difference in temperature between the equatorial and polar tropopause (ΔT_{tp}) (as summarised in table 3.1). The difference in the relaxation temperature profile (T_{ref}) between these experiments and the control run are shown in Fig 3.4. In each of these the stratospheric T_{ref} is altered but the tropospheric T_{ref} remains unchanged. The equatorial heating case (E5) consists of a maximum increase of 5K in the equatorial stratosphere decreasing to 0K at the poles. The uniform heating case (U5) consists of a uniform increase in T_{ref} of 5K throughout the whole stratosphere whereas the polar heating case consists of an increase in T_{ref} of 10K at the poles decreasing to 0K at the equator.

Equatorial heating (E5) most closely resembles that seen over the solar cycle although the applied temperature perturbation is considerably larger than that observed (Haigh, 2003; Labitzke *et al.*, 2002). However, it was found by HBD05 that the results were qualitatively independent of the magnitude of the applied heating, with the magnitude of the response varying linearly in the stratosphere and with a slightly larger response than linear in the troposphere. This suggests that, although the applied temperature perturbation in the E5 case is large, the mechanisms involved in the tropospheric response will be the same as with a smaller stratospheric heating perturbation. This experiment is not intended to be a direct simulation of the climate response over the solar cycle but it can be of use in investigating the mechanisms involved in a tropospheric response to enhanced heating of the equatorial lower stratosphere over the solar cycle.

Although we are primarily investigating mechanisms by which the tropospheric response to solar activity is produced, our results apply equally to other situations where there is a thermal perturbation to the stratosphere,

such as the cooling expected with increased greenhouse gas concentrations (Lorenz & DeWeaver, 2007). The U5 heating case could be thought of as the opposite of a greenhouse gas stratospheric cooling scenario whereas the P10 case could be of use in interpreting any circulation changes associated with a warming of the polar stratosphere such as might occur with ozone recovery (Son *et al.*, 2008a).

A 10 000 day control run simulation has been performed with the original Held-Suarez relaxation temperature parameters (See Figs. 3.1 and 3.2). For each of the heating perturbation cases (E5, U5 and P10), a spin-up ensemble

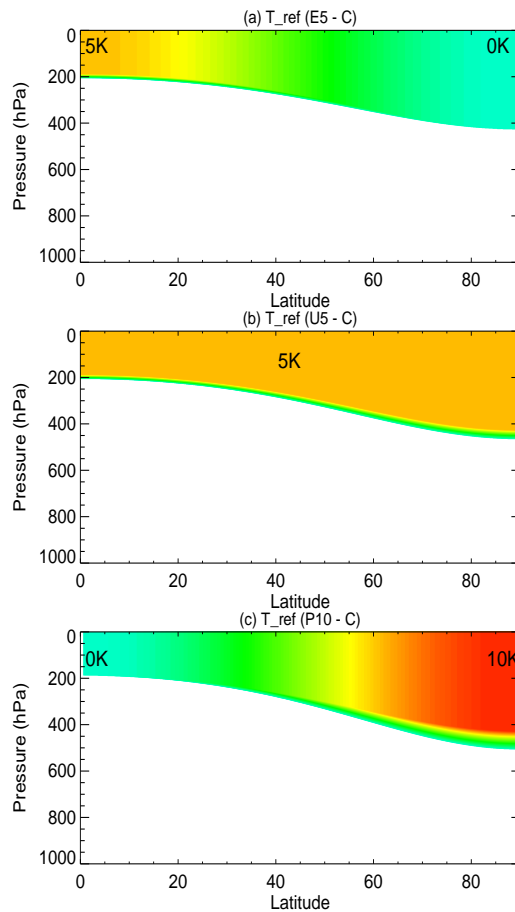


Fig. 3.4: Change in relaxation temperature profile (*Experiment - Control*) for the (a) E5, (b) U5 and (c) P10 heating experiments.

has been performed consisting of 200, 50-day runs. Each ensemble member starts from different initial conditions taken at 50 day intervals from the control run simulation in which no stratospheric heating perturbation was applied. In this way the starting conditions are different for each ensemble member but remain within the natural variability of the control run. The stratospheric heating perturbation is then switched on by altering the parameters as given in table 3.1 and the model is allowed to respond over the following 50 day period. By averaging over the ensemble a statistical signal emerges from internally generated variability and the evolution in response to the applied heating perturbation is clearly demonstrated. The number of data points can be doubled by averaging over both hemispheres as the model is symmetric about the equator. It was noted in HBD05 that the temporal correlation between the equivalent points in the two hemispheres is very low.

In addition to the spin-up ensembles an equilibrium run has been performed for each heating case. For each of these the model is spun-up from rest with the stratospheric heating perturbation continuously applied and the results taken from a 5000 day average after an initial spin-up period of 200 days¹.

3.2.2 *Zonally asymmetric boundary conditions*

Recently the sensitivity of simplified GCM's with zonally symmetric boundary conditions has come under much investigation. This has largely followed from the work of Gerber & Vallis (2007) and Gerber *et al.* (2008).

¹ These experiments were presented in HBD05 for 1000 day runs. However, it was found that, due to variability in the model, the magnitude from a 1000 day mean response is not completely representative. The equilibrium runs have therefore been extended to 5000 days. In fact it will be demonstrated in Chapters 5 and 6 that even a 5000 day run is not of sufficient length for accurate determination of the magnitudes. As Chapters 5 and 6 are looking at the magnitude of response, much longer runs have been used there. However, for the purposes of Chapter 4 which is looking at the qualitative patterns of response, the 5000 day equilibrium runs are used. This has no effect on the qualitative pattern of response but there are uncertainties in the magnitude of response with runs of this length.

Gerber & Vallis (2007) showed that under many circumstances the decorrelation timescale of the leading mode of annular variability in sGCM's is unrealistically long compared to the observed values in the atmosphere which are of the order of 10 to 20 days (Baldwin *et al.*, 2003). Moreover, there is found to be a strong dependence of the annular mode decorrelation timescale on various model parameters including vertical and horizontal resolution (Gerber & Vallis, 2007), equator to pole temperature gradient, the temperature relaxation timescale and the surface frictional timescale (Gerber *et al.*, 2008). This is potentially important when looking at annular mode-like responses to forcing in these models.

Often the tropospheric circulation response to forcing has a pattern that closely resembles that of the models leading mode of variability: its annular mode, which normally represents North-South displacements of the mid-latitude jet (Ring & Plumb, 2007). Indeed, it has been shown by Haigh *et al.* (2005) that this is the case for the response to stratospheric heating. It is possible to relate the magnitude of a models response to forcing that projects onto its annular mode to the characteristics of its unforced internal variability (at least qualitatively) through the fluctuation-dissipation theorem (Gerber & Vallis, 2007; Ring & Plumb, 2008). This predicts that the magnitude of the annular mode response to a small forcing is linearly related to the projection of that forcing onto the annular mode by a factor that is simply the

Zonally asymmetric boundary conditions			
Name	Type	Length	Description
Q	Control	10×5000 days	T_{ref} given by Eq. 3.6
Q_E5	Equilibrium	10×5000 days	as Q but with E5 heating
R	Control	10×5000 days	2000m ridge centred at 0° lon, 45° lat
R_E5	Equilibrium	10×5000 days	as R but with E5 heating

Tab. 3.2: Summary of model runs with zonally asymmetric boundary conditions.

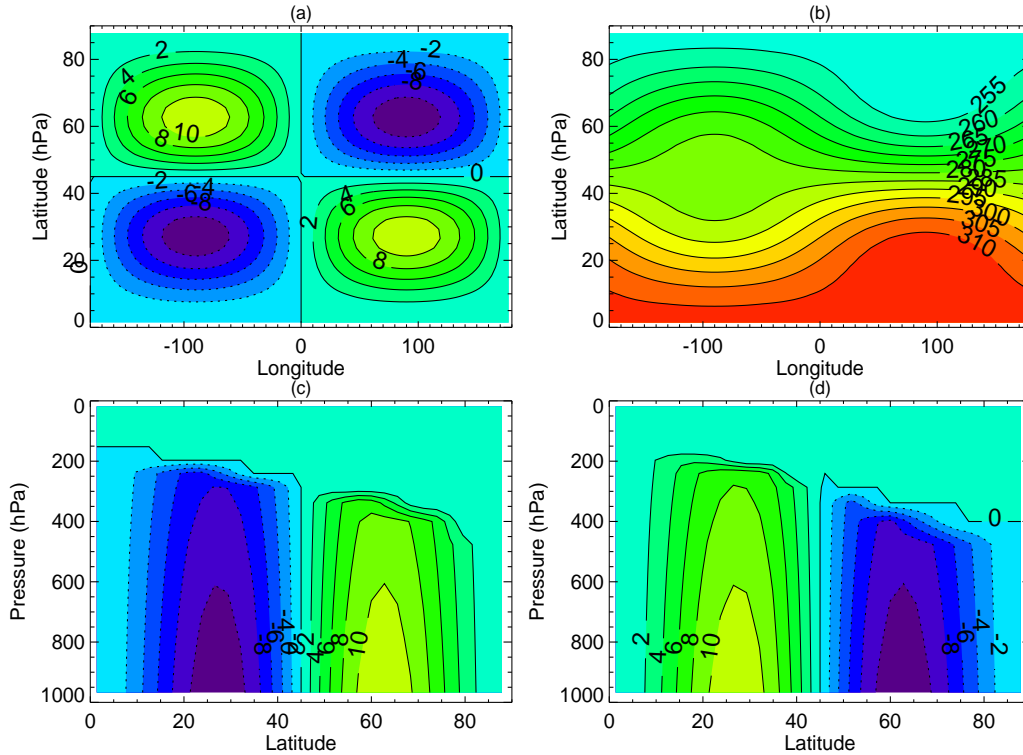


Fig. 3.5: T_{ref} for the Q experiments: (a) Anomaly from original Held-Suarez forcing (3.5) at the surface, (b) surface T_{ref} , (c) meridional cross section of the anomaly from Held-Suarez at 90° longitude, (d) as (c) but for 270° longitude.

decorrelation timescale of the annular variability in the unforced control run situation (Leith, 1975). Therefore, the longer the decorrelation timescale, the larger the annular mode-like response to a given forcing. Gerber *et al.* (2008) attributed the long decorrelation timescales that occur in sGCMs to a strong feedback between the eddy forcing and the mean flow. Furthermore, they demonstrate that the characteristic timescales are reduced with the introduction of zonal asymmetries such as land-sea temperature contrasts or topography. Therefore, it is possible that when the jet is broken up into storm track regions, such as is the case in the real atmosphere, particularly in the northern hemisphere, this strong feedback between the eddies and the mean

flow is reduced along with the decorrelation timescale and the magnitude of the models annular mode-like response to forcing.

We have therefore performed some additional experiments to investigate the sensitivity of the model response to the introduction of zonally asymmetric boundary conditions. These are summarised in table 3.2. In experiment Q a quadrupole perturbation in tropospheric relaxation temperature has been applied. This has been done by modifying Eq. 3.5 for $T_{ref}(\phi, p)$ to include a quadrupole term as follows

$$T_{ref}(\phi, p) = \max \left\{ (T_{tpeq} - \Delta T_{tp} \sin^2 \phi), \left[T_o - \Delta T_y \sin^2 \phi - (\Delta \theta_{eq} \cos^2 \phi + \Delta \theta_{pl} \sin^2 \phi) \log \left(\frac{p}{p_0} \right) - Q(\lambda, \phi) \right] \left(\frac{p}{p_o} \right)^\kappa \right\}, \quad (3.6)$$

where

$$Q(\lambda, \phi) = \bar{Q} \sin(\lambda) \cos(2(\phi - \pi/4)) \sin(4(\phi - \pi/4)). \quad (3.7)$$

\bar{Q} is the amplitude of the quadrupole perturbation which has been chosen to be 15K. This is the maximum amplitude which does not introduce unrealistic reversed latitudinal temperature gradients in T_{ref} . This amplitude of perturbation is large but it will be shown in Chapter 5 that the model response to this is considerably smaller due to the weak relaxation towards T_{ref} and temperature advection in the zonal direction acting to spread out the quadrupole anomalies. The relaxation temperature profile of Eq. 3.6 is shown in figure 3.5. It was chosen to have this form so that the maximum change in latitudinal temperature gradient occurs in mid-latitudes with zero change at the equator and poles. This T_{ref} has enhanced baroclinicity in mid-latitudes and decreased baroclinicity at high and low latitudes between 0° and 180° longitude and vice-versa between -180° and 0° longitude. This should have the effect of enhancing the storm track region between 0° and 180° longitude and reducing it between -180° and 0° longitude. It will be demonstrated in Chapter 5 that a 5000 day run is not sufficient to accurately determine the magnitude of response to stratospheric heating. Therefore an

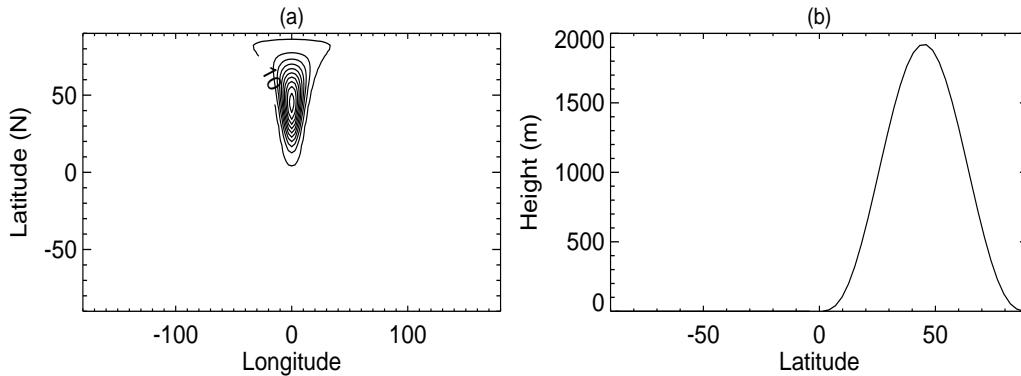


Fig. 3.6: (a) Topographic height in metres (b) Cross section of topographic height through 0° longitude.

ensemble of 10, 5000 day runs has been performed for the control and E5 stratospheric heating experiments with this quadrupole change in T_{ref} . Each ensemble member differs only in the random number seed that is used to introduce noise into the model at the beginning of each integration.

In addition to this an experiment has been performed with the introduction of topography. A 2000m high ridge orientated north-south has been placed in the northern hemisphere centred on 0° longitude and 45° latitude as shown in Fig. 3.6.

This has been orientated so as to block the jet. It was noted by Gerber *et al.* (2008) that their results are robust for various shapes and heights of idealised topography provided it is put in a position that blocks the extratropical jet. The topography is introduced into the model through a change in the surface geopotential height² as shown in Fig. 3.6. It is elliptical in shape with an eccentricity of 4 and a half width of 20° longitude. An ensemble of 10, 5000 day runs has been performed for the control run and E5 stratospheric heating experiments with the introduction of this topography.

² Geopotential height values provided by Mike Blackburn.

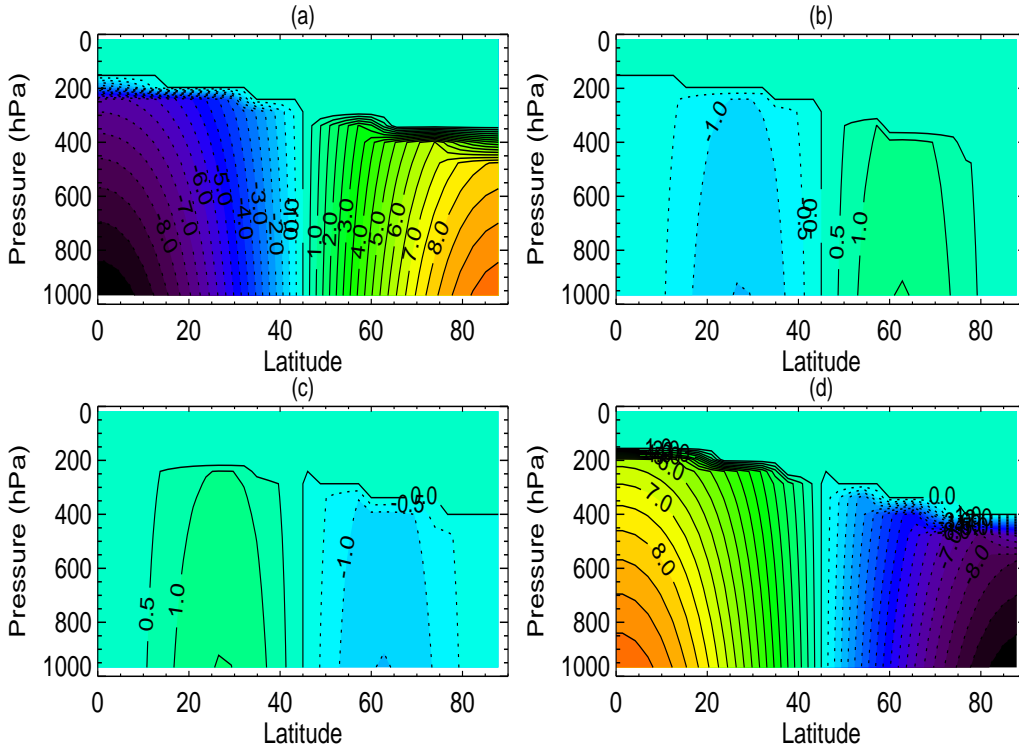


Fig. 3.7: Meridional cross section of the perturbation to the original Held-Suarez relaxation temperature profile to produce experiments TR1(a), TR2(b), TR4(c), TR5(d).

3.2.3 Varying tropospheric baroclinicity

The final set of experiments that have been performed were designed to study the effect of slightly different zonally symmetric tropospheric situations on the response to stratospheric heating.

In these experiments the troposphere is altered by modifying the Held-Suarez relaxation temperature profile (T_{ref} , Eq. 3.5). This has been done for 4 different tropospheric relaxation temperature profiles. Thus including the original Held-Suarez T_{ref} we have 5 different tropospheric situations that will be denoted by TR1-TR5 and are summarised in table 3.3.

TR3 has the original Held-Suarez relaxation temperature profile. TR2

and TR4 take slices through the quadrupole change to T_{ref} of experiment Q at -90° and $+90^\circ$ longitude respectively and apply that T_{ref} at all longitudes. In other words TR2 has weakened baroclinicity in midlatitudes and enhanced baroclinicity at the highest and lowest latitudes and vice-versa for TR4. However, only a 2K amplitude (\overline{Q}) has been used as there is no longer a problem with advection and spreading out of the temperature increase/decrease in the zonal direction as a zonally symmetric change to T_{ref} is applied. TR1 and TR5 also have varied tropospheric baroclinicity but now the maximum and

Different tropospheric reference states					
Name	Type	Length	T_o	ΔT_y	T_{ref}
TR1	Control	2*5*5000days	305	40	3.5
TR1E5	Equilibrium	2*5*5000days	305	40	as TR1 with E5 heating
TR1P5	Equilibrium	2*5*5000days	305	40	as TR1 with P5 heating
TR2	Control	2*5*5000days	315	60	3.6 with $\lambda=-90^\circ$, $\overline{Q}=2K$
TR2E5	Equilibrium	2*5*5000days	315	60	as TR2 with E5 heating
TR2E5	Spin-up	100*250days	315	60	as TR2 with E5 heating
TR2P5	Equilibrium	2*5*5000days	315	60	as TR2 with P5 heating
TR3	Control	2*5*5000days	315	60	3.5
TR3E5	Equilibrium	2*5*5000days	315	60	as TR3 with E5 heating
TR3P5	Equilibrium	2*5*5000days	315	60	as TR3 with P5 heating
TR4	Control	2*5*5000days	315	60	3.6 with $\lambda=90^\circ$, $\overline{Q}=2K$
TR4E5	Equilibrium	2*5*5000days	315	60	as TR4 with E5 heating
TR4E5	Spin-up	100*350days	315	60	as TR4 with E5 heating
TR4P5	Equilibrium	2*5*5000days	315	60	as TR4 with P5 heating
TR5	Control	2*5*5000days	325	80	3.5
TR5E5	Equilibrium	2*5*5000days	325	80	as TR5 with E5 heating
TR5P5	Equilibrium	2*5*5000days	325	80	as TR5 with P5 heating

Tab. 3.3: Summary of experiments with different tropospheric reference states.

minimum change in T_{ref} are applied at the equator and poles rather than in the subtropical and subpolar regions as in TR2 and TR4. This is done by simply altering the surface temperature at the equator (T_o) and the equator to pole temperature difference (ΔT_y) in Eq. 3.5. TR1 has a weakened equator to pole temperature gradient whereas TR5 has a strengthened equator to pole temperature gradient. Meridional cross sections of the alteration that is added on to the original Held-Suarez T_{ref} to create these new tropospheres are shown in Fig. 3.7.

An ensemble of 5, 5000 day runs has been performed for the control run and E5 stratospheric heating experiments as well as a P5 stratospheric heating experiment. P5 is similar to P10 but with $\Delta T_{tp}=-5\text{K}$. P5 has been used instead of P10 as it is easier to compare this with the E5 runs as there isn't the additional complication of double the stratospheric heating. As these experiments are symmetric about the equator, each hemisphere will be treated separately so there are effectively 10 ensemble members of 5000 days length from which the magnitude of response and its uncertainty can be estimated.

In addition to the equilibrium runs, 100 member spin-up ensemble experiments have been run for the TR2 and TR4 tropospheres. The TR2 ensemble members are 250 days long and the TR4 ensemble members are 300 days long.

3.3 Diagnostics

In order to investigate the model response to stratospheric heating, several diagnostics will be used. Each of these stem from the primitive equations which govern the global atmospheric flow. In spherical coordinates with (λ, ϕ) denoting longitude and latitude respectively, and using $z \equiv -H \ln(p/p_s)$ as a vertical coordinate, these can be written as

$$\frac{Du}{Dt} - \left(f + \frac{u \tan \phi}{a} \right) v + \frac{\Phi_\lambda}{a \cos \phi} = \mathcal{F}^{(\lambda)} \quad (3.8)$$

$$\frac{Dv}{Dt} + \left(f + \frac{u \tan \phi}{a} \right) u + \frac{\Phi_\phi}{a} = \mathcal{F}^{(\phi)} \quad (3.9)$$

$$\Phi_z = H^{-1} R \theta \exp\left(-\frac{\kappa z}{H}\right) \quad (3.10)$$

$$\frac{1}{a \cos \phi} \frac{\partial u}{\partial \lambda} + \frac{1}{a \cos \phi} \frac{\partial(v \cos \phi)}{\partial \phi} + \frac{1}{\rho_o} \frac{\partial(\rho_o w)}{\partial z} = 0 \quad (3.11)$$

$$\frac{D\theta}{Dt} = Q \quad (3.12)$$

where the meaning of each symbol is given in the list of symbols and subscripts represent derivatives (see e.g. Andrews *et al.* (1987)). The first two equations represent momentum balance in the zonal and meridional directions. Equation 3.10 represents hydrostatic balance, 3.11 is conservation of mass and 3.12 is the thermodynamic equation. The derivative D/Dt is given by

$$\frac{D}{Dt} \equiv \frac{\partial}{\partial t} + \frac{u}{a \cos \phi} \frac{\partial}{\partial \lambda} + \frac{v}{a} \frac{\partial}{\partial \phi} + w \frac{\partial}{\partial z} \quad (3.13)$$

and gives the rate of change following the fluid motion.

In order to investigate the interaction between eddies (deviations from the zonal mean) and the mean flow it is useful to divide each quantity into a zonal mean part and an eddy part. In the following overbars will denote zonal means and dashed quantities represent the deviations from the zonal mean. For example the zonal wind can be written as

$$u = \bar{u} + u' \quad (3.14)$$

where \bar{u} is the zonal mean zonal wind and u' is the eddy part of the zonal wind. Applying this to each of the quantities in 3.8, taking the zonal mean and making use of the equation 3.11 gives the following equation governing the time rate of change of the zonal mean zonal wind:

$$\begin{aligned} \frac{\partial \bar{u}}{\partial t} + \frac{\bar{v}}{a \cos \phi} \frac{\partial(\bar{u} \cos \phi)}{\partial \phi} - f \bar{v} + \bar{w} \frac{\partial \bar{u}}{\partial z} - \overline{\mathcal{F}^{(\lambda)}} = \\ - \frac{1}{a \cos^2 \phi} \frac{\partial(\overline{u'v'} \cos^2 \phi)}{\partial \phi} - \frac{1}{\rho_o} \frac{\partial(\rho_o \overline{u'w'})}{\partial z} \end{aligned} \quad (3.15)$$

A further approximation that is appropriate for large scale circulation in the mid-latitudes is the quasi-geostrophic approximation. In this approximation it is assumed that the flow is almost horizontal so that any term involving the vertical advection of momentum can be neglected. Furthermore, considering the typical lengths and velocities associated with synoptic scale mid-latitude weather systems (see e.g. Holton (2004)) leaves the following dominant terms in zonal mean momentum balance:

$$\frac{\partial \bar{u}}{\partial t} = f\bar{v} - \frac{1}{a\cos^2\phi} \frac{\partial(\overline{u'v'}\cos^2\phi)}{\partial\phi} + \overline{\mathcal{F}}^{(\lambda)} \quad (3.16)$$

That is the acceleration in the zonal mean zonal wind is given by the imbalance between the coriolis force on the zonal mean meridional wind, the convergence of horizontal eddy momentum flux ($\overline{u'v'}$) and friction.

In a similar manner the thermodynamic equation (3.12) can be written as

$$\frac{\partial \bar{\theta}}{\partial t} + \frac{\bar{v}}{a} \frac{\partial \bar{\theta}}{\partial \phi} + \bar{w} \frac{\partial \bar{\theta}}{\partial z} - \bar{Q} = -\frac{1}{a\cos\phi} \left(\frac{\partial(\overline{v'\theta'}\cos\phi)}{\partial\phi} \right) - \frac{1}{\rho_o} \frac{\partial(\rho_o \overline{w'\theta'})}{\partial z} \quad (3.17)$$

which in the quasi-geostrophic approximation reduces to

$$\frac{\partial \bar{\theta}}{\partial t} = -\bar{w} \frac{\partial \bar{\theta}_o}{\partial z} + \bar{Q} - \frac{1}{a\cos\phi} \frac{\partial(\overline{v'\theta'}\cos\phi)}{\partial\phi} \quad (3.18)$$

i.e. the rate of change of potential temperature is given by the imbalance between vertical advection, diabatic heating and the convergence of heat flux due to the eddies.

3.3.1 The vertically integrated momentum budget

Another useful way of looking at zonal momentum balance (Eq. 3.15) is in the vertical integral. This has been used by HBD05 to look at the dominant terms in maintaining the equilibrium zonal wind anomalies in response to changes in stratospheric temperature and will be used in the following to look at the dominant terms producing the zonal wind anomalies during the spin-up. The zonal mean of Eq. 3.8 can be written as

$$\frac{\partial \bar{u}}{\partial t} = -\frac{1}{a\cos^2\phi} \frac{\partial}{\partial\phi} (\overline{uv}\cos^2\phi) - \frac{\partial}{\partial z} (\overline{uw}) + f\bar{v} + \overline{\mathcal{F}}^{(\lambda)} \quad (3.19)$$

Again, dividing each quantity into a zonal mean and an eddy part and now multiplying by density, integrating in the vertical and making use of the fact that $dp = -\rho g dz$, the balance of vertically integrated westerly momentum can be written as:

$$\frac{1}{g} \frac{\partial}{\partial t} \int_0^{p_s} \bar{u} dp = -\frac{1}{g a \cos^2 \phi} \frac{\partial}{\partial \phi} \left\{ \cos^2 \phi \int_0^{p_s} (\bar{u} \bar{v} + \overline{u'v'}) dp \right\} + \frac{1}{g} \int_0^{p_s} \overline{\mathcal{F}^{(\lambda)}} dp \quad (3.20)$$

The advantage of looking at momentum balance in this way is that the term involving the coriolis force on the mean meridional wind cancels out between the upper and lower parts of the overturning circulation. Additionally, the terms involving surface pressure variations and the surface momentum flux associated with the resolved flow are small and can be neglected. The result is three terms which contribute to the vertical integral of westerly momentum:

$$\frac{1}{g} \frac{\partial}{\partial t} \int_0^{p_s} \bar{u} dp = C_{ZONAL} + C_{EDDY} - \overline{\tau_{s\lambda}} \quad (3.21)$$

where C_{ZONAL} is the zonally averaged convergence of the poleward flux of westerly momentum by the mean circulation $\bar{u} \bar{v}$, C_{EDDY} is the zonally averaged convergence of westerly momentum due to the eddies $\overline{u'v'}$ and $\overline{\tau_{s\lambda}}$ is the contribution due to the zonally averaged surface stress.

3.3.2 Stationary and transient eddies

Until now eddies have been defined as the deviation from the zonal mean (see Eq. 3.14). Thus, the eddy momentum and heat fluxes that have been described so far represent the fluxes due to any zonal asymmetries in the flow whether they be stationary or transient. For the most part, where simulations with zonally symmetric boundary conditions are being considered the flux due to transient eddies by far outweighs that due to stationary eddies. However, when zonal asymmetries are introduced into the model it is likely that the contribution due to stationary eddies will increase. It is therefore useful to decompose the eddies into stationary and transient components. Another way of looking at each quantity is that it consists of a time mean

component and a part that varies in time e.g.

$$u = [u] + u^*, \quad (3.22)$$

where $[]$ represents the time mean and $*$ the deviation from the time mean. Thus, for example, the zonal wind at any longitude and time can be thought of as consisting of four components

$$u = [\bar{u}] + [u'] + \bar{u}^* + u'^*, \quad (3.23)$$

where $[\bar{u}]$ is the time mean-zonal mean zonal wind, $[u']$ is the time mean of the deviation from the zonal mean (or a stationary eddy component), \bar{u}^* represents instantaneous fluctuations of the zonal mean zonal wind and u'^* represents instantaneous fluctuations of the deviations from the zonal mean (or transient eddies). In this way the time mean, zonal mean spatial eddy momentum flux that has been used until now can be divided up into two components, one due to transient eddies, and one due to stationary eddies as follows:

$$[\overline{u'v'}] = \overline{[u']'[v]'} + \overline{[u'^*v'^*]}, \quad (3.24)$$

where $\overline{[u']'[v]}'$ is the poleward momentum flux due to stationary eddies and $\overline{[u'^*v'^*]}$ is that due to transient eddies.

For ease of calculation from the model output, the transient fluxes that are presented in Chapter 5 will actually be of the form $[u^*v^*]$ (taking eddy momentum flux as an example). This differs from the transient eddy momentum flux $[u'^*v'^*]$ by a contribution due to the transient zonally symmetric part of the circulation $[\bar{u}^*\bar{v}^*]$. Analysis has shown that this term is negligible compared to the contribution due to the transient asymmetric part of the circulation.

3.3.3 The Transformed Eulerian Mean and Eliassen-Palm flux

The above equations govern the atmospheric flow in the Conventional Eulerian Mean (CEM). However, when looking at the interaction between eddies

and the mean flow it is often useful to use the Transformed Eulerian Mean (TEM) formulation as defined by Andrews & McIntyre (1976).

The reason for this is, for example looking at Eq. 3.16, it is not clear how the zonal flow might react to an altered horizontal eddy heat flux as it does not explicitly appear in the equation for zonal flow acceleration. It is not the case that a change in horizontal eddy heat flux has no effect on the zonal flow, it is just not apparent from the CEM equations. In the atmosphere, the dominant balance in the thermodynamic equation is between the convergence/divergence of horizontal eddy heat flux and adiabatic cooling/heating. Therefore, an altered horizontal eddy heat flux tends to alter the mean meridional circulation in such a way that the altered adiabatic cooling/heating associated with this circulation balances the convergence/divergence of horizontal eddy heat flux. So, clearly an altered horizontal eddy heat flux will have an effect on the mean flow through the meridional circulation it induces. In order to see the net effect of eddies on the mean flow, Andrews & McIntyre (1976) defined a residual circulation such that

$$\bar{v}^* \equiv \bar{v} - \rho_o^{-1} \left(\rho_o \frac{\overline{v'\theta'}}{\bar{\theta}_z} \right)_z \quad (3.25)$$

$$\bar{w}^* \equiv \bar{w} + \frac{1}{a \cos \phi} \frac{\partial}{\partial \phi} \left(\frac{\cos \phi \overline{v'\theta'}}{\bar{\theta}_z} \right) \quad (3.26)$$

where \bar{v}^* and \bar{w}^* are the zonal mean meridional wind and vertical velocity in the TEM formulation. Therefore, \bar{w} is the vertical velocity residual whose adiabatic heating/cooling effect is not balancing the divergence/convergence or horizontal eddy heat flux. Substitution of this into equation 3.18 for \bar{w} leaves the thermodynamic equation in the quas-geostrophic TEM formulation as

$$\frac{\partial \bar{\theta}}{\partial t} + \bar{w}^* \frac{\partial \bar{\theta}}{\partial z} - \bar{Q} = 0 \quad (3.27)$$

That is, the dominant balance between the adiabatic heating/cooling and the divergence/convergence of horizontal eddy heat flux has been removed. Furthermore, substitution of 3.25 and 3.26 into equation 3.16 for \bar{v} and \bar{w}

leaves the following equation for the acceleration of the zonal mean zonal wind in the quasi-geostrophic TEM formulation:

$$\frac{\partial \bar{u}}{\partial t} - f\bar{v}^* - \overline{\mathcal{F}}^{(\lambda)} = \frac{1}{\rho_o a \cos \phi} \vec{\nabla} \cdot \vec{F}. \quad (3.28)$$

The vector \vec{F} is the Eliassen-Palm (E-P) flux which will be used extensively in the following. This was first introduced by Eliassen & Palm (1961). It is a vector in the latitude-height plane which, in the quasi-geostrophic approximation and spherical coordinates, is given by

$$\vec{F} = (F_\phi, F_z) = \left(-\rho_o a \cos \phi \overline{u'v'}, -a f \cos \phi \frac{\overline{v'\theta'}}{\theta_{oz}} \right) \quad (3.29)$$

i.e. it's latitudinal component is proportional to the negative of the horizontal eddy momentum flux and it's vertical component is proportional to the horizontal eddy heat flux. Thus, from Eq. 3.28 it is clear that both the horizontal eddy momentum flux and horizontal eddy heat flux act to change the zonal mean zonal wind in the combination given by the divergence of \vec{F} . Moreover, the E-P flux can be useful in determining what properties of the waves are changing in order to drive an acceleration in the mean flow as its direction demonstrates the relative importance of eddy heat and momentum fluxes (Edmon *et al.*, 1980).

One aspect of the E-P flux which is of importance for this study is that when the eddies can be thought of as being wavelike, then the direction of the E-P flux is the same as the direction of the group velocity of the eddies in the latitude-height plane (see e.g. Andrews *et al.* (1987) pg 187). This is demonstrated in the appendix. Thus when eddies can be thought of as wavelike, their net effect on the mean flow can be related to their direction of propagation through the E-P flux.

3.3.4 The quasi-geostrophic index of refraction

In order to investigate the influence that the mean flow has on eddy fluxes we will make use of the quasi-geostrophic index of refraction. This was

first introduced by Matsuno (1970) for investigating the propagation of stationary planetary waves but can be modified for studying the propagation of transient waves (Karoly & Hoskins, 1982). In spherical coordinates the quasi-geostrophic index of refraction is given by:

$$n^2 = \left\{ \frac{\bar{q}_\phi}{a[\bar{u} - c]} - \left(\frac{k}{a \cos \phi} \right)^2 - \left(\frac{f}{2NH} \right)^2 \right\} a^2, \quad (3.30)$$

where c is the zonal phase speed, N is the buoyancy frequency and H is the density scale height. The meridional gradient of potential vorticity is given by:

$$\bar{q}_\phi = 2\Omega \cos(\phi) - \left[\frac{(\bar{u} \cos \phi)_\phi}{a \cos \phi} \right]_\phi + \frac{af^2}{R} \left(\frac{p\theta}{T} \frac{\bar{u}_p}{\theta_p} \right)_p. \quad (3.31)$$

This refractive index can be interpreted in a similar manner to that of light. Light is refracted toward regions of higher refractive index and the same is true for waves in the atmosphere. Karoly & Hoskins (1982) demonstrated that under linear WKB theory, waves will be refracted by gradients of n^2 such that they will tend to propagate away from regions of low refractive index and toward regions of high refractive index. The derivation of n^2 is given in the appendix along with an explanation following that of Karoly & Hoskins (1982) for why waves should tend to propagate up the gradient of n^2 .

The crucial assumption is that linear WKB theory applies. That is, that the waves can be approximated as plane waves with a phase that varies more rapidly than do the quantities of the basic flow or the amplitude of the waves. This is not strictly true throughout the whole atmosphere, but it will be shown in the following that for synoptic scale eddies in the mid-latitude, middle and upper troposphere/tropopause region, the refractive index is of use in explaining changes in the direction of eddy propagation indicating that, here, this approximation is a reasonable assumption. Furthermore, other authors have demonstrated that the refractive index can be used to predict wave behaviour even when the WKB conditions do not strictly apply (Chen & Robinson, 1992; Hartmann & Zuercher, 1998; Lorenz & Hartmann, 2003).

The above diagnostics will be used in the following chapters to investigate the mechanisms involved in producing the tropospheric response to stratospheric heating perturbations.

3.3.5 Significance testing

For some of the differences between experiment and control in Chapter 4, significance testing will be presented. The significance values have been calculated using the Students t-test to determine whether the difference between experiment and control is significantly different from zero. The t-value of the difference between two populations x_1 and x_2 is given by

$$T = \frac{\bar{x}_1 - \bar{x}_2}{\left[\frac{s_1^2}{n_1} + \frac{s_2^2}{n_2} \right]^{1/2}}, \quad (3.32)$$

where $n_1 = N_1/T_{o1}$ and $n_2 = N_2/T_{o2}$ are the effective number of degrees of freedom of the populations of size N_1 and N_2 and $s_1^2 = \frac{1}{N_1 - T_{o1}} \sum_{i=1}^{N_1} (x_{1i} - \bar{x}_1)^2$ and $s_2^2 = \frac{1}{N_2 - T_{o2}} \sum_{i=1}^{N_2} (x_{2i} - \bar{x}_2)^2$ are the variances of populations 1 and 2 respectively. The factor T_o takes into account the fact that all the members of the population are not necessarily independent. As described by Trenberth (1984) this factor effectively reduces the number of degrees of freedom by an amount that is dependent on the autocorrelation within the population. It is given by

$$T_o = 1 + 2 \sum_{L=1}^{L_C} \left(1 - \frac{L}{N} \right) r_L, \quad (3.33)$$

where r_L is the autocorrelation at lag L

$$r_L = \frac{\sum_{i=1}^{N-1} (x_i - \bar{x})(x_{i+L} - \bar{x})}{\sum_{i=1}^N (x_i - \bar{x})^2}. \quad (3.34)$$

L_C is a cut-off lag over which the autocorrelation is calculated. As was stated by Trenberth (1984) the calculation of r_L becomes unreliable at large lags. In these simulations, as there is a large amount of variability, it can lead to strong autocorrelations at large lags which are clearly just due to variability and not actually a real correlation. If the runs were long enough then the

various autocorrelations at different lags would cancel out but in runs of 5000 days length, as used in Chapter 4, they have a significant influence on the number of degrees of freedom. Thus in what follows, the autocorrelation has only been calculated until the lag where it drops below zero. This is not the most sophisticated of methods and Trenberth (1984) proposed a procedure that involved fitting an autoregressive noise model to the autocorrelation. However, for the purposes of the significance testing used here it is found that, although the cut-off lag chosen can have a significant influence on the number of degrees of freedom, the significance of the difference between experiment and control is so great in most regions that it only has a slight influence on the significance around the edges of the regions of strong response.

The number of degrees of freedom used for the t-test is given by

$$DF = \frac{(s_1^2/n_1 + s_2^2/n_2)^2}{(s_1^2/n_1)^2/(n_1 - 1) + (s_2^2/n_2)^2/(n_2 - 1)}, \quad (3.35)$$

(Welch, 1947). In Chapter 4, significance values will be calculated using consecutive 50 day means as the sample members.

In Chapters 5 and 6, ensembles of 5000 day runs are performed. Thus, for these runs there are, in most cases, 10 independent estimates of the magnitude of response. For these ensembles the error estimate on the ensemble mean that is quoted is the 95% confidence interval. This is given by

$$\frac{s}{\sqrt{N}} \times T_{95}, \quad (3.36)$$

where s is the standard deviation of the ensemble members, N is the number of degrees of freedom (10 in most cases) and T_{95} is a constant from the t distribution which, for 10 degrees of freedom and the 95% confidence limit, is 2.262.

4. STRATOSPHERIC HEATING EXPERIMENTS

In this chapter, spin-up ensemble experiments of the model response to three stratospheric heating perturbations (E5, U5 and P10) will be presented. The purpose of these experiments is to perform detailed investigation of the mechanisms involved in producing the tropospheric response found in the results of HBD05. First, an overview of the equilibrium response to the E5, U5 and P10 stratospheric heating perturbations will be given. Then, the results of the spin-up ensemble experiment will be discussed, first in terms of the E5 heating case as this most closely resembles the solar cycle response. The ideas presented for the E5 case will then be confirmed by comparison with the U5 and P10 stratospheric heating experiments.

4.1 *The equilibrium response to E5, U5 and P10 stratospheric heating*

As was described in section 3.2.1, a 5000 day equilibrium run has been performed for the E5, U5 and P10 experiments. Fig. 4.1 shows the difference in zonal mean temperature and zonal mean zonal wind between the 5000 day equilibrium run and the control run for each of the experiments. The control run temperature and zonal wind is shown again for comparison. It should be noted that for these, and all of the plots in the remainder of this chapter, only one hemisphere is shown as results have been averaged over both hemispheres. Regions where the difference between the equilibrium and control runs are not statistically significant at the 95% level (as calculated using the Students t-test) are shaded in grey.

The response to the stratospheric heating perturbations for these 5000

day runs is qualitatively the same as that for the 1000 day runs of HBD05. In fact they are quantitatively the same for the E5 and P10 experiments. However, the response of the U5 case is roughly between 1/2 and 1/3 of the magnitude of the response in the HBD05 runs. As was mentioned previously this is due to the magnitude of the response in a 1000 day average being not representative due to internal variability. In fact in the chapter to follow it will be shown that 5000 days is also not sufficient to accurately determine the magnitude of response. However, for now we shall not be concerned with this as we are focussing on the qualitative patterns of response and these are robust even for the short 1000 days runs. Problems only arise if one is trying to determine the exact magnitude of response accurately.

From Fig. 4.1. it is apparent that by simply heating the stratosphere, a significant response is found in the tropospheric circulation. In each of the experiments this consists of a shift in position of the mid-latitude jet along with banded anomalies in temperature. Focussing first on the E5 heating case. In the stratosphere there is maximum heating at low latitudes, decreasing toward the poles as expected from the imposed change in T_{ref} . However, accompanying this is a tropospheric response which consists of a banded increase in temperature in the mid-latitudes with a decrease on either side. These temperature changes are in thermal wind balance with the zonal wind response which consists of a decreased westerly wind on the equatorward side of the mid-latitude jet and an increase on the poleward side. Accompanying this is also an increased westerly wind anomaly in the subtropics. This E5 heating case most closely resembles the heating of the lower stratosphere over the solar cycle as can be seen by comparison between Figs. 4.1 and 1.6. Moreover, this produces a tropospheric response that is qualitatively similar to that found over the solar cycle (compare with Figs. 1.6 and 1.7). Specifically, the equatorial heating case produces a poleward shift of the mid-latitude jet along with a banded increase in temperatures in the mid-latitudes similar to that observed for the solar signal in the troposphere.

In contrast the U5 and P10 experiments give an equatorward shift of the

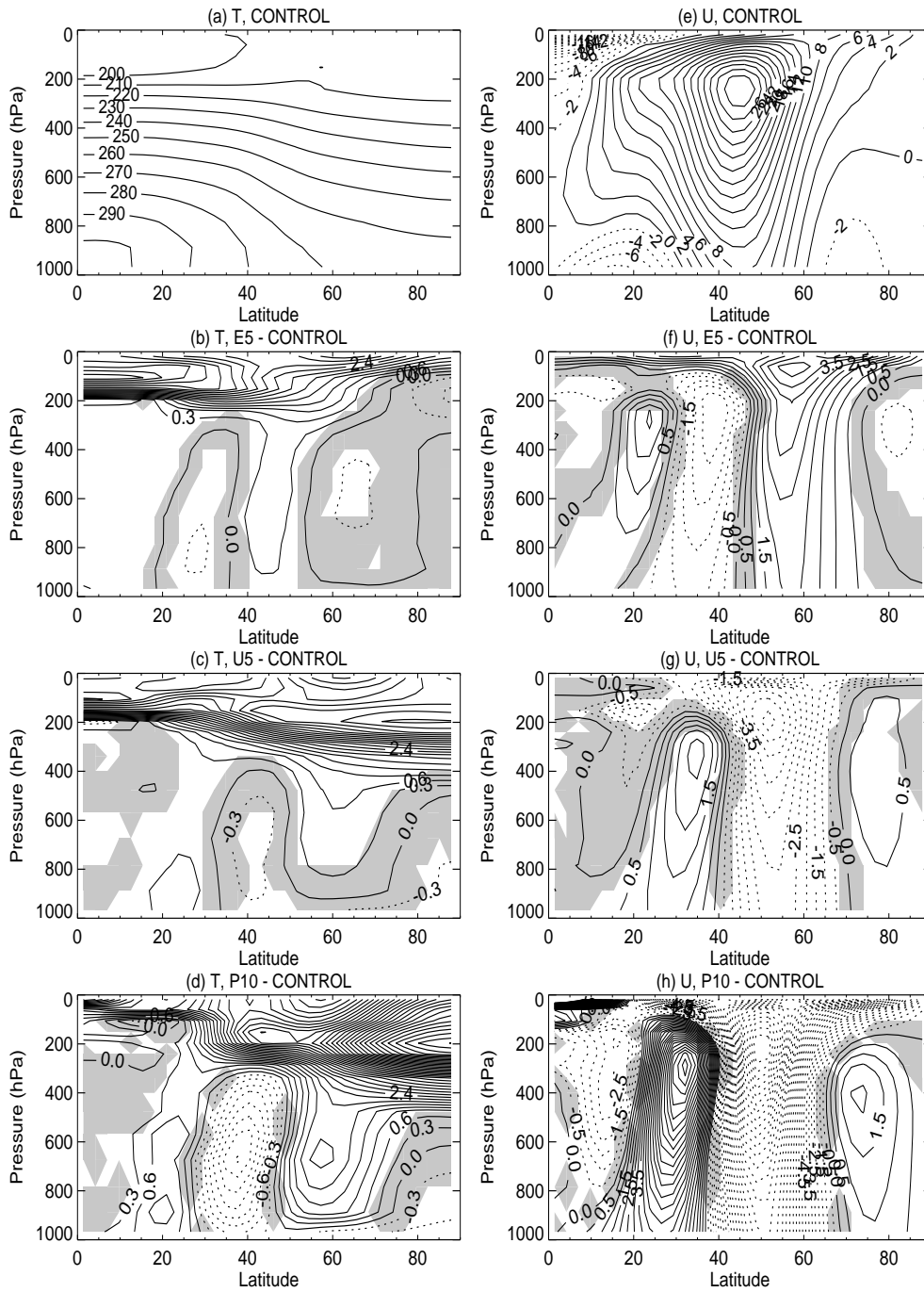


Fig. 4.1: (LHS) zonal mean temperature, (RHS) zonal mean zonal wind. The top panel shows the control run values (contour intervals: 10K and 2ms^{-1}) and the lower three panels show the difference between the equilibrium run and the control run for the E5, U5 and P10 experiments (contour intervals: 0.3K and 0.5ms^{-1}).

mid-latitude jet i.e. an increased westerly wind on the equatorward side of the jet centre and a decrease on the poleward side which is associated with banded temperature changes in the troposphere at different latitudes from the E5 experiment.

HBD05 demonstrated that altered horizontal eddy momentum fluxes were crucial in maintaining the anomalous tropospheric zonal flow against low level drag. In the following analysis of the spin-up ensembles we shall demonstrate that, not only are the changing eddy momentum fluxes important in maintaining the anomalous circulation, but they are also instrumental in creating it. Moreover, by comparison between the three different heating perturbations we shall investigate the reason for the differences in the tropospheric response depending on the latitudinal extent of the applied heating.

4.2 Spin-up ensemble results for the E5 experiment

The spin-up ensemble allows the evolution of the model response to the applied stratospheric heating to be observed in order to further investigate the mechanisms involved in producing the response in Fig. 4.1.

The spin-up ensemble average evolution of zonal mean temperature (\overline{T}), zonal mean zonal wind (\overline{u}) and stream function of the zonal mean meridional circulation ($\overline{\psi}$) for the E5 case are shown in Fig. 4.2. The control run and equilibrium response are also shown for comparison. The spin-up results are presented as 10-day averages with the difference taken relative to the average of the equivalent 10 days of the control run following the start day of the spin-up to limit any apparent evolution that is due to internal variability. The spin-up evolution of each of the fields is clearly heading towards the equilibrium response implying that these results are robust and statistically significant.

In the initial 10 days after the perturbation is switched on there is an increase in the temperature of the stratosphere, with warming that is largest at the equator and decreasing towards the poles. This reduces the reversed

latitudinal temperature gradient of the control run and induces poleward flow which results in a broad increase in vertical wind shear in the stratosphere to maintain thermal wind balance. The tropopause in the equilibrium temperature distribution slopes down from equator to pole (See Fig. 3.1), so the perturbation also increases the meridional temperature gradient equatorward of $\sim 30^\circ$ latitude around the 200hPa level. This induces equatorward flow and an easterly anomaly with decreased vertical wind shear immediately below it at the subtropical tropopause.

As the spin-up progresses a response begins to be seen in the troposphere. This consists of a band of increased temperature in the mid-latitudes centred on $\sim 45^\circ$ latitude and a decrease on either side (see Fig. 4.2). This banded structure is already very similar to the equilibrium response by days 20 to 29. It continues to intensify through the spin-up period but the equilibrium response has not yet been reached after 50 days.

In thermal wind balance with these tropospheric temperature changes there is an increased westerly wind on the poleward side of the jet and a decrease on the equatorward side. This corresponds to a weakening and poleward shift of the mid-latitude jet. Again, this zonal wind response is small initially but continues to amplify throughout the spin-up period while the features in the subtropical upper troposphere migrate slowly poleward leading to a poleward tilt with height.

A response in mean meridional circulation is also apparent near the beginning of the spin-up (column c of Fig. 4.2). In days 0 to 9 it consists of a weakening of the Hadley cell and the equatorward side of the Ferrell cell which starts in the upper troposphere. This is qualitatively consistent with the response to the temperature gradients directly generated by the stratospheric heating, as already discussed. By days 20 to 29 the meridional circulation has extended throughout the depth of the troposphere and an anomalous indirect circulation has also appeared at high latitudes. This three cell pattern continues to increase in magnitude as time progresses. The regions of anomalous descent and adiabatic warming coincide with the re-

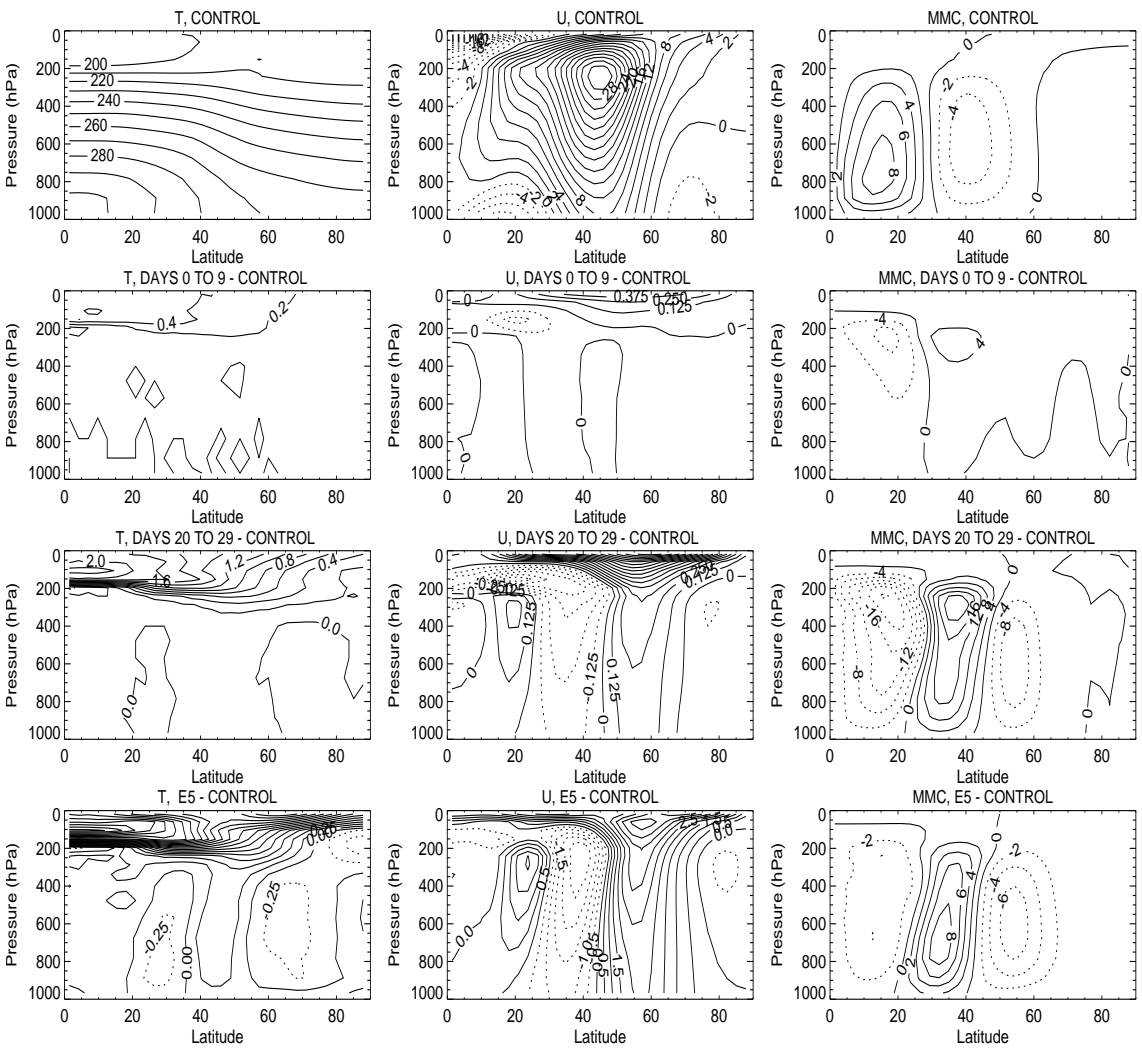


Fig. 4.2: Evolution of zonal mean fields for the E5 experiment. (Top panel) control run values. (Bottom panel) equilibrium E5 - C. (Middle panels) difference between the 10 day averages of the spin-up and the equivalent 10 days of the control run for days 0 to 9 and 20 to 29. (LHS) Temperature (K), (Middle) Zonal wind (ms^{-1}), (RHS) Stream function of the mean meridional circulation ($\text{Top} = 10^{10} \text{ kgs}^{-1}$, Middle = 10^8 kgs^{-1} , Bottom = 10^9 kgs^{-1}). Dashed contours are negative. Note the different contour intervals between panels.

gions of increased temperature in the troposphere and vice-versa. The change in the convergence of poleward eddy heat flux (not shown) acts to oppose these tropospheric temperature changes such that, by equilibrium, there is a balance between the adiabatic heating/cooling and divergence/convergence of the poleward eddy heat flux (See HBD05 for the equilibrium poleward eddy heat flux).

It is apparent that there is a balanced response in the troposphere to the stratospheric heating but how is such a response produced when the temperature perturbation is only applied in the stratosphere?

4.2.1 The importance of changing eddy momentum fluxes

The results of the previous section have demonstrated that altered temperature gradients in the stratosphere and around the tropopause region result in zonal wind accelerations there. Fig. 4.3 demonstrates that this is also accompanied by altered horizontal eddy momentum fluxes and it becomes apparent when looking at momentum balance that these are important in driving the meridional wind changes in the upper troposphere which are in turn important in producing the zonal wind anomalies in the lower troposphere. Throughout the following we use horizontal eddy momentum flux to refer to momentum flux in the equator to pole direction.

The momentum balance in the conventional Eulerian mean, given by Eq. 3.15 can be written

$$\frac{\partial \bar{u}}{\partial t} = f\bar{v} - \frac{1}{a \cos^2 \phi} \frac{\partial \overline{u'v'} \cos^2 \phi}{\partial \phi} - k_f \bar{u} + \text{AGEOSTROPHIC TERMS}, \quad (4.1)$$

where overlined quantities represent zonal means and dashed quantities represent the deviations from the zonal mean, a is the radius of the Earth and k_f is the boundary layer frictional damping coefficient.

The difference in zonal wind between E5 and Control (\bar{u}_{anom}) at any time

during the spin-up can then be given by

$$\bar{u}_{anom} = \frac{1}{e^{k_f t}} \left[\int_0^t e^{k_f t} f \bar{v} dt + \int_0^t -e^{k_f t} \frac{1}{a \cos^2 \phi} \frac{\partial \overline{u'v'}}{\partial \phi} dt + \int_0^t e^{k_f t} (\text{AGEOSTROPHIC TERMS}) dt \right], \quad (4.2)$$

where each of the terms in the integrals on the right hand side are the difference between E5 and control. To derive this solution, the dependence of the ageostrophic terms on \bar{u} has been ignored. Given the good agreement between the sum of the terms on the RHS of equation 4.2 and the \bar{u} anomaly (as will be shown in the following) this appears to be a reasonable approximation. Note that for $p < 700\text{hPa}$, $k_f=0$ and the solution is exact. The advantage of looking at momentum balance in this way is that, below 700hPa, the strong cancellation between the terms that act to accelerate \bar{u} and the anomalous frictional force which acts against them is removed so it can be seen clearly exactly what terms are resulting in the change in \bar{u} .

Thus, in this formulation, there are three terms which act to give the change in \bar{u} : the Coriolis force acting on the anomalous meridional wind, the change in horizontal eddy momentum flux convergence and the ageostrophic terms. Mean meridional wind anomalies will arise in response to thermal wind imbalances created directly by the anomalous heating and by anomalous eddy fluxes. So, as the altered eddy momentum flux acts to accelerate \bar{u} , a change in mean meridional circulation must also accompany this in order to maintain thermal wind balance in the presence of the altered zonal wind.

Comparing the right hand column of Fig. 4.2 with 4.3 (a) it is evident that the anomalous mean meridional circulation is in the correct sense to (at least partially) balance the anomalous horizontal eddy momentum flux. In response to the stratospheric heating there is a horizontal dipole in the change in horizontal eddy momentum flux, consisting of a decrease around the tropopause on the equatorward side of the jet maximum and an increase poleward of this. This gives a tripole of forcing in equation 4.1. This tripole corresponds to the latitudes of the 3 cell pattern in the meridional circulation

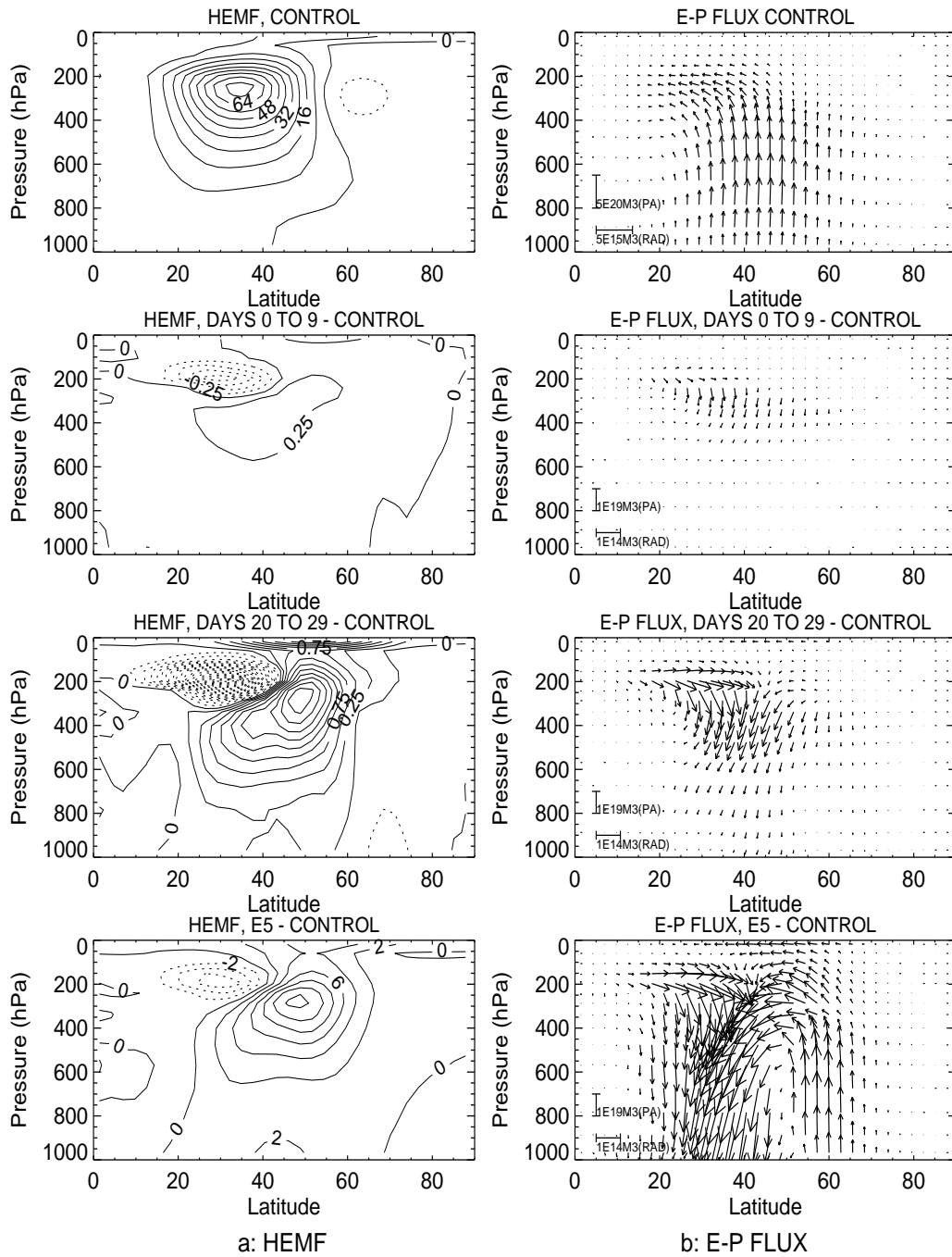


Fig. 4.3: As Fig. 4.2 but for (a) $\overline{u'v'}$ and (b) E-P flux scaled as in Edmon et al. (1980) for the E5 experiment. Note the different scale of the E-P flux vectors and the different contour intervals between plots.

anomalies. By days 20 to 29 the increase in horizontal eddy momentum flux on the poleward side of the jet has become more prominent and stretches downward and equatorward into the troposphere.

The altered temperature gradients around the tropopause will tend to drive an anomalous indirect circulation equatorward of $\sim 30^\circ$ latitude and a direct circulation poleward of this. These circulations will drive easterly winds equatorward of 30° latitude and westerly winds poleward of this near 200hPa via coriolis torque. During days 0 to 9, the $\overline{u'v'}$ anomalies result in a region of increased convergence equatorward of around 30° latitude. This will tend to drive changes in the zonal wind, but will induce a mean meridional circulation opposing these changes. The dipole in momentum flux convergence associated with the negative $\overline{u'v'}$ anomaly is located such as to enhance the mean meridional circulations and weaken the zonal winds driven directly by the heating. At the highest latitudes there is an increased convergence of $\overline{u'v'}$ but this does not initially dominate over the effect of the altered temperature gradient. By days 20 to 29 the positive part in the dipole of eddy momentum flux has become much more prominent and, in the region poleward of $\sim 50^\circ$ latitude, this results in an anomalous indirect circulation.

Thus regions of increased/decreased convergence of horizontal eddy momentum flux coincide with regions of decreased/increased meridional wind, as would be expected from Eq. 4.1. This is further demonstrated in the top panels of Fig. 4.4 which show time series' of the change in each of the forcing terms in Eq. 4.2 over the spin-up, along with their sum and the zonal wind anomaly (difference between spin-up and control run at time t), averaged between 700hPa and the top of the model. Fig. 4.4 (a) shows the average over 34 to 37° latitude (in the region of decreased \bar{u} on the equatorward side of the jet) and Fig. 4.4 (b) shows the average over 54 to 57° latitude (in the region of acceleration on the poleward side of the jet). This demonstrates that over these latitudes, in the vertical average outside the boundary layer, the dominant balance is between anomalous horizontal eddy momentum flux

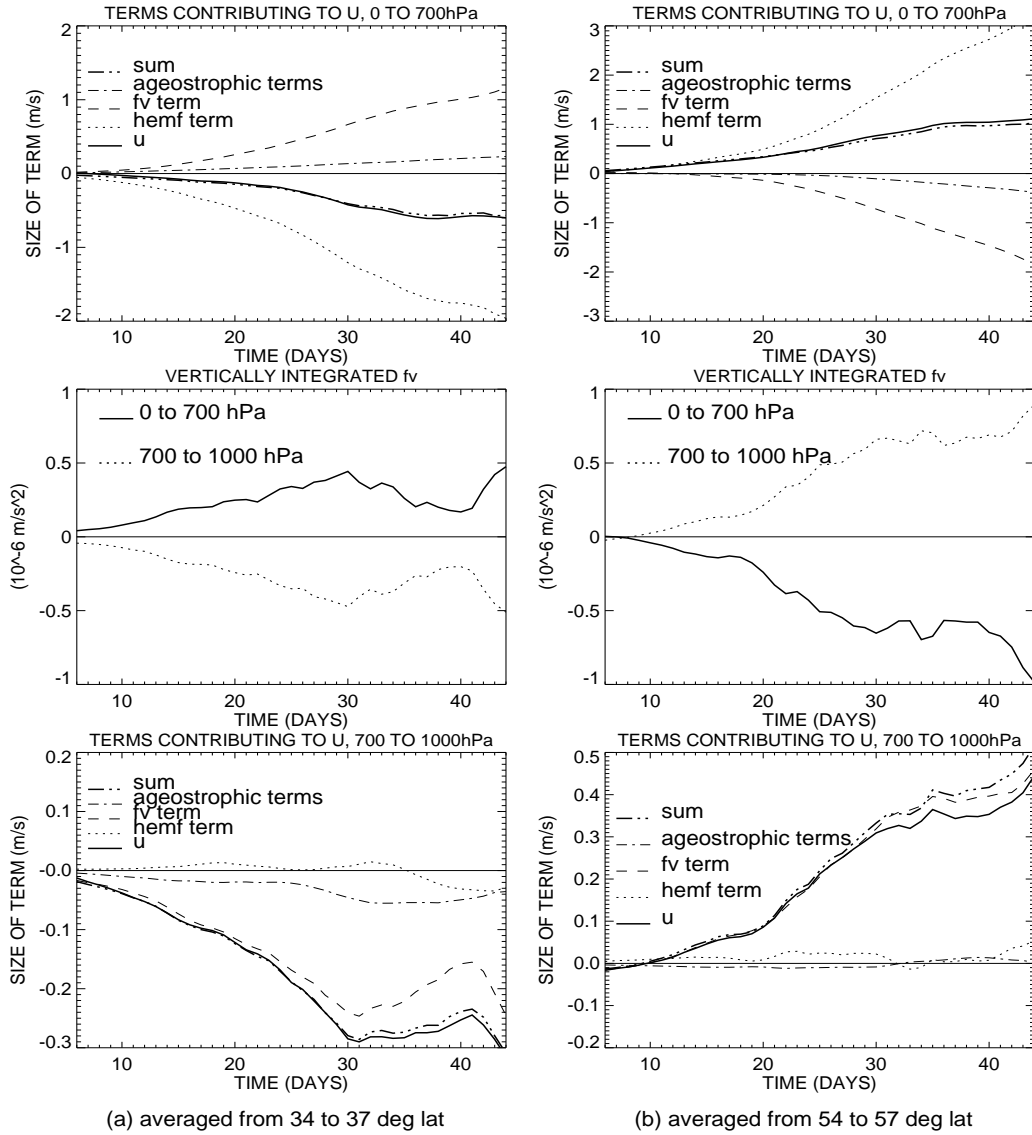


Fig. 4.4: (Top panel) 11-day running means of the change in each of the terms in Eq. 4.2 along with their sum and the difference in \bar{u} from the control run (hemf = 2nd term in Eq. 4.2), averaged from the top of the model to 700hPa. (Middle panel) 11-day running means of $f\bar{v}$ anomaly vertically integrated from 0 to 700hPa and from 700hPa to the surface. (Bottom panel) as top panel but averaged over 700hPa to the surface. (a) average over 34 to 37° latitude, (b) averaged over 54 to 57° latitude.

and anomalous $f\bar{v}$ with the imbalance giving a net acceleration in \bar{u} .

In almost all regions the change in horizontal eddy momentum flux is considerably larger than the change in vertical eddy momentum flux. However, the latter does become important around the 30° latitude region, where the change in horizontal eddy momentum flux convergence approaches zero. Thus the vertical eddy momentum flux is important in determining the exact latitude of zero meridional/zonal wind changes in the subtropics. At certain pressure levels on the equatorward side of the jet the ageostrophic terms become important, but their contribution to the change in \bar{u} cancels out when integrating over the upper half of the atmosphere, leaving the dominant balance between the horizontal eddy momentum flux and the $f\bar{v}$ anomalies, as shown.

The middle panel of Fig. 4.4 shows the anomalous $f\bar{v}$ vertically integrated over the free atmosphere and within the frictional boundary layer (i.e. above and below 700hPa), averaged over the same latitudes (note this is the instantaneous $f\bar{v}$ acceleration in Eq. 4.1, not the time integrated value from Eq. 4.2 shown in the upper and lower panels). The anomalous meridional wind in upper levels clearly mirrors that at lower levels, so that meridional wind anomalies produced in response to eddy momentum flux changes in the upper troposphere are balanced by meridional wind anomalies in the lower troposphere of opposite sign, as expected through downward control (Haynes *et al.*, 1991).

Comparison of Figs. 4.2 (b) and (c) shows that the regions of anomalous poleward meridional wind in the lower troposphere correspond to regions of increased westerly zonal wind and vice-versa, suggesting that the $f\bar{v}$ term at lower levels gives rise to the zonal wind accelerations there.

This is confirmed in the lower panel of Fig. 4.4, which shows each of the terms in Eq. 4.2 for the region of acceleration on the poleward side of the jet and the region of deceleration on the equatorward side of the jet now averaged from 700hPa to the surface. Here it is $f\bar{v}$ which is the dominant contribution to the change in \bar{u} . Thus, changes in horizontal eddy momentum

flux in the upper troposphere drive altered meridional circulations which lead to zonal wind accelerations in the lower troposphere. Fig. 4.4 suggests that this occurs in two stages with an initial slow acceleration of the zonal wind in the first 20 days followed by faster changes, particularly on the poleward side of the jet.

The vertically integrated momentum budget as given by Eqs. 3.20 and 3.21 has also been analysed. This is shown for the E5 spin-up and equilibrium in Fig. 4.5. The 10000 day average of the control run is shown, along with the anomalies for days 0 to 9 and 20 to 29 of the spin-up and the anomalies for the E5 equilibrium run. In the control run it can be seen that it is the convergence of horizontal eddy momentum flux that is important in producing the strong westerly momentum in mid-latitudes. For the spin-up, the vertically integrated momentum budget demonstrates that, in the region of zonal wind acceleration on the poleward side of the jet (between ~ 45 and 70°), there is a significant increase in horizontal eddy momentum flux convergence which is not balanced by the surface stress associated with the anomalous zonal wind at the beginning of the spin-up. This creates a positive momentum budget residual which acts to accelerate the zonal wind. Changes of the opposite sign are seen in the latitudes of deceleration on the equatorward side of the jet. Equatorward of $\sim 30^\circ$ latitude, the changes in eddy momentum flux are smaller (particularly at the beginning of the spin-up) resulting in a more complex balance where the momentum flux due to the zonally averaged circulation is also important. During the spin-up the zonal wind anomalies extend down to the surface and the anomalous surface stress increasingly balances the anomalous eddy forcing so that, by equilibrium (bottom panel of Fig. 4.5), there is almost a complete balance.

The vertically integrated momentum budget therefore confirms that the altered eddy momentum flux is important in driving the vertically integrated zonal wind accelerations.

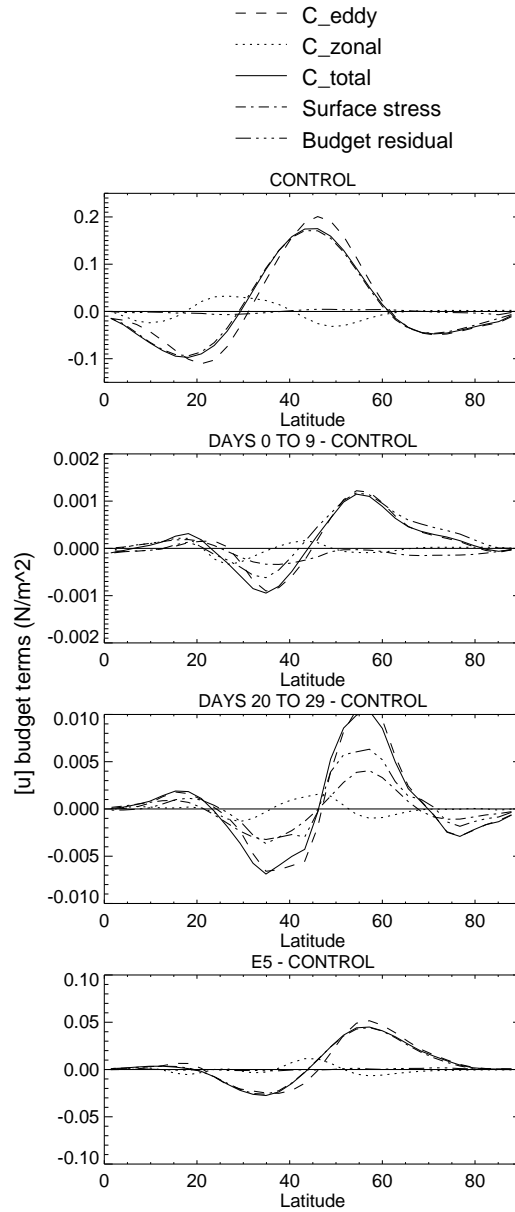


Fig. 4.5: Vertically integrated momentum budget. (Top panel) control run, (Bottom panel) difference between the vertically integrated momentum budget of the equilibrium E5 run and the control run and (Middle panels) difference between the vertically integrated momentum budget for days 0 to 9 and 20 to 29 of the E5 run and the vertically integrated momentum budget for the equivalent 10 day chunks of the control run.

In the Transformed Eulerian Mean

The above analysis has been shown for the Conventional Eulerian Mean (CEM) but the Transformed Eulerian Mean (TEM) momentum budget has also been studied. However, it is found that this does not aid in the interpretation of the results.

In the vertical integral the two formulations are equivalent but the local TEM balances in the meridional plane are quite different. Fig. 4.6 shows the anomalies in E-P flux divergence and the residual circulation ($f\bar{v}^*$) for the average of days 20 to 29 of the E5 spin-up. These are the two dominant terms which act to accelerate the zonal wind when friction can be neglected (see Eq. 3.28). This shows that the change in E-P flux divergence has a very broad latitudinal structure which is closely balanced by the residual circulation term and neither of these correspond to the structure of the change in zonal wind seen in Fig. 4.2. This broad structure is dominated by the vertical E-P flux component in the early spin-up as shown in Fig. 4.3 (b). The TEM will be shown to be of particular use through the E-P flux vector and its dependence on properties of the mean flow, but analysis of the local TEM momentum budget does not add to the conclusions already obtained from

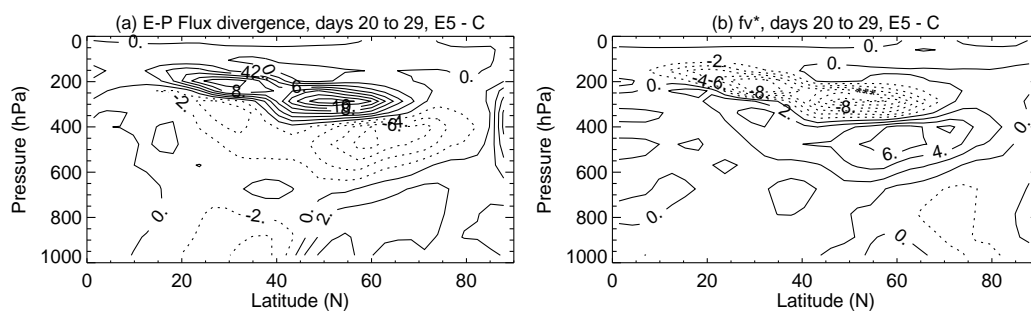


Fig. 4.6: (Top panel) difference in E-P flux divergence between days 20 to 29 of the E5 spin-up and the equivalent days of the control run. (Bottom panel) as top panel but for $f\bar{v}^*$. Contour interval = $2e^{-6} \text{ ms}^{-2}$.

the CEM. This is due to the dominant balance between the contribution to the E-P flux divergence from the vertical component of the E-P flux and the residual circulation.

4.2.2 *Comparison with a zonally symmetric model*

The above analysis of the zonal momentum budget has shown there to be a dominant balance around the tropopause between altered horizontal eddy momentum flux convergence and the Coriolis force on the anomalous mean meridional wind in response to stratospheric heating. From this dominant balance it is implied that mean meridional circulations are induced through the thermal wind imbalances created by changes in horizontal eddy momentum flux convergence. However, it is difficult to attribute, with absolute certainty, the altered meridional circulations to the change in eddy momentum flux convergence as we do not have a prognostic equation for the meridional wind in terms of the eddy momentum flux convergence. In order to confirm that it is indeed the eddy momentum flux convergence that is the driving force of the tropospheric response we have performed the same experiment but with a zonally symmetric model.

Exactly the same runs have been performed as described in Table 3.1 but this time with the model run in a zonally symmetric mode. As the model is zonally symmetric there are no explicit eddies. The eddy fluxes of heat and momentum are prescribed as those required to maintain the control run equilibrium state. In doing this we are allowing everything, except for the eddy fluxes, to change in response to the stratospheric heating. Thus, if the changes in the eddies are the driving force of the tropospheric response then it would be expected that with stratospheric heating of this zonally symmetric model, where the eddies are effectively held fixed, the tropospheric response should be absent. Due to the lack of eddy feedback in the zonally symmetric model there is much less variability and so only one ensemble member was required for the spin-up runs and the equilibrium response was determined from a 200 day average after an initial spin-up period of 200 days.

Fig. 4.7 shows the response in temperature, zonal wind and mean meridional circulation of the zonally symmetric model to E5 heating for days 0 to 9 and 20 to 29 of the spin-up. Comparison with Fig. 4.2 demonstrates that, initially, the temperature and zonal wind response in the stratosphere is rather similar to that in the full model. The meridional circulation changes are, however, considerably reduced (note the contour interval for mean meridional circulation in Fig. 4.7 is half that in Fig. 4.2). There is a weak indirect circulation anomaly equatorward of 30° latitude and a weak direct circulation anomaly poleward of around 30° latitude. This is the symmetric circulation response to maintain thermal wind balance in the presence of altered meridional temperature gradients around the tropopause. Coriolis torques on these meridional circulations drive changes in zonal wind. However, the changes in horizontal eddy momentum flux convergence that enhance these circulation

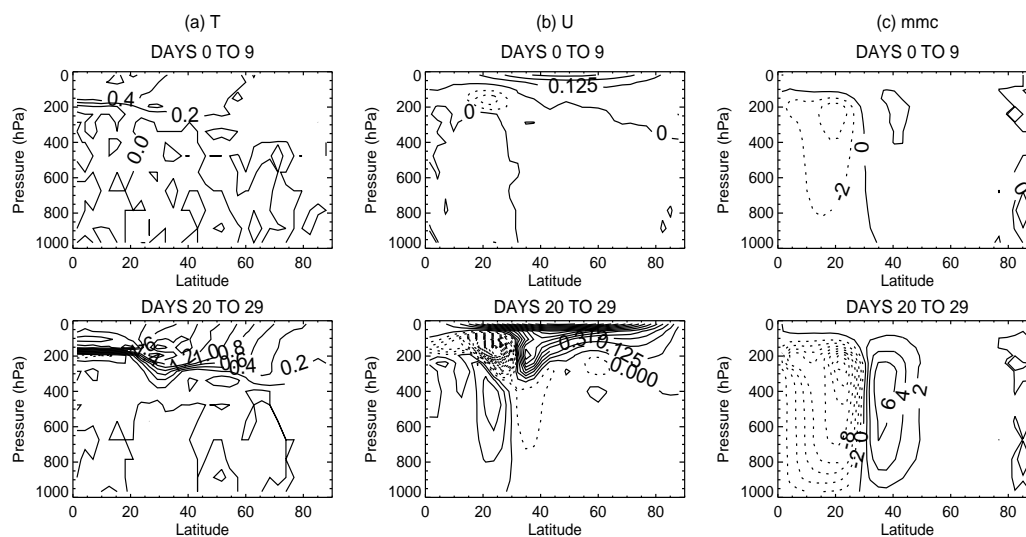


Fig. 4.7: Response of the zonally symmetric model to E5 heating for days 0 to 9 and days 20 to 29 of the spin-up. Differences relative to day zero of the spin-up are shown. (a) zonal mean temperature, (b) zonal mean zonal wind and (c) stream function of the mean meridional circulation (10^8 kgs^{-1}).

anomalies in the 3D model are absent in the zonal model.

After days 0 to 9, the tropospheric circulation responds differently. There is a large response in the zonal wind in the subtropical upper troposphere of the zonally symmetric model, associated with a temperature increase that

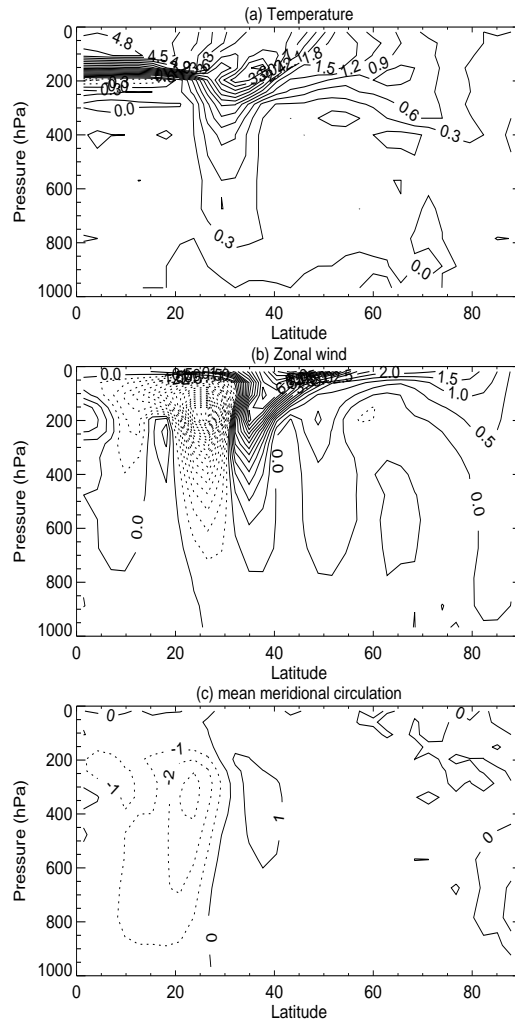


Fig. 4.8: Equilibrium response to E5 heating for the zonally symmetric response (a) Zonal mean temperature, (b) Zonal mean zonal wind and (c) stream function of the mean meridional circulation (10^9 kgs^{-1}).

stretches down into the troposphere in the sub-tropics. No such temperature increase is present in the 3D model. In the zonal model, examination of the terms in the thermodynamic equation (not shown) demonstrate that this tropospheric temperature increase is due to vertical advection (the $\overline{w}\partial\overline{\theta}/\partial z$ term in Eq. 3.18). The climatological meridional circulation is acting to advect the stratospheric temperature increase down into the subtropical troposphere. This does not occur as much in the 3D model runs because, in the subtropics, there is a stronger anomalous upward vertical motion throughout the spin-up which counteracts the warming effect of the control run mean meridional circulation acting on the anomalous vertical temperature gradient around the tropopause.

It is clear that the full tropospheric response that occurs in the 3D simulations is not being produced in the zonally symmetric model. Throughout the spin-up the weakening and poleward shift of the jet and the banded increase in temperature in mid-latitudes are not produced. Furthermore, the magnitude of the two lower latitude cells of the meridional circulation response is reduced compared to the 3D runs and the anomalous indirect cell at high latitudes is absent. This is also apparent in the equilibrium response in the zonally symmetric model shown in Fig. 4.8. By equilibrium the response in the subtropics has increased in magnitude but it is still clear that the full tropospheric response of the 3D model is not produced. Thus, these experiments using the zonally symmetric model in which the eddy fluxes are held fixed have confirmed that it is changes in the eddy fluxes that are important in producing the tropospheric response to stratospheric heating perturbations.

4.2.3 Diagnosing the cause of the altered eddy momentum fluxes

The preceding sections have demonstrated the importance of eddy fluxes, in particular eddy momentum fluxes around the tropopause, in producing the tropospheric response. In the following it shall be investigated further what is causing these altered eddy fluxes.

Changing phase speeds?

One mechanism that has recently been suggested for a stratospheric influence on tropospheric eddy momentum fluxes, and consequently circulation, is the effect that changes in the stratosphere can have on eddy phase speeds. This was mentioned briefly in Chapter 2. This mechanism was proposed by Chen *et al.* (2007) to explain the mid-latitude jet shift that they found in response to reduced surface friction in an sGCM much like the one use here. They found that by reducing the surface friction the mid-latitude jet was shifted poleward and that this was due to an increase in eddy phase speed. Reducing the surface friction resulted in an acceleration of the westerly wind at the surface and an increase in the eastward eddy phase speed. Consequently there was a poleward shift in the latitude of eddy breaking associated with a poleward shift of the critical line. This then resulted in a poleward shift of the region of eddy momentum flux convergence and correspondingly a poleward shift of the mid-latitude jet. The experiments of Chen *et al.* (2007) are, of course, fundamentally different from those presented here in that they are imposing changes to the zonal wind directly at the surface. However, Chen & Held (2007) noted that the recent poleward shift in the SH westerly jet which is thought to be associated with trends in the stratosphere is, too, accompanied by an increase in eddy phase speed. They suggest that changes in zonal wind near the tropopause or in the lower stratosphere may be sufficient to alter the eddy phase speed and result in the poleward shift of the westerly jet. However, they also state that it remains to be seen whether the shift in phase speed is a consequence or a cause of the altered tropospheric circulation. Here, we investigate whether an altered eddy phase speed is important in producing the tropospheric response to the stratospheric heating perturbations.

The phase speed of the eddies has been estimated by tracking of regions of maximum potential vorticity (PV) as they move from West to East in the mid-latitude region. PV has been output daily at each longitude, latitude and pressure level. As eddies are associated with regions of large PV at their

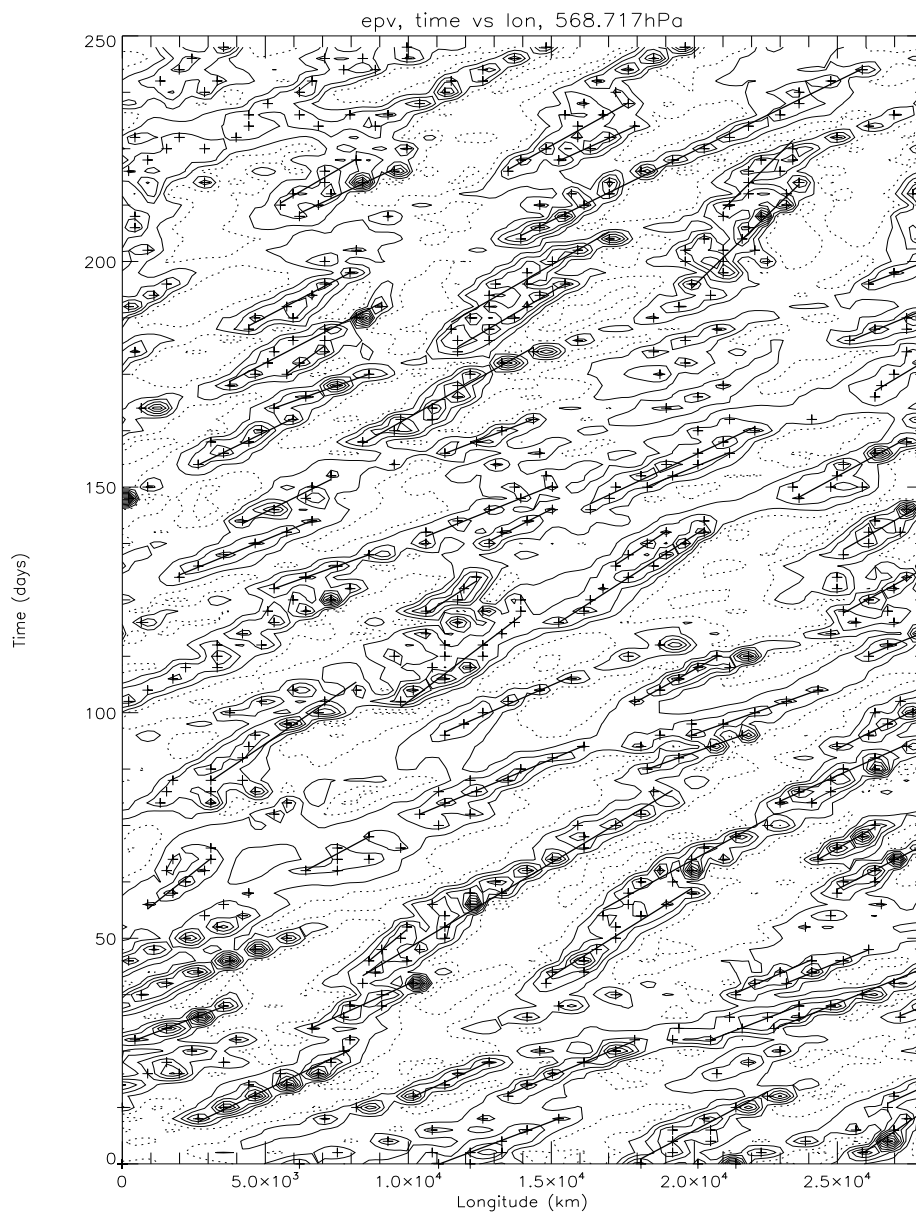


Fig. 4.9: Potential vorticity (anomaly from the zonal mean) at the 568hPa level averaged between 40° and 50° latitude. Contour interval = 0.02PVU , Threshold for large PV regions = 0.02PVU . Crosses = points of maximum PV, Solid lines = best fitting lines through the crosses for each PV track.

centre, an estimate of the phase speed can be obtained by tracking the speed of the movement of a region of maximum PV.

From the daily output of PV a Hövmoller plot of longitude versus time of PV averaged over a particular latitude band can be produced. An example is shown in Fig. 4.9 which shows PV averaged over the 40° to 50° latitude band i.e. around the centre of the jet. This shows PV anomalies from the zonal mean for a 250 day chunk of the control run. There are clearly tracks of regions of higher PV moving along from west to east associated with the eddies. By estimating how fast they are moving an estimate of the phase speed is obtained.

In order to do this the tracks where the PV reaches above some threshold value have been selected. The longitude of the point of maximum PV at the beginning of each of these tracks is found. The point of maximum PV on the next day of the track is found and so on until the PV falls below a threshold value again. In this way the longitude of the maximum PV in each track at daily intervals is obtained. The best fitting line to each of these tracks can then be calculated. The inverse gradient of these best fitting lines then gives the zonal phase speed.

By doing this for the full 10000 day control run and both hemispheres, a large number of tracks can be obtained to give a distribution of phase speeds centred on some value which will be taken to be the mean phase speed of the most dominant wavenumbers. The threshold PV should be chosen to be high enough that each track is considered separately but low enough that there are enough points in each track to provide a good estimate of the best fitting line. Fig. 4.10 shows the distribution of phase speeds calculated from the 10000 day control run (a) using a threshold value of 0.02PVU ($1\text{PVU} = 10^{-6}\text{Km}^2\text{kg}^{-1}\text{s}^{-1}$) and (b) a threshold value of 0.05PVU and tracking regions of maximum PV on the 569hPa level. The distributions show the percentage of PV tracks that have their phase speeds within a 1ms^{-1} bin e.g. the point with a phase speed of 0.5ms^{-1} shows the percentage of tracks that have a phase speed between 0 and 1ms^{-1} .

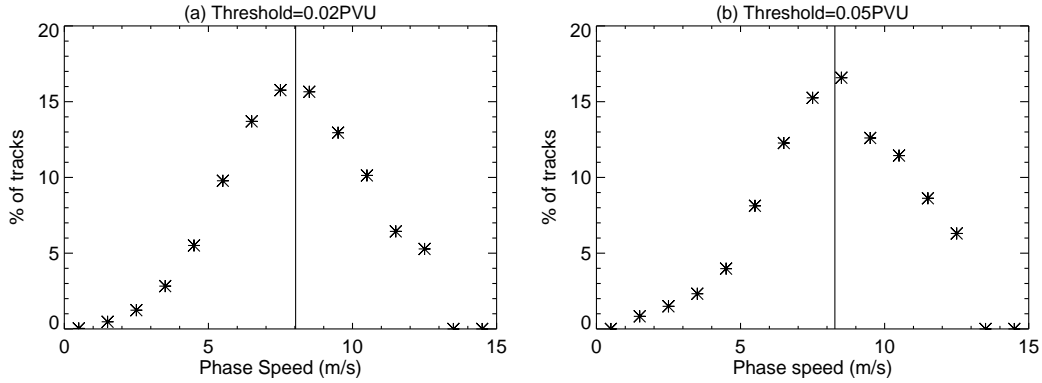


Fig. 4.10: Distribution of phasespeeds (a) using a threshold PV value of 0.02 PVU and (b) using a threshold PV value of 0.05PVU. Percentage of phase speed tracks in 1ms^{-1} bins is shown. Vertical line shows the mean phase speed.

For the threshold of 0.02PVU, the distribution has been produced from 12933 tracks and gives a mean phase speed of $8\pm 2\text{ms}^{-1}$. The mean phase speed was found to be fairly insensitive to the threshold value used as can be seen from Fig. 4.10 (b). Here, because the threshold value has been raised there are now only 927 tracks making up the distribution. Nevertheless, it still gives a mean zonal phase speed of around 8ms^{-1} .

Figure 4.11 shows the phase speed distribution for a threshold value of 0.03PVU at the 286, 400, 568 and 784hPa levels. It can be seen that the zonal phase speed is consistently around 8ms^{-1} . So, in the control run the mean phase speed of the most dominant wavenumbers around the latitude of the jet seems to be around 8ms^{-1} . Now we investigate whether there is a change in this phase speed in response to the stratospheric heating perturbations.

Figure 4.12 shows the distribution of phase speeds calculated from PV anomalies from the zonal mean averaged between 40 and 50° latitude at the 286hPa level using a threshold PV of 0.01PVU. The distribution of phase speeds is shown for days 0 to 9, 20 to 29 and 40 to 49 for the E5 and U5 spin-ups as well as the distribution for the equivalent 10 days of the control

run simulation. In this section we are primarily focussing on the E5 response but here the U5 phase speed distributions are given for comparison as, if the phase speed mechanism is at work, the U5 case should show a shift in the opposite direction to E5. The RHS gives the difference in the percentage at a particular phase speed between the E5 or U5 run and the control run. It can be seen that the E5, U5 and control run phase speed distributions become less and less similar as time progresses and the runs diverge from each other in response to the stratospheric heating. But, the main point that can be taken from these phase speed distributions is that there is not a consistent

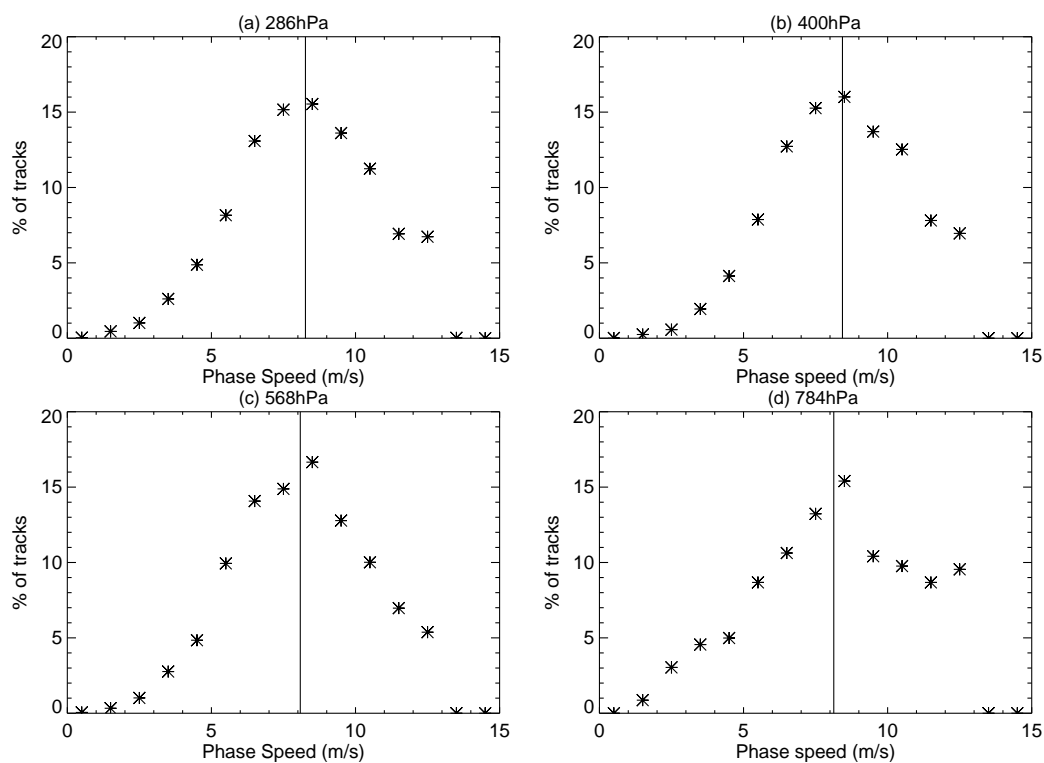


Fig. 4.11: Distribution of phase speeds calculated from PV (anomalies from the zonal mean) averaged between 40 and 50° latitude using a PV threshold value of 0.03 . Percentage of tracks with phase speeds in 1ms^{-1} bins is shown for (a) 286hPa , (b) 400hPa , (c) 568hPa and (d) 784hPa .

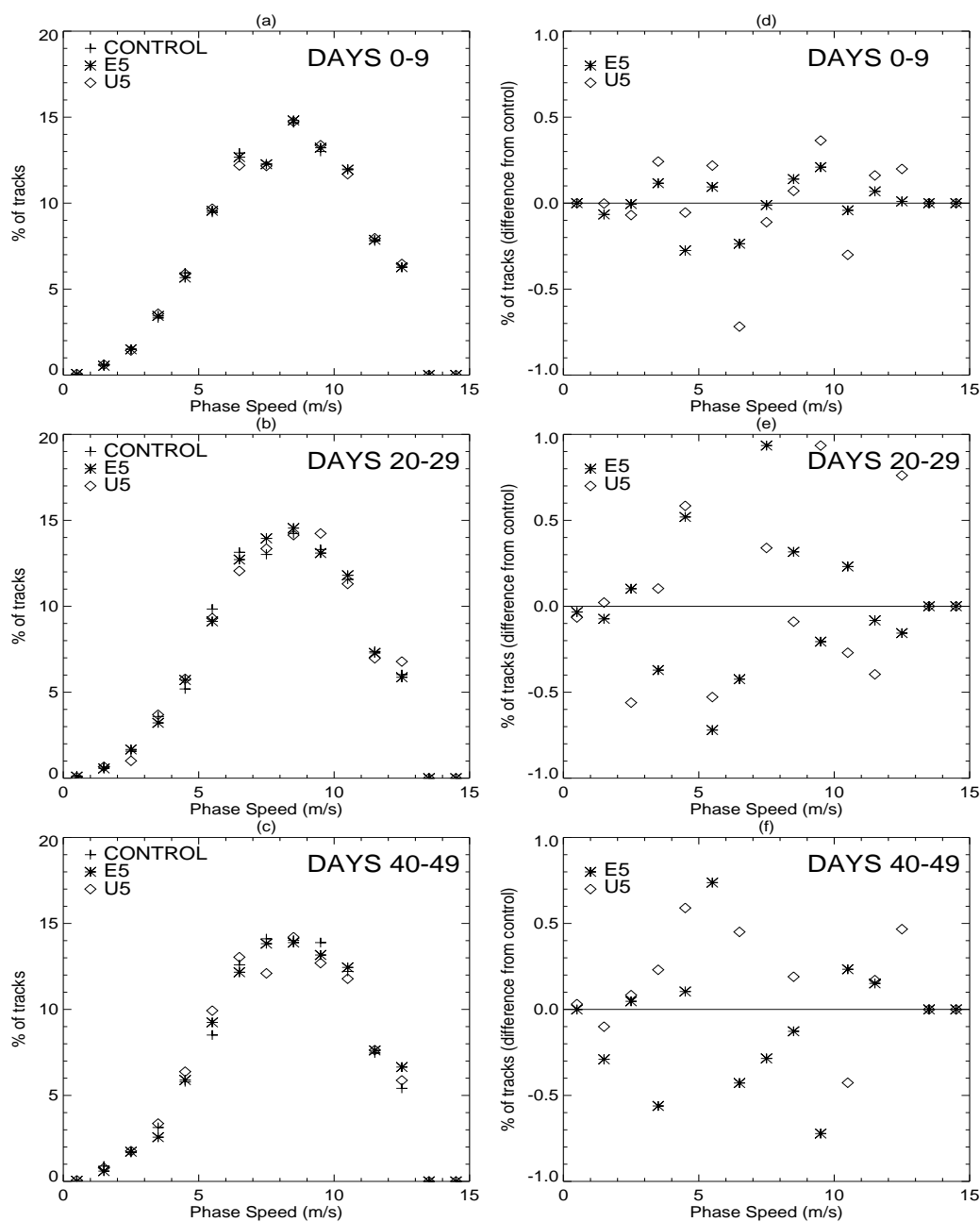


Fig. 4.12: (a)-(c): Phase speed distributions for days 0 to 9, 20 to 29 and 40 to 49 of the spin-up. (d)-(f): difference in the phase speed distributions for the E5 and U5 spin-ups from the control run for days 0 to 9, 20 to 29 and 40 to 49.

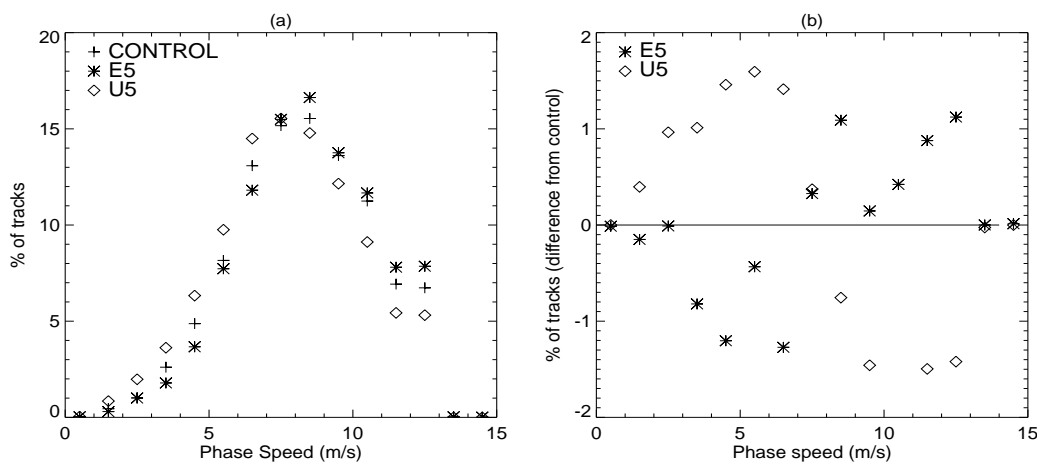


Fig. 4.13: Phase speed distributions for the equilibrium E5 and U5 runs and the control run. RHS = difference in the phase speed distributions between the equilibrium E5 and U5 runs and the control run.

shift in phase speed in either the U5 or the E5 spin-ups. If the phase speed mechanism is at work in producing the tropospheric response then it would be expected that there should be a shift in the phase speed distributions to higher phase speeds in the E5 spin-up and a shift to lower phase speeds in the U5 spin-up (as the U5 heating produces an equatorward shift in the jet). It is clear from the difference figures (4.12 (d), (e) and (f)) that there is not an increased percentage of tracks at higher phase speeds and a decrease at lower phase speeds for the E5 case and vice versa for the U5 case. The troposphere has definitely started to show the equilibrium pattern of response during the spin-up and therefore it is unlikely that a change in phase speed plays an important role in producing the tropospheric response.

However, there is found to be a shift in phase speed in the equilibrium response which is toward higher phase speeds for the E5 case and lower phase speeds for the U5 case. This can be seen in Fig. 4.13 which shows the phase speed distribution for the control run and equilibrium E5 and U5 runs along with the difference between the equilibrium E5 and U5 runs and the control

run. The E5 run has an increased percentage of phase speed tracks with phase speeds in the faster half of the distribution and a decreased percentage of tracks with phase speeds in the slower half of the distribution. The opposite is true for the U5 heating. This is in the correct sense for the Chen *et al.* (2007) phase speed mechanism but the fact that this is not apparent during the spin-up, where the response is clearly starting to take place, leads us to conclude that this is not a cause of the tropospheric response but rather a consequence.

For each of the experiments, PV has been averaged over 40 to 50° latitude but, of course, the jet has shifted in response to the E5 and U5 heating. Perhaps the shift in phase speed seen at equilibrium is a consequence of sampling PV from a different location relative to the jet maximum in the E5 and U5 equilibrium runs. Alternatively, it could be in response to altered zonal wind speeds which have been produced in response to the stratospheric heating, in a similar manner to the response to reduced surface friction in the Chen *et al.* (2007) study. Finding out the cause of this change in phasespeed requires further investigation and perhaps a more sophisticated method for the calculation of phase speeds. Nevertheless, a change in phase speed does not seem to be important in producing the tropospheric response which occurs during the spin-up.

Changes in eddy refraction

Another possibility for the production of these eddy momentum flux changes is through the effect that the stratospheric heating can have on the direction of eddy propagation. Here, the E-P flux and refractive index will be used to attribute the altered eddy momentum fluxes to changes in the direction of eddy propagation which can be further attributed to various properties of the change in the state of the atmosphere.

Fig. 4.3 (b) shows the evolution of the change in Eliassen-Palm (E-P) flux throughout the E5 spin-up, where the arrows have been scaled for graphical purposes following the conventions of Edmon *et al.* (1980). Recall that, in the

quasi-geostrophic approximation, $\vec{F} = (F_\phi, F_z)$, where $F_\phi = -a \cos\phi \overline{u'v'}$ and $F_z = -af \cos\phi \frac{\overline{v'\theta'}}{\theta_z}$. As is shown in the Appendix 1, when eddy propagation can be thought of as wavelike then the direction of the E-P flux also indicates the direction of wave propagation. In the control run (top panel), eddies develop due to baroclinic instability of the temperature gradient below the jet and propagate upward along the jet axis. This upward propagation is associated with poleward eddy heat flux through the definition of F_z . The high static stability of the tropopause prevents further upward propagation and the eddies refract primarily equatorwards to break anticyclonically on the equatorward side of the jet. The equatorward propagation corresponds to the region of poleward eddy momentum flux in the top panel of Fig. 4.3a by definition of F_ϕ .

Even at the beginning of the spin-up (days 0 to 9) there are changes to the direction of eddy propagation around the tropopause, with a weakening of the upward E-P flux particularly at lower latitudes i.e. equatorward of the jet maximum. This is accompanied by reduced equatorward E-P flux around the tropopause (~ 100 to 250 hPa), equatorward of $\sim 40^\circ$ corresponding to the decrease in horizontal eddy momentum flux seen on the equatorward side of the jet. Below this in the upper troposphere there is increased equatorward propagation associated with the increased horizontal eddy momentum flux which extends equatorward and downward from the poleward side of the jet. The weakened upward E-P flux extends down to the surface by days 20 to 29 and, by days 40 to 49 (not shown), is accompanied by increased upward E-P flux on the poleward side of the jet, consistent with the shift in the region of maximum baroclinicity with the shift in the jet. This is further amplified at equilibrium (bottom panel).

To determine whether the changes in E-P flux throughout the spin-up are consistent with changes in wave refraction by the evolving zonal mean state, the zonal mean quasi-geostrophic refractive index (Matsuno, 1970) as given by equations 3.30 and 3.31 has been calculated. Karoly & Hoskins (1982) demonstrate that, under linear WKB theory, waves will be refracted

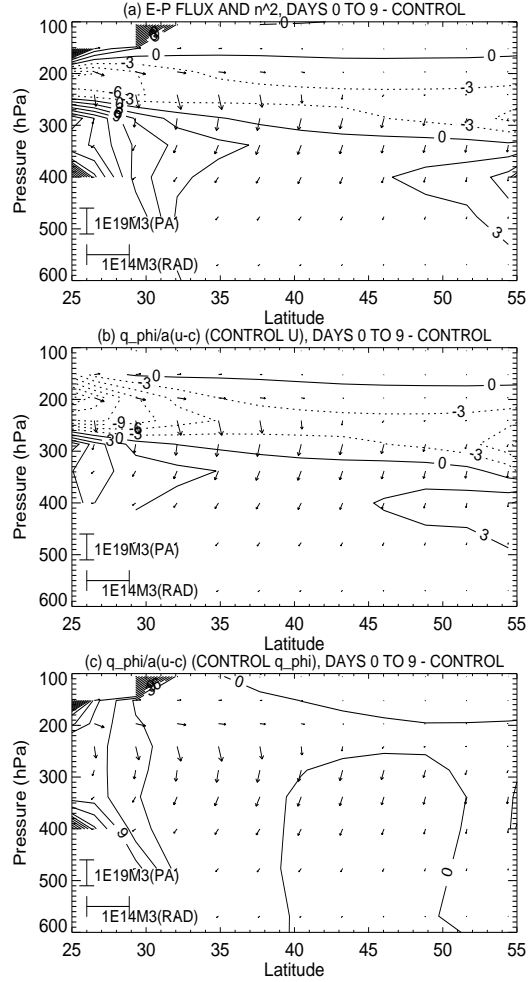


Fig. 4.14: (a) change in n^2 (contours) and scaled E-P flux (arrows) for days 0 to 9 of the E5 spin-up, (b) change in $\bar{q}_\phi/a(\bar{u} - c)$ using the change in \bar{q}_ϕ for the spin-up and \bar{u} from the control run and (c) change in $\bar{q}_\phi/a(\bar{u} - c)$ using the change in \bar{u} from the spin-up and \bar{q}_ϕ from the control run. Contours have been blanked out in regions where $c > u$. Note: values in the middle and bottom panels have been scaled by a^2 to make them non-dimensional for comparison with total n^2 . The E-P flux anomalies are the same in all panels.

by gradients of n^2 , such that they will tend to propagate away from regions of low refractive index and towards regions of high refractive index (see also the Appendix).

The top panel of Fig. 4.14 shows the change in refractive index together with the change in E-P flux for days 0 to 9 of the spin-up for the upper troposphere/tropopause region around the jet latitude, where the change in E-P flux is most significant. When calculating differences in the refractive index the term involving wavenumber cancels out for any particular wavenumber. The refractive index calculations have assumed a phase speed of 8ms^{-1} as was calculated in the previous section. The patterns of change in refractive index are found to be qualitatively similar for any choice of phase speed between 6 and 16ms^{-1} . The following discussion of refractive index and E-P flux anomalies applies to wavenumbers 5-7 as these dominate the E-P flux and horizontal eddy momentum flux anomalies and also dominate in the calculation of the phase speed.

It can be seen that the changes in E-P flux are generally consistent with those in the refractive index. There is a vertical dipole change in refractive index consisting of a reduction around the tropopause and an increase below i.e. a reduced upward gradient of refractive index, with the refractive index changes being larger on the flanks of the jet. The reduced upward gradient of n^2 is accompanied by reduced upward E-P flux, with the anomalies being larger on the equatorward side of the jet (particularly at $\sim 300\text{hPa}$). By continuity this reduced upward E-P flux would be expected to be accompanied by a reduced equatorward E-P flux above, as is indeed the case. This can be seen to be consistent with refraction away from a minimum in n^2 in low latitudes at around 200hPa . Thus the initial weakening of the upward E-P flux (and associated change in horizontal E-P flux above) appears to stem from the decrease in refractive index around the tropopause and the increase below which reduces the upward gradient of refractive index and thus weakens upward eddy propagation.

The individual contributions to the change in n^2 in Eq. 3.30 have been

examined to determine what aspects of the change in the zonal mean state lead to the changes in wave propagation. The change in n^2 is calculated for a given wavenumber so the middle term of Eq. 3.30 is fixed. Comparison of the other two terms show that the change in the third term is insignificant compared to the change in $\bar{q}_\phi/a(\bar{u} - c)$. The lower two panels of Fig. 4.14 compare the effect on $\bar{q}_\phi/a(\bar{u} - c)$ of changes in \bar{q}_ϕ and of changes in \bar{u} in the denominator. The middle panel shows the effect of the change in \bar{q}_ϕ only, by calculating the change in $\bar{q}_\phi/a(\bar{u} - c)$ using the spin-up values of \bar{q}_ϕ and the control run values of \bar{u} in the denominator. Conversely the bottom panel shows the change in $\bar{q}_\phi/a(\bar{u} - c)$ using the spin-up value of \bar{u} in the denominator and the control run value of \bar{q}_ϕ .

Comparison with the top panel of Fig. 4.14 shows that most of the refractive index change is explained by the change in \bar{q}_ϕ except at the lowest latitudes. The contribution due to the change in \bar{u} in the denominator is small and confined to the low latitude tropopause region.

Initially it is the change in the meridional gradient of potential vorticity at the tropopause that alters the refractive index and thus eddy propagation. The top panel of Fig. 4.15 shows the change in meridional PV gradient for days 0 to 9 which consists of this dipole change with a decrease around the tropopause and an increase below. Comparing this with the change in E-P flux (Fig. 4.3 (b)) it can be seen that the reduced upward E-P flux only occurs in the latitudes where the dipole change in \bar{q}_ϕ occurs. The components of \bar{q}_ϕ are next diagnosed to understand how this change in \bar{q}_ϕ arises. Eq. 3.31 gives the meridional gradient of quasi-geostrophic potential vorticity as a function of the zonal-mean zonal wind (\bar{u}) and potential temperature ($\bar{\theta}$) gradients. The second term measures the meridional curvature of the zonal wind and augments the planetary vorticity gradient. The third term is influenced by changes in the vertical shear and curvature of the zonal wind and the vertical shear and curvature of the potential temperature. The change in the third term

$$\frac{a f^2}{R} \left(\frac{p \bar{\theta}}{T} \frac{\bar{u}_p}{\bar{\theta}_p} \right)_p \quad (4.3)$$

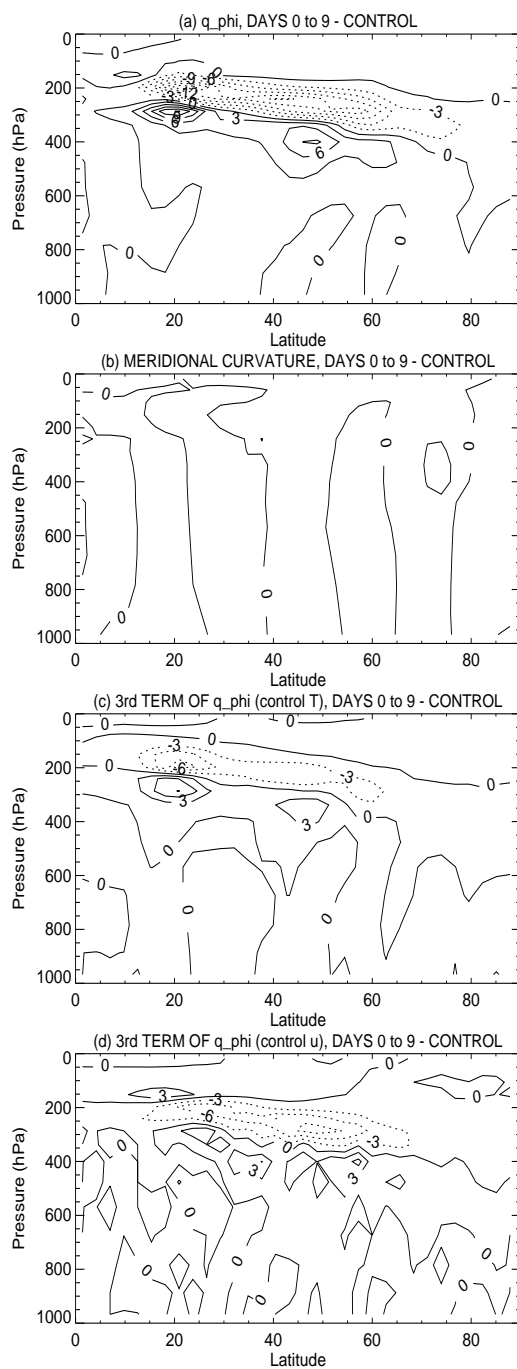


Fig. 4.15: Change in individual components of \bar{q}_{ϕ} ($10^{-6} \text{s}^{-1} \text{rad}^{-1}$). (a) change in \bar{q}_{ϕ} , (b) meridional curvature, (c) change in third term of \bar{q}_{ϕ} due to altered \bar{u} , (d) change in third term of \bar{q}_{ϕ} due to altered $\bar{\theta}$.

can be linearised in terms of the contributions from the change in $\bar{\theta}$ or \bar{T} and the change in \bar{u} where the non-linear part is small.

The lower three panels of Fig. 4.15 show the separate contributions to the change in meridional PV gradient for days 0 to 9 of the E5 spin-up. The contribution to the change from the meridional curvature is negligible compared to the contributions from the other terms. The contributions to the change in term 4.3 from the changes in \bar{u} and $\bar{\theta}$, shown in the third and fourth panels respectively, are both important, with the change due to the vertical temperature gradient being about twice as large as that due to vertical zonal wind gradients (or equivalently horizontal temperature gradients) except perhaps at low latitudes. These both act to give this dipole change in meridional PV gradient which then results in the dipole change in n^2 . The n^2 anomalies on the flanks of the jet are amplified by the effect of low values of $(\bar{u} - c)$ in the denominator. This initial change in n^2 produces refraction of the E-P flux of the form shown in Fig. 4.3 (b) which results in changes in horizontal eddy momentum flux. This then drives zonal wind anomalies in the upper troposphere as well as anomalous meridional circulations which result in zonal wind and temperature changes in the lower troposphere.

The importance of the change in vertical temperature gradient around the tropopause in causing this weakened upward E-P flux is further confirmed by examining the relative importance of the horizontal eddy heat flux $(\overline{v'\theta'})$ and the vertical temperature gradient $\bar{\theta}_z$ in the definition of E-P flux (Eq. 3.29). Fig. 4.16 (a) shows the full change in vertical E-P flux for days 0 to 9 in response to the stratospheric heating (including the ageostrophic contributions) whereas Fig. 4.16 (b) shows the change in vertical E-P flux as calculated using the quasi-geostrophic definition of E-P flux (3.29). It can be seen that there is reasonable agreement between the two indicating that the ageostrophic terms are small.

The change in quasi-geostrophic vertical E-P flux has then been linearised in terms of the change in vertical temperature gradient and the change in horizontal eddy heat flux. i.e. Fig. 4.16 (c) shows the change in F_z as

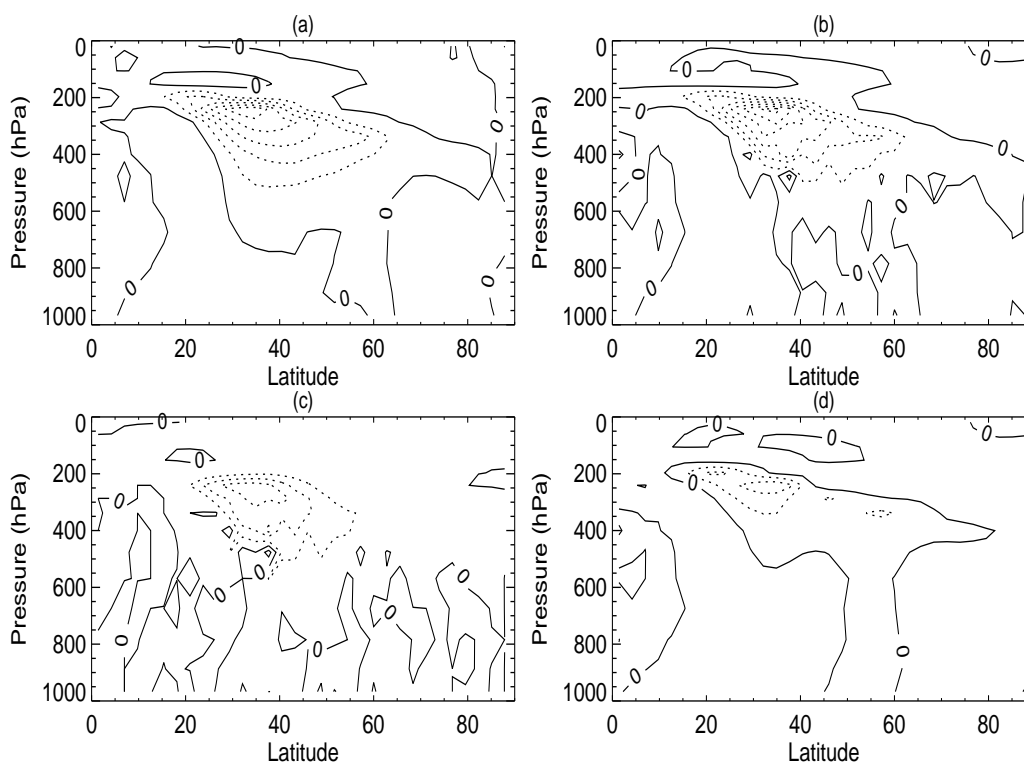


Fig. 4.16: (a) The full change in vertical E-P flux during days 0 to 9 of the spin-up. (b) The change in vertical E-P flux as calculated using Eq. 3.29 i.e. omitting the ageostrophic terms, (c) as (b) but using control run horizontal eddy heat flux and spin-up vertical temperature gradient for the calculation of F_z , (d) as (c) but using spin-up horizontal eddy heat flux and control run vertical temperature gradient in the calculation of F_z .

calculated using Eq. 3.29 with the spin-up value of vertical temperature gradient but the control run horizontal eddy heat flux and vice-versa in Fig. 4.16 (d). The contributions due to the altered vertical temperature gradient and the altered horizontal eddy heat flux approximately add up to the full change in vertical E-P flux. From this it can be seen that a large fraction of the reduction in upward E-P flux is actually due to the increased vertical temperature gradient that occurs within the definition of E-P flux.

This, together with the analysis of the refractive index and its contributions has shown that initially the increased static stability around the tropopause has weakened the upward eddy propagation and resulted in corresponding changes to the momentum fluxes. There is also a smaller contribution to the refraction of the eddies from the altered vertical wind shear and curvature associated with the meridional temperature gradient through thermal wind balance.

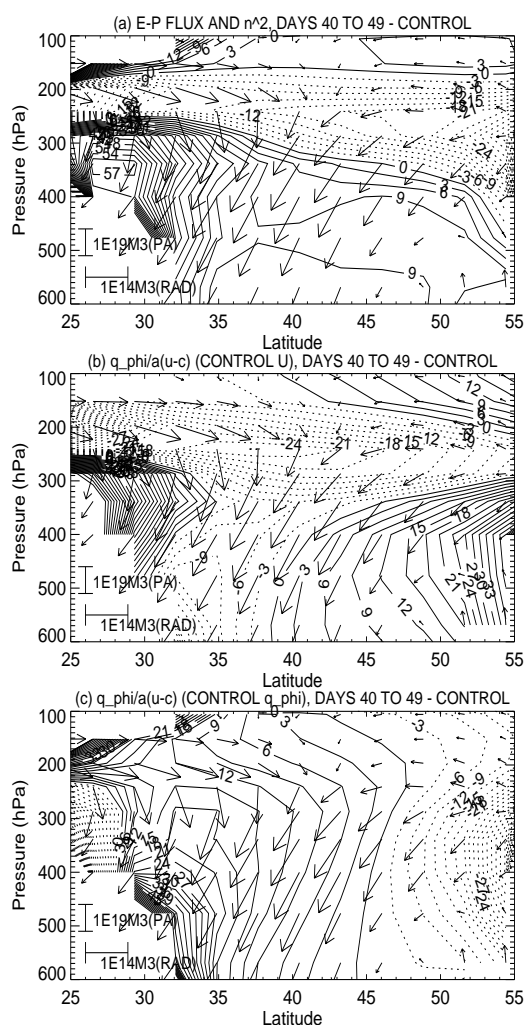


Fig. 4.17: As Fig. 4.14 but for days 40 to 49.

As time progresses an important feedback becomes apparent. This can be seen in Fig. 4.17 which is equivalent to Fig. 4.14 but now for days 40 to 49. The refractive index and E-P flux changes are now considerably larger and there is a positive gradient of refractive index from pole to equator in the troposphere accompanied by anomalous equatorward refraction of E-P flux in the troposphere. This leads to the increase in horizontal eddy momentum flux stretching down into the troposphere seen in Fig. 4.3 (a). Comparing the total change in refractive index with the individual components demonstrates that the change in \bar{q}_ϕ no longer completely explains the change in n^2 . There is now a much larger contribution from the altered zonal wind in the denominator. As the zonal wind in the troposphere starts to change, the \bar{u} and \bar{q}_ϕ contributions become comparable. In the region of zonal wind deceleration between $\sim 30^\circ$ and 45° the zonal wind (in the denominator) contribution to $\bar{q}_\phi/a(\bar{u} - c)$ actually dominates the refractive index changes in the troposphere by days 10 to 19. However, the change in PV gradient remains the dominant contribution to the change in n^2 around the tropopause. The lower panel of Fig. 4.17 demonstrates that the altered zonal wind is responsible for the positive gradient of refractive index from pole to equator in the troposphere and corresponding E-P flux and eddy momentum flux changes in the troposphere. These results suggest a feedback: as the zonal wind starts to respond to the initial changes in meridional temperature gradient and eddy momentum flux around the tropopause this influences eddy propagation in the troposphere resulting in changes in horizontal eddy momentum flux throughout the troposphere. This acts to further accelerate the tropospheric zonal wind. The initial response followed by a feedback involving the tropospheric eddies is likely to be the reason for the two stage response seen in Fig. 4.4: as the feedback becomes important there is a stronger acceleration of the zonal wind.

4.3 Comparison with the U5 and P10 experiments

The above analysis has been performed for the E5 experiment and suggests the following mechanism for producing the tropospheric response to stratospheric heating. Heating the stratosphere alters the vertical temperature gradient which weakens the upward propagation of eddy activity and thus alters the horizontal eddy momentum flux around the tropopause. There is also a contribution to the change in eddy refraction from the altered vertical wind shear associated with the change in meridional temperature gradient. These initial changes in eddy momentum flux around the tropopause drive mean meridional circulation anomalies which result in zonal wind accelerations lower down in the troposphere. There is then an important feedback. As the zonal wind starts to change in the troposphere it influences eddy propagation there which results in altered tropospheric eddy momentum fluxes which then feed back onto the zonal wind anomalies.

To confirm that the above mechanism is also valid for other stratospheric heating perturbations this will now be compared with the U5 and P10 heating perturbations, focussing first on the initial changes in meridional PV gradient around the tropopause and then demonstrating that the feedback involving tropospheric zonal wind changes also occurs in these experiments. By comparing the different heating cases we also seek to understand what determines the direction of jet displacement since, in both these experiments, the jet is displaced equatorward, as opposed to poleward in E5.

Fig. 4.18 shows the anomalies of various fields from the control run values for the average of days 0 to 9 of the U5 and P10 spin-ups. As expected from the applied heating perturbations the change in vertical temperature gradient is fairly uniform for U5 and is more localised toward the poles for P10. It was demonstrated for E5 that the change in vertical temperature gradient around the tropopause was important in the initial change in \bar{q}_ϕ and the weakening of the upward E-P flux. It can be seen from Fig. 4.18 that the differences in the \bar{q}_ϕ anomaly between the experiments are associated with differences in the location of the change in vertical temperature gradient.

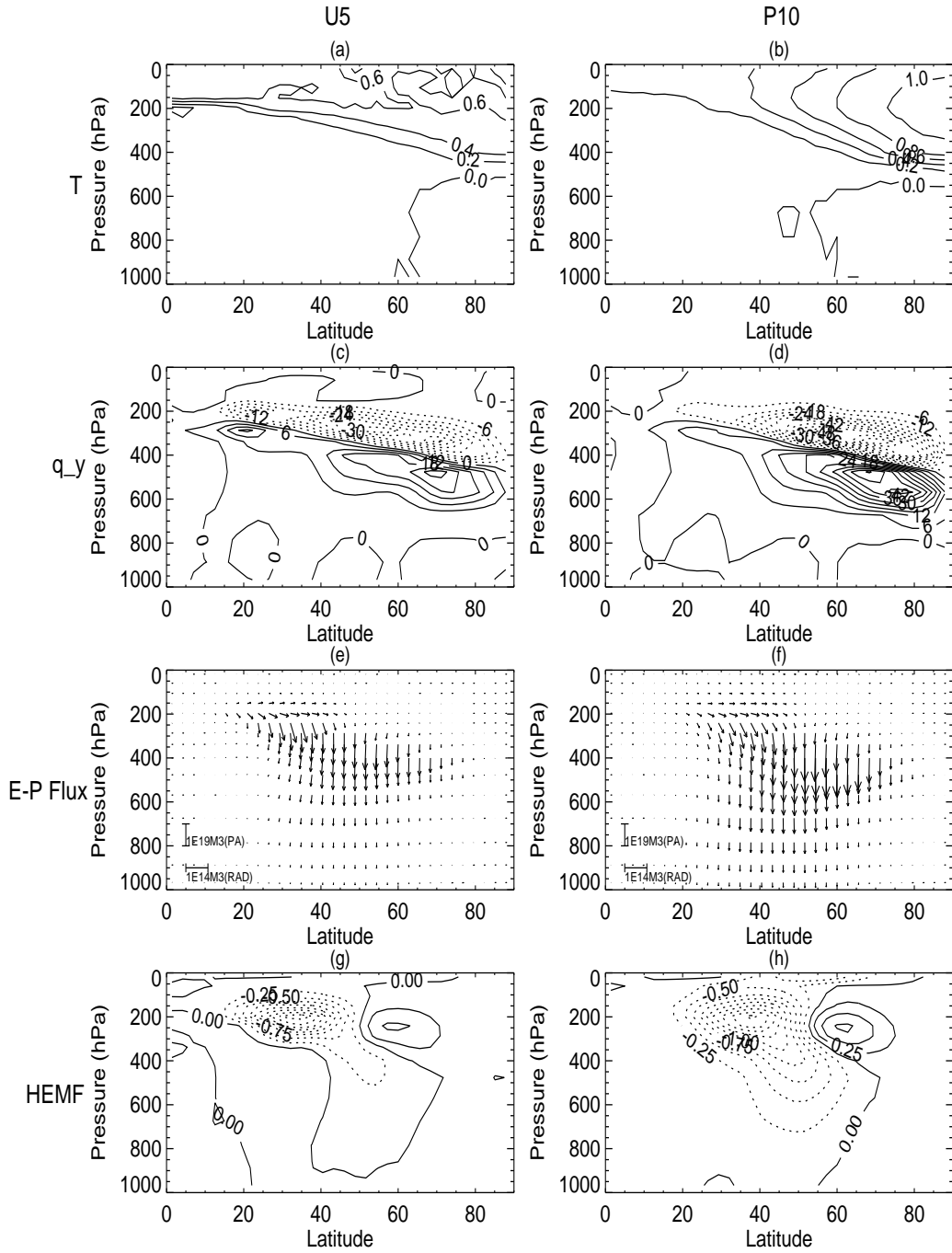


Fig. 4.18: Difference between days 0 to 9 of the spin-up and the control run for (a) U5 \bar{T} , (b) P10 \bar{T} , (c) U5 \bar{q}_ϕ ($10^{-6} s^{-1} rad^{-1}$), (d) P10 \bar{q}_ϕ ($10^{-6} s^{-1} rad^{-1}$), (e) U5 E-P flux, (f) P10 E-P flux, (g) U5 $\overline{u'v'}$ and (h) P10 $\overline{u'v'}$.

In U5 the stratosphere is heated uniformly at all latitudes. As a result the vertical temperature gradient changes at all latitudes and the anomalous \bar{q}_ϕ has a greater meridional extent than in either of the other experiments. In P10 the change in \bar{q}_ϕ is largest in the polar regions whereas in the E5 run it is largest at lower latitudes in association with where the vertical temperature gradient is changing the most.

Figs. 4.18 (e) and (f) then demonstrate that the reduced upward E-P flux occurs in the region where the PV gradient is most changed. Therefore U5 shows a more latitudinally uniform decrease in upward E-P flux than either P10 or E5 in which the change is largest at high or low latitudes respectively. The spatial correspondence between the reduction in vertical E-P flux and the change in \bar{q}_ϕ arises through both the change in refractive index and the direct dependence of vertical E-P flux on static stability.

The different locations of the reduced vertical E-P flux between different experiments then result in different locations of the change in horizontal eddy momentum flux as can be seen in Figs. 4.18 (g) and (h). Both experiments show a dipole change in eddy momentum flux but with the maxima and minima occurring at slightly different latitudes. As U5 shows a fairly uniform weakening in upward E-P flux, the eddy momentum flux anomalies are simply a weakening of the control run eddy momentum flux around the tropopause but with a slight equatorward displacement of the zero line. In P10 the weakening of the upward E-P flux is stronger at higher latitudes and so the strength of the anomalies in eddy momentum flux are biased toward higher latitudes compared to U5.

So, through the different latitudinal extents of the applied temperature perturbation and corresponding change in vertical temperature gradient there are different latitudinal locations of the strongest weakening of the upward eddy propagation and corresponding eddy momentum flux changes between experiments. The different locations of anomalous horizontal eddy momentum flux in each experiment lead to different latitudinal extents of the regions of anomalous momentum flux convergence/divergence and hence of

initial zonal wind accelerations/decelerations around the tropopause and direct/indirect meridional circulations changes. This can be seen in Fig. 4.19 which shows the $\overline{u'v'}$, $\overline{\psi}$ and \overline{u} anomalies for days 20 to 29 of the U5 and P10 spin-ups.

As in E5, the locations of the anomalous direct/indirect circulations and

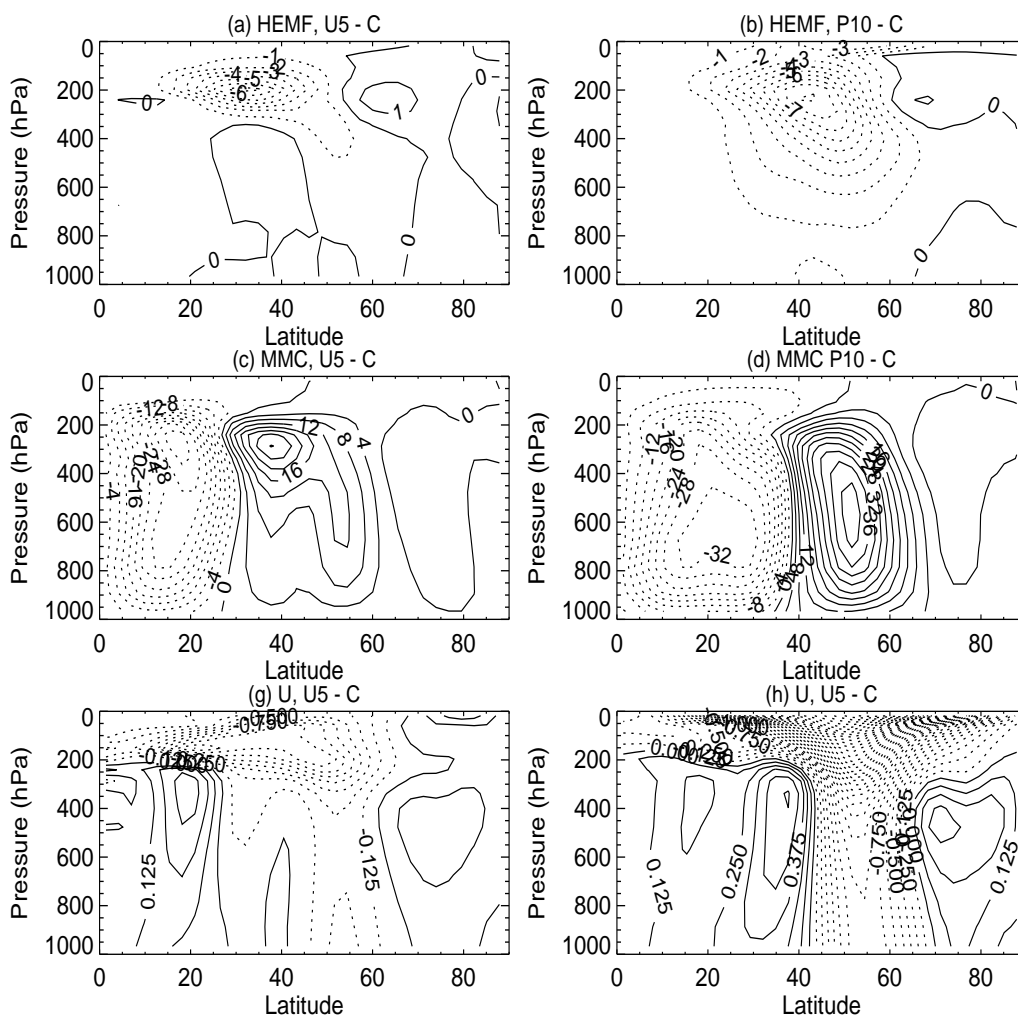


Fig. 4.19: Difference between days 20 to 29 of the spin-up and the equivalent control run values for (a) U5 $\overline{u'v'}$, (b) P10 $\overline{u'v'}$, (c) U5 $\overline{\psi}$ (10^8 kgs^{-1}), (d) P10 $\overline{\psi}$, (e) U5 \overline{u} and (f) P10 \overline{u} .

deceleration/acceleration of zonal wind correspond to the latitudes of eddy momentum flux divergence/convergence around the tropopause. The maximum decrease in eddy momentum flux occurs at a slightly higher latitude in P10 than in U5. Therefore the anomalous indirect circulation at low latitudes has a slightly larger latitudinal extent in P10 than in U5. Comparing Fig. 4.19 with the corresponding plots for E5 (Figs 4.2 and 4.3), it can be seen that in both U5 and P10 the negative part of the dipole extends up to higher latitudes than in E5 and there is an increase in $\overline{u'v'}$ which occurs at a much higher latitude than the positive part of the dipole in E5. As a result, the region of increased divergence of eddy momentum flux which is responsible for the anomalous direct circulation in mid-latitudes has a much greater latitudinal extent in U5 and P10 than in E5. The anomalous direct circulation extends between ~ 30 and $\sim 65^\circ$ latitude in U5 compared ~ 25 to $\sim 45^\circ$ latitude in E5. As a result the decreased zonal wind only stretches between around 25 and 45° latitude in E5 whereas during days 20 to 29 there is a decreased zonal wind between around 25 and 65° latitude in U5.

In P10, as the eddy momentum flux anomalies are localised to higher latitudes, the region of eddy momentum flux convergence stretches only between around 40 and 70° latitude and so the decreased zonal wind anomaly is occurring more on the poleward side of the jet than in E5 or U5.

Thus, through the different latitudinal extents of the applied heating perturbation and weakened upward E-P flux, there are different latitudinal locations of the regions of eddy momentum flux convergence/divergence. This then results in different latitudinal locations and extents of the various mean meridional circulation and zonal wind anomalies.

Fig. 4.20 then demonstrates that the feedback involving tropospheric eddy momentum flux anomalies is also occurring in the U5 and P10 experiments. Due to the different latitudinal extents of the zonal wind anomalies it is occurring in the opposite sense to that in E5 but in the correct sense to be further accelerating the zonal wind anomalies produced at the start of the U5 and P10 spin-ups.

Focussing first on P10. The zonal wind anomalies consist of a decreased westerly wind between ~ 40 and 70° latitude and an increased westerly wind anomaly equatorward of $\sim 40^\circ$ latitude. The dependence of n^2 on $1/(\bar{u} - c)$ results in these zonal wind anomalies producing an increased n^2 on the poleward side of the jet and a decrease on the equatorward side i.e. in the opposite sense to E5. This results in a poleward refraction of the E-P flux across the mid-latitudes and a corresponding decrease in eddy momentum flux throughout the mid-latitude troposphere with a maximum around 45° latitude. This therefore results in an increased divergence poleward of around 45° latitude resulting in a deceleration of the zonal wind and vice-versa equatorward of 45° latitude i.e. a feedback on the tropospheric zonal wind anomalies.

In U5, by days 40 to 49 the changes in tropospheric eddy momentum flux are not as strong and they are not completely acting to feedback on the initial zonal wind changes. The initial zonal wind anomalies produced in response to the altered eddy momentum flux anomalies around the tropopause do not result in as strong a gradient in \bar{u} across the jet latitude as in E5 and P10. Rather they are acting to decelerate the zonal wind across the whole of the mid-latitude region (i.e. between around 30 and 60° latitude). This is unlike the E5 and P10 runs where the initial wind anomalies change sign over the region of the jet center ($\sim 45^\circ$ latitude). Thus the initial U5 wind anomalies are less effective at creating this strong meridional gradient in n^2 across the jet centre and so are less effective initially at producing the tropospheric feedback. However, some poleward refraction can be seen toward the maximum in n^2 on the poleward side of the jet in the troposphere associated with the zonal wind decrease there. The tropospheric eddy momentum flux changes are not completely feeding back on the zonal wind anomalies. There is an increased convergence of eddy momentum flux around 40 to 45° latitude where the zonal wind has actually decreased. This results in an acceleration of the zonal wind there. Comparing the U5 zonal wind anomalies in Fig. 4.20 with the equilibrium response in Fig. 4.1, they can be seen to be quite different.

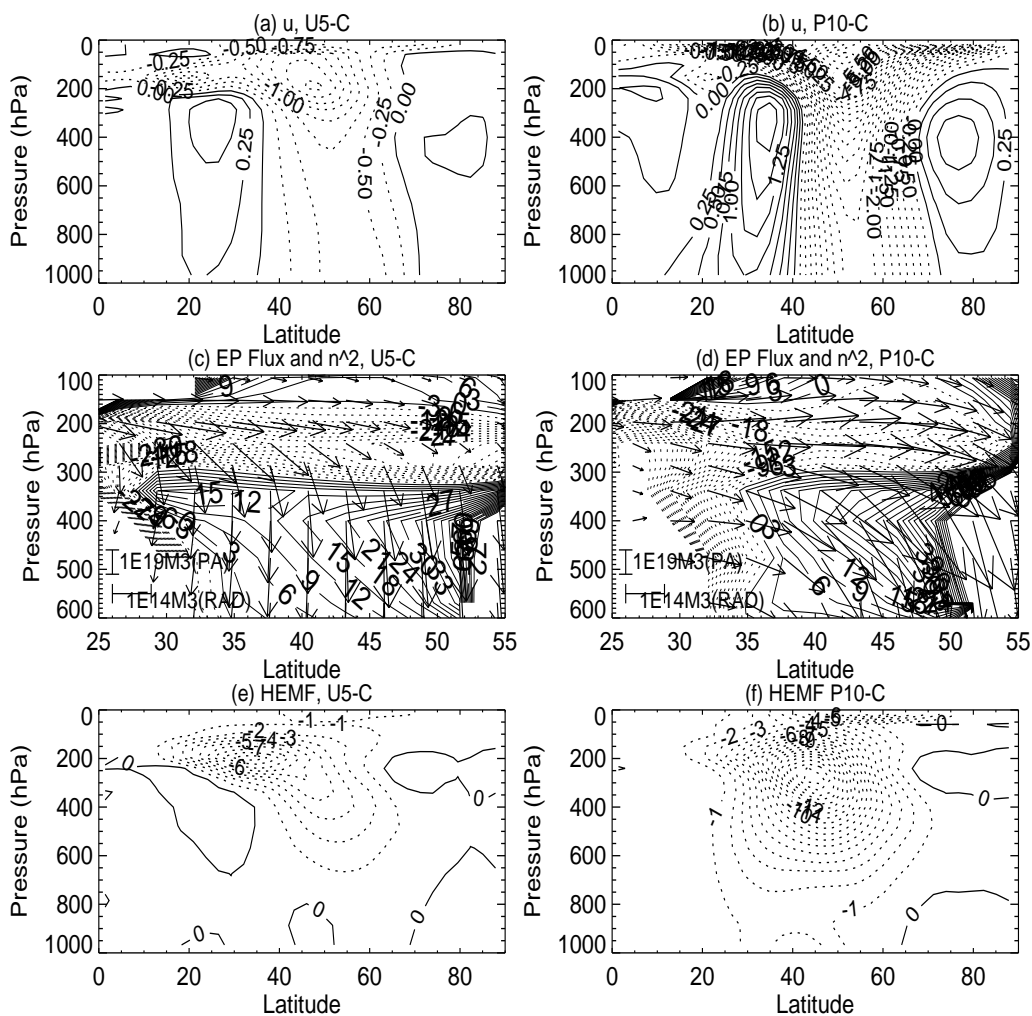


Fig. 4.20: Difference between days 40 to 49 and the equivalent 10 days of the control run for (a) U5 \bar{u} , (b) P10 \bar{u} , (c) U5 E-P flux and n^2 , (d) P10 E-P flux and n^2 , (e) U5 $\overline{u'v'}$ and (f) P10 $\overline{u'v'}$.

By equilibrium the response is a lot more annular mode-like with an increased westerly wind equatorward of $\sim 45^\circ$ latitude and a decrease poleward of this. In fact, by equilibrium the U5 and P10 zonal wind responses look rather similar. It seems that the tropospheric eddy momentum flux changes are acting to migrate the increased westerly wind on the equatorward side of

the jet poleward. The positive wind anomaly is centred around 25° latitude during days 20 to 29 but by equilibrium it is centred around 35° latitude. As this wind anomaly migrates poleward it will become more effective at producing a strong meridional gradient in n^2 across the jet centre and the tropospheric eddy momentum flux anomalies become larger.

The analysis above of the U5 and P10 experiments has confirmed that the same processes as found for E5 are acting to produce the tropospheric anomalies. Moreover, it has shown how the direction of the jet shift depends on the latitudinal extent of the applied heating perturbations. Different latitudinal locations of the heating perturbation result in different latitudinal locations of the change in vertical temperature gradient. This localises the weakening of the upward eddy propagation which then results in different locations of the strongest change in eddy momentum flux. As a result the latitudes at which there is eddy momentum flux convergence/divergence differ between runs and thus the latitudes of anomalous direct/indirect circulation and zonal wind deceleration/acceleration differ. This results in different tropospheric eddy momentum flux feedbacks which act to accelerate the zonal wind anomalies further and/or make them more annular mode like.

4.4 *Discussion and Conclusion*

The results of HBD05 and several other authors (Kushner & Polvani, 2004, 2006; Polvani & Kushner, 2002; Williams, 2006; Lorenz & DeWeaver, 2007) have demonstrated that heating perturbations applied to the stratospheres of simplified GCM's result in annular mode - like responses in the troposphere i.e. they result in anomalous wind speeds of opposite sign on the equatorward and poleward side of the time mean jet with accompanying tropospheric temperature and mean meridional circulation anomalies. Here, we have taken the analysis a step further by using spin-up ensembles to look at the evolution of the model in response to stratospheric heating to determine the mechanisms involved in producing the tropospheric response and determine

the factors controlling the direction of the tropospheric jet shift.

The analysis of the model results, described above, leads us to propose the following mechanism (summarised in Fig. 4.21) whereby thermal perturbations to the stratosphere influence tropospheric circulation: Heating the stratosphere causes the vertical and meridional temperature gradients around the tropopause region to change. Changes in vertical shear and curvature of the zonal wind, associated with the change in meridional temperature gradient, alter the meridional PV gradient around the tropopause. But, more importantly, the change in vertical temperature gradient has a direct effect on the meridional PV gradient. This produces a change in refractive index which influences eddy propagation. Specifically, there is a reduced vertical gradient of n^2 in the upper troposphere/tropopause region which weakens the upward propagation of eddy activity. In fact this initial change can be identified directly through the definition of vertical E-P flux without the need for refractive index. It has been demonstrated that a large fraction of the initial weakening of the upward E-P flux occurs directly through the change in vertical temperature gradient within the definition of E-P flux. This result is consistent with the analysis of refractive index and the dominant cause of this change in refractive index.

The initial change in eddy propagation results in eddy momentum flux anomalies which act to drive changes in the zonal wind locally around the tropopause and in the upper troposphere. They also drive anomalous meridional circulations which result in zonal wind and temperature changes throughout the troposphere. These tropospheric zonal wind changes alter the refractive index in a local positive feedback as follows. Reduced zonal wind increases the ambient positive refractive index, since the term $(\bar{u} - c)$ appears in the denominator of n^2 . Wave activity is then refracted toward that latitude, increasing the E-P flux convergence which drives further easterly acceleration (and vice-versa for westerly anomalies). The spreading of zonal wind anomalies throughout the depth of the troposphere also creates an implicit feedback. An easterly anomaly with easterly vertical shear reduces

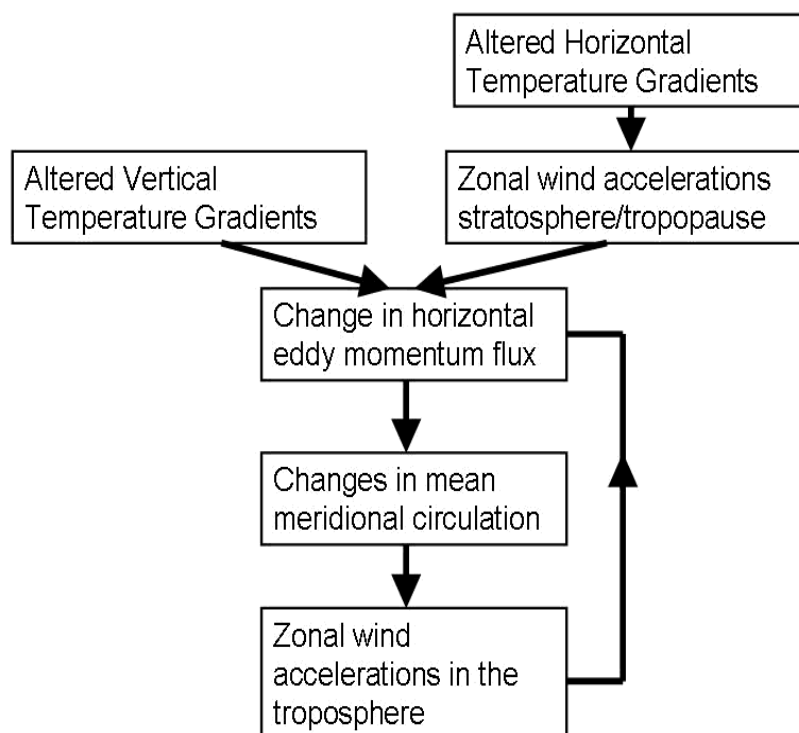


Fig. 4.21: Summary of the mechanism proposed for the production of tropospheric circulation changes in response to stratospheric heating perturbations.

the local baroclinicity: this weakens the E-P flux source and thus weakens the eddy forcing of westerly flow at that latitude. This is analogous to the mechanism proposed by Lorenz & Hartmann (2003) and Robinson (2000) to explain the persistence of annular mode variability. Both of these mechanisms cause the eddies to provide a positive feedback on displacements of the mid-latitude jet.

It is interesting that each of the heating perturbations produce an annular mode-like response. In particular that the U5 and P10 responses end up looking rather similar when they start of quite differently at the beginning of the spin-up. The U5 response starts with a weakened westerly wind over most of the mid-latitude region with no change in sign of the wind anomalies

around the jet centre as in the E5 and P10 runs. But, then the tropospheric eddy feedback results in a poleward migration of the zonal wind anomaly at low latitudes to make the U5 response more annular mode - like. It seems that the initial changes in eddy momentum flux around the tropopause result in a small perturbation in the troposphere which then starts off this tropospheric feedback resulting in a strong annular mode - like response to any perturbation in stratospheric temperature. Perhaps this is not surprising as the annular mode is the dominant mode of variability in the mid-latitudes and so is clearly the preferred way for the circulation to shift in response to perturbations. It could be predicted from the above results that any heating perturbation produces an annular mode - like response, the sign of which depends on the latitudinal extent of the applied heating perturbation. Heating preferentially at lower latitudes produces a poleward shift of the jet whereas uniform heating or heating preferentially at higher latitudes results in an equatorward shift of the jet.

The importance of changes in eddy momentum flux around the tropopause region in driving the tropospheric response has been demonstrated by the 3D spin-up experiments and has been confirmed by the lack of response in the troposphere of the zonally symmetric model with fixed eddy forcing. The requirement for a feedback involving tropospheric eddy momentum fluxes to produce the full zonal wind anomalies is in agreement with several previous studies (Polvani & Kushner, 2002; Kushner & Polvani, 2004, 2006; Song & Robinson, 2004). The idea of tropospheric eddy feedbacks has been developed further in this study by using the refractive index to show that, as the zonal wind changes in the troposphere, it results in meridional gradients of refractive index in the troposphere to produce changes in tropospheric eddy momentum fluxes which act to enhance the annular mode - like anomalies.

There has been some debate as to whether the refractive index can be used to predict wave behaviour when the waves are not strictly in the WKB limit. However, several authors have demonstrated that the refractive index can give useful predictions as to the behaviour of waves even when the

WKB conditions do not strictly apply (Chen & Robinson, 1992; Hartmann & Zuercher, 1998; Lorenz & Hartmann, 2003). Moreover, it has been demonstrated in Figs. 4.14 and 4.17 that the refractive index in these results is consistent with the altered E-P flux and so is useful in predicting the changes in eddy propagation in the mid-latitude upper troposphere/tropopause region.

The model used here differs from some previous studies, such as those of Kushner & Polvani (2004, 2006), in that it does not have a stratospheric polar vortex but still produces a significant tropospheric response to stratospheric heating perturbations. Furthermore, as there is no large scale zonally asymmetric forcing in our model, planetary waves are weak and eddy forced. The dominant wavenumbers are 5-7. The results therefore confirm the possibility that smaller scale baroclinic eddies alone can produce a tropospheric response to stratospheric heating perturbations, although larger scale planetary waves may play a role in other modelling studies and in the real atmosphere. A mechanism by which the tropospheric response can be produced by small scale baroclinic eddies is also consistent with observed signals that are symmetric about the equator and/or seen in all seasons, such as the zonal wind and temperature response observed over the solar cycle (Haigh (2003) and HBD05).

Moreover, the results suggest that it is a change in eddy propagation near the eddy source latitudes that is important in producing the jet displacement rather than a process affecting the critical latitude of eddy breaking in the subtropics. Following the results of Chen *et al.* (2007) who showed the importance of a change in eddy phase speed in the poleward shift of mid-latitude westerlies in response to reduced surface friction, Chen & Held (2007) have suggested that a similar mechanism could produce a tropospheric response to stratospheric zonal wind anomalies. By this hypothesis, changes in lower stratospheric and upper tropospheric zonal wind could produce a shift in the mid-latitude jet through a shift in the region of sub-tropical wave breaking caused by a change in phase speed. However, Chen & Held (2007) state that the question still remains as to whether the shift in phase speed is a conse-

quence or a cause of the tropospheric circulation changes. In our experiments a change in phase speed shifting the critical line does not appear to be an important factor in producing the tropospheric response. However, a change in phase speed as found by the time that equilibrium is reached which leads us to believe that the shift in phase speed is a consequence rather than a cause of the tropospheric circulation changes.

The primary aim of these experiments was to study how the response to changing solar activity could be produced in the troposphere but our results could equally apply to other situations where a heating or cooling perturbation is applied to the stratosphere. For example, Lorenz & DeWeaver (2007) showed, in model studies investigating the response to stratospheric cooling, that a complete understanding of the mechanisms involved must consider both the effects of the change in vertical temperature gradient and the change in horizontal temperature gradient. Our results have confirmed this since the change in vertical temperature gradient and how it is localised in latitude is key to the latitudinal distribution of the response and therefore the direction of meridional jet displacement.

With regards to the solar cycle response, the above has presented a mechanism whereby the tropospheric circulation changes could be produced in response to heating of the equatorial lower stratosphere. HBD05 have demonstrated that a qualitatively similar pattern to that seen in the data over the solar cycle is produced by heating of the equatorial lower stratosphere in the model. A 5K heating perturbation is considerably larger than that seen in the equatorial lower stratosphere over the solar cycle. However, HBD05 showed that a similar pattern of response is produced with a more realistic 1K perturbation with the magnitude of the tropospheric response scaling almost linearly with the magnitude of the applied heating perturbation. Clearly we are not attempting to simulate exactly the tropospheric response to changing solar activity given the simplicity of the model and the applied heating perturbation. Rather, we are investigating the mechanisms involved in producing the tropospheric response to perturbations in lower stratospheric

temperature. However, a concern may arise if we do attempt to compare the magnitude of the model response to the magnitude of the tropospheric response found in the data. Comparing the magnitude of the zonal wind and temperature response to E5 heating (Fig. 4.1) with the solar cycle signal in zonal wind and temperature (Figs. 1.6 and 1.7) and scaling the magnitude of the model response down by e.g. a factor of five, it can be seen that the magnitude of the model tropospheric response is not quite comparable to that seen in the data. For example the model shows a maximum zonal wind anomaly (when scaled down by 5) of around 0.5ms^{-1} at the surface on the poleward side of the jet compared to around 1ms^{-1} seen in the data. There is an even larger difference in the temperature response. The banded increase in temperature in the mid-latitude troposphere in the data is approximately the same as the E5 response. i.e. scaling down the E5 heating perturbation to more realistic values means the tropospheric temperature response is about one fifth of the magnitude seen in the data. There are many possible reasons for the differences in the magnitudes of response. First and foremost, the simplifications in the model such as the lack of moisture. However, it will be shown in Chapter 6 that there is a very strong dependence of the magnitude of the tropospheric response on the state of the troposphere. By having a slightly different structure of tropospheric jet, a response can be produced which is of more comparable magnitude to that seen in the data.

Another concern with using simplified GCM's with zonally symmetric boundary conditions is that they can be overly sensitive to external forcing. Gerber & Vallis (2007) and Gerber *et al.* (2008) have shown that these models can have unrealistically long annular mode decorrelation timescales compared to the real atmosphere. This can lead to them being overly sensitive to external forcing, as implied by the fluctuation-dissipation theorem (Leith, 1975). The sensitivity of the results to the introduction of zonal asymmetries will be investigated in Chapter 5.

To summarise the results of this chapter: HBD05 have demonstrated that tropospheric circulation changes, similar in nature to those seen over the so-

lar cycle, can be produced by heating the stratosphere of a simplified GCM preferentially over the equatorial region. Here, we have investigated the mechanism by which such a response is produced and have demonstrated the importance of changes in eddy momentum flux in driving the tropospheric response and of the presence of tropospheric eddy feedbacks on the zonal wind anomalies. The quasi-geostrophic refractive index has demonstrated the initial importance of altered vertical temperature gradient and, to a lesser extent, vertical wind shear, in changing the eddy momentum flux. Furthermore, it has shown that the tropospheric zonal wind anomalies act to refract the eddies there to produce the tropospheric eddy momentum flux feedback. Comparison of three different heating perturbation experiments has shown that the change in vertical temperature gradient and how it is localised in latitude are key to determining the direction of the tropospheric jet shift.

5. ZONALLY ASYMMETRIC BOUNDARY CONDITIONS

In the following chapter, the effect of introducing zonally asymmetric boundary conditions on the model response to E5 stratospheric heating will be investigated (experiments described in section 3.2.2). Specifically, the effect of introducing a zonally asymmetric tropospheric relaxation temperature profile in the form of the Q experiments and the effect of introducing topography in the form of the R experiments will be examined.

The reason for doing these experiments is that the real atmosphere is indeed zonally asymmetric, particularly in the Northern hemisphere, with the presence of topography and land-sea temperature contrasts. It is therefore useful to check whether the processes found to be responsible for the production of the tropospheric response in chapter 4 still hold in the presence of zonal asymmetries which bring the simplified GCM a step closer to the real atmosphere. Clearly the simplified asymmetries used here cannot be compared with the complex topography and land-sea temperature contrast of the real Earth but it is still useful as a first check that the tropospheric response holds in the presence of some form of zonal asymmetry.

Another one of the main motivations for doing this comes from the work of Gerber & Vallis (2007). As has previously been discussed, there is a close relationship between a model's response to a forcing and the timescale of its unforced internal variability (Leith, 1975; Gerber & Vallis, 2007; Ring & Plumb, 2008). Gerber & Vallis (2007) find that simplified GCMs with zonally symmetric boundary conditions have unrealistically long e-folding timescales of the autocorrelation of the model's annular mode. As a consequence they may be overly sensitive to a forcing which projects onto that annular mode. It is found that the introduction of zonal asymmetries (particularly topog-

raphy) reduces the decorrelation timescale to more realistic values implying that it may also reduce the magnitude of the annular mode-like response to stratospheric heating.

Initially, experiments were performed for 5000 days for the Q experiment and 10000 days for the R experiment (as the R experiment cannot be averaged over both hemispheres). However, these experiments, rather than giving any conclusions about the effect of zonal asymmetries on the model response, have elucidated the need for much longer runs to accurately determine the magnitude of response to stratospheric heating. In light of the results of these runs, much longer integrations of 50 000 days have been used to investigate whether the introduction of zonal asymmetries does have an influence on the response to stratospheric heating. The data for these long runs have been provided by Fenwick Cooper, DAMTP, University of Cambridge.

However, even with these long runs there is still uncertainty as to the magnitude of response. In short the results show that the introduction of zonal asymmetries does not have a dramatic effect on the response to stratospheric heating. Qualitatively similar patterns of response are found in both the Q and R experiments. If the statistics of the results of the 50 000 day runs are reliable, there is a slight decrease in the magnitude of response in the presence of asymmetries but, given the large amount of variability present in the response, it is difficult to say this with certainty and it is definitely not possible to assign a value to the difference in the magnitudes of response between the different experiments.

The structure of this chapter will therefore be as follows: first the effect of the zonal asymmetries on the control run troposphere will be discussed. Then there will be a discussion of the issues of accurately determining the magnitude of response with model runs of 5000 and 10000 days. This will be followed by an examination of the zonal mean magnitude of response to stratospheric heating for the 50000 day runs.

5.1 The control run simulations

5.1.1 The Q control run

In order to introduce zonally asymmetric boundary conditions into the model, a quadrupole change in the tropospheric relaxation temperature profile has been introduced of the form shown in Fig. 3.5 and given by equation 3.6. Between -180° and 0° (referred to as the left hand (LH) hemisphere hereafter) this consists of a weakening of the meridional temperature gradient across the mid-latitudes and a strengthening of it in the subtropical and subpolar regions. Between 0 and 180° (referred to as the right hand (RH) hemisphere hereafter) the change in T_{ref} is opposite, i.e. a weakening of the meridional temperature gradient in the mid-latitudes and a strengthening of it in the sub-tropical and sub-polar regions. The magnitude of the change to T_{ref} falls off with $(p/p_o)^\kappa$.

Fig. 5.1 shows latitude-longitude cross sections of surface temperature and zonal wind at the 286hPa level for the Q run as well as the anomalies from the original C control run. It can be seen from Fig. 5.1 (a) that the perturbation to T_{ref} has been effective at increasing the mid-latitude baroclinicity, (i.e. the increase in the latitudinal temperature gradient) in the RH hemisphere and decreasing it in the LH hemisphere. However, the difference in surface temperature between the Q run and the original control run demonstrates that the amplitude of the temperature change is considerably lower than the applied change in T_{ref} (See Fig. 3.5 (a)). This is due to advection of the temperature anomalies, predominantly in the zonal direction, acting to spread out and cancel the temperature anomalies. Hence, the reason for applying a perturbation of amplitude 15K. This increased meridional temperature gradient in the RH hemisphere and decrease in the LH hemisphere is found throughout the troposphere but with decreasing magnitude with increasing height corresponding to the decrease in the magnitude of the applied perturbation to T_{ref} with increasing height.

Figs. 5.1 (c) and (d) demonstrate that the zonal wind speed at 286hPa in

the mid-latitudes is increased in the RH hemisphere and decreased in the LH hemisphere relative to the original control run. The peak zonal wind speed in the RH hemisphere is around 36ms^{-1} , around 10ms^{-1} faster than the peak wind speed in most of the LH hemisphere. This pattern of stronger westerly winds in the RH hemisphere and weaker westerlies in the LH hemisphere is consistently found throughout the whole of the troposphere although the difference in peak wind speed between the two hemispheres decreases at lower levels. There is also a general decrease in zonal wind at the lowest and highest latitudes in the RH hemisphere and vice-versa in the LH hemisphere.

Thus, the application of this zonally asymmetric perturbation to T_{ref} breaks up the jet into a storm track region with increased westerly wind in the RH hemisphere and decreased in the LH hemisphere. This is further confirmed by examination of the eddy statistics.

Fig. 5.2 presents latitude-longitude cross-sections of the transient horizontal eddy heat flux [v^*T^*] on the 784hPa level, the transient eddy kinetic energy [$1/2(u^{*2} + v^{*2})$] on the 286hPa level and the transient horizontal eddy momentum flux [u^*v^*], also on the 286hPa level. The horizontal eddy heat flux shows a significant difference between the LH and the RH hemispheres. In the RH hemisphere, consistent with the enhanced mid-latitude baroclinicity, there is a much greater poleward eddy heat flux compared to the LH hemisphere. This is true at all pressure levels in the troposphere. This enhanced poleward eddy heat flux is what would be expected from a storm track region with enhanced baroclinicity and thus increased eddy growth rate and vertical eddy propagation.

Consistent with a lifecycle view of baroclinic eddies (see e.g. Orlandi & Gross (2000)), the maximum in eddy kinetic energy is found downstream of the maximum in poleward eddy heat flux. Again, this is true of all pressure levels in the troposphere. So eddies are formed in the region of strong meridional temperature gradient but then as they grow and obtain their maximum kinetic energy they are being advected downstream by the mean westerly flow. The eddy kinetic energy at 286hPa is about twice as large at

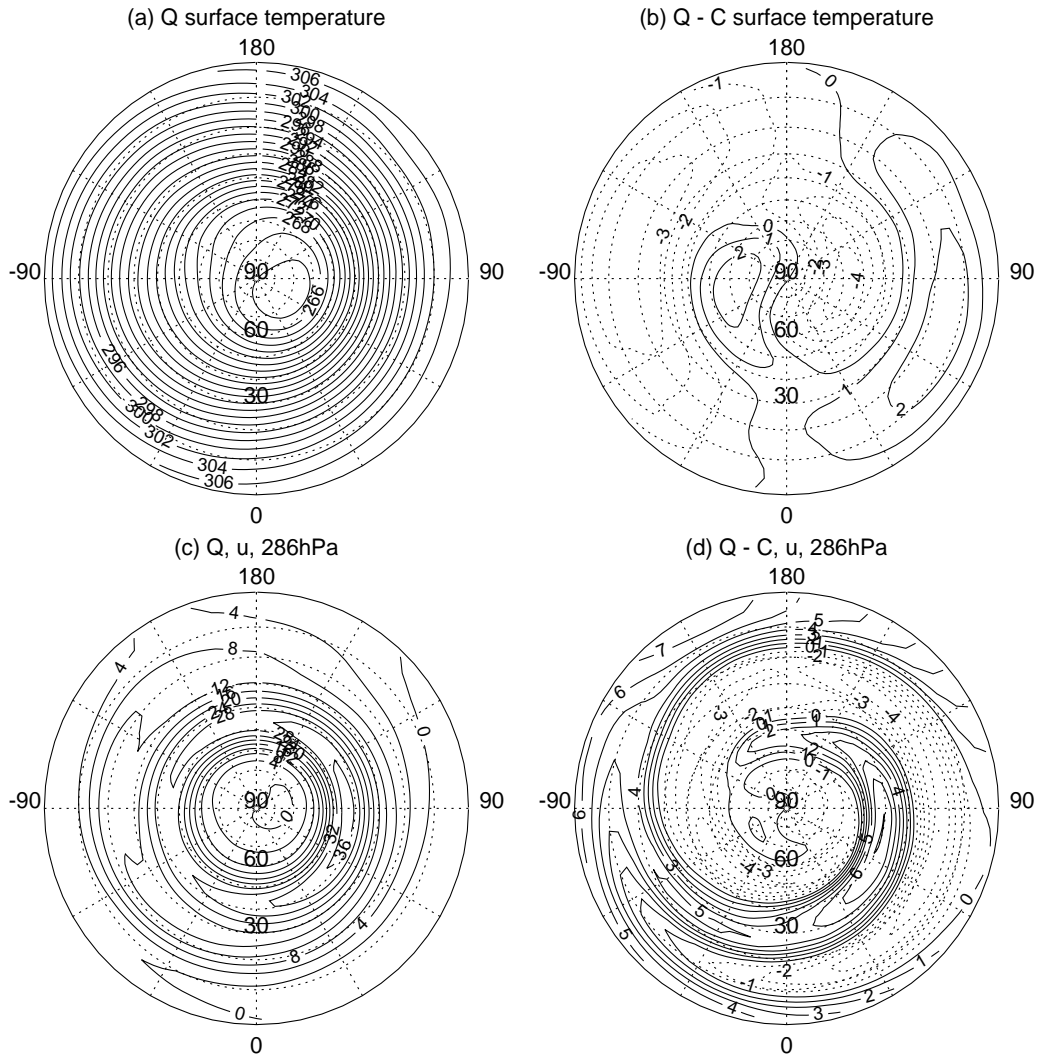


Fig. 5.1: (a) Q control run surface temperature (K), (b) difference in surface temperature between the Q control run and the C control run, (c) as (a) but for zonal wind (ms^{-1}) at the 286hPa level, (d) as (b) but for the zonal wind (ms^{-1}) at the 286hPa level.

$\sim 180^\circ$ longitude than at $\sim 0^\circ$ longitude.

Perhaps surprisingly, despite the zonal asymmetry in the locations of eddy production and maximum eddy kinetic energy, the poleward eddy momentum flux at upper levels is fairly zonally uniform. It seems that by the

time the eddies have reached the decay stage characterised by strong eddy momentum fluxes, advection by the mean flow has acted to smooth out the zonal asymmetry that is apparent in the eddy growth regions.

Thus, the introduction of this quadrupole perturbation in tropospheric

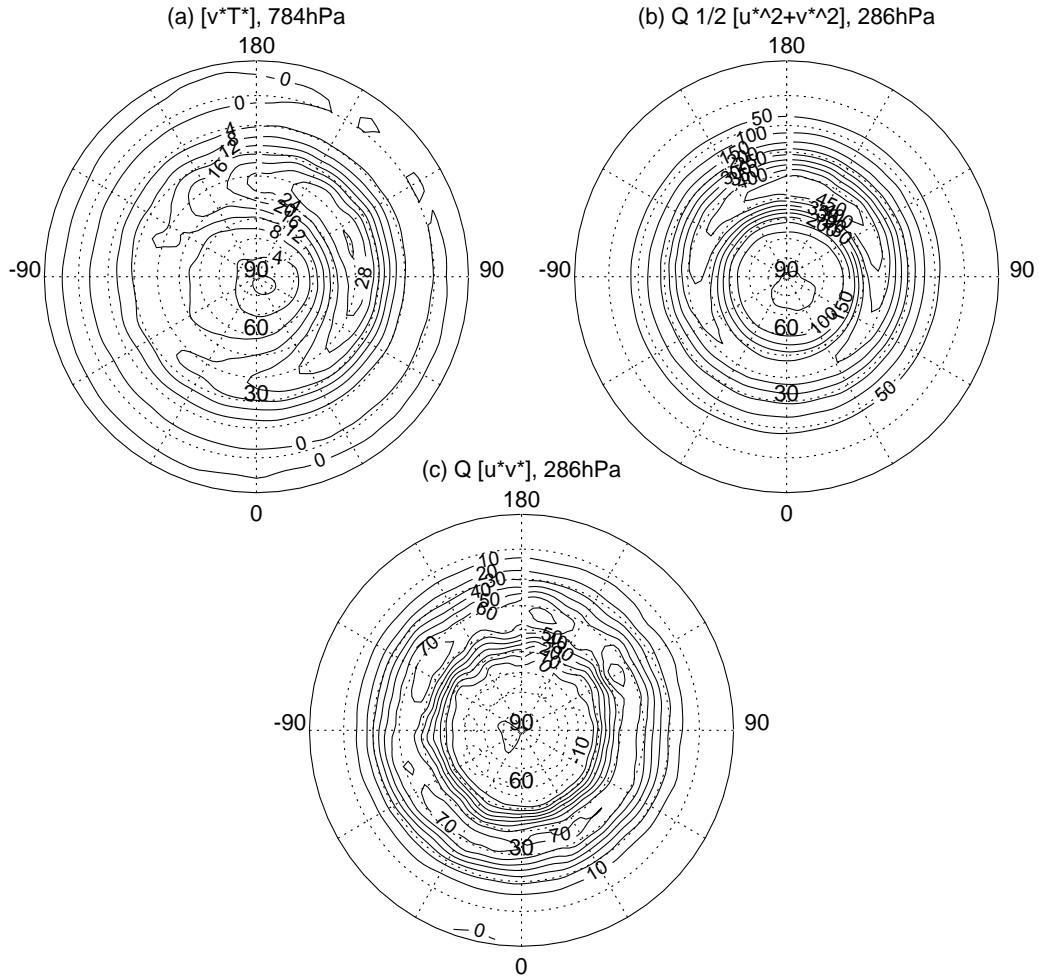


Fig. 5.2: Transient eddy fields for the average of the Q control run. (a) transient poleward eddy heat flux (Kms^{-1}) on the 784hPa level, (b) transient eddy kinetic energy (m^2s^{-2}) on the 286hPa level and (c) transient poleward eddy momentum flux (m^2s^{-2}) on the 286hPa level.

T_{ref} seems to have been effective at introducing a storm track region in the RH hemisphere with stronger zonal wind speeds and much greater baroclinic eddy production and poleward eddy heat flux. It has also been effective at localising the eddy kinetic energy. However, despite this, it has not been very effective at localising the horizontal eddy momentum flux.

5.1.2 The R control run

The second experiment that has been performed to investigate the effect of zonally asymmetric boundary conditions on the model response to stratospheric heating is the introduction of topography. A 2000m high ridge has been placed in the Northern hemisphere centred on 0° longitude and 45° latitude as described in section 3.2.2. This is similar to the ridge used in the experiments of Gerber & Vallis (2008) to investigate the effect of topography on their models internal intraseasonal variability. As the model is no longer symmetric about the equator the number of data points can no longer be doubled by averaging over both hemispheres. Both the control run and E5 integrations were therefore initially run for 10000 days to be comparable to the 2 hemispheres of the 5000 day equilibrium runs of Chapter 4.

When Gerber *et al.* (2008) and Gerber & Vallis (2008) investigated the effect of zonal asymmetries on the internal variability of their GCM it was found that the topography in particular was efficient at reducing the annular mode autocorrelation timescale to more realistic values. Moreover, it was found that the overall strength of the annular mode patterns was around 30% larger in the runs without topography even when land-sea temperature contrast was present (Gerber & Vallis, 2008). They suggest that the presence of topography breaks up and weakens the eddy-mean flow interaction preventing hemispheric scale motions of the jet. Thus, it may be expected that topography will have a more dramatic effect on the tropospheric response to stratospheric heating than does the land-sea temperature contrast.

Fig. 5.3 shows latitude-longitude cross-sections of the control run mean zonal wind at 240hPa and the temperature at 967hPa when including topography. Values have been interpolated from model sigma levels onto pressure levels.

The introduction of topography has had the effect of breaking up the zonal symmetry of the mid-latitude westerly jet. There is a reduced zonal wind speed over the topography with enhanced zonal wind downstream of it. This region of enhanced zonal wind has a meridional tilt from South-West to North-East. A similar structure of zonal wind is found at all heights but the magnitude of the downstream enhancement decreases as you go into the stratosphere and as you go down to higher pressures. Thus there is an enhanced vertical wind shear downstream of the topography which is consistent with the increased meridional temperature gradient there (Fig. 5.3 (b)). The zonal wind contours also hint at the presence of a standing wave introduced by the topography e.g. the 8 and 12 ms^{-1} contours show quite a pronounced wave structure downstream of the topography.

Fig. 5.4 examines the transient eddy fluxes of the R control run. Fig. 5.4

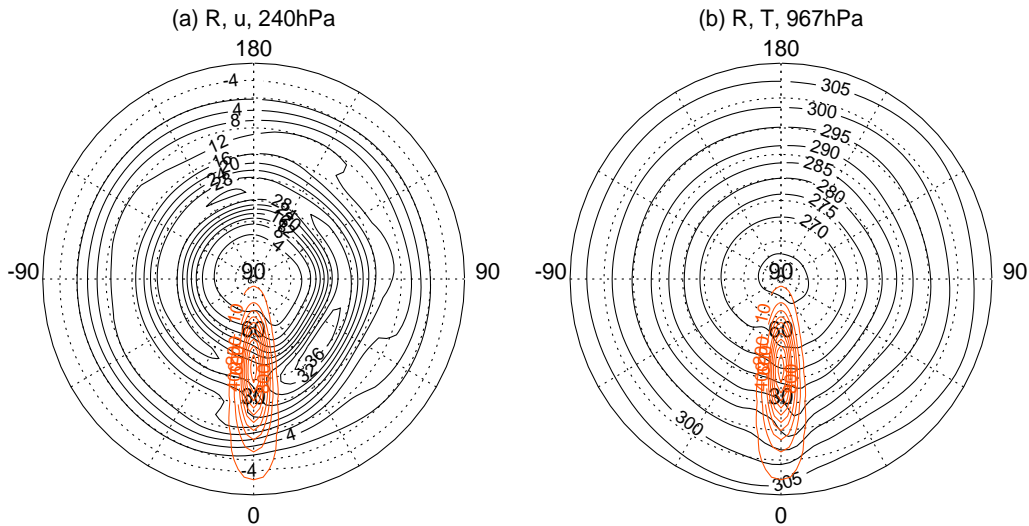


Fig. 5.3: (a) Control run zonal wind (ms^{-1}) on the 240hPa level and (b) control run temperature (K) on the 967hPa level. Orographic height is overplotted in Red.

(a) presents the horizontal eddy heat flux on the 784hPa level. In agreement with the findings of Gerber & Vallis (2008), the standing wave generated by the topography localises the baroclinicity (and thus eddy growth and horizontal eddy heat flux). It creates several maxima in $[v^*T^*]$ with decreasing

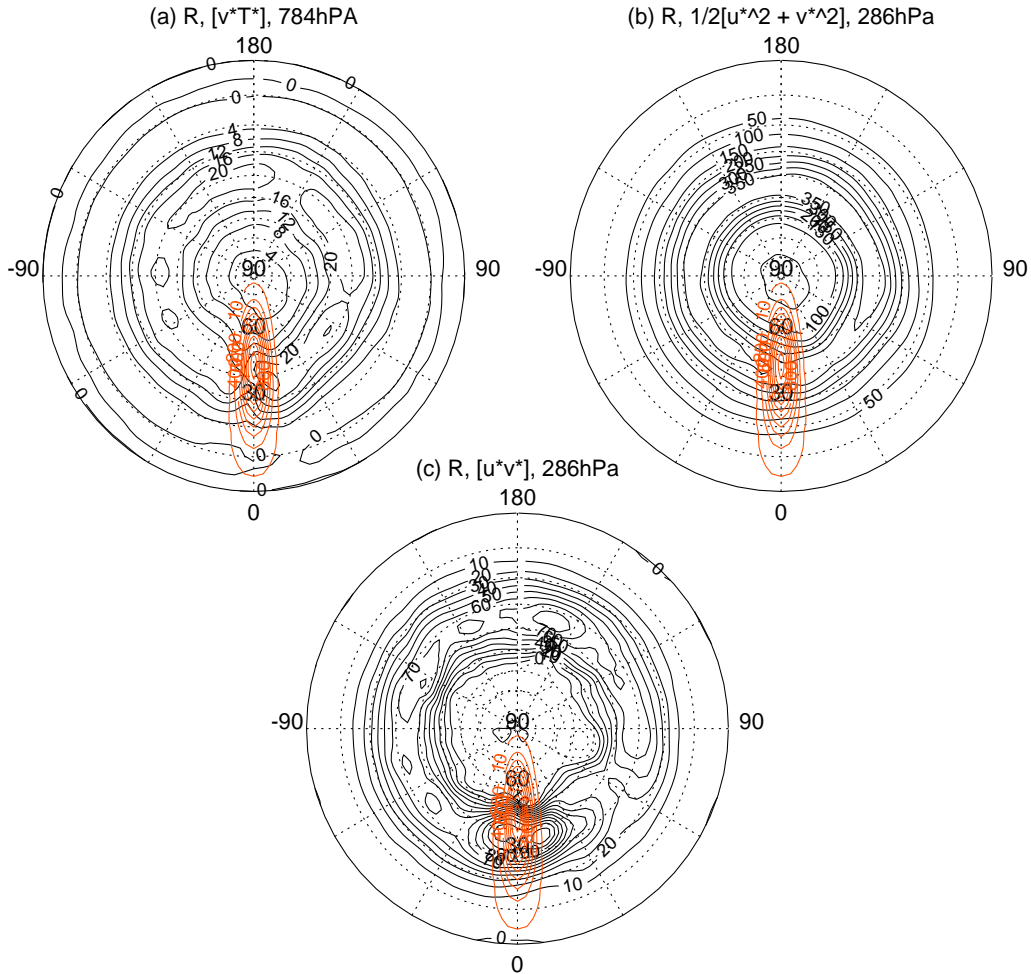


Fig. 5.4: (a) Control run transient horizontal eddy heat flux (Kms^{-1}) on the 784hPa level, (b) control run transient eddy kinetic energy (m^2s^{-2}) on the 286hPa level and (c) control run transient horizontal eddy momentum flux (m^2s^{-2}) on the 286hPa level. Topographic height is overplotted in Red.

magnitude with distance from the topography as the damping of the standing wave increases. The first peak in $[v^*T^*]$ which occurs $\sim 50^\circ$ downstream of the topography is strongest and this is then followed by a secondary maximum $\sim 110^\circ$ downstream of the topography. Also, in agreement with Gerber & Vallis (2008), despite this localisation in baroclinicity the eddy kinetic energy remains fairly zonally uniform except for a slight reduction just downstream of the ridge (Fig. 5.4 (b)). The most prominent zonal variation in the horizontal eddy momentum flux (Fig. 5.4 (c)) is a maximum occurring over the longitude of the ridge. Gerber & Vallis (2008) suggest this could be due to shearing of the eddies by the standing wave generated by the ridge. Furthermore, they suggest that this breaking of the eddies over the topography prevents them from propagating further downstream and is responsible for the breaking up of the eddy-mean flow interactions which gives rise to the more realistic annular mode autocorrelation timescale. The slight reduction in eddy kinetic energy and horizontal eddy momentum flux that occurs downstream of the topography is consistent with this.

In the following the effect that introducing these zonal asymmetries has on the response to stratospheric heating will be investigated with 50000 day runs. But, first, the issues that these experiments have revealed with accurately determining the magnitudes of response will be discussed.

5.2 *Issues with accurately determining the magnitude of response.*

The initial plan of these experiments was to demonstrate the impact of the zonal asymmetries on the response to stratospheric heating for 10000 days worth of data. Runs of this order of length are commonly used in studies with simplified GCMs, such as this, to look at the control run variability and also the impact of various forcings on the climatology and the application of the fluctuation/dissipation theorem (e.g. Ring & Plumb (2007, 2008); Gerber & Vallis (2007); Gerber *et al.* (2008)). For qualitative examination of the

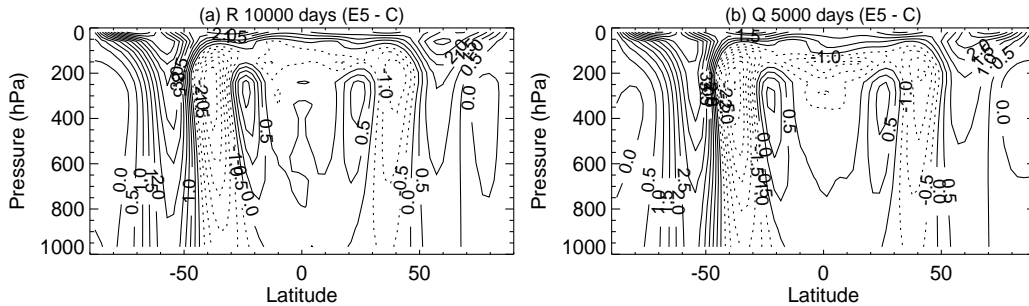


Fig. 5.5: Difference in zonal mean zonal wind (ms^{-1}) between E5 and Control for (a) the 10000day runs with topography and (b) the 5000 day runs with a quadrupole perturbation to T_{ref} .

control run variability or the response to a forcing this length of integration is likely to be sufficient. It is, indeed, found that all 5000 day runs of individual experiments to be presented in this chapter and Chapter 6 show qualitatively similar patterns of response to each other. However, problems arise when accurately determining the magnitude of response as it is found that there is a large amount of variability in the magnitudes between different ensemble members of the same experiment.

The problem can be demonstrated by examination of the zonal wind response to E5 heating for each of the experiments. The equilibrium difference between E5 and Control is shown in Fig. 5.5 for the 10000 day R response and the 5000 day Q response. Focussing first on the response with topography (Fig. 5.5 (a)) and comparing with the equilibrium response for the original model configuration (Fig. 4.1), it can be seen that in the SH where no topography is present there is a very similar magnitude of response as in the original runs, as expected. However, in the NH, where the Gaussian topography has been placed, the response to E5 heating is considerably reduced. This is consistent with the ideas of the results presented by Gerber & Vallis (2007) and it could have been rather convincingly concluded that the presence of topography is having the effect of reducing the magnitude of response to stratospheric heating.

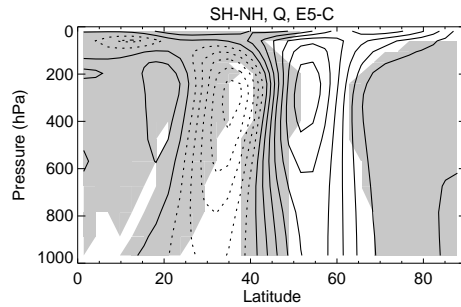


Fig. 5.6: Difference between SH and NH of the Q response to E5 stratospheric heating. Grey regions are not statistically significantly different from zero at the 95% level

However, Fig. 5.5 (b) demonstrates that there is a comparable, if not slightly larger, difference between the hemispheres of the Q experiment. This is an experiment which is symmetric about the equator but clearly the magnitude of response for this length of run is not. It therefore demonstrates just how much variability is present in the magnitude of response.

Fig. 5.6 shows the difference in zonal wind response between the SH and NH of the Q experiments along with significance values at the 95% level as calculated by the t-test. This demonstrates that the NH and SH are significantly different which is quite unexpected given the hemispherically symmetric nature of the experiments. This leads to uncertainty as to whether the magnitude of the response to the Q experiments when averaging over both hemispheres is accurate enough and also whether the difference between the NH and SH of the R experiment is real or is an artefact of sampling issues with runs of 10000 days length. Moreover, it demonstrates that there is a problem in using the t-test in this way to determine significance values as the NH and SH of the Q experiments are the same and so should not be significantly different.

Part of the reason for the difference between the hemispheres of the Q run can be found by examination of the daily wind anomalies from the time mean of the control and E5 runs. This is shown in Fig. 5.7 which shows the

daily wind anomalies for (a) the Q control run, (b) the QE5 run and (c) the difference between them on the 286hPa level. The difference plot shows two regions of rather anomalous wind response for an extended period of time (highlighted by the black squares). These anomalies can be seen to be in the correct sense to produce an enhanced poleward shift of the mid-latitude jet in the SH and a decreased poleward shift in the NH which is the sense of the discrepancy shown in Figs. 5.5 and 5.6. Moreover, it can be seen that the reason for the SH anomaly is a time in the control run where there is an anomalously large positive zonal wind anomaly on the equatorward side of the time mean jet and a negative anomaly on the poleward side. Similarly the NH anomaly is due to a time when the E5 run has an anomalous increased zonal wind on the equatorward side of the time mean jet and decrease on the poleward side. The model appears to jump between different regimes. For the most part the timescale of zonal wind variability is short with the anomalies from the time mean being relatively small and a tendency for poleward propagation of these anomalies. However, on occasion the jet gets into an anomalous regime where there are large zonal wind anomalies on either side of the time mean jet for an extended period of time. Both these different types of variability have been observed in models and in the real atmosphere previously (Son & Lee (2006) and references therein). It is not completely clear why the jet goes into these anomalous states but more on the control run variability can be found in Chapter 6.

To illustrate the effect that these anomalous times have on the time mean response, Fig. 5.8 (a) presents E5 - C for the Q experiment but with the anomalous times around the squared regions in Fig. 5.7 omitted from the average. Conversely, Fig. 5.8 (b) shows the difference between E5 and C for the mean of only the anomalous days. Fig. 5.8 (a) demonstrates that when the anomalous times are omitted the asymmetry between the hemispheres is reduced. There is still some asymmetry but this is perhaps more reasonable within the errors expected on the magnitude of response. Fig. 5.8 (b) shows the large effect these anomalous days can have. The NH and SH response

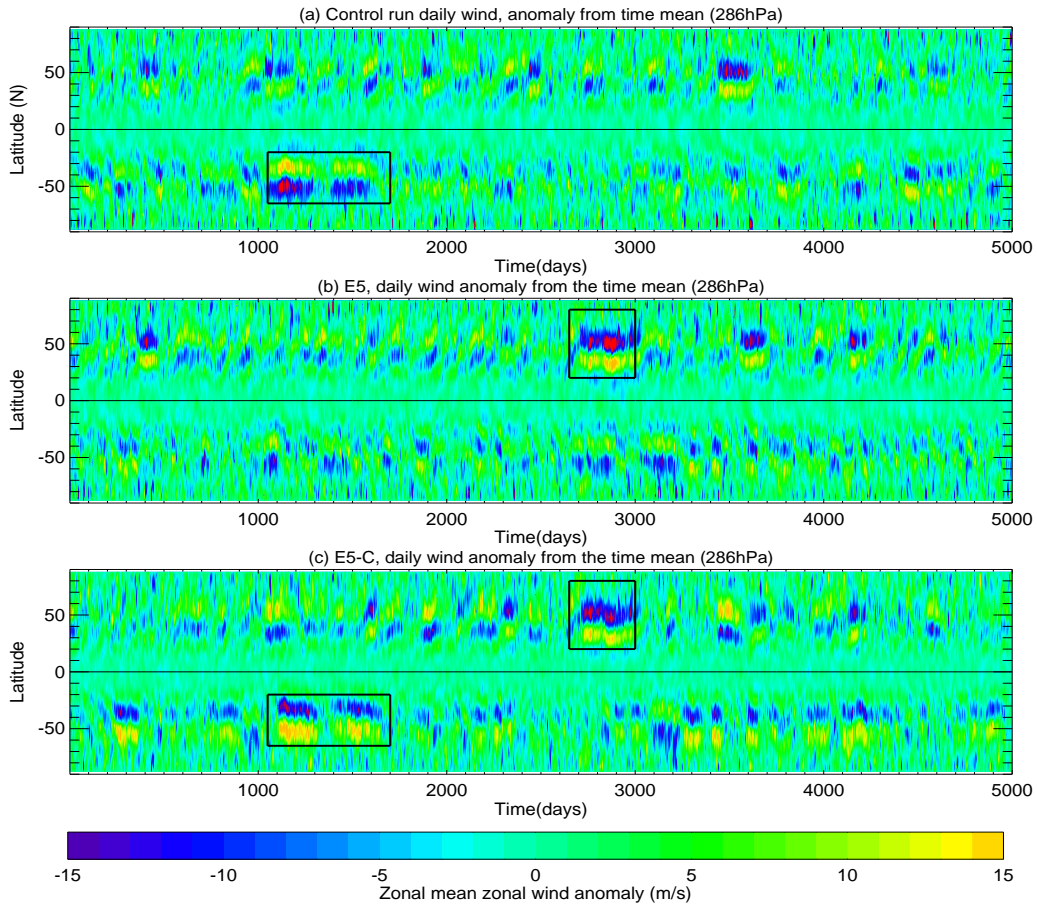


Fig. 5.7: Daily zonal mean zonal wind anomalies from the time mean (ms^{-1}) on the 286hPa level for (a) the Q control run, (b) the QE5 run and (c) the difference between QE5 and Q.

are of opposite sign and with completely different magnitudes of response. The NH part of Fig. 5.8 (b) is just from a 300 day average and one cannot hope to get realistic estimates of the magnitude of response from that. But, the SH part is a 700day average which is quite a significant amount of time when e.g. a run of 1000 days length is used.

Given the large difference in the magnitude of response between the two hemispheres of the Q experiment, which are supposed to be the same, it is clearly difficult to state with confidence whether the reduction in the mag-

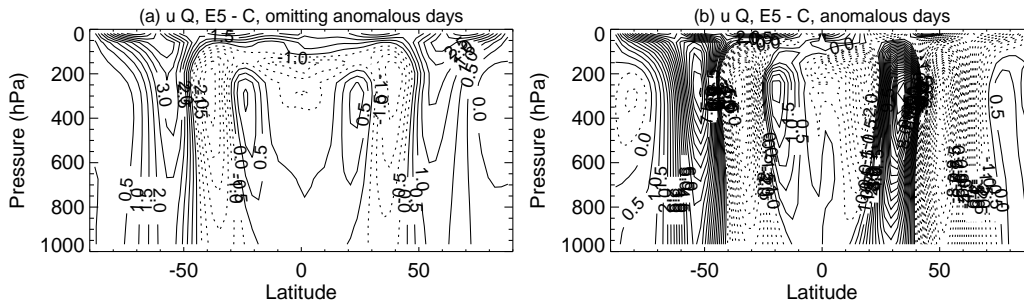


Fig. 5.8: Difference in zonal mean zonal wind between E5 and Control for (a) time mean excluding anomalous days and (b) anomalous days. Anomalous days are considered to be between days 1000 and 1700 in the NH and days 2700 and 3000 in the SH.

nitude of the NH of the R run is really due to topography or simply natural variability. To examine this further, the results of ensembles of 10, 5000 day runs will be discussed in the following section.

5.3 50000 day integrations of the Q and R experiments

The results of the 5000 and 10000 day integrations in the previous section have demonstrated large uncertainties in the magnitude of response to stratospheric heating. It was shown that the SH and NH of the Q response were significantly different. This clearly cannot be the case for a statistically representative sample of the two hemispheres because the SH and NH are the same experiment. This demonstrates that a 5000 day integration is not sufficient to accurately determine the magnitude of response.

In order to investigate further the effect of zonal asymmetries on the model response, an ensemble of runs has been performed for each of the Q and R experiments. 10 runs of 5000 days for each control and E5 equilibrium experiment have been run (data provided by Fenwick Cooper, DAMTP, University of Cambridge). Each one differs only in the random number seed that determines the noise introduced into the model at the beginning of each

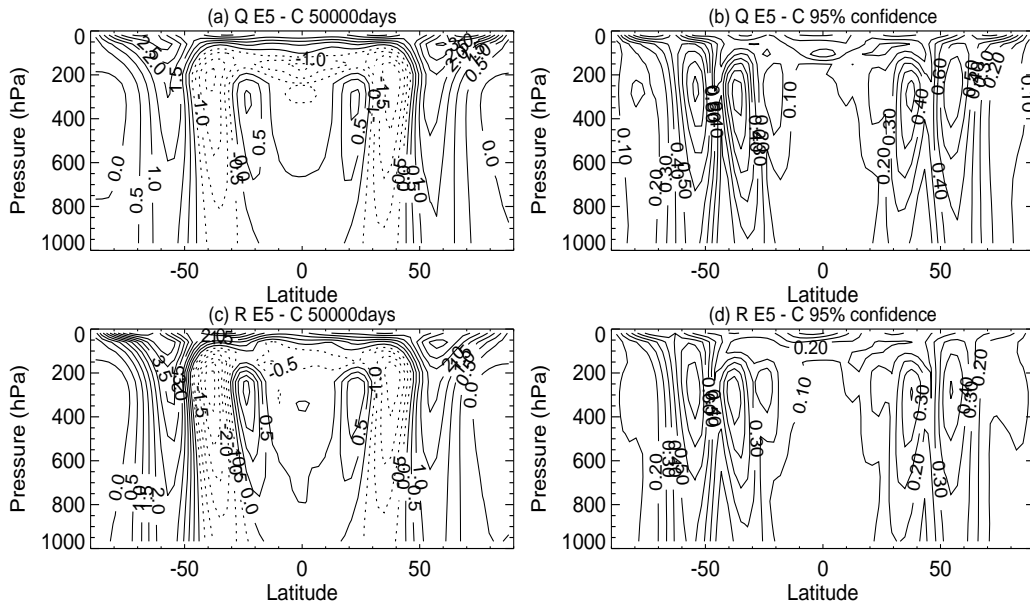


Fig. 5.9: (a) and (c) the 50000 day mean response to E5 stratospheric heating for the Q and R runs respectively. (b) and (d) the 95% confidence interval of the mean response to E5 heating for the Q and R runs respectively.

integration. Thus we have 50000 days for each run or 10 independent runs of 5000 days. From this we can more accurately determine the magnitude of response to stratospheric heating and its uncertainty.

Fig. 5.9 shows the zonal mean zonal wind response to E5 stratospheric heating for the 50000 day ensemble mean together with the 95% confidence level which has been calculated from the 10 different ensemble members as described in section 3.3.5. It can be seen that introducing these zonal asymmetries has not had an impact on the qualitative patterns of the tropospheric response. The zonal wind response shows the same poleward shift as the original run (Fig. 4.1(f)) and the other fields (not shown) show a qualitatively similar pattern of response. Therefore, the mechanism discussed in chapter 4 is clearly still dominant in the presence of the zonal asymmetries. Moreover, comparison of the stationary and transient eddy momentum flux (not shown)

demonstrates that even when zonal asymmetries are introduced the transient eddy momentum flux still dominates in the response to stratospheric heating by far.

This is a promising result that, even when asymmetries are introduced, the tropospheric response to stratospheric heating is still present. The question is whether the asymmetries have had an effect on the magnitude of the tropospheric response. First, examination of Fig. 5.9 (a) demonstrates that the two hemispheres of the Q experiment are now symmetric about the equator and they are no longer significantly different. They agree within the errors which is reassuring that this length of run is considerably more accurate than the 5000 day run used previously. Moreover, both these hemispheres appear to show a slight reduction in the magnitude of response compared to the original run without asymmetries (see e.g. the SH of Fig. 5.9 (c)).

Examination of the R response (Fig. 5.9 (c)) shows that there is still asymmetry in the magnitude of response between the hemispheres with the magnitude in the NH being about half that of the SH. These results suggest that the presence of either asymmetry (Q or R) slightly reduces the magnitude of response.

However, these differences are small signals on top of a massive amount of variability. A sense of the amount of variability can be obtained from Fig. 5.10 which shows for each of the hemispheres of the Q and R runs, the mean magnitude of response at two points on the 286hPa level: 54deg latitude and 37deg latitude. These are around the maximum zonal wind increase on the poleward side of the jet and the maximum zonal wind decrease on the equatorward side of the jet respectively. For each of the hemispheres there is a large spread in the magnitude of response over the 10 different 5000 day ensemble members. In the extreme cases there can be up to an order of magnitude difference in the size of the peak wind anomaly. Nevertheless, the mean values and 95% confidence levels suggest that there is a reduction in the magnitude of response for those runs that have zonal asymmetry in them but given the large spread of the data it is difficult to assign a value to

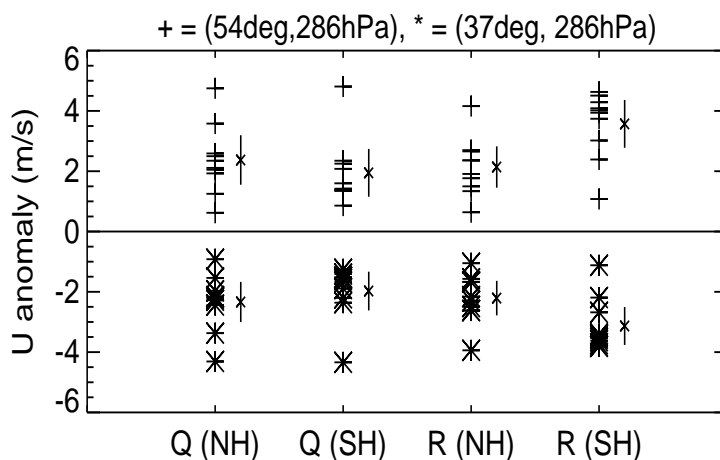


Fig. 5.10: 5000 day mean \bar{u} anomaly ($E5 - C$) at 286hPa and 54 deg latitude (crosses) and 37deg latitude (asterisks) for each hemisphere and each ensemble member of the Q and R runs. Mean values and 95% confidence intervals are shown along side.

this reduction. Not much more can be said than that there is a reduction in magnitude of response between both the Q and R responses and the original (or R(SH)), but this reduction is only just significant based on this amount of data. One thing that can be said for certain is that in order to obtain sufficiently accurate results to determine whether there is a difference in magnitudes of response for experiments like these, very long runs are required and it is not possible to do this with runs of several thousand days that are commonly used in studies with simplified GCM's.

5.3.1 Decorrelation timescales

One of the main motivations for these experiments was the result of Gerber & Vallis (2007) that when zonal asymmetry, particularly topography, was introduced into their sGCM, it reduced the decorrelation timescale of the models annular variability to more realistic values. The decorrelation timescales for each of the ensemble members for the NH and SH of the R and Q runs have been calculated (S.Sparrow, personal communication) and

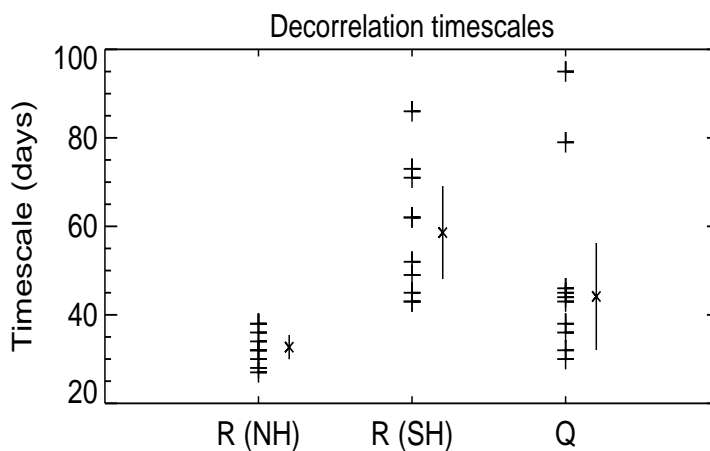


Fig. 5.11: Decorrelation timescale for each ensemble member of the NH and SH of the R control run and the two hemispheres combined of the Q run. Ensemble mean and 95% confidence interval are shown alongside. (These values have been calculated by S.Sparrow).

the values are shown in Fig. 5.11.

These timescales are calculated by finding the first Empirical Orthogonal Function (EOF) of the zonal mean zonal wind variability for each 5000 day run. Then projecting the zonal wind anomaly from the time mean onto that EOF and calculating the mean e-folding timescale of the autocorrelation of that projection (this is the same method as used in e.g. Chan & Plumb (2009)). Fig. 5.11 shows both the timescale for each individual ensemble member together with the mean and 95% confidence interval. It is apparent that there is a clear separation in the timescales between the NH and SH of the R run, both in their mean values and in their spread.

In the presence of topography the decorrelation timescale has been reduced to about half that of the hemisphere with zonally symmetric boundary conditions consistent with the results of Gerber & Vallis (2007). This timescale is getting towards more realistic values for the Earth's atmosphere (~ 10 to 20 days (Baldwin *et al.*, 2003)). But, what is also apparent is the much larger spread in the timescales for the southern hemisphere where

there are no zonal asymmetries present. The decorrelation timescale for the model in its original configuration is clearly much more uncertain than when topography is present. Perhaps this is because when there are no zonal asymmetries present the model is jumping between these two regimes: one of long timescale variability and the other of shorter timescale variability. It is possible that the presence of the topography is breaking up the zonal jet such as to prevent such long timescale anomalous behaviour and so maintaining the model in the usual regime of shorter timescale variability. This could then have the effect of reducing the mean decorrelation timescale and also the spread of values obtained for the decorrelation timescale of runs like these. This is in agreement with the suggestions of Gerber *et al.* (2008) and also the results of Son *et al.* (2008b) who showed that in some of their sGCM experiments where the control run exhibited 'zonal index' behaviour characterized by long timescale poleward or equatorward shifts of the jet, the introduction of topography shifted the model into a different regime characterized by shorter timescale poleward propagating zonal wind anomalies.

The details of the reason for this reduction in decorrelation timescale requires further investigation but there is clearly a reduction in timescale when topography is present. In terms of the fluctuation-dissipation theorem which suggests that the magnitude of the part of the response which projects onto the annular mode in these runs should be proportional to the decorrelation timescale: if the estimate of the mean values of response for the NH and SH R runs are robust, this could appear to be the case. In the NH the decorrelation timescale has been reduced to about half that of the Southern hemisphere and so has the mean magnitude of response. However, given the spread in the magnitudes of response it is difficult to say this with certainty.

The mean decorrelation timescale of the Q ensemble is around 10 to 15 days lower than that of the original Held-Suarez configuration (R(SH)) but this is not a significant difference. Unlike the introduction of topography, the Q experiment has not had the dramatic effect on the spread of the decorrelation timescales calculated from the ensemble members.

5.4 Discussion and conclusions

At the outset of these experiments the main aim was to examine the effect of zonal asymmetries on the tropospheric response to stratospheric heating with 5000 day model runs. It was even hoped that something could be said about the zonal variations of the response in the presence of zonally asymmetric storm tracks. However, these runs have demonstrated that it is not possible to say anything with certainty about the magnitude of response in the zonal mean, with runs of this length, let alone the zonal variations.

Rather, these experiments have demonstrated that there is a huge amount of variability in the magnitude of the tropospheric response, even when runs of 5000 days length are used and thus it is important to ensure that runs of sufficient length are used to determine the magnitude of the response accurately.

However, despite this it has been possible to examine the impact of the zonal asymmetries with ensembles of 10, 5000 day runs from which several conclusions can be drawn:

- Qualitatively similar patterns of response to E5 stratospheric heating are found in each ensemble member of each experiment and these are qualitatively similar to the pattern of response in the original model with zonally symmetric boundary conditions as shown in HBD05 and Chapter 4. This pattern of response is therefore robust and is not affected by the presence of zonal asymmetries. The mechanism producing the tropospheric response found in Chapter 4 is still dominant.
- There is a clear impact of the topography on the decorrelation timescale of the control run variability. The presence of the ridge reduces the decorrelation timescale to around half that of the hemisphere with zonally symmetric boundary conditions. Not only is the actual decorrelation reduced in the presence of topography but so is the spread of the calculated decorrelation timescale between ensemble members.

- The ensemble means and 95% confidence intervals suggest a slight reduction in the magnitude of response in the presence of either the Q or R experiments. However, this is barely significant and it is very difficult to assign accurately a magnitude to this decrease. Combining this evidence together with the reduction in the decorrelation timescale for the R runs, and what is expected from the fluctuation-dissipation theorem, it seems likely that the topography, and probably the asymmetric T_{ref} , is having an impact on the magnitude of response. However, this impact is small when compared with the variability demonstrated between different ensemble members of the same experiment.
- Runs of several thousand days, as commonly used in experiments like these, are likely to be sufficient to look at control run variability or the qualitative patterns of response to a forcing. But, with responses of relatively small magnitude like these, it is not possible to say anything concrete about the magnitude of response. This is because these are relatively small signals on top of a much larger background variability. Presumably this is also the case for the real atmosphere.

It was shown that the NH and SH of the 5000 day Q response were significantly different by the t-test. This suggests that care has to be taken when using the t-test in this way to determine significance levels. It assumes Gaussian statistics and, although for the most part this is likely to be a reasonable assumption, on some occasions the model goes into an anomalous regime where the mid-latitude jet is anomalously poleward or equatorward for an extended period of time. When this happens the distribution of zonal wind values is unlikely to remain Gaussian and the t test is unlikely to give an accurate significance level. This raises the question of how long a run is required to determine accurately the magnitude of response and it has not been possible to answer that question definitively in this study. It depends on the frequency of occurrence of these anomalous periods.

Often the variability of e.g. the annular mode index is modelled as an autoregressive noise process of first order (see e.g. Gerber *et al.* (2008)). From

this, the length of run required to obtain a value at a particular significance level can be obtained as was done by Gerber *et al.* (2008) to obtain the length of run required to accurately determine the autocorrelation timescale. But, this relies on certain assumptions, namely that the process in question has a stationary probability distribution. That is, the likelihood of the annular mode index having a value at one time based in the value at a previous time remains constant. Perhaps this is not a valid assumption when a model like this appears to be jumping between different regimes: one of short timescale variability and one of much longer timescale variability where the probability of remaining in the same state as that of a previous time is a lot higher.

The purpose of these experiments was not to provide a detailed analysis of the statistics of the model runs and clearly further work is required on this topic. Rather we were concerned with the effect that introducing zonal asymmetries has on the response to stratospheric heating and the main conclusion that can be drawn from the 50000 day model runs is that it is possible the introduction of zonal asymmetries is having a small impact on the magnitude of the tropospheric response but it has no impact on the qualitative patterns of response.

The concerns as to the length of run required to accurately determine the magnitude of response have very little impact on the results of Chapter 4 as there we are focussing on the qualitative patterns of response and those are robust. In chapter 6 we will go on to investigate the effect of varying tropospheric jet structure on the magnitude of response. The differences in the magnitude of response are a lot larger than those due to topography and the change in tropospheric T_{ref} and we will also be using 50 000 day ensembles for these.

6. THE EFFECT OF VARYING TROPOSPHERIC JET STRUCTURE

The third and final set of experiments are designed to investigate the effect that varying tropospheric jet structure has on the response to stratospheric heating. This is useful as the real atmosphere does not always have a zonal wind structure that is similar to that produced by the T_{ref} used in chapter 4. Indeed it varies with both season (Piexoto & Oort, 1992) and location (Eichelberger & Hartmann, 2007). Moreover, it has been demonstrated by other authors that a change in the tropospheric relaxation temperature structure of simplified GCMs such as these brings with it changes in the natural variability of the mid-latitude westerlies (Gerber & Vallis, 2007; Son & Lee, 2006) which is likely to have an impact on the response to stratospheric heating as predicted by the fluctuation-dissipation theorem.

Here, as described in section 3.2.3, four new tropospheres have been created by altering the Newtonian relaxation temperature profile in the troposphere. Given the problems with accurately determining the magnitude of response found in chapter 5, an ensemble of experiments has been performed for each of the different tropospheres. These each consist of 5, 5000 day runs, each one differing only in the random noise perturbation at the beginning of the integration. Thus, taking each hemisphere separately there are 10, 5000 day runs for each troposphere and each experiment to provide a more accurate determination of the magnitude of response and its uncertainty.

Thus, including the original troposphere described in Chapter 4, there are 5 different tropospheres and for each of these an ensemble of runs for the control, E5 and P5 experiments has been performed. An intriguing pattern in the magnitude of response to stratospheric heating is found, with

lower latitude/narrower jets generally having a much larger magnitude of response than higher latitude/wider jets for both the E5 and P5 experiments. This appears to be related to the variability of the mid-latitude westerlies in the control run simulations which is fundamentally different for the lower latitude/narrower jets than the higher latitude/wider jets.

The structure of this chapter will begin with a discussion of the control run states of each troposphere. Then the equilibrated response to E5 and P5 stratospheric heating will be presented. Finally there will be an attempt at explaining the differing responses with altered tropospheric jet structure. This will include a discussion of the variability present in the control run simulations together with an examination of the E5 spin-ups for TR2 and TR4 and the equilibrated response to stratospheric heating.

6.1 *The control run tropospheres*

As described in section 3.2.3, four new tropospheres have been created by altering the tropospheric relaxation temperature profile. Two of these new tropospheres TR1 and TR5 are simply formed by altering the equator-to-pole temperature difference by changing the parameters T_o and ΔT_y to 305 and 40 and 325 and 80 respectively. So, TR1 has a weakened equator-to-pole temperature gradient and TR5 has a strengthened equator-to-pole temperature gradient as compared to the original run, denoted by TR3. Tropospheres TR2 and TR4 consist of a slice through the quadrupole T_{ref} (experiment Q), used in chapter 5, at 90° and 270° longitude respectively and applying that at all longitudes. Thus TR2 has a decreased T_{ref} in the subtropics and an increase in the sub-polar regions whereas TR4 has an increased T_{ref} in the subtropics and a decrease in the sub-polar regions (see Fig. 3.7 for the relaxation temperature profiles).

We therefore have five different tropospheres of varying mid-latitude baroclinicity going from TR1 being the weakest to TR5 being the strongest. To begin a discussion of these different tropospheric states it is simplest to first

consider the tropospheres TR1, TR3 and TR5 as these each have the same structure of tropospheric T_{ref} (given by Eq. 3.5) but with a simple alteration of the equator-to-pole temperature difference. TR2 and TR4 have the additional complication of an oppositely signed change to the tropical and polar meridional temperature gradient.

As was stated in section 3.1, the dynamical response of the model to the imposed T_{ref} is to cause warming in mid-high latitudes in the troposphere and cooling at low latitudes such as to reduce the negative latitudinal temperature gradient in the troposphere. From the temperature plots in Fig. 6.1 (top) it can be seen that this is being done more (less) effectively in TR5 (TR1) than in the original TR3. By examination of the difference in surface temperature between equator and pole it can be seen that it is approximately 32K, 42K and 52K for TR1, TR3 and TR5 respectively whereas the imposed equator-to-pole temperature differences are 40K, 60K and 80K respectively.

This enhancement of the poleward heat flux going from TR1 to TR3 to TR5 can be explained by both an enhanced tropical Hadley cell and poleward eddy heat flux in mid-latitudes. The meridional stream function plots (Fig. 6.1 (bottom)) demonstrate that the peak meridional stream function associated with the tropical Hadley cell is around twice that in TR5 compared to TR1.

The decent and adiabatic warming in the subtropics caused by the thermally direct Hadley cell, together with the imposed meridional temperature gradient in T_{ref} means that going from TR1 to TR3 to TR5 there is a greatly enhanced meridional temperature gradient in the mid-latitudes. This results in enhanced baroclinicity and thus increased eddy production in TR5 as compared to TR1 as can be seen in the E-P flux (Fig. 6.2 (top)). Associated with this stronger eddy growth and vertical E-P flux is a strong poleward eddy heat flux in the lower mid-latitude troposphere. The poleward eddy heat flux can be seen to be greatly enhanced going from TR1 to TR3 to TR5 with peak values being around 10Kms^{-1} , 20Kms^{-1} and 30Kms^{-1} respectively. Thus, the eddies in TR5 more effectively reduce the meridional

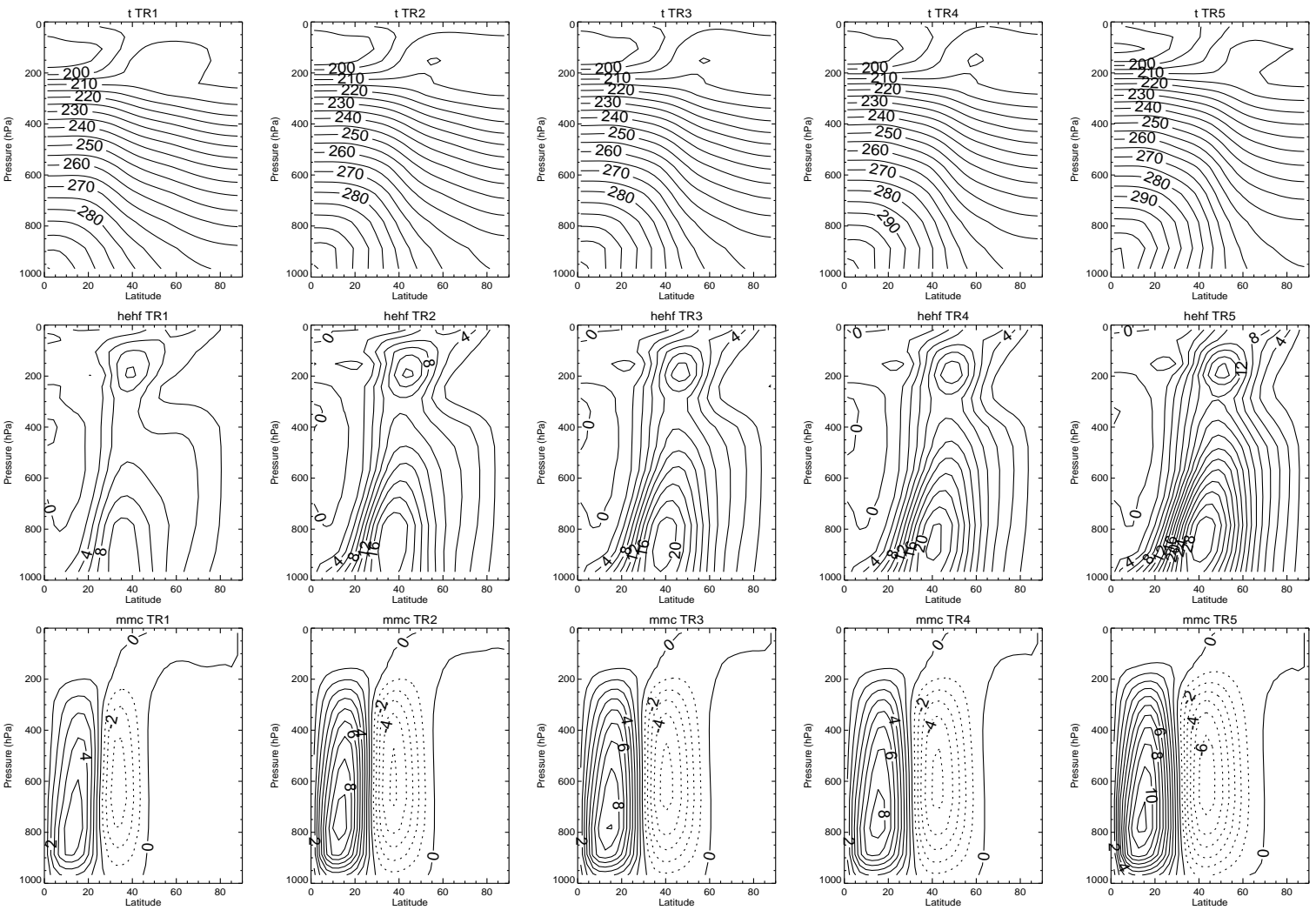


Fig. 6.1: Control run (top) zonal mean temperature (K), (middle) horizontal eddy heat flux (Km s^{-1}) and (bottom) stream function of the mean meridional circulation ($10^{10} \text{ kg s}^{-1}$) for the ensemble means of (column 1) TR1, (column 2) TR2, (column 3) TR3, (column 4) TR4 and (column 5) TR5.

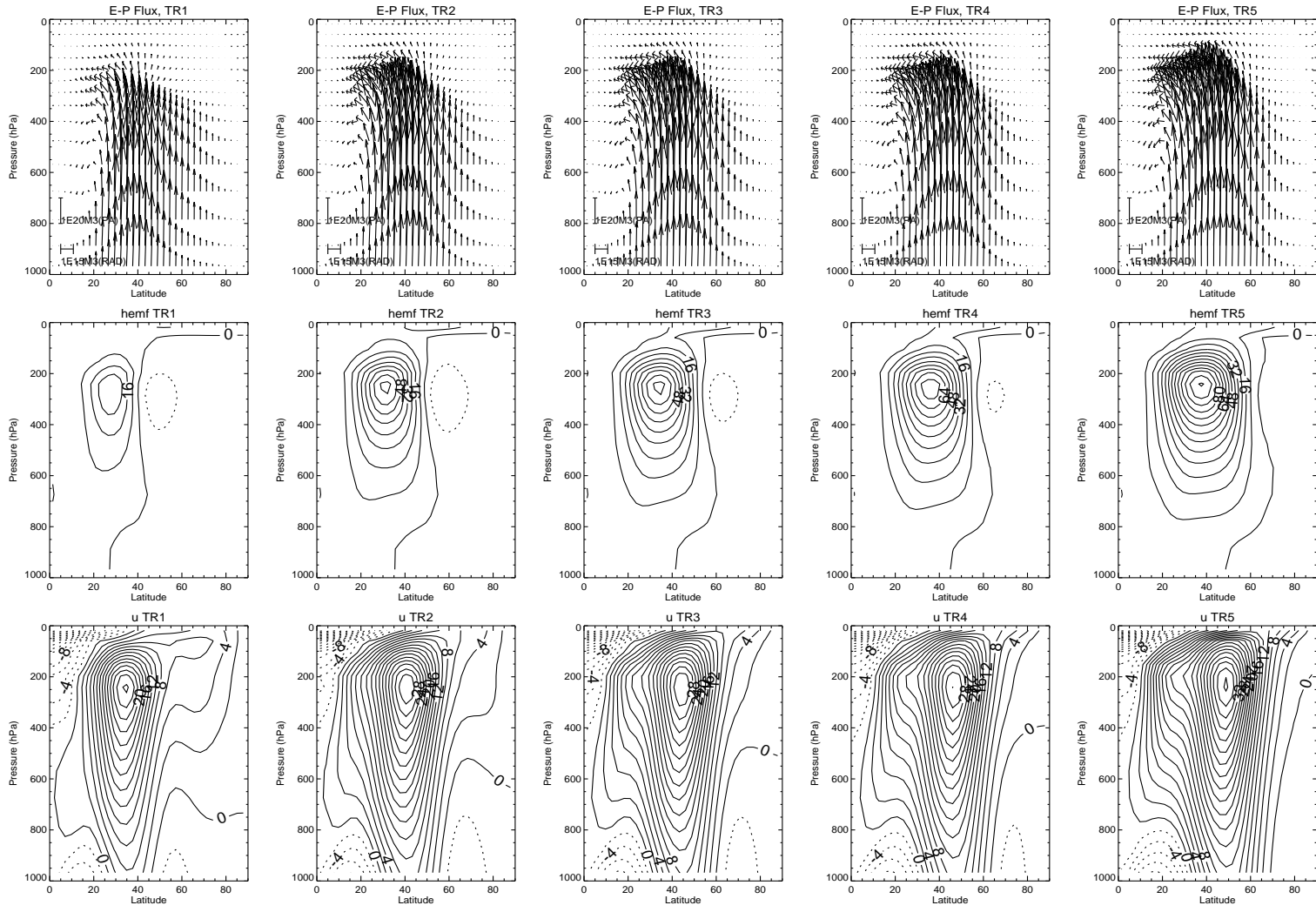


Fig. 6.2: As Fig. 6.1 but for (top) E-P flux, (middle) horizontal eddy momentum flux (m^2s^{-2}) and (bottom) zonal wind (ms^{-1}).

temperature gradient as compared to TR1.

The combination of eddy heat and momentum fluxes act to induce a thermally indirect circulation in mid-latitudes in order to maintain thermal wind balance in the presence of the low level poleward eddy heat fluxes and the upper level poleward eddy momentum fluxes. As the eddies reach the higher static stability of the tropopause the effects of the Earth's sphericity and rotation (the presence of $2\Omega\cos\phi$ in Eqs. 3.30 and 3.31) acts to refract them mostly equatorward. This is associated with a large poleward flux of momentum. It can be seen that in going from TR1 to TR3 to TR5, associated with the increased production of eddies there is an increased poleward momentum flux in the upper troposphere (Fig. 6.2 (middle)). The momentum flux convergence associated with this acts to accelerate the zonal flow at upper levels in order to maintain thermal wind balance in the presence of the meridional temperature gradient. But, it is also offset by the coriolis force on the equatorward branch of the eddy driven thermally indirect circulation. Thus, associated with the increased eddy fluxes in going from TR1 to TR3 to TR5 there is a stronger thermally indirect circulation in mid-latitudes and a stronger more poleward peak in mid-latitude westerly wind e.g. the peak wind speed in TR1 is around 26ms^{-1} at around 35° latitude as compared to around 38ms^{-1} at around 50° latitude in TR5.

The net effect of enhancing the meridional temperature gradient is to enhance the Hadley cell as well as increase the production of eddies and their associated fluxes, which then results in a stronger and more poleward mid-latitude jet and a stronger thermally indirect circulation. It can be seen that in TR1 the sub-tropical and mid-latitude jets are merged into a single jet whereas TR3 and TR5 have increasingly broader regions of strong westerly wind with increasingly separated sub-tropical and mid-latitude jets.

The tropospheres TR2 and TR4 have the additional complication that the imposed change in meridional T_{ref} gradient is of the opposite sign in the tropical and polar regions as compared to in the mid-latitudes. In TR2 there is a reduction in T_{ref} in the subtropics. As a result the meridional temper-

TR1	—————→	TR5
Weaker mid-latitude \bar{T} gradient		Stronger mid-latitude \bar{T} gradient
Weaker eddy heat flux		Stronger eddy heat flux
Weaker eddy momentum flux		Stronger eddy momentum flux
Weaker mid-latitude jet		Stronger mid-latitude jet
More equatorward mid-latitude jet		More poleward mid-latitude jet
Single jet state		Double jet state
Narrower region of $\bar{u} > c$		Wider region of $\bar{u} > c$

Tab. 6.1: Summary of the differences in tropospheric jet structure in going from TR1 to TR5.

ature gradient in the tropics is increased and there is a slightly enhanced Hadley cell as compared to the original TR3 run. The opposite is true of TR4, it has a slightly weaker Hadley cell. However, in the mid-latitudes, TR2 has a weakened meridional temperature gradient as compared to TR3 and thus weaker eddy fluxes and a weaker, more equatorward and narrower mid-latitude jet although not as dramatic a change as for TR1. The opposite is true in TR4; there is an enhanced mid-latitude temperature gradient, stronger eddy fluxes and a stronger, more poleward, mid-latitude jet, but again not as pronounced as in TR5. Thus, TR2 and TR4 fit in with the pattern of the change in climatology in going from TR1 to TR5 with the exception of the strength of their Hadley cell. Table 6.1 summarises the changes in tropospheric jet structure in going from TR1 to TR5. It is not intended to suggest that the changes are occurring linearly between TR1 and TR2, TR2 and TR3, etc but rather to give an indication of the qualitative differences in the tropospheric jet structures.

6.2 The equilibrated response to stratospheric heating.

The effect that having a different tropospheric jet structure has on the response to stratospheric heating will now be investigated. In keeping with the

previous chapters there will be a focus on the response to E5 heating but the response to P5 heating will also be briefly discussed.

6.2.1 *The E5 response.*

Figs. 6.3 and 6.4 show the difference between ensemble means of E5 and Control of some of the key fields for each of the different tropospheres.

Qualitatively the patterns of response for each troposphere are similar. Each shows the familiar patterns of TR3 which has been discussed extensively in chapter 4. There is a strengthened westerly wind and enhanced vertical wind shear on the poleward side of the jet maximum and a reduced westerly wind and vertical wind shear on the equatorward side of the jet (Fig. 6.3 (middle)). In thermal wind balance with this is an increased temperature around the centre of the control run jet with a decrease on either side (Fig. 6.3 (top)). At the latitudes of zonal wind decrease there is an anomalous clockwise circulation and at the latitudes of zonal wind increase there is an anomalous anti-clockwise circulation (Fig. 6.3 (bottom)). Accompanying these circulation changes are eddy momentum flux anomalies (Fig. 6.4 (middle)). There is a decreased eddy momentum flux around the tropopause on the equatorward side of the jet associated with anomalous poleward E-P flux (Fig. 6.4 (top)). This is more apparent for the stronger, higher latitude jets¹. There is also the increased eddy momentum flux on the poleward side of the jet stretching down into the troposphere.

Thus, there is a qualitatively similar response to E5 heating in each of the tropospheres but there is a large difference in the magnitudes of the response in going from TR1 to TR5 with TR1 having a much stronger response and TR5 having a weaker response than the original TR3 experiment. There is almost an order of magnitude difference in the zonal wind response between TR1 and TR5 with e.g. a peak zonal wind acceleration on the poleward side

¹ The reason for this will be discussed later and it is not inconsistent with the mechanism presented in Chapter 4 where it is shown that an initial decrease in eddy momentum flux on the equatorward side of the jet triggers the tropospheric response.

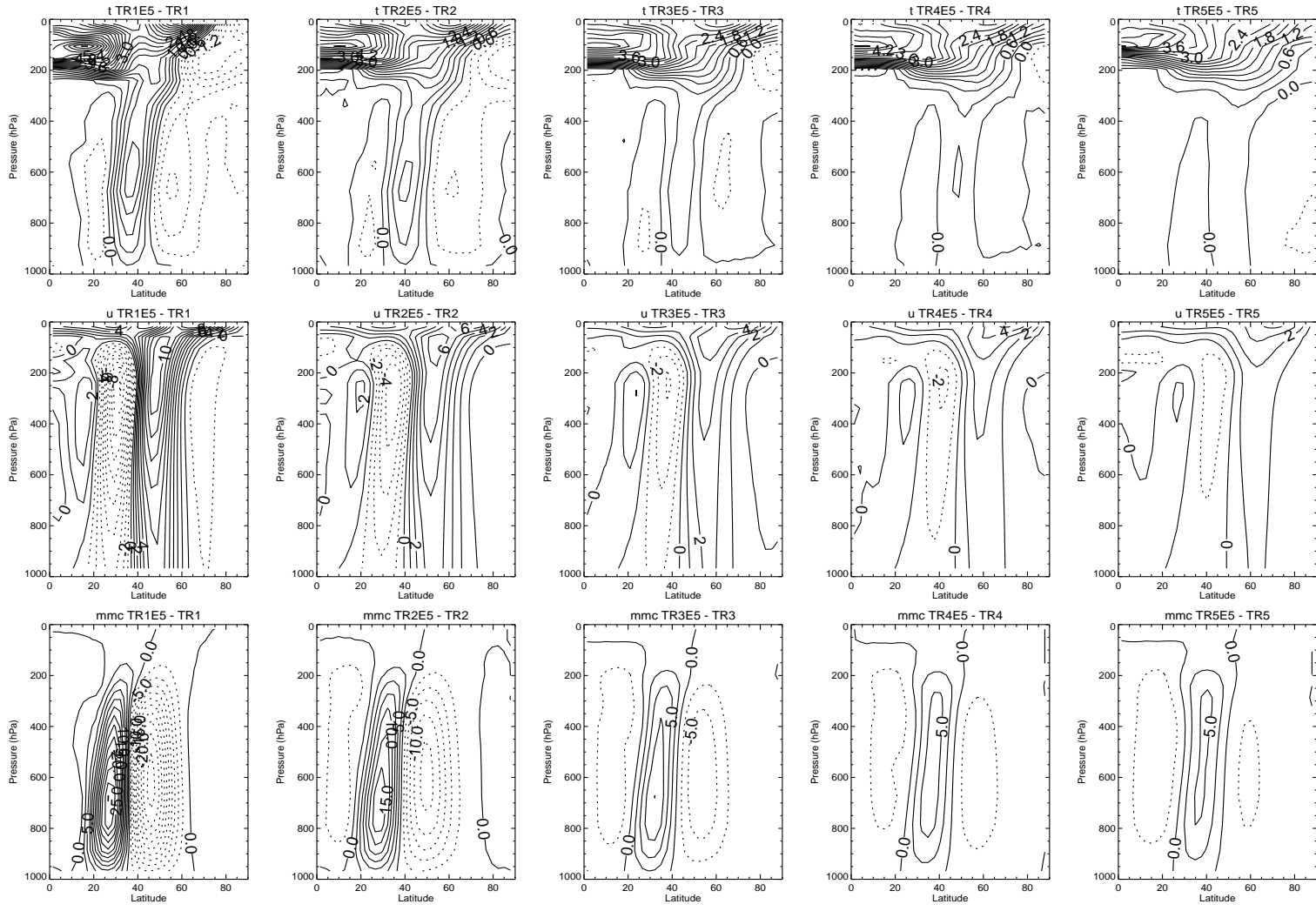


Fig. 6.3: E5 - C for (top) Temperature (K), (middle) zonal wind (ms^{-1}) and (bottom) stream function of the mean meridional circulation (10^9 kgs^{-1}) for (left to right) ensemble mean of TR1 to TR5.

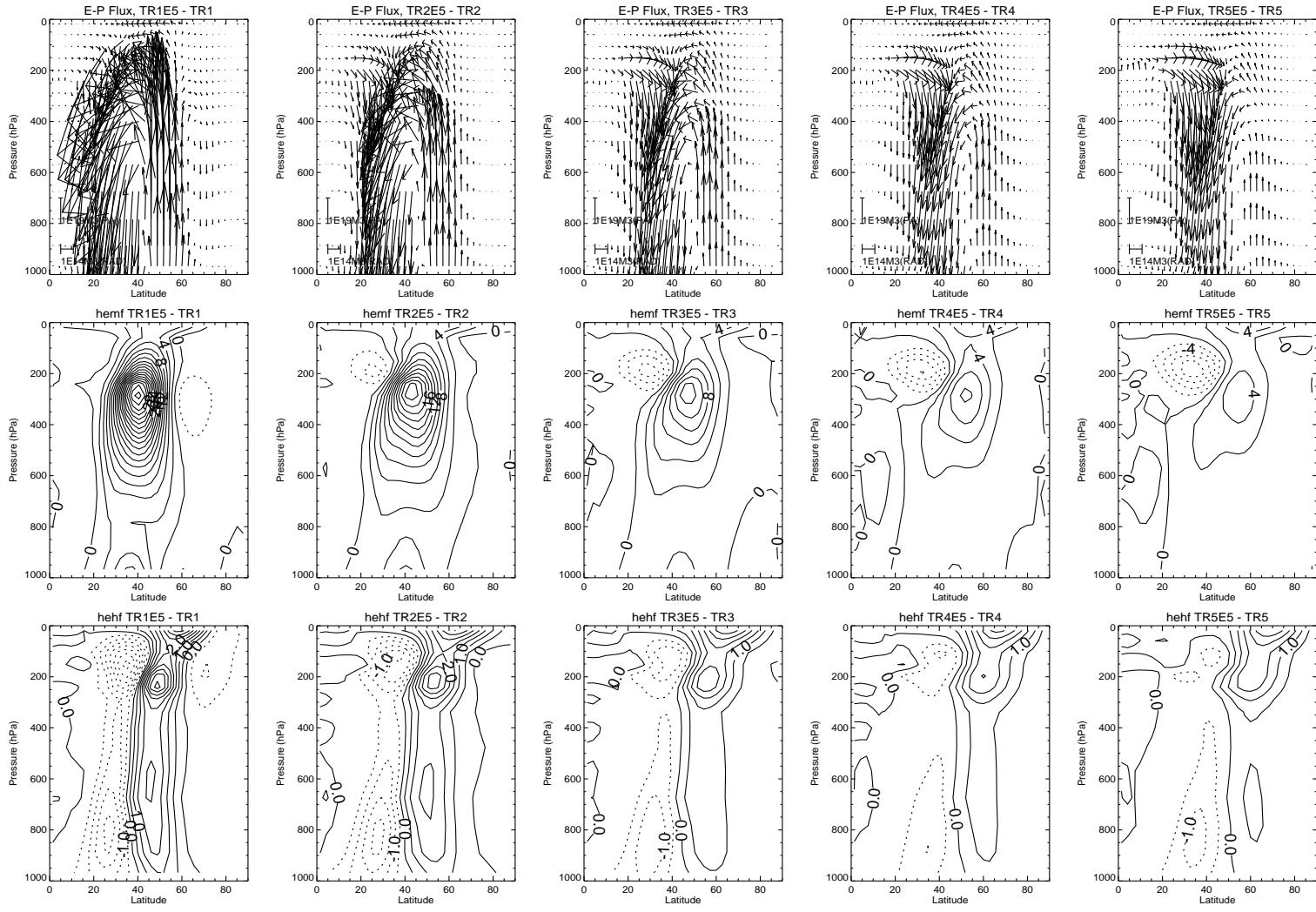


Fig. 6.4: As Fig. 6.3 but for (top) E-P flux, (middle) horizontal eddy momentum flux and (bottom) horizontal eddy heat flux.

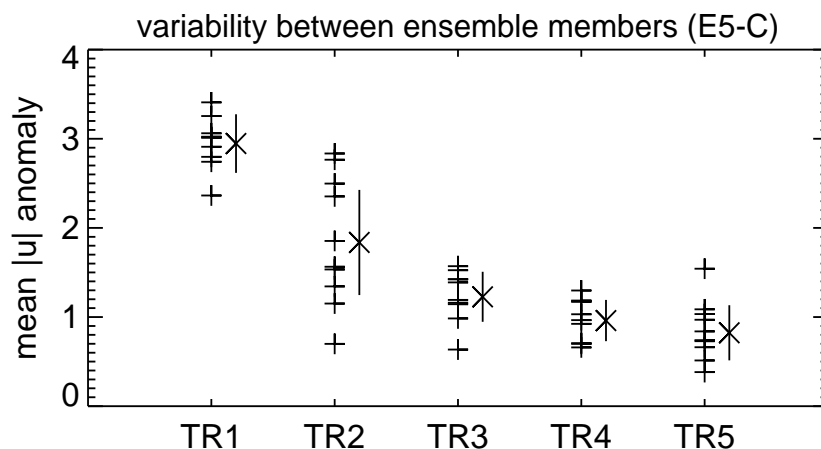


Fig. 6.5: Mean anomaly over all latitudes and pressures for each ensemble member (+’s) of each experiment. Ensemble mean and 95% confidence intervals are shown alongside.

of the jet at $\sim 300\text{hPa}$ being around 10ms^{-1} compared to around 1.5ms^{-1} in TR5 ².

Chapter 5 demonstrated the difficulty in accurate determination of the magnitude of response for runs of 5000 days length. It must be stressed that these differences between the ensemble means of the different tropospheres are occurring concurrently with a large amount of variability between the different ensemble members of each individual troposphere. This is demonstrated in Fig. 6.5 which takes the mean magnitude of the zonal wind anomaly at all latitudes and pressures as a measure of the magnitude of the response. This magnitude of response is shown for each individual

² It has been demonstrated that the tropospheric response to polar stratospheric cooling in the studies of Polvani & Kushner (2002) and Kushner & Polvani (2004) were unrealistically large because their tropospheric state was on the border line between two regimes which constituted a bimodal distribution of where the latitude of maximum surface westerlies occurred (Chan & Plumb, 2009; Gerber & Polvani, 2008). This bifurcation is not present in either control or E5 runs of the tropospheres which appear to show a much larger response, so the reason for the large response in the Polvani & Kushner (2002) experiments does not apply to these runs.

ensemble member together with the mean and 95% confidence interval. It is clear that there is a large spread in the magnitude of response between the different 5000 day ensemble members of each experiment, again highlighting the need for very long runs to determine the magnitudes accurately. It is interesting to note that there is a particularly large variations in the magnitude of response for TR2 and a smaller variation for TR4. It's possible that applying the T_{ref} perturbation in the subtropics and sub-polar regions affects the variability in the magnitude of response but this requires further investigation.

As the averages are being taken over 10, 5000 day ensemble members and given the large magnitude of the difference between the different ensemble means and the clear pattern of the variation in the magnitude of response with differing tropospheric jet structure we believe that despite the large uncertainty in the magnitude of response there is a robust variation in this magnitude with different tropospheric jet states. This is further verified by the difference in spin-up evolution of TR2 and TR4 to be presented in section 6.3.2. Weaker, lower latitude, narrower jets have a much larger response than higher latitude, stronger, wider jets. However, care should be taken when making conclusions about the exact magnitudes of response.

Another difference to note between the experiments is the difference in the equilibrated temperature response in the stratosphere. Fig. 6.3 (top) shows an enhanced heating in the low latitudes and enhanced cooling in the high latitudes compared to the imposed change in T_{ref} for each of the tropospheres. However, this gets progressively weaker going from TR1 to TR5. Examination of the individual terms in the thermodynamic equation (3.18) (not shown) demonstrates that differences in the horizontal eddy heat flux response account for the difference in stratospheric temperature at the poles whereas differences in the mean meridional circulation anomalies account for the difference in temperature response in the tropical stratosphere through the adiabatic heating term.

In the following we will focus on trying to explain the dramatic differences

in the tropospheric mid-latitude responses i.e. the dipole zonal wind anomaly centred on the mid-latitude jet maximum.

6.2.2 *The P5 response*

An ensemble of P5 equilibrium runs have also been performed for each of the tropospheres. Here, the polar stratosphere has been heated preferentially by 5K decreasing to zero at the equator.

This can be used to investigate whether the difference in the tropospheric response magnitude is due to the proximity of the jet to the stratospheric heating. Intuitively, it may be expected that the response to E5 stratospheric heating would be stronger for lower latitude jets simply because they are closer to the heating. However, the response to P5 heating demonstrates that the trend of lower latitude jets having a stronger response remains and thus is not related to the proximity of the heating.

Fig. 6.6 presents the equilibrated zonal wind and temperature response to P5 stratospheric heating for the ensemble mean of each of the tropospheres, TR1 to TR5. The patterns of response in the troposphere are qualitatively similar to that of P10 but with a smaller magnitude. It can be seen that much like in the E5 experiment, TR5 shows the smallest magnitude of response. Thus, it is not the case that the closer the jet is to the stratospheric heating, the stronger the response. There must be something else associated with the jet structure that results in a weaker response for higher latitude/wider jets to stratospheric heating. The trend that lower latitude/narrower jets have a stronger response is true in the P5 runs with the exception of TR1 which shows a weaker response. Perhaps this jet is just so far from the stratospheric heating that the initial influence of the heating on the eddies is not felt as strongly leading it to evolve slightly differently. Further, investigation is needed to confirm this, perhaps involving a spin-up experiment.

As for the E5 experiments, an indication of the spread in the magnitudes of response is given in Fig. 6.7 which shows the mean magnitude of zonal wind response over all latitudes and pressures together with the ensemble

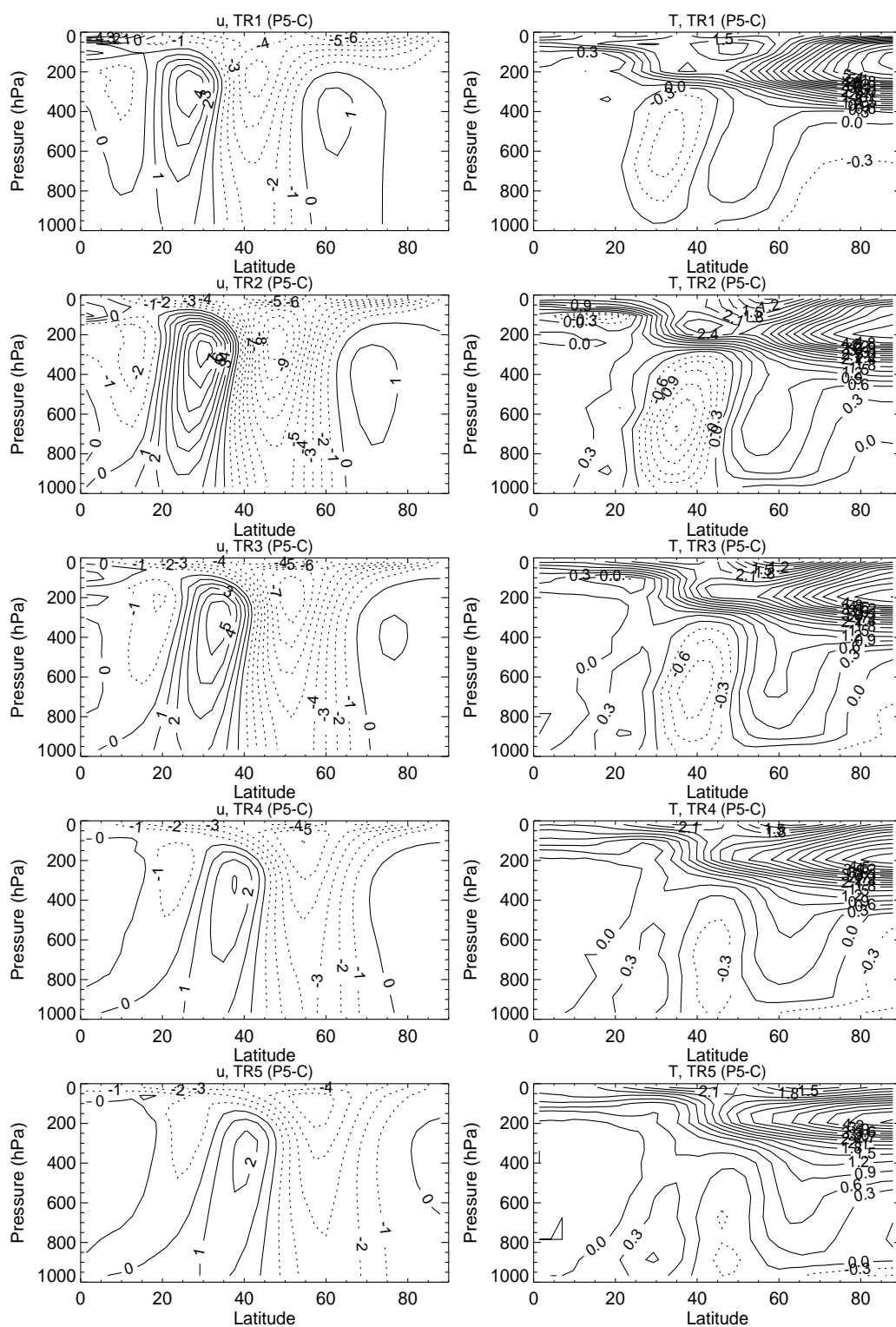


Fig. 6.6: (Left) zonal wind (ms^{-1}) and (Right) temperature (K) response to P5 stratospheric heating for the ensemble means of TR1 to TR5 from top to bottom.

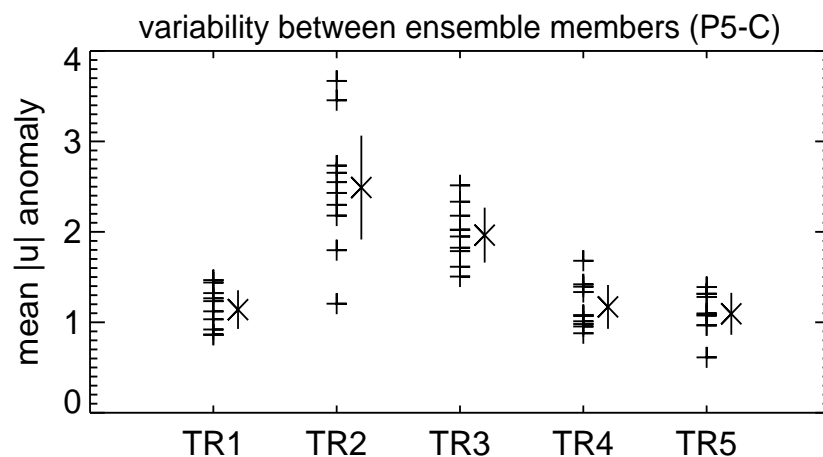


Fig. 6.7: Mean magnitude of zonal wind anomaly over all latitudes and pressures for each individual ensemble member of each experiment (+’s). The ensemble means and 95% confidence intervals are shown alongside.

mean and 95% confidence interval. Again the TR2 response seems to be a lot more variable than the others.

The main conclusion to be taken from the P5 runs is that the magnitude of response does not appear to be related to the proximity of the stratospheric heating to the jet and the trend of lower latitude/narrower jets having a larger magnitude of response appears to remain (with the exception of TR1).

6.3 Why the difference in magnitude of the tropospheric response?

Examination of equilibrated responses like these carries with it the usual difficulty of separating cause from effect, particularly as the eddies and the mean flow are highly coupled.

It was demonstrated in chapter 4 that altered eddy momentum fluxes are responsible for the tropospheric response to stratospheric heating. Initial changes in vertical temperature gradient around the tropopause region

influence eddy propagation there, producing eddy momentum flux anomalies which generate meridional circulation changes that are responsible for the accelerations at lower levels. An important feedback was demonstrated; altered meridional gradients in the zonal wind across the jet centre refract the eddies in the troposphere such as to produce momentum fluxes there that reinforce and enhance the wind anomalies.

An obvious answer to the differing magnitudes might be the dramatic differences in the eddy momentum flux anomalies in the troposphere. The tropospheric increase in eddy momentum flux is much larger in TR1 than in TR5 (Fig. 6.4 (middle)) and thus so is the eddy momentum flux convergence/divergence and the acceleration of the mean flow. But, this change in eddy momentum flux is due to refraction by the altered zonal flow. Therefore, the magnitude of the change in eddy momentum flux in the troposphere and the zonal wind anomalies are intrinsically linked and it cannot be said that the smaller wind anomalies in TR5 are due to smaller tropospheric eddy momentum flux anomalies as these smaller tropospheric eddy momentum flux anomalies are in turn, due to the smaller wind anomalies.

This demonstrates the difficulty in separating cause from effect. It is not obvious why the lower latitude, weaker, narrower jets should have a much larger response to E5 heating, particularly given the importance of eddies in driving the response and the weaker eddies in those jets. Nevertheless, making use of the knowledge gained from the spin-up experiments of chapter 4 together with information present in other literature on the subject along with examination of the control run variability in each of the different jet states and spin-up experiments of TR2 and TR4 we shall attempt to offer some explanation of the differing magnitudes of response. The results are not entirely conclusive but suggest a relationship between the width of the jet and the ability of the tropospheric eddy momentum flux anomalies to feed back onto the zonal wind anomalies.

6.3.1 *Control run variability*

Several studies have recently demonstrated that the simulated response of the tropospheric mid-latitude westerly jets to various forcings is closely related to the natural variability that occurs in the unforced control run simulations (Gerber & Vallis, 2007; Ring & Plumb, 2008). It is therefore instructive to examine the control run simulations of TR1 to TR5. In doing this it is revealed that there is also a trend in the natural variability of the control run in going from TR1 to TR5. The natural variability of the lower latitude/narrower jets is fundamentally different from that of the higher latitude/wider jets which can provide some clues as to the reason for the larger magnitude of response found in the lower latitude/narrower jets (with the exception of TR1 P5).

Fig. 6.8 presents, on the left hand side, time series of the zonal mean wind anomaly from the time mean on the 286hPa level for one ensemble member of each of the control run simulations. The right hand side shows one point correlation maps for the wind anomalies of each troposphere with the base latitude chosen to be the latitude of maximum variability on the equatorward side of the jet maximum (similar results are produced for any base latitude chosen that is within the region of dipole variability around the jet centre).

The one point correlation maps confirm what can be seen by eye in the wind anomaly plots. TR4 and TR5 have much shorter timescale wind anomalies with a tendency for poleward propagation. An example can also be seen in Fig. 6.9 (a) which shows such an anomaly occurring between around days 2170 and 2280 of one ensemble member of the TR5 control run. However, the variability in TR1 and TR2 appears to be fundamentally different. Rather than having short timescale poleward migrations there are much longer timescale wind anomalies occurring around the jet centre which show no real poleward migration. Such an example can be seen in Fig. 6.9 (b). The differences in the timescales is also apparent from the e-folding timescale of the autocorrelation of the first EOF of zonal mean zonal wind variability (characterised by North-South displacements of the mid-latitude jet) of each

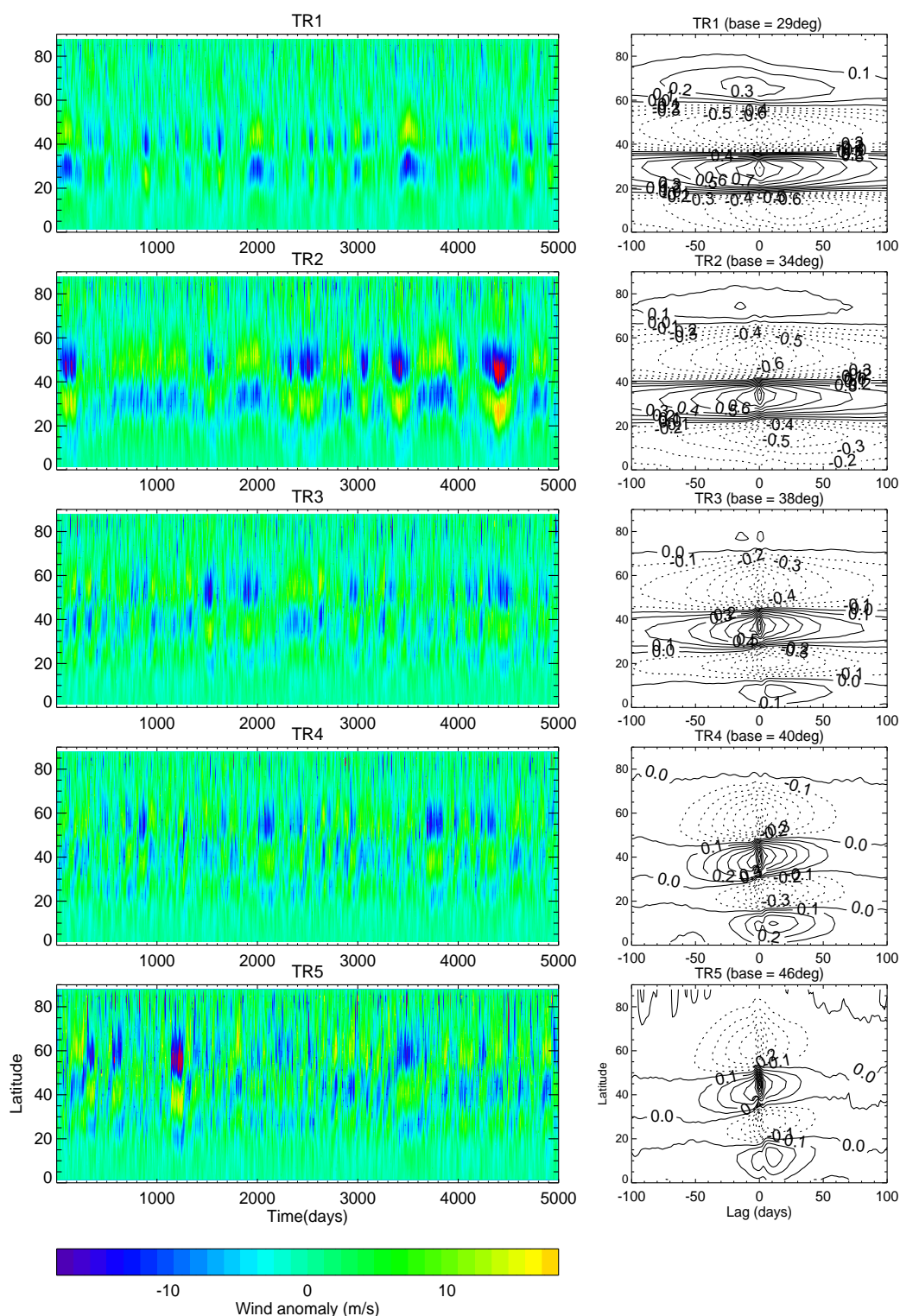


Fig. 6.8: (LHS) Time series of the zonal wind anomaly from the time mean of the control run on the 286hPa level of one ensemble member. (RHS) One-point correlation maps of the zonal mean zonal wind anomaly as a function of latitude for the ensemble mean. Top to Bottom = TR1 to TR5.

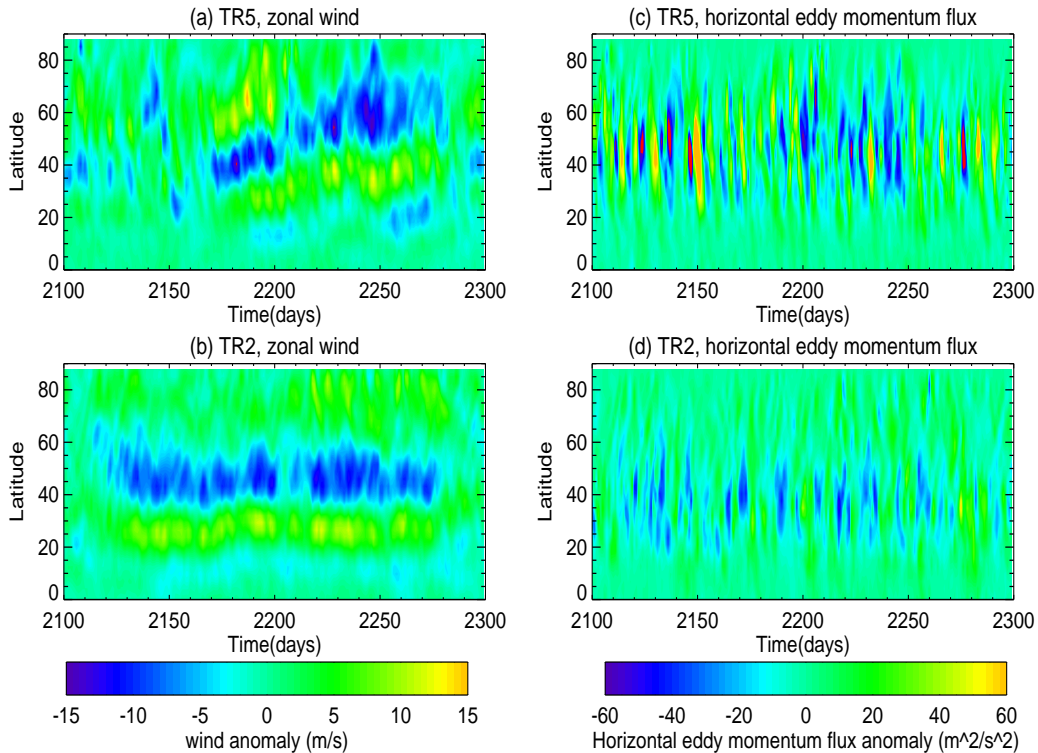


Fig. 6.9: Zonal mean zonal wind anomaly from the time mean for days 2100 to 2300 of the control run simulation of one ensemble member of (a) TR5 and (b) TR2. (c) and (d) show the corresponding horizontal eddy momentum flux anomalies from the time mean.

run as summarised in Fig. 6.10 (Sarah Sparrow, personal communication). This shows that TR1 and TR2 have considerably longer timescales of variability than TR4 and TR5 and TR3 lies somewhere in the middle. There is a general trend of a decrease in the decorrelation timescale in going from TR1 to TR5. Although as the timescale increases, so to does the uncertainty in the calculated value. Perhaps this reflects the fact that the uncertainty of the calculated decorrelation timescale for a fixed length of run increases as the timescale increases (Gerber *et al.*, 2008) i.e. as the decorrelation timescale increases the estimated value from a 5000 day run becomes more uncertain.

TR3, which is the original Held-Suarez configuration control run appears

to lie somewhere in between the two regimes. It tends to exhibit mostly short timescale poleward propagating anomalies but there are occasions where longer timescale stationary anomalies occur with either an equatorward or a poleward shift of the jet for an extended period of time.

It is interesting to note that there is a consistent pattern in all equilibrium runs, whether they be control or stratospheric heating experiments, that lower latitude/narrower jets exhibit this longer timescale stationary behavior whereas higher latitude/wider jets exhibit the shorter timescale poleward propagation. Indeed it is found that for the TR2, E5 equilibrium run that as the E5 heating has shifted the mid-latitude jet poleward it has also shifted it into the regime of shorter timescale poleward propagating variability. Conversely the P10 perturbation on the original Held-Suarez configuration run has shifted it into the regime of longer timescale variability as it has shifted the mid-latitude jet more equatorward.

The occurrence of these two different types of variability is a common fea-

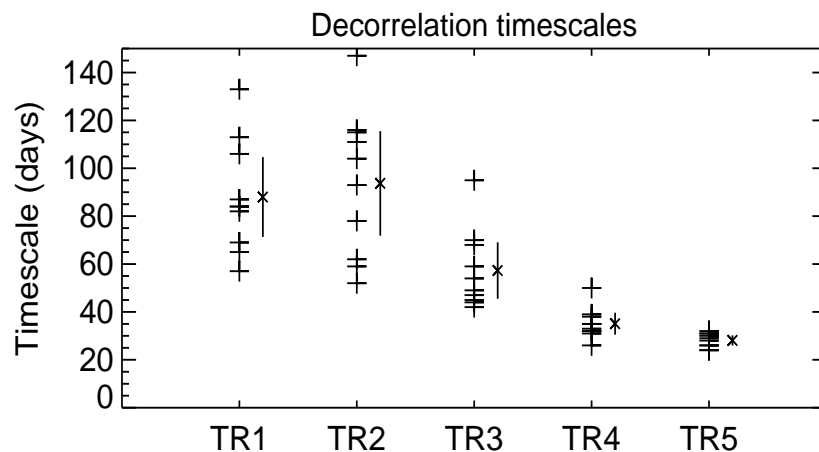


Fig. 6.10: *e*-folding/decorrelation timescale of the autocorrelation of the first EOF of variability in the zonal mean zonal wind for each ensemble member of each troposphere (+’s). Ensemble mean and 95% confidence interval are shown alongside. Decorrelation timescales calculated by Sarah Sparrow.

ture that has been observed in many other modeling studies and indeed in the real atmosphere (Son & Lee (2006) and references therein). In a suite of experiments using a simplified GCM Son & Lee (2006) clearly demonstrated this. Many simulations were performed with varying tropical heating and high latitude cooling. This had a similar impact on the tropospheric circulation as varying T_{ref} in the experiments described here but not identical as the heating and cooling were applied over more localised regions and thus did not have such an effect on the mid-latitude temperature gradient and mid-latitude baroclinicity. It was found that there were two distinct regions of tropical heating-high latitude cooling parameter space. With high tropical heating and low high latitude cooling, strong single jets were formed and these were characterised by 'zonal index' behavior i.e. longer timescale fluctuations in the jet position. Conversely, with low tropical heating and high, high latitude cooling, weaker double jet states were formed with variability that was characterised by poleward propagation.

Lee *et al.* (2007) offer an explanation of the mechanism behind this poleward propagation and demonstrate the importance of meridional radiation of waves in producing it. They suggest that the difference between the states that show poleward propagation and those that exhibit the zonal index behavior lies in the structure of the meridional PV gradient of the basic state. This is discussed further in Son *et al.* (2008b). It is shown that there is a one-to-one correspondence in time between individual wave breaking events and extrema of the principal component time series of the first EOF of annular variability (which represents north-south displacements of the mid-latitude jet). This leads them to conclude that the feedback that is maintaining the zonal index anomalies is associated with breaking of the mid-latitude eddies. They suggest that when the PV gradient is strong and sharp the wave breaking is weaker and the eddies and their momentum fluxes are more meridionally confined. However, for the states where the PV gradient is weaker and broader (i.e. their double jet states), the wave breaking is much more violent and the eddy momentum fluxes have a greater meridional extent

which allows for the poleward propagation.

The variability in TR1 and TR5 is partly in agreement with this. Examination of the eddy momentum flux anomalies associated with the example of zonal index behavior of TR2 and the poleward propagating behavior of TR5 in Fig. 6.9 demonstrates that for the period of TR2 where the zonal index behavior is exhibited there are a series of eddy momentum flux anomalies in the correct sense to maintain it and these eddy momentum flux anomalies are rather meridionally confined with the peaks each occurring at similar latitudes. In Fig. 6.9 (c) which corresponds to the poleward propagating period of TR5 it can be seen that the momentum flux anomalies have a much greater meridional extent and there is quite a lot more variation in the latitudes of peak eddy momentum flux anomaly.

It is true that the zonal index behavior occurs when the region of high positive PV gradient is narrower whereas the poleward propagation occurs when the region of high PV gradient is wider. However, in contrast to the jets in the Son & Lee (2006) study there is little difference in the peak magnitude of the PV gradient. This can be seen on the left hand side of Fig. 6.11 which shows meridional cross-sections of the PV gradient for each troposphere at the 286hPa level. Another difference between these experiments and those of Son & Lee (2006) is that here the lower latitude/narrower jets are also weaker whereas in Son & Lee (2006) their narrower jet states were also stronger leading to the stronger peak in PV gradient. This suggests that perhaps the differences in wave breaking and variability are associated with the width of this region of strong westerly winds and high PV gradient rather than the magnitude of the PV gradient.

The ideas discussed above, namely that variations in the position of the mid-latitude jet are associated with momentum fluxes due to individual eddies is in agreement with other studies. Vallis *et al.* (2004) demonstrated that patterns of variability similar to the annular modes and the NAO can be produced by simple stochastic forcing or stirring of a barotropic model. Variability of the eddy momentum flux convergence produced annular mode-like

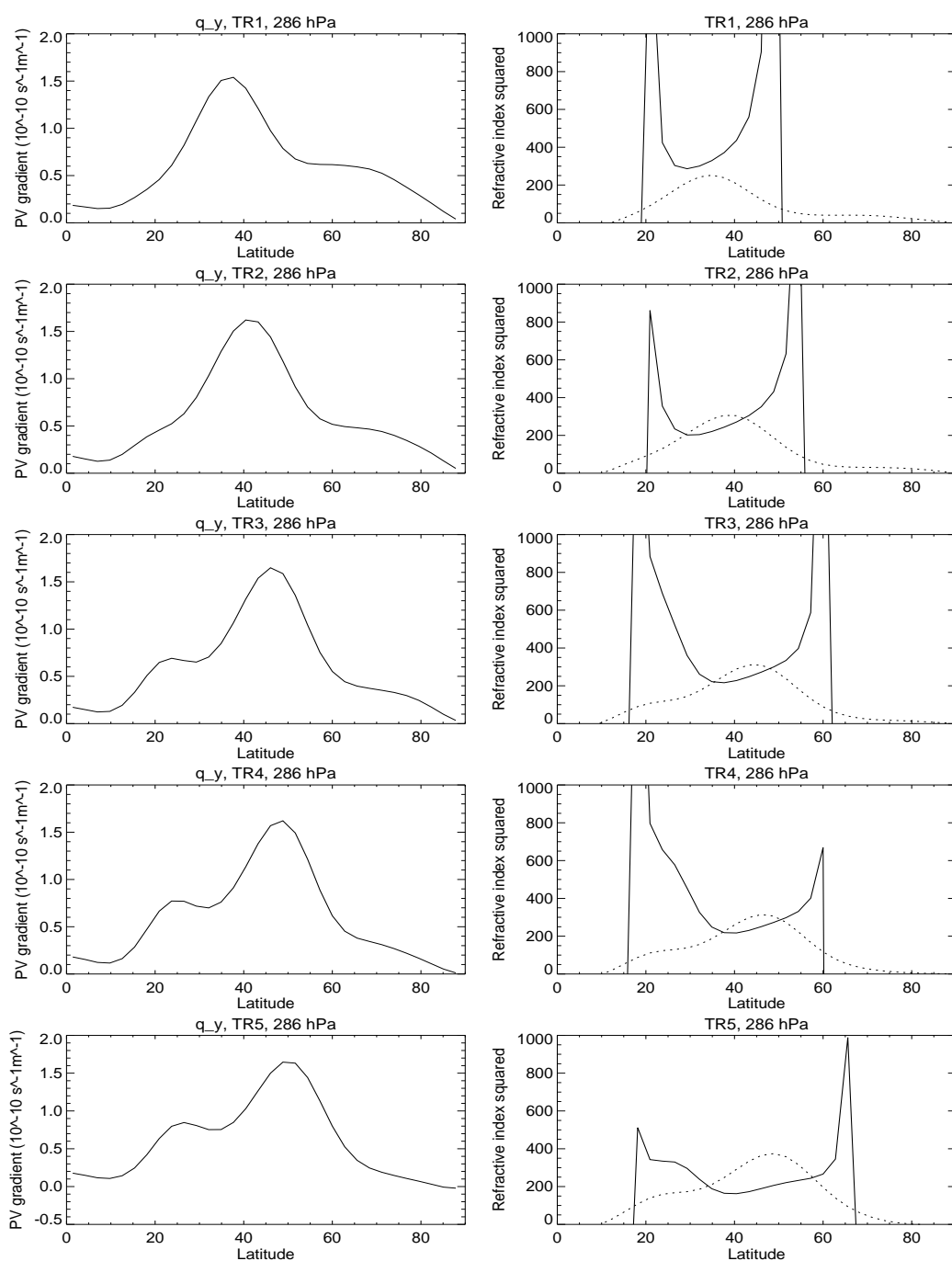


Fig. 6.11: (LHS) meridional PV gradient on the 286hPa level for TR1 (top) to TR5 (bottom). (RHS) solid lines - refractive index, dashed=zonal wind on the 286hPa level scaled by a factor of 10.

anomalies, but they state that the annular mode-like variability, rather than being hemispheric, is associated with the projection of eddy dynamics onto the zonally averaged flow. Similarly Cash *et al.* (2002) demonstrated using a GCM with zonally symmetric lower boundaries that, although composites of high and low annular mode are zonally symmetric in nature, individual times corresponding to high or low annular mode index are dominated by zonally localised events. This implies zonally symmetric variations in the zonal wind are, rather than actually being zonally symmetric, statistical in nature and built up of many zonally localised events.

It is apparent from the above discussion that the tropospheres which have a larger response to stratospheric heating are those which have longer timescale variability in their unforced control run simulations. This is of course consistent with the fluctuation-dissipation theorem (Leith, 1975; Ring & Plumb, 2008) but is also what would be expected for simulations in which the feedback between the eddies and the mean flow is stronger. Therefore, to understand both the timescale of the control run variability and the magnitude of the response to stratospheric heating it is necessary to understand what determines the strength of the eddy feedback onto the mean flow.

In the following we shall attempt to reconcile the differences in the response to stratospheric heating with the ability of individual eddies to feed back onto the zonal wind anomalies which is affected by the width of the jet and the region over which eddy propagation is possible.

Wave breaking latitude/Life cycle index

The wave breaking latitude (WBL) (or life cycle index) as defined by Akahori & Yoden (1997) and used in Son *et al.* (2008b) has been calculated for each day of each ensemble member of the control and E5 runs of TR1 to TR5 to examine the difference in eddy behavior between them. Akahori & Yoden (1997) introduced what they termed the 'Life cycle index' in order to obtain a statistical relationship between vacillations of the mid-latitude jet and the behavior of individual eddy life cycles. It makes use of the fact that breaking

of baroclinic eddies is associated with a reversal of the potential vorticity (PV) gradient on an isentropic surface and involves summing over all latitudes where the potential vorticity is negative with a weighting according to how negative the PV gradient is. Thus, a mean latitude of eddy breaking is obtained at a particular time.

In the following we have closely followed the procedure used by Son *et al.* (2008b). A particular latitude band must be chosen over which the calculation is performed. Son *et al.* (2008b) chose to examine PV values between 0.5 and 6PVU which corresponded for the 330K isentrope to a region between 25° and 65° latitude. Here, a slightly extended region has been used to ensure that the wave breaking region for each of the different jets is captured. The PV values of the time mean which corresponds to between 20° and 70° latitude have been used on the 350K isentropic surfaces. This surface was chosen as it is in the upper troposphere at all latitudes. Given the different jet structures, this latitude band corresponds to slightly different bounds in terms of the time mean PV.

Within the bounds of maximum and minimum PV that have been chosen the PV gradient (q_y) is calculated. Then each latitude at which q_y is negative is included in a summation with a weighting of the value of that PV gradient. Thus, latitudes where the PV gradient is most strongly negative i.e. where the wave breaking is stronger, are more dominant in the summation. This summation is performed over all longitudes to give a mean WBL at each time as follows:

$$WBL = \frac{\sum_{\phi,\lambda} \phi A}{\sum_{\phi,\lambda} A}, \quad (6.1)$$

where

$$A = \begin{cases} \text{Min}(q_y, 0) \cos \phi & \text{if } PV_{min} < q < PV_{max} \\ 0 & \text{otherwise} \end{cases} \quad (6.2)$$

Fig. 6.12 shows the WBL distributions for the ensemble means of the control and E5 and the difference between them for each jet. There is a striking difference in the control run WBL's between TR1 and TR5. The WBL distribution of TR1 is much more sharply defined and the distribution

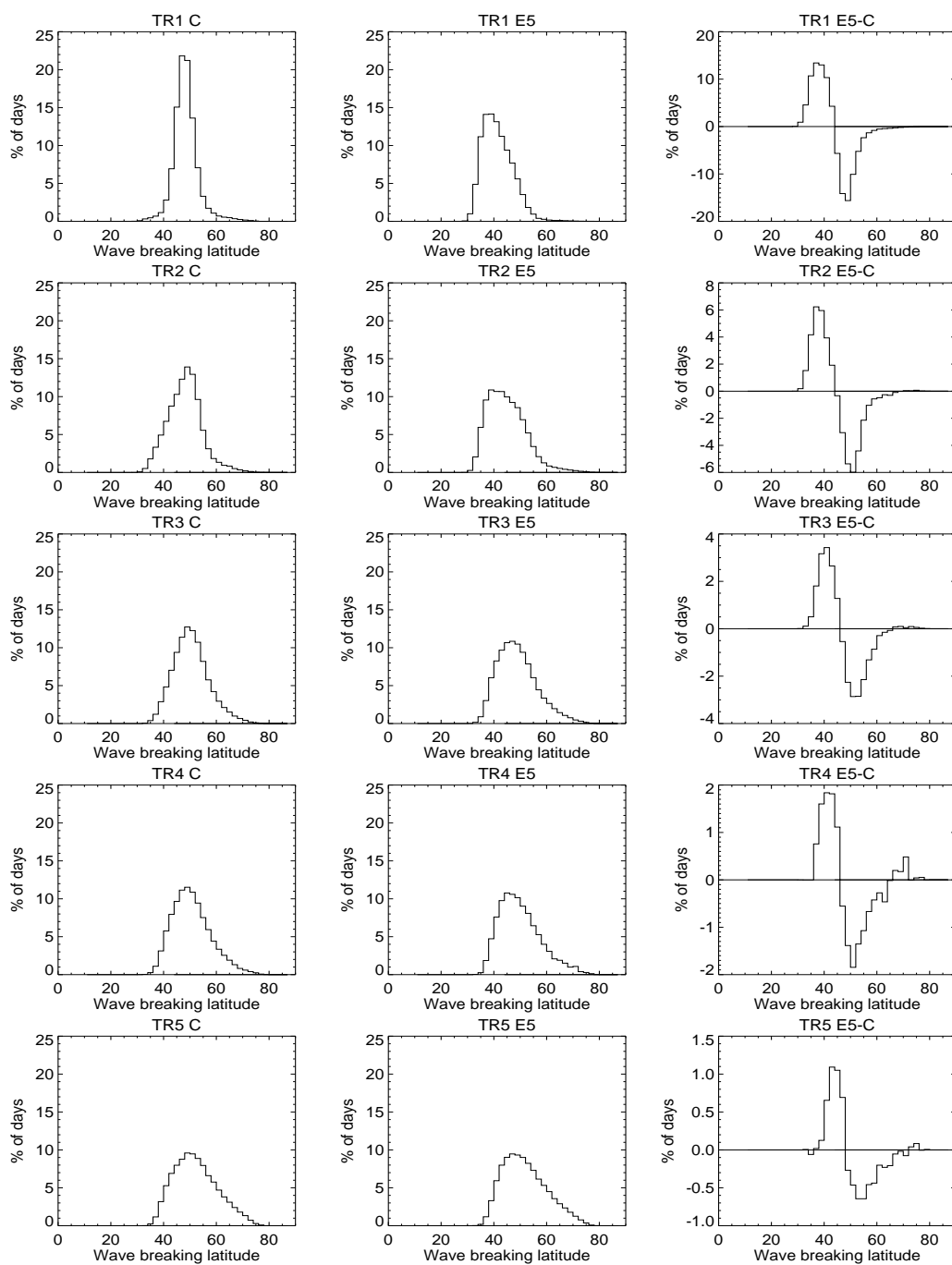


Fig. 6.12: Wave breaking latitude distribution of the ensemble means (50000 days) of the (left) Control, (middle) E5 and (right) E5 - Control, for each troposphere (top to bottom) TR1 to TR5.

gets increasingly broader when going from TR1 to TR5. This is consistent with the greater meridional restriction on eddy propagation and therefore a greater restriction on their breaking latitude in the more meridionally confined jet. For, the higher latitude/broader jet, the region over which the eddies can propagate is a lot broader and so there are a greater number of possible latitudes over which breaking is likely to occur.

An indication of the region over which eddy propagation is allowed is given on the right hand side of Fig. 6.11 which shows meridional profiles of the refractive index at the 286hPa level. Waves can only propagate in regions where the zonal wind is greater than the phase speed. Where the zonal wind becomes comparable to the phase speed, a critical line is formed which is where the refractive index goes to extreme positive or negative values. Outside of this region $\bar{u} < c$ and eddy propagation is inhibited. Thus, the region over which eddy propagation is occurring can be thought of as being the region between these two latitudes of extreme values of refractive index. As expected from the meridional confinement of the jet in TR1 and TR2, this region is a lot narrower than for the higher latitude/wider jets. This is consistent with the narrower distribution of latitudes at which eddy breaking is occurring.

Another difference in the WBL distributions in going from TR1 to TR5 is that the distribution becomes increasingly skewed towards lower latitudes indicative of the increased dominance of anticyclonic wave breaking. This can be seen in the horizontal eddy momentum flux plots of Fig. 6.2 (middle) which shows that in going from TR1 to TR5, the ratio of poleward eddy momentum flux on the equatorward side of the jet to the equatorward eddy momentum flux on the poleward side of the jet increases. Son *et al.* (2008b) suggest that this skew towards anticyclonic wave breaking is what is responsible for the poleward propagating zonal wind anomalies. The calculation of WBLs for these different jets is consistent with this, those that have poleward propagating variability have a skew toward lower WBLs.

Akahori & Yoden (1997) and Son *et al.* (2008b) have used this to show

that times corresponding to a poleward shift of the jet are associated with lower WBL's and thus dominated by anticyclonic wave breaking whereas times at which the jet is at a lower latitude are associated with higher values of the WBL. Son *et al.* (2008b) show that the eddy feedback required to produce the zonal index behaviour in their jets is associated with this preference for anticyclonic wave breaking and thus poleward momentum fluxes when the jet is more poleward and vice-versa. The difference plots of the WBL distributions between E5 and Control show that this is also true of the response to E5 heating. When the jet is more poleward there is an increase in the percentage of days of low WBL and a decrease in the percentage of days with high WBL. This is another way of looking at the eddy refraction and feedback ideas of chapter 4. Anomalous positive meridional wind shear across the jet centre refracts the eddies more equatorward and thus increases the amount of anticyclonic wave breaking. However, it is difficult to determine any reasons for the differences between the different tropospheres, again, due to the problem of separating cause from effect. There are much larger increases in the percentage of low latitude wave breaking days for the lower latitude jets which is consistent with a stronger feedback onto the tropospheric wind anomalies, but, then this larger difference in WBL is due to the larger wind anomalies, and thus larger anomalous meridional shear, acting to refract the eddies equatorward.

However, one thing that can be said about the shape of the difference in WBL distributions is that for the lower latitude/narrower jets the WBLs at which there is a change in the percentage of days in response to the E5 stratospheric heating is more meridionally confined than for the higher latitude/wider jets.

To summarise what can be concluded from these WBL distributions: examination of the control run WBL distributions have demonstrated that meridional confinement of the jet brings with it meridional confinement of the region over which eddies can propagate and where wave breaking is likely to occur. This means that more eddies are likely to be breaking in the same

position for narrower jets than for wider jets.

The poleward shift of the mid-latitude jet in response to E5 heating brings with it enhanced anticyclonic wave breaking. The reason for looking at the distribution of WBLs is that in the following we shall attempt to relate the greater meridional confinement of the eddies and their latitudes of wave breaking for the lower latitude/narrower jets to the magnitude of the response to stratospheric heating by examining the projection of the tropospheric eddy momentum flux anomaly onto the wind anomaly as a measure of the eddy feedback.

6.3.2 *TR2 and TR4 E5 spin-ups*

In order to gain some insight into the differences in the response to E5 heating between the lower latitude/narrower jets and the higher latitude/wider jets a 100 member spin-up ensemble has been performed for TR2 and TR4 with E5 heating as described in section 3.2.3. The TR2 spin-up was run for 300 days and the TR4 spin-up for 250 days. It will become apparent in the following that there is quite a major difference in the time taken to reach equilibrium between the two tropospheres and hence the reason for these long spin-up ensembles. Given the length of these spin-ups, the ensemble size is reduced to half that used in chapter 4. This brings with it the difficulty of increased signal to noise when looking at patterns of anomalies such as eddy momentum flux over e.g. 10 day averages as used in chapter 4.

Firstly, the spin-up ensembles have demonstrated that the differences in the eddy momentum flux anomalies shown in Fig. 6.13 are not in contradiction with the mechanism described in chapter 4. The TR1 and TR2 equilibrium $\overline{u'v'}$ anomalies (Fig. 6.4 (bottom)) show very little in the way of the decrease around the tropopause on the equatorward side of the jet. This decrease was found in chapter 4 to be the initial trigger of the tropospheric response. Fig. 6.13 demonstrates that both TR2 and TR4 show this initial decrease around the tropopause in the spin-up and so the initial response is triggered in the same way. The evolution of the TR2 spin-up demonstrates

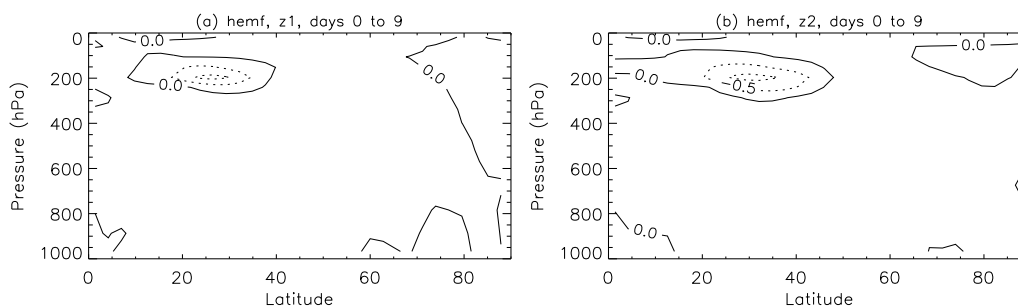


Fig. 6.13: Horizontal eddy momentum flux anomaly for days 0 to 9 of (a) the TR2 spin-up and (b) the TR4 spin-up.

that as the response progresses the much larger response in zonal wind and resulting equatorward refraction of eddies and increase in eddy momentum flux begins to dominate over this decrease.

The evolution over the spin-ups of TR2 and TR4 progress in a similar manner to that of chapter 4 and indeed over the first 100 days it is hard to distinguish between the TR2 and TR4 runs other than in the latitudinal distributions of their anomalies.

In order to examine the differences between TR2 and TR4, Fig. 6.14 presents the evolution of various parameters averaged over various regions of the latitude-pressure plane. The difficulty of looking at the wind anomaly at a particular latitude as a measure of the response is that the jets and their wind responses are centred at different latitudes. It is therefore difficult to ensure that the wind anomaly is measured at equivalent latitudes relative to the jet centre. Thus, as a measure of the magnitude of the tropospheric zonal wind response the mean absolute magnitude of the zonal wind anomaly at all latitudes and pressures between 196hPa and the surface has been calculated. This gives an approximate measure of the amplitude of the tripole wind anomalies seen in Fig. 6.3 (middle). The evolution of this mean magnitude of the wind anomalies over the TR2 and TR4 spin-ups is shown in Fig. 6.14 (a). It is clear that there is a dramatic difference in the evolution of this wind anomaly between TR2 and TR4.

They start of in a similar fashion with the wind anomaly increasing at a similar rate. However, TR4 reaches equilibrium much earlier and at a much lower value than TR2. The wind anomaly in TR2 continues to increase and in fact does not appear to have reached equilibrium by 300 days. In contrast the evolution of the temperature anomaly in the stratosphere is very similar in the TR2 and TR4 spin-ups. So, although the time taken for the stratosphere to respond is similar in each experiment, the time during which the troposphere responds is dramatically different between the two. Given the mechanism presented in Chapter 4 and the importance of the feedback between the eddies and the mean flow this suggests that the feedback is occurring more effectively in TR2 than TR4. It is allowing the wind anomalies and corresponding eddy

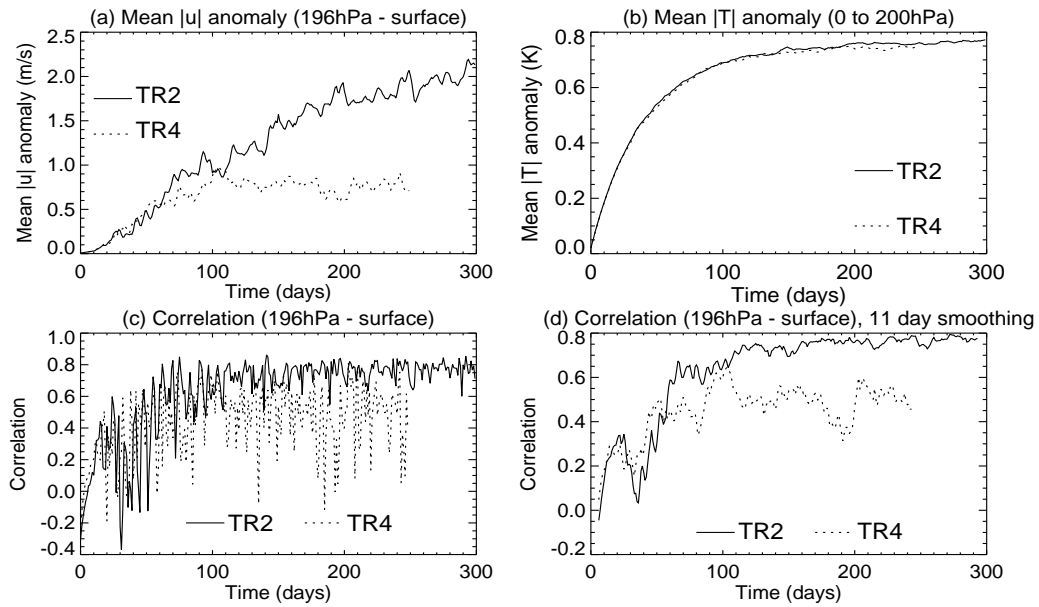


Fig. 6.14: Spin-up evolution for the E5 response in TR2 and TR4 (a) mean $|\bar{u}|$ anomaly between 196hPa and the surface, (b) mean $|\bar{T}|$ anomaly from 0 to 200hPa, (c) correlation between anomalies in horizontal eddy momentum flux convergence and zonal wind between 196hPa and the surface and (d) as (c) but with 11-day smoothing.

momentum flux anomalies to continue to increase for longer before they reach an equilibrated state in which they are balanced by surface friction and the temperature anomalies are balanced by the newtonian relaxation.

As a measure of the effectiveness of the tropospheric eddy momentum fluxes feeding back onto the zonal flow anomalies, the correlation between the eddy momentum flux convergence and the wind anomalies over all latitudes and pressures below 196hPa has been calculated and is presented in figures 6.14 (c) (daily) and (d) (11 day running mean). After around 10 days into the spin-up there begins to be a positive correlation between the eddy momentum flux convergence anomalies and the zonal wind anomalies as the feedback begins. The correlation then increases but it can be seen to be a lot higher for TR2 than TR4. This agrees with the suggestion above that the tropospheric feedback is occurring more efficiently in TR2 than TR4 which allows the wind anomalies to continue to grow for longer before reaching an equilibrium state in which the tropospheric response is of a larger magnitude.

Now to attempt to relate this to the discussion of the control run variability and the wave breaking latitudes in the previous section, it can be seen that the correlation for the TR4 run is considerably more variable than that for the TR2 run. In fact, for several of the days throughout the spin-up they are anti-correlated, whereas for the majority of the TR2 spin-up the correlation between eddy momentum flux convergence and zonal wind anomaly is above 0.5. It can also be seen from the 11-day smoothing that the mean correlation is considerably lower for TR4 than TR2. This suggests that the feedback involving tropospheric eddy momentum fluxes projecting back onto the zonal wind anomalies is much more efficient in TR2 than in TR4. Moreover, this decreased efficiency in TR4 appears to coincide with a much greater variability in the projection of eddy momentum flux anomalies onto the zonal wind. This is consistent with the previous discussion that for wider jets there is a much larger region over which eddy propagation is possible and thus many more possibilities for the behavior of each individual eddy. It is therefore less likely that the momentum flux due to each individual eddy will project back

onto the zonal wind anomalies exactly.

6.3.3 *Eddy feedback in the equilibrated situation.*

The discussion of these different tropospheric responses will be concluded with an examination of the feedback between the eddies and the mean flow at equilibrium. Fig. 6.15 shows the eddy momentum flux convergence anomalies along with the zonal wind anomalies from the control run for the ensemble mean of each E5 and P5 run. Apart from the different magnitudes of response between TR1 and TR5, this shows that there is also more of an offset between the eddy momentum flux convergence and the wind anomalies in the troposphere for those that show a smaller magnitude of response, particularly below around 250hPa. This is most apparent for the region of divergence on the equatorward side of the jet in the E5 runs. The offset is not as dramatic on the poleward side of the jet nor is it as dramatic for the P5 runs. Nevertheless, the trend is still there with the tropospheres that have a smaller magnitude of response to stratospheric heating having more of an offset between the eddy momentum flux convergence and the wind anomalies.

This can be summed up in Fig. 6.16 which shows the mean magnitude of zonal wind anomaly and the correlation between the eddy momentum flux convergence and wind anomaly over all latitudes and pressures. Figs. 6.16 (a) and (c) show the ensemble means and 95% confidence intervals for each E5 and P5 experiment respectively whereas (b) and (d) show the equivalent plot for each ensemble member individually. In the ensemble mean it is apparent that generally a larger magnitude of response is accompanied by a higher correlation between the eddy momentum flux convergence and the zonal wind anomalies i.e. a more efficient feedback between the eddies and the mean flow anomalies. There are large uncertainties on the ensemble mean values (particularly on the cross correlation of the E5 runs). Nevertheless, examination of the individual ensemble members shows a definite trend with the larger magnitude of response being concurrent with a higher cross correlation between the eddy momentum flux convergence and the zonal wind anomalies.

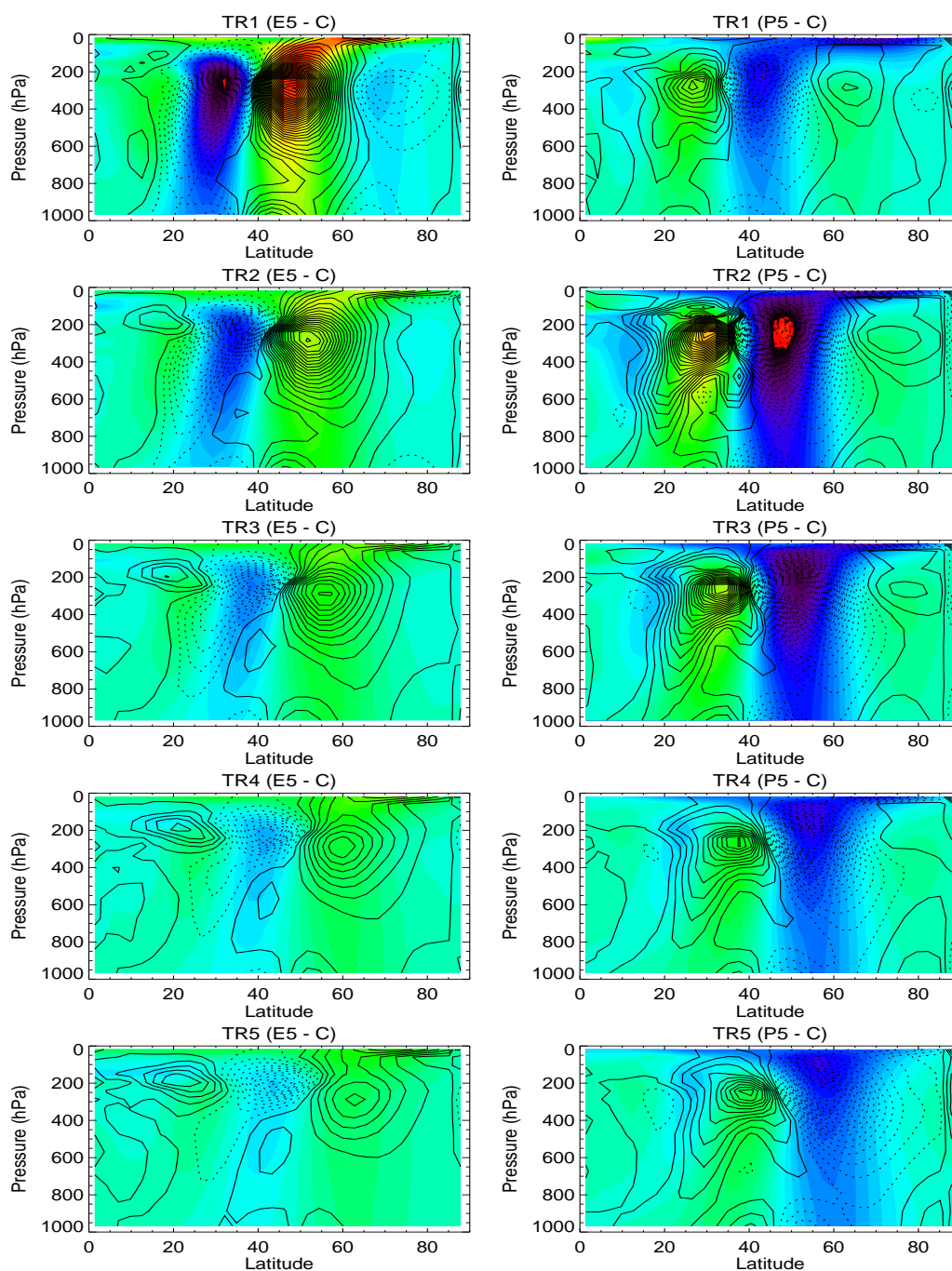


Fig. 6.15: (LHS) E5 equilibrium response, colours = zonal wind, contours = eddy momentum flux convergence, (solid = convergence, dashed = divergence), (RHS) as LHS but for the P5 response. Top to Bottom = TR1 to TR5.

Moreover, the ensemble members of each troposphere are clustered with the lower latitude/narrower jets generally having larger responses/higher cross correlations. The exception to this is the TR1 P5 experiment and further investigation is required to understand this.

6.4 Discussion and Conclusion

The effect that altered tropospheric jet structure has on the response to stratospheric heating has been investigated. Results have shown that similar

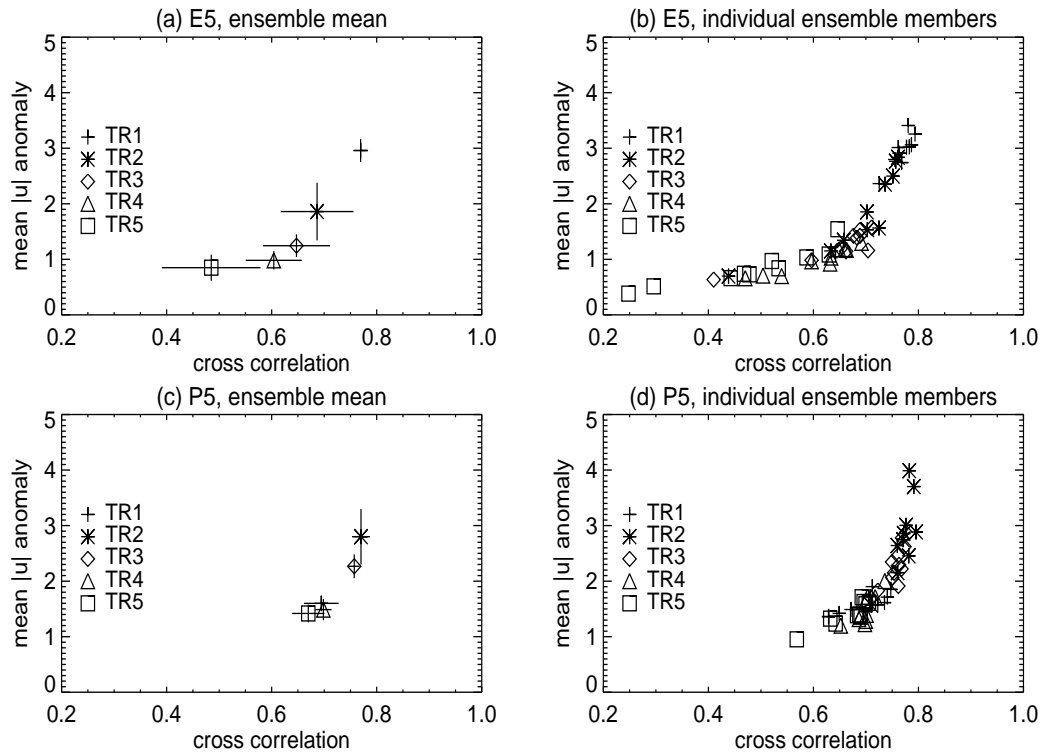


Fig. 6.16: (a) mean magnitude of zonal wind anomaly vs correlation between $\overline{u'v'}$ convergence and zonal wind anomaly at all latitudes and pressures for the E5 runs, (b) as (a) but for each of the individual ensemble members of the E5 experiments. (c) and (d) are as (a) and (b) but for P5.

patterns of response to the stratospheric heating are produced for each troposphere but with dramatically different magnitudes. It is demonstrated that for lower latitude/narrower jets the magnitude of response to E5 stratospheric heating is considerably larger than for higher latitude/wider jets. There is also a tendency for lower latitude/narrower jets to have a larger magnitude of response to P5 heating which suggests that it is not the proximity of the jet to the stratospheric heating that is important. Rather, it suggests that there is something about the structure of the lower latitude/narrower jets which allows it to have a larger response to a forcing. This is, perhaps, counterintuitive given the importance of eddies in producing the response and the much weaker eddies in those jets that tend to show the larger response.

The control run variability of each troposphere has also been examined and it is found that those jets which have a larger magnitude of response exhibit longer timescale variability of the mid-latitude westerlies in the control run. This is consistent with the ideas of the fluctuation-dissipation theorem and suggests that there is something about those jets which allows the feedback between the eddies and the mean flow to be stronger which results in both longer timescale variability in the control run and a larger magnitude of response to stratospheric heating.

It is proposed that the important factor in determining the strength of the eddy-mean flow feedback is the width of the jet region over which eddy propagation is possible. A calculation of the latitudes of wave breaking has demonstrated that for a lower latitude/narrower jet the distribution of wave breaking latitudes is much more meridionally confined compared to the broad distribution of the higher latitude/wider jets. As there is a larger region over which eddy propagation is possible in the wider jets there are a greater number of ways in which the eddies can behave and thus a greater number of ways in which the momentum fluxes due to those eddies can feed back onto the zonal wind anomalies.

It is demonstrated in an E5 spin-up ensemble for two of those tropospheres (TR2 and TR4) that for TR4, which has the wider jet, the projection of the

eddy momentum flux convergence anomalies onto the mean flow anomalies is much more variable, consistent with the above. Moreover, it is demonstrated in the equilibrium response to stratospheric heating that the correlation between the eddy momentum flux convergence in the troposphere and the zonal wind anomalies there is larger for those jets that exhibit a larger response. This is all consistent with a weaker feedback between the eddies and the mean flow in the higher latitude/wider jets and it is proposed that the reason for this is the greater variability in the ways in which individual eddies can behave, thus limiting the likelihood of the momentum flux due to each individual eddy projecting back onto the zonal wind anomalies in a consistent manner.

The evidence for this is limited by the statistical nature of the response i.e. that it is made up of a contribution due to many individual eddies at all longitudes and is also on top of a huge amount of natural variability. It is thus difficult to examine the response of the behavior of individual eddies to the stratospheric heating. Perhaps it could be useful to perform baroclinic life cycle experiments to examine the response of individual eddies to altered meridional wind shear for each of the jet structures to see whether it is indeed true that for the narrower jet, the way in which the eddies can respond is much more limited and thus results in them each being more likely to feed back onto the mean flow in the same way.

Recently, a great deal of research has been done into the variability of simplified GCMs such as this one. This is motivated by the fact that they appear to have unrealistically long decorrelation timescales as compared to the real atmosphere which exhibits variability on the timescale of the order of 10 to 20 days (Baldwin *et al.*, 2003). It is found that the timescale of variability is sensitive to various parameters including vertical resolution (Gerber *et al.*, 2008), equator to pole temperature gradient, the Newtonian relaxation timescale (k_T) and the friction timescale (k_f) (Gerber & Vallis, 2007). But, it is interesting that accompanying the changes in each of these parameters and lengthening of the decorrelation timescale is, consistently, an equator-

ward shift of the mid-latitude eddy driven jet and therefore a meridional confinement of the region of strong westerly winds (Gerber, 2006).

Another idea which is consistent with the reasoning presented in this chapter is the explanation of Gerber & Vallis (2007) for the enhanced persistence of those runs that exhibit the longer decorrelation timescale. They demonstrate that accompanying the enhanced persistence of their run with $\Delta T_{eq} = 40K$ as compared to $\Delta T_{eq} = 80K$ is a much greater zonal coherence i.e. there is a much greater correlation between the variability at one longitude and that at another longitude. Perhaps this is consistent with the greater meridional confinement of the eddies and the increased likelihood of them behaving the same way at each longitude.

This brings us onto the effect that introducing zonal asymmetries might have on both the natural variability of the control run simulations and the response to stratospheric heating as it has been demonstrated by Gerber & Vallis (2007) that the zonal coherence is reduced, as is the sensitivity of the autocorrelation timescale described above, when topography is present in the model. Moreover, Son *et al.* (2008b) have demonstrated that introducing topography into their runs which previously exhibited the longer timescale zonal index behavior shifted them into the regime of shorter timescale poleward propagation. Whereas for those jets that were already in this regime, the introduction of the mountain had little effect. The effect of introducing topography on the E5 response to stratospheric heating was investigated in Chapter 5 for TR3. With hindsight it would have been useful to investigate the impact of topography on either TR1 or TR2 to see whether this impacts on the control run variability, and the response to stratospheric heating, and, if so, what aspects of the zonal flow are changing to produce this impact.

By comparison of the magnitude of the response to E5 heating in chapter 4 with the observational signal over the solar cycle it may have been difficult to be convinced that the magnitude of the model response (when scaled down by e.g. a factor of 5) was sufficient to explain the observed signal. But, here it has been demonstrated that this magnitude of response is highly variable and

an order of magnitude larger response can be produced by a slight alteration of the tropospheric jet structure. If this magnitude of response were to remain in the presence of zonal asymmetries then it could easily account for the magnitude of the solar signal seen in the observations. This remains for further study.

It would also be interesting to see whether the differing magnitudes of response hold for zonally localised regions where, for example, the jet was more equatorward and merged with the sub-tropical jet or vice-versa. If this was the case then it may be expected that, for example, a different magnitude of response would occur over the Pacific than the Atlantic oceans or the magnitude of response may vary with season. Very long runs would be required to get a statistically representative sample to examine this.

There are, therefore, many more experiments that could be performed to investigate the impact of various aspects of the model on the magnitude of the response to stratospheric heating and the results of both this chapter and Chapter 5 have demonstrated just how variable the magnitude of response in a GCM such as this can be. It is therefore important to investigate this and determine which would be the most realistic situation for the real atmosphere.

7. CONCLUSIONS AND FUTURE WORK

In this study a simplified GCM has been used to investigate the tropospheric response to stratospheric heating perturbations. This work has been motivated by many previous studies (Haigh *et al.*, 2005; Kushner & Polvani, 2004, 2006; Polvani & Kushner, 2002; Williams, 2006; Lorenz & DeWeaver, 2007) that have shown that perturbations to the temperature of the lower stratosphere of sGCMs can have a significant impact on the tropospheric circulation. In each of the above studies a perturbation to the lower stratospheric temperature results in an annular mode-like response in the troposphere i.e. an equatorward or poleward shift of the mid-latitude jets. The sign of this shift has been shown to depend on both the sign of the applied heating perturbation and its meridional distribution (Lorenz & DeWeaver, 2007; Haigh *et al.*, 2005). Here, spin-up ensemble experiments have been used to investigate further the mechanisms involved in driving the tropospheric response to the stratospheric heating perturbations. With increasing understanding of the mechanism involved in producing the response, the reason for the dependence of the sign of the response on the latitudinal distribution of the applied temperature perturbation has also become apparent.

Following this, the impact of various changes in the tropospheric climatology on the magnitude of response has been investigated. Specifically, the effect of introducing zonal asymmetries and the effect of varying tropospheric jet structure.

The primary aim of these experiments was to investigate the mechanism that may be responsible for the tropospheric response to changing solar activity. However, the results could equally be applied to any perturbation that results in a change in lower stratospheric temperature such as ozone

depletion (Hartmann *et al.*, 2000), ozone recovery (Eyring *et al.*, 2007) or the increased abundance of greenhouse gases (Santer *et al.*, 2003). Indeed in modelling studies and observations of the response to these forcings, the change in stratospheric temperature is accompanied by a shift in the position of the mid-latitude jet that is consistent with the results of this study (Son *et al.*, 2008a; Lorenz & DeWeaver, 2007). Temperature perturbations of the lower stratosphere in response to these forcing and others are therefore likely to have an impact on tropospheric circulation and the mechanism presented in Chapter 4 is likely to play a role. Detailed conclusions are given at the end of each chapter but, here, a brief summary of the main conclusions to be taken from each chapter will be given along with some suggestions for future work.

7.1 Conclusions

7.1.1 The mechanism

In Chapter 4, spin-up ensemble experiments have been used to investigate the mechanism whereby temperature perturbations in the lower stratosphere can influence the tropospheric circulation. This followed on from the work of Haigh *et al.* (2005) where it was shown that an increase in temperature of the equatorial lower stratosphere resulted in a poleward shift of the mid-latitude jet whereas a uniform or polar heating of the lower stratosphere resulted in an equatorward shift of the mid-latitude jet. The equatorial heating case is thought of as being qualitatively similar to the solar cycle response in lower stratospheric temperature and is found to give qualitatively similar patterns of response, in the troposphere, to those found over the solar cycle.

The equilibrium responses of Haigh *et al.* (2005) revealed the importance of changes in the eddy momentum flux anomalies in maintaining the tropospheric response. The spin-up ensembles have verified that not only are the eddies important in maintaining the tropospheric response but they are also instrumental in creating it. Moreover, examination of the evolution of the

model in response to the heating has revealed what aspects of the changing zonal flow and temperature structure influence the eddies to produce the response. The proposed mechanism whereby changes in lower stratospheric temperature can influence the troposphere is shown schematically in Fig. 4.21 and can be summarised as follows:

- The change in temperature of the lower stratosphere alters the meridional and vertical temperature gradients around the tropopause.
- The initial response to the altered meridional temperature gradients is to produce changes in zonal wind and mean meridional circulation through thermal wind adjustment.
- The change in vertical temperature gradient changes the static stability around the tropopause. For the case of a warming of the lower stratosphere there is an increase in static stability which weakens the upward E-P flux around the tropopause. The quasi-geostrophic refractive index also shows a slight impact of altered vertical wind shear in response to altered meridional temperature gradient on eddy propagation. The primary influence, however, seems to be the altered vertical temperature gradient around the tropopause which weakens the upward eddy propagation.
- This weakening of the upward eddy propagation brings with it horizontal eddy momentum flux anomalies around the tropopause.
- These horizontal eddy momentum flux anomalies are important in driving zonal wind accelerations directly in the upper troposphere and meridional circulation changes result in zonal flow accelerations in the lower troposphere.
- These initial zonal flow changes in response to both the altered meridional temperature gradients and the altered horizontal eddy momentum fluxes appear to trigger an important feedback.

-
- Altered meridional wind shear across the jet centre results in refraction of the eddies in such a way that produces tropospheric eddy momentum flux anomalies which act to feed back onto the initial zonal flow anomalies.
 - There is another implicit feedback that comes with the spreading of the zonal flow anomalies throughout the depth of the troposphere. An easterly anomaly with easterly vertical shear reduces the local baroclinicity which weakens the E-P flux source and weakens the eddy forcing of westerly flow at that latitude and vice-versa for westerly anomalies. This is similar to the mechanism of eddy feedback onto the zonal index anomalies proposed by Robinson (2000) and Lorenz & Hartmann (2003).
 - The effects of meridional wind shear on refractive index then acts to refract these anomalous eddies produced in the region of increased vertical wind shear in such a way as to further reinforce the zonal wind anomalies. Thus, when there is an anomalous westerly wind on the poleward side of the jet there is increased eddy production there with these eddies being refracted equatorward by the anomalous meridional wind shear producing poleward momentum fluxes across the jet maximum which act to reinforce the wind anomalies. Conversely, when there is an anomalous westerly wind on the equatorward side of the jet there is increased eddy production there with these eddies being refracted poleward resulting in equatorward eddy momentum flux in the troposphere across the jet centre which, again, reinforces the zonal wind anomalies.

Comparison of each of the E5, U5 and P10 heating perturbations has revealed that it is the altered vertical temperature gradient and its localisation in latitude that is important in determining the direction of the jet shift. The latitudinal extent of the altered vertical temperature gradient determines the latitudinal extent of the altered horizontal eddy momentum flux around the

tropopause, and thus the latitude at which the initial mean meridional circulation changes and zonal wind accelerations/decelerations are occurring. This then results in different senses of the tropospheric eddy momentum flux anomalies which act to feedback onto the zonal flow anomalies. This results in heating of the lower stratosphere that is localised to low latitudes producing a poleward shift of the jet whereas heating that is latitudinally uniform or localised towards the poles results in an equatorward shift of the jet. Here, stratospheric cooling experiments have not been performed but if this mechanism holds for those the opposite would be true. Cooling of the equatorial stratosphere would result in an equatorward shift of the jet whereas uniform or polar cooling would result in a poleward shift of the jet. This has, indeed, been the case in other studies (Lorenz & DeWeaver, 2007; Polvani & Kushner, 2002; Williams, 2006).

The above mechanism could be useful in explaining the solar cycle signal as well as any other tropospheric responses to perturbations in lower stratospheric temperature. As discussed in the conclusions of Chapter 4, there may be a concern as to whether the magnitude of response is sufficient to explain the observed tropospheric response to solar activity. But, the results of Chapters 5 and 6 have shown that the magnitude of response in the model is highly variable and depends on a number of different factors.

7.1.2 The effect of zonal asymmetries

In Chapter 5, the effect of introducing zonal asymmetries in the form of topography and a quadrupole perturbation to the tropospheric relaxation temperature profile was investigated. The motivation for this was to see whether the mechanism and response found in the zonally symmetric situation of Chapter 4 holds in the presence of zonal asymmetries which bring the model closer to the real atmosphere. Moreover, Gerber & Vallis (2007) have demonstrated that simplified GCMs with zonally symmetric boundary conditions have unrealistically long annular mode decorrelation timescales. The fluctuation-dissipation theorem implies that this may lead to these models

being overly sensitive to forcing that projects onto the models annular mode. The presence of zonal asymmetries (particularly topography) tends to reduce the decorrelation timescale to more realistic values. These experiments were therefore designed to test whether the same pattern of response to stratospheric heating is produced and, if so, whether there is a reduction in the magnitude of response in the presence of zonal asymmetries.

It was found that there is a large amount of variability in the magnitude of the model response even for runs of 5000 days length. The results of Chapter 5 have demonstrated that runs of several thousand days, as commonly used with sGCMs like these, are insufficient for accurate determination of the magnitude of response. Nevertheless, ensembles of 10, 5000 day E5 experiments for the Q and R experiments have shown that, despite this variability, qualitatively similar patterns are produced for each ensemble member and each experiment and these are qualitatively similar to the patterns produced in the E5 experiments of Chapter 4. It is found that even in the presence of these zonal asymmetries, the tropospheric response is still produced and the forcing by small scale baroclinic eddies remains the dominant mechanism.

Determination of the influence of asymmetries on the magnitude of response was made difficult by the large variability in the magnitude between individual ensemble members of the same experiment. However, there is an indication from the ensemble means that there is a slight reduction in the magnitude of response in the presence of either the Q or R asymmetry. This is consistent with the reduction in the decorrelation timescale of the control run variability in the presence of either asymmetry. Thus, the main conclusions to be taken from these experiments are that:

- Runs of several thousand days are not sufficient for accurate determination of the magnitude of response.
- Qualitatively, the patterns of response to E5 stratospheric heating are unchanged in the presence of zonal asymmetries. The mechanism of Chapter 4 is still dominant.

- There is a reduction in the magnitude of response in the presence of asymmetries but the large uncertainty in the magnitude of response even with these 10 member ensembles makes it difficult to assign a value to this reduction.

7.1.3 The effect of varying tropospheric jet structure

The final set of experiments examined the effect of varying the tropospheric jet structure on the response to stratospheric heating. Five different tropospheres were created by changing the relaxation temperature profile in the troposphere. This resulted in five different jets of varying latitude, strength and width going from lower latitude/weaker/narrower jets to higher latitude/stronger/wider jets. An ensemble of E5 and P5 stratospheric heating experiments were then performed for each of these different tropospheres. It was found that there is quite a dramatic influence on the magnitude of response with generally a stronger response to stratospheric heating for lower latitude/weaker/narrower jets than for higher latitude/stronger/wider jets. The only exception to this is TR1 P5 and further work is required to understand this. It may be that this low latitude jet is so far from the polar stratospheric heating that the distance from the stratospheric heating is having more of an effect on the magnitude of response than the tropospheric jet structure.

This is accompanied by much longer timescales of variability in the control run simulations of the lower latitude/weaker/narrower jets. This is consistent with what is expected from the fluctuation-dissipation theorem. Indeed it is true that for all the experiments performed, the tropospheres that show a larger response to stratospheric heating tend to have longer timescale variability in their control runs. This is summarised in Fig. 7.1 which shows the mean magnitude of zonal wind anomaly at every latitude and pressure versus the control run decorrelation timescale for the ensemble mean of all the E5 heating experiments of Chapters 5 and 6. 95% confidence intervals are shown for each of the values. Again, this demonstrates , particularly for those runs

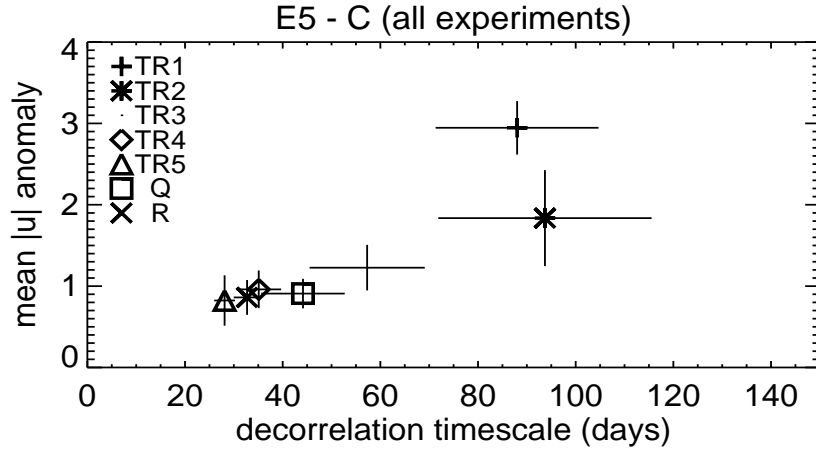


Fig. 7.1: Mean magnitude of zonal wind anomaly over all latitudes and pressures versus control run decorrelation timescale for the ensemble means of each E5 stratospheric heating experiment. 95% confidence intervals are also shown.

that have a long decorrelation timescale, that there is a large uncertainty in both the decorrelation timescale and the magnitude of response, highlighting the need for long runs to accurately determine these values. But, generally, it can be seen that those tropospheres that have a larger magnitude of response to stratospheric heating also exhibit longer timescale variability in their control runs.

As it is also true, in general, that for the P5 runs the lower latitude jets have a larger magnitude of response to stratospheric heating, the difference in the magnitude of response does not appear to be related to the proximity of the stratospheric heating to the jet. Rather there seems to be some aspect of the structure of the lower latitude/narrower jets which leads them to have a stronger feedback between the eddies and the mean flow, which results in both longer timescale variability in the control run and a larger magnitude of response to stratospheric heating.

In Chapter 6 it is suggested that the key to determining the strength of the eddy feedback is the width of the jet. It is suggested that for narrower jets,

where the region over which eddy propagation is possible is more meridionally confined, when eddies are refracted by the changes in the mean flow there is a greater chance that the momentum flux due to each eddy will be feeding back onto the zonal flow in the same manner simply because the region over which the eddies can propagate is more meridionally confined.

Evidence for this is presented in the form of wave breaking latitude calculations. These demonstrate that in the control run simulations, for the lower latitude/narrower jets, the region over which wave breaking is occurring is much more meridionally confined. The response to E5 stratospheric heating is then shown to result in enhanced anticyclonic wave breaking. Although it is difficult to determine much from the equilibrium differences due to the difficulty in separating cause from effect, it can be seen that, for more meridionally confined jets, the latitude region over which the percentage of days of a particular wave breaking latitude is changing is more meridionally confined. It is suggested that the meridional confinement of the eddies leads them to each be feeding back onto the zonal wind anomalies in a more consistent manner.

The correlation of the patterns of eddy momentum flux convergence with the patterns of zonal wind anomalies in the meridional plane is also presented. Those jets that have a larger magnitude of response to stratospheric heating have a higher degree of correlation between the eddy momentum flux convergence and the zonal wind anomalies. In other words, the feedback between the eddies and the mean flow is more effective.

Moreover, a spin-up ensemble for two of the tropospheres (TR2 and TR4) has demonstrated that for TR4 (the wider jet) the projection of the eddy momentum flux onto the mean flow anomalies is much more variable throughout the spin-up than for the narrower jet which is consistent with the idea that for wider jets, where there is a much larger region over which eddy propagation is possible, there are more ways in which the eddies can behave and thus the likelihood that their momentum fluxes will feed back onto the zonal wind anomalies in the same way is reduced. The evidence for this is not com-

pletely conclusive and further work is required to see if this really is the main factor in determining the strength of the eddy feedback and the magnitude of response to stratospheric heating.

But what can be taken away from this chapter with certainty is that the magnitude of the response to stratospheric heating is significantly different with altered tropospheric jet structures (at least in these simulations with zonally symmetric boundary conditions). If this were to remain true in the presence of zonal asymmetries then it may be more convincing that the magnitude of the observed tropospheric signal over the solar cycle could be produced by the $\sim 1\text{K}$ heating in the lower stratosphere. But, this remains for further work.

7.2 *Future work*

The response to stratospheric heating and the importance of small scale baroclinic eddy momentum fluxes in producing it is robust in all of the sGCM experiments of this study.

The two main avenues for future work should probably be to see whether this remains valid for increasing complexity of models i.e. getting closer to the real atmosphere, and also further investigation into the magnitude of response and what controls it.

Considering the first of these: one of the major simplifications of this model is the lack of moisture. All moist processes are parameterised by the Newtonian relaxation of the temperature field. It would be interesting to see the effect of introducing moisture into the model on the response. Also, it would be interesting to look at the effects of having realistic topography and land-sea temperature contrasts. If the introduction of zonal asymmetries does reduce the magnitude of response then realistic topography may have a dramatic influence on the magnitude. Also, given the importance of small scale baroclinic eddies in producing the response, this may result in the response being localised in the storm track regions which would be interesting

to check. However, given that it was difficult to do this with the simplified Q and R asymmetries, this may be very noisy and thus require very long runs.

The results of Chapter 6 showed a dramatic impact of the altered tropospheric jet structure on the magnitude of response. It would be interesting to introduce a seasonal cycle into the model, which would result in changes in tropospheric jet structure, and then see the impact of that on the magnitude of response.

The other avenue for future work would be to continue investigating what determines the magnitude of response in the sGCM. Chapters 5 and 6 have shown that there is an influence of the structure of the troposphere on the magnitude of the response.

Firstly, the impact of topography was investigated with the original Held-Suarez configuration (TR3). However, the studies of Son *et al.* (2008b) have shown that topography may have a more dramatic impact on jets that are in the longer timescale 'zonal index' regime. It would therefore be useful to check whether introducing a ridge of the form of the R experiments results in a large reduction in the magnitude of response for the TR1 and TR2 experiments. If this is the case then, although it may be interesting, from the perspective of looking at the dynamics of sGCM's with zonally symmetric boundary conditions, to continue looking at the impact of tropospheric jet structure on the magnitude of response, it may not be all that relevant for the real atmosphere. What may be more important is to determine exactly what about the topography results in this reduction in magnitude.

However, it would also be interesting to research further into why the tropospheric jet structure with zonally symmetric boundary conditions does have such an effect. The reasoning proposed in Chapter 6 is not completely conclusive and requires further investigation. Baroclinic lifecycle experiments, to look at the effect of altered meridional shear on individual baroclinic eddies, must be able to determine whether the hypothesis of Chapter 6 is at least true in the lifecycle context.

Finally, it has been shown that there is a large amount of variability in the

magnitude of response and the results have clearly demonstrated that runs of 5000 days length are insufficient to determine the magnitude of response accurately. Further work is required to determine how long a run is required to obtain magnitudes of response and decorrelation timescales to the desired accuracy.

To conclude, there is a lot of work that remains to be done in examining this mechanism. The evidence from this study and others, as well as from observations suggests that temperature perturbations of the lower stratosphere do have an impact on tropospheric circulation and that the mechanism presented in Chapter 4 is likely to be important. An sGCM has been used here as it is the best way of gaining a detailed understanding of dynamical processes. In the future it is important to determine how these processes translate into more realistic atmospheric situations and to determine whether this mechanism is indeed responsible for the production of the tropospheric response to stratospheric heating perturbations.

Appendix

Derivation of quasi-geostrophic refractive index

Here the quasi-geostrophic refractive index is derived following similar procedures to that used by Matsuno (1970) for stationary planetary waves and Karoly & Hoskins (1982) for transient planetary waves. For ease of notation the derivation is presented for the quasi-geostrophic approximation on a β plane (i.e. $f = f_o + \beta y$) but this can easily be translated into the equivalent equations for spherical coordinates.

We take as a starting point, the primitive equations in the quasi-geostrophic approximation on a β plane in the absence of friction (see e.g. Andrews *et al.* (1987)):

$$D_g u_g - f_o v_a - \beta y v_g = 0 \quad (\text{A1})$$

$$D_g v_g + f_o u_a + \beta y u_g = 0 \quad (\text{A2})$$

$$\frac{\partial u_a}{\partial x} + \frac{\partial v_a}{\partial y} + \frac{1}{\rho_o} (\rho_o w_a)_z = 0 \quad (\text{A3})$$

$$\Phi_z = \frac{R\theta}{H} \exp\left(-\frac{\kappa z}{H}\right) \quad (\text{A4})$$

$$D_g \theta_d + w_a \frac{d\theta_o}{dz} = 0 \quad (\text{A5})$$

where the ageostrophic velocities are given by $u_a = u - u_g$, $v_a = v - v_g$, $w_a = w$ and are assumed to be small. These are the quasi-geostrophic, β plane equivalents of Eqs. 3.8 to 3.12 but now using cartesian coordinates (x, y, z) . The geostrophic velocities u_g and v_g are the velocities that when acted on by the coriolis force balance the horizontal pressure gradients and $D_g = \partial/\partial t + u_g \partial/\partial x + v_g \partial/\partial y$ is the advective derivative following the geostrophic

flow. The potential temperature and density are assumed to consist of a background state which is a function of z only plus a small departure from that state such that $\theta = \theta_o(z) + \theta_d(x, y, z, t)$ and $\rho = \rho_o(z) + \rho_d(x, y, z, t)$. Taking $\partial(A2)/\partial x - \partial(A1)/\partial y$ and making use of the continuity equation (A3) gives the vorticity equation:

$$D_g \zeta_g + \beta v_g - \frac{f_o}{\rho_o} \frac{\partial(\rho_o w_a)}{\partial z} = 0. \quad (A6)$$

where $\zeta_g = \partial v_g / \partial x - \partial u_g / \partial y$ is the geostrophic vorticity. The geostrophic stream function is then defined by $\psi = f_o^{-1} (\Phi - \Phi_o)$ where Φ is the geopotential height and Φ_o is the geopotential height of the background state which is a function of z only. The geostrophic velocities can be written in terms of this stream function:

$$u_g = -\frac{\partial \psi}{\partial y}, \quad v_g = \frac{\partial \psi}{\partial x}. \quad (A7)$$

Using the definition of stream function together with hydrostatic balance, (A4), the departure of potential temperature from the reference state (θ_d) can be written in terms of the geostrophic stream function

$$\theta_d = HR^{-1} \exp\left(\frac{\kappa z}{H}\right) f_o \psi_z. \quad (A8)$$

Combining this with the thermodynamic equation (A5), the vertical velocity can be written in terms of the stream function

$$w_a = -D_g \left(\frac{f_o \psi_z}{N^2} \right) \quad (A9)$$

where N^2 is the buoyancy frequency given by

$$N^2 = \frac{g}{\theta} \frac{d\theta_o}{dz} = H^{-1} \text{Re} \exp\left(-\frac{\kappa z}{H}\right) \frac{d\theta_o}{dz}. \quad (A10)$$

w_a can then be eliminated from the vorticity equation (A6) and also making use of the fact that $\beta v_g = D_g f$ gives the potential vorticity equation

$$D_g q = 0 \quad (A11)$$

where

$$q = f + \zeta_g + \frac{1}{\rho_o} \frac{\partial}{\partial z} \left(\frac{f_o^2 \rho_o}{N^2} \frac{\partial \psi}{\partial z} \right) \quad (A12)$$

is the potential vorticity (PV) which is conserved following the geostrophic flow in the absence of friction or diabatic heating.

Next, considering a perturbation to a purely zonal basic state denoted by $u_o(y, z)$, ($v_o = w_o = 0$) such that

$$u = u_o + u' \quad (\text{A13})$$

$$v = v' \quad (\text{A14})$$

$$q = q_o + q' \quad (\text{A15})$$

where the perturbation (dashed) quantities are assumed to be small compared to the basic state quantities. Substituting these into the PV equation gives the perturbation PV equation

$$\frac{\partial q'}{\partial t} + u_o \frac{\partial q'}{\partial x} + v' \bar{q}_y = 0 \quad (\text{A16})$$

where

$$q' = \zeta'_g + \frac{1}{\rho_o} \frac{\partial}{\partial z} \left(\frac{f_o^2 \rho}{N^2} \frac{\partial \psi'}{\partial z} \right) \quad (\text{A17})$$

$$\bar{q}_y = \beta - \bar{u}_{oyy} - \frac{1}{\rho_o} \frac{\partial}{\partial z} \left(\frac{f_o^2 \rho_o}{N^2} \frac{\partial \bar{u}_o}{\partial z} \right) \quad (\text{A18})$$

Using equations A7, this can be written in terms of the perturbation stream function (ψ'):

$$\left(\frac{\partial}{\partial t} + u_o \frac{\partial}{\partial x} \right) \left\{ \left[\frac{\partial^2}{\partial x^2} + \frac{\partial^2}{\partial y^2} + \frac{1}{\rho_o} \frac{\partial}{\partial z} \left(\rho_o \frac{f_o^2}{N^2} \frac{\partial}{\partial z} \right) \right] \psi' \right\} + \bar{q}_{oy} \frac{\partial \psi'}{\partial x} = 0 \quad (\text{A19})$$

So, this gives an equation for the perturbation stream function associated with a perturbation to the zonal mean basic state. If we assume that the amplitude of any perturbation to this stream function grows exponentially with height in association with the exponential decrease in density with height then we can put in a solution of the form

$$\psi'(x, y, z, t) = \exp\left(\frac{z}{2H}\right) \Re(\Psi(y, z) \exp(i(k_m x - k_m c t))) \quad (\text{A20})$$

where k_m is the zonal wavenumber in m^{-1} and c is the zonal phase speed in ms^{-1} . Then we obtain the following equation for the amplitude of the

perturbation as a function of y and z .

$$\Psi_{yy} + \frac{f_o^2}{N^2} \Psi_{zz} + n^2 \Psi = 0 \quad (\text{A21})$$

where

$$n^2 = \frac{q_y}{u_o - c} - \frac{k^2}{a^2 \cos^2 \phi} - \frac{f^2}{4N^2 H^2} \quad (\text{A22})$$

and k is a dimensionless zonal wavenumber. This is a wave equation for the two-dimensional propagation of the perturbation streamfunction. The quantity n^2 can be thought of as the refractive index for the propagation of the atmospheric wave, which is a function of latitude and height. It will be shown in the following that the wave will propagate up the gradient of refractive index.

The spherical analogues of Eqs. A18, A21 and A22 are

$$\frac{1}{a^2 \cos^2 \phi} \frac{\partial}{\partial \phi} \left(\cos \phi \frac{\partial \Psi}{\partial \phi} \right) + \frac{f_o^2}{N^2} \Psi_{zz} + n^2 \Psi = 0 \quad (\text{A23})$$

$$n^2 = \frac{q_\phi}{a(u - c)} - \frac{k^2}{a^2 \cos^2 \phi} - \frac{f^2}{4N^2 H^2} \quad (\text{A24})$$

$$q_\phi = 2\Omega \cos \phi - \frac{1}{a} \frac{\partial}{\partial \phi} \left(\frac{1}{a \cos \phi} \frac{\partial (u \cos \phi)}{\partial \phi} \right) + \frac{a}{\rho_o} \frac{\partial}{\partial z} \left(\frac{f_o^2 \rho_o}{N^2} \frac{\partial \bar{u}}{\partial z} \right) \quad (\text{A25})$$

Eqs. A24 and A25 are equivalent to Eqs. 3.30 and 3.31.

Why are waves refracted up the gradient of n^2 ?

In order to investigate the properties of equation A21 the WKB approximation can be used. In this approximation you can assume that the disturbance stream function in the y - z - plane (Ψ) is linear i.e. can be written as:

$$\Psi = \hat{\Psi}(y, z) \exp(i\chi(y, z)) \quad (\text{A26})$$

where χ is the phase which is real. The major assumption of the WKB approximation is that the phase varies more rapidly with y and z than do the quantities of the basic flow (\bar{u} , \bar{q}_y or n^2) or the amplitude of the disturbance stream function $\hat{\Psi}$ or the derivatives of χ . Under this approximation the

terms $\partial^2\chi/\partial z^2$, $\partial^2\chi/\partial y^2$, $\partial\hat{\Phi}/\partial y$ and $\partial\hat{\Phi}/\partial z$ can be neglected compared to $\partial\chi/\partial y$ and $\partial\chi/\partial z$. The wavenumbers in the meridional and vertical directions are defined as

$$l \equiv \frac{\partial\chi}{\partial y}, \quad m \equiv \frac{\partial\chi}{\partial z} \quad (\text{A27})$$

Thus, putting a solution of the form A26 into equation A21 gives:

$$n^2 = l^2 + \frac{f_o^2}{N^2}m^2 = \tilde{l}^2 + \tilde{m}^2 \quad (\text{A28})$$

where \tilde{l} and \tilde{m} are the meridional and vertical wavenumbers in a stretched coordinate system $((\tilde{y}, \tilde{z}) = (y, \frac{N}{f_o}z))$. So, the refractive index squared (n^2) can be thought of as the sum of the meridional and vertical wavenumbers squared in this stretched coordinate system.

Karoly & Hoskins (1982) demonstrated that under certain assumptions waves will be refracted up the gradient of the total wavenumber $K^2 = k^2 + l^2 + m^2$. One of the assumptions is that the waves follow a dispersion relation which is isotropic in the y and z wavenumbers.

Upon putting in the above plane wave solution into equation A21, the following dispersion relation is obtained:

$$\omega = ck_m = k_mu_o - \frac{\bar{q}_{oy}k_m}{k_m^2 + l^2 + \frac{f_o^2}{N^2}m^2 + \frac{f_o^2}{4N^2H^2}} \quad (\text{A29})$$

This is isotropic in the y and z wavenumbers if you consider the wavenumbers in the stretched vertical coordinates $\tilde{z} = \frac{N}{f_o}z$.

Following Karoly & Hoskins (1982), if you consider a dispersion relation which is isotropic in the y and z wavenumbers to have the form

$$\omega = F(y, z, K_\omega^2) \quad (\text{A30})$$

where $K_\omega^2 = k^2 + l^2 + m^2$ is the total wavenumber of a wave of fixed frequency ω . Considering a wave of fixed zonal wavenumber k , the group velocity in the y - z - plane is given by

$$c_{gr} = (v_{gr}, w_{gr}) = \left(\frac{\partial\omega}{\partial l}, \frac{\partial\omega}{\partial m} \right) = \left(2l \frac{\partial F}{\partial K_\omega^2}, 2m \frac{\partial F}{\partial K_\omega^2} \right) \quad (\text{A31})$$

So, in the y - z plane the wave can be thought of as following a ray with this group velocity in the y and z directions. The angle θ of the direction of propagation in the y - z plane to the horizontal is therefore given by

$$\tan\theta = \frac{w_{gr}}{v_{gr}} = \frac{m}{l} \quad (\text{A32})$$

A small change in F or equivalently ω , with a small change in the y direction can be written

$$\Delta F = \frac{\partial F}{\partial y} \Delta y + \frac{\partial F}{\partial K_\omega^2} \Delta K_\omega^2 \quad (\text{A33})$$

and as we are considering waves of a fixed frequency this is equal to zero. Therefore in the limit $\Delta \rightarrow 0$

$$\frac{\partial F}{\partial y} + \frac{\partial F}{\partial K_\omega^2} \frac{\partial K_\omega^2}{\partial y} = 0 \quad (\text{A34})$$

Under the WKBJ approximation

$$\frac{\partial F}{\partial y} = -\frac{d_{gr}l}{dt} \quad (\text{A35})$$

(see e.g. Andrews *et al.* (1987) pg 215) where $\frac{d_{gr}}{dt} = \frac{\partial}{\partial t} + c_{gr} \cdot \nabla$ is the advective derivative moving with the group velocity. Combining this with equation A34 and using A31 gives

$$m \frac{d_{gr}l}{dt} = w_{gr} K_\omega \frac{\partial K_\omega}{\partial y} \quad (\text{A36})$$

In a similar way considering a small change in the z direction it can be shown that

$$l \frac{d_{gr}m}{dt} = v_{gr} K_\omega \frac{\partial K_\omega}{\partial z} \quad (\text{A37})$$

Taking the rate of change of equation A32 following the ray gives

$$\frac{d_{gr}\theta}{dt} = \sec^2\theta \frac{d_{gr}\theta}{dt} = l^{-2} \left(l \frac{d_{gr}m}{dt} - m \frac{d_{gr}l}{dt} \right) \quad (\text{A38})$$

and then using equations A36 and A37 and the fact that $\sec^2\theta = (\cos\theta)^{-2} = (l^2 + m^2)/l^2$ gives

$$\frac{d_{gr}\theta}{dt} = \frac{1}{l^2 + m^2} \left(v_{gr} K_\omega \frac{\partial K_\omega}{\partial z} - w_{gr} K_\omega \frac{\partial K_\omega}{\partial y} \right) = \frac{K_\omega}{K_\omega^2 - k^2} \tilde{\mathbf{i}} \cdot (c_{gr} \times \nabla K_\omega) \quad (\text{A39})$$

So, from this it can be seen that waves will always be refracted toward the gradient of K_ω e.g. if the group velocity was in the same direction as ∇K_ω then $d_{gr}\theta/dt = 0$ whereas if they are perpendicular then $d_{gr}\theta/dt$ is maximum and the angle of the direction of propagation of the ray will be changed such that it is more in the direction of ∇K_ω .

So, Karoly & Hoskins (1982) showed that, if the WKB approximation can be applied and you have a dispersion relation which is isotropic in the y and z wavenumbers, then waves of a fixed zonal wavenumber k and frequency ω will be refracted up the gradient of total wavenumber squared. For planetary waves in the stretched coordinate system we do have a dispersion relation that is isotropic in the y and z wavenumbers and the results of Karoly & Hoskins (1982) are equivalent to saying that waves will be refracted up the gradient of $K^2 = k^2 + l^2 + \frac{f_o^2}{N^2}m^2$. For a fixed zonal wavenumber this is equivalent to waves being refracted up the gradient of n^2 by A28 if you neglect any variation in f^2/N^2 .

The relationship between E-P flux and group velocity

Thus, it has been demonstrated that the refractive index can be useful in determining the direction of propagation of the eddies but we now need to determine how that is related to the E-P flux and thus eddy heat and momentum fluxes. It can be shown that, in fact, under the assumptions of WKB theory, the E-P flux is in the same direction as the group velocity (See e.g. Andrews *et al.* (1987) pg 187).

On a β plane in the quasi-geostrophic approximation the E-P flux is given by

$$\vec{F} = \left(0, -\rho_o \overline{u'v'}, \frac{\rho_o f_o \overline{v'\theta'}}{\theta_{oz}} \right) \quad (\text{A40})$$

which using A7, A8 and A10 can be written in terms of the perturbation stream function as follows

$$\vec{F} = \left(0, \rho_o \overline{\psi'_x \psi'_y}, \frac{\rho_o f_o^2 \overline{\psi'_x \psi'_z}}{N^2} \right). \quad (\text{A41})$$

Putting in the plane wave solution as above in the WKB approximation gives

$$\vec{F} \simeq \frac{1}{2} \rho_o k |\hat{\psi}|^2 \left(0, l, \frac{f_o^2}{N^2} m \right) \quad (\text{A42})$$

Similarly putting in the wave solution to equation A17 gives

$$q' = - \left(k^2 + l^2 + \frac{f_o^2}{N^2} \left(m^2 + \frac{1}{4H^2} \right) \right) \psi' \quad (\text{A43})$$

Combining A42 and A43 with the definition of group velocity A31 and the dispersion relation A29 it can be shown that the E-P flux is given by

$$\vec{F} = (0, v_{gr}, w_{gr}) A \quad (\text{A44})$$

where A , the wave activity density is given by

$$A = \frac{1}{2} \rho_o \frac{\overline{q'^2}}{q_y} \quad (\text{A45})$$

i.e. the E-P flux is always parallel or anti-parallel to the group velocity.

BIBLIOGRAPHY

- Akahori, K., & Yoden, S. 1997. Zonal flow vacillation and bimodality of baroclinic eddy life cycles' in a simple global circulation model. *Journal of the Atmospheric Sciences*, **54**(19), 2349–2361.
- Ambaum, M. H. P., & Hoskins, B. J. 2002. The NAO troposphere-stratosphere connection. *Journal of Climate*, **15**(14), 1969–1978.
- Andrews, D. G., & McIntyre, M. E. 1976. Planetary Waves in Horizontal and Vertical Shear - Generalized Eliassen-Palm Relation and Mean Zonal Acceleration. *Journal of the Atmospheric Sciences*, **33**(11), 2031–2048.
- Andrews, D. G., Holton, J. R., & Leovy, C. B. 1987. *Middle Atmosphere Dynamics*. London: Academic Press Inc.
- Baldwin, M. P., & Dunkerton, T. J. 1999. Propagation of the Arctic Oscillation from the stratosphere to the troposphere. *Journal of Geophysical Research-Atmospheres*, **104**(D24), 30937–30946.
- Baldwin, M. P., & Dunkerton, T. J. 2001. Stratospheric harbingers of anomalous weather regimes. *Science*, **294**(5542), 581–584.
- Baldwin, M. P., Stephenson, D. B., Thompson, D. W. J., Dunkerton, T. J., Charlton, A. J., & O'Neill, A. 2003. Stratospheric memory and skill of extended-range weather forecasts. *Science*, **301**(5633), 636–640.
- Baldwin, M. P., Dameris, M., & Shepherd, T. G. 2007. Atmosphere - How will the stratosphere affect climate change? *Science*, **316**(5831), 1576–1577.

- Bates, J. R. 1981. A Dynamical Mechanism Through Which Variations in Solar Ultraviolet-Radiation Can Influence Tropospheric Climate. *Solar Physics*, **74**(2), 399–415.
- Berg, P., Christiansen, B., Thejll, P., & Arnold, N. 2007. The dynamical response of the middle atmosphere to the tropospheric solar signal. *Journal of Geophysical Research-Atmospheres*, **112**.
- Black, R. X. 2002. Stratospheric forcing of surface climate in the Arctic oscillation. *Journal of Climate*, **15**(3), 268–277.
- Black, R. X., & McDaniel, B. A. 2004. Diagnostic case studies of the northern annular mode. *Journal of Climate*, **17**(20), 3990–4004.
- Bond, G., Kromer, B., Beer, J., Muscheler, R., Evans, M. N., Showers, W., Hoffmann, S., Lotti-Bond, R., Hajdas, I., & Bonani, G. 2001. Persistent solar influence on north Atlantic climate during the Holocene. *Science*, **294**(5549), 2130–2136.
- Boville, B. A. 1984. The Influence of the Polar Night Jet on the Tropospheric Circulation in A Gcm. *Journal of the Atmospheric Sciences*, **41**(7), 1132–1142.
- Camp, C. D., & Tung, K. K. 2007. Surface warming by the solar cycle as revealed by the composite mean difference projection. *Geophysical Research Letters*, **34**(14).
- Carslaw, K. S., Harrison, R. G., & Kirkby, J. 2002. Cosmic rays, clouds, and climate. *Science*, **298**(5599), 1732–1737.
- Cash, B. A., Kushner, P. J., & Vallis, G. K. 2002. The structure and composition of the annular modes in an aquaplanet general circulation model. *Journal of the Atmospheric Sciences*, **59**(23), 3399–3414.
- Chan, C. J., & Plumb, R. A. 2009. *The response to stratospheric forcing and its dependence on the state of the troposphere*. In Press.

-
- Chen, G., & Held, I. M. 2007. Phase speed spectra and the recent poleward shift of Southern Hemisphere surface westerlies. *Geophysical Research Letters*, **34**(21).
- Chen, G., Held, I. M., & Robinson, W. A. 2007. Sensitivity of the latitude of the surface westerlies to surface friction. *Journal of the Atmospheric Sciences*, **64**(8), 2899–2915.
- Chen, P., & Robinson, W. A. 1992. Propagation of Planetary-Waves Between the Troposphere and Stratosphere. *Journal of the Atmospheric Sciences*, **49**(24), 2533–2545.
- Christiansen, B. 1999. Stratospheric vacillations in a general circulation model. *Journal of the Atmospheric Sciences*, **56**(12), 1858–1872.
- Coughlin, K., & Tung, K. K. 2004. Eleven-year solar cycle signal throughout the lower atmosphere. *Journal of Geophysical Research-Atmospheres*, **109**(D21).
- Coughlin, K., & Tung, K. K. 2005. Tropospheric wave response to decelerated stratosphere seen as downward propagation in northern annular mode. *Journal of Geophysical Research-Atmospheres*, **110**(D1).
- Crooks, S. A., & Gray, L. J. 2005. Characterization of the 11-year solar signal using a multiple regression analysis of the ERA-40 dataset. *Journal of Climate*, **18**(7), 996–1015.
- Douglass, D. H., & Clader, B. D. 2002. Climate sensitivity of the Earth to solar irradiance. *Geophysical Research Letters*, **29**(16).
- Douglass, D. H., Clader, B. D., & Knox, R. S. 2004. *Climate sensitivity of Earth to Solar irradiance: update*. Unpublished Work.
- Eddy, John A. 1976. The Maunder Minimum. *Science*, **192**(4245), 1189–1202.

- Edmon, H. J., Hoskins, B. J., & McIntyre, M. E. 1980. Eliassen-Palm Cross-Sections for the Troposphere. *Journal of the Atmospheric Sciences*, **37**(12), 2600–2616.
- Eichelberger, S. J., & Hartmann, D. L. 2007. Zonal jet structure and the leading mode of variability. *Journal of Climate*, **20**, 5149–5163.
- Eliassen, A., & Palm, E. 1961. On the transfer of energy in stationary mountain waves. *Geofysiske Publikasjoner*, **22**(3), 1–23.
- Eyring, V., Waugh, D. W., Bodeker, G. E., Cordero, E., Akiyoshi, H., Austin, J., Beagley, S. R., Boville, B. A., Braesicke, P., Bruhl, C., Butchart, N., Chipperfield, M. P., Dameris, M., Deckert, R., Deushi, M., Frith, S. M., Garcia, R. R., Gettelman, A., Giorgetta, M. A., Kinnison, D. E., Mancini, E., Manzini, E., Marsh, D. R., Matthes, S., Nagashima, T., Newman, P. A., Nielsen, J. E., Pawson, S., Pitari, G., Plummer, D. A., Rozanov, E., Schraner, M., Scinocca, J. F., Semeniuk, K., Shepherd, T. G., Shibata, K., Steil, B., Stolarski, R. S., Tian, W., & Yoshiki, M. 2007. Multimodel projections of stratospheric ozone in the 21st century. *Journal of Geophysical Research-Atmospheres*, **112**(D16).
- Forster, P., Ramaswamy, V., Artaxo, P., Berntsen, R., Betts, R., Fahey, D. W., Haywood, J., Lean, J., Lowe, G., Myhre, J., Nganga, J., Prinn, R., Raga, G., Schulz, M., & Dorland, R. Van. 2007. *Changes in atmospheric constituents and in Radiative forcing*. Report.
- Fröhlich, & Lean, J. 2004. Solar radiative output and its variability: evidence and mechanisms. *Astronomy and Astrophysics Review*, **12**(4), 273–320.
- Fröhlich, C., & Lean, J. 1998. The Sun's total irradiance: Cycles, trends and related climate change uncertainties since 1976. *Geophysical Research Letters*, **25**(23), 4377–4380.
- Gerber, E. P. 2006. *A Dynamical and Statistical Understanding of the North*

-
- Atlantic Oscillation and Annular Modes*. Thesis/Dissertation, Princeton University.
- Gerber, E. P., & Polvani, L. M. 2008. *Stratosphere-troposphere Coupling in a Relatively Simple AGCM: The importance of Stratospheric Variability*. In Press.
- Gerber, E. P., & Vallis, G. K. 2007. Eddy-zonal flow interactions and the persistence of the zonal index. *Journal of the Atmospheric Sciences*, **64**, 3296–3311.
- Gerber, E. P., Voronin, S., & Polvani, L. M. 2008. Testing the annular mode autocorrelation time scale in simple atmospheric general circulation models. *Monthly Weather Review*, **136**(4), 1523–1536.
- Gerber, Edwin P., & Vallis, Geoffrey K. 2008. *On the Zonal Structure of the North Atlantic Oscillation and Annular Modes*. In Press.
- Gleisner, H., & Thejll, P. 2003. Patterns of tropospheric response to solar variability. *Geophysical Research Letters*, **30**(13).
- Gray, L. J., Crooks, S. A., Palmer, M. A., Pascoe, C. L., & Sparrow, S. 2006. A possible transfer mechanism for the 11-year solar cycle to the lower stratosphere. *Space Science Reviews*, **125**(1-4), 357–370.
- Grise, K. M., Thompson, D. W. J., & Forster, P. M. 2009. *On the role of radiative processes in stratosphere-troposphere coupling*. In Press.
- Haigh, J. D. 1994. The Role of Stratospheric Ozone in Modulating the Solar Radiative Forcing of Climate. *Nature*, **370**(6490), 544–546.
- Haigh, J. D. 1996. The impact of solar variability on climate. *Science*, **272**(5264), 981–984.
- Haigh, J. D. 1999. A GCM study of climate change in response to the 11-year solar cycle. *Quarterly Journal of the Royal Meteorological Society*, **125**(555), 871–892.

-
- Haigh, J. D., & Blackburn, M. 2006. Solar influences on dynamical coupling between the stratosphere and troposphere. *Space Science Reviews*, **125**(1-4), 331–344.
- Haigh, J. D., Blackburn, M., & Day, R. 2005. The response of tropospheric circulation to perturbations in lower-stratospheric temperature. *Journal of Climate*, **18**(17), 3672–3685.
- Haigh, Joanna D. 2003. The effects of solar variability on the Earth’s climate. *Phil. Trans. R. Soc. Lond. A*, **361**(1802), 95–111.
- Hartley, D. E., Villarin, J. T., Black, R. X., & Davis, C. A. 1998. A new perspective on the dynamical link between the stratosphere and troposphere. *Nature*, **391**(6666), 471–474.
- Hartmann, D. L., & Zuercher, P. 1998. Response of baroclinic life cycles to barotropic shear. *Journal of the Atmospheric Sciences*, **55**(3), 297–313.
- Hartmann, D. L., Wallace, J. M., Limpasuvan, V., Thompson, D. W. J., & Holton, J. R. 2000. Can ozone depletion and global warming interact to produce rapid climate change? *Proceedings of the National Academy of Sciences of the United States of America*, **97**(4), 1412–1417.
- Haynes, P. H., & Shepherd, T. G. 1989. The Importance of Surface Pressure Changes in the Response of the Atmosphere to Zonally-Symmetric Thermal and Mechanical Forcing. *Quarterly Journal of the Royal Meteorological Society*, **115**(490), 1181–1208.
- Haynes, P. H., Marks, C. J., McIntyre, M. E., Shepherd, T. G., & Shine, K. P. 1991. On the Downward Control of Extratropical Diabatic Circulations by Eddy-Induced Mean Zonal Forces. *Journal of the Atmospheric Sciences*, **48**(4), 651–679.
- Haynes, Peter. 2005. Stratospheric Dynamics. *Annual Review of Fluid Mechanics*, **37**(1), 263–293.

-
- Held, I. M., & Suarez, M. J. 1994. A Proposal for the Intercomparison of the Dynamical Cores of Atmospheric General-Circulation Models. *Bulletin of the American Meteorological Society*, **75**(10), 1825–1830.
- Herschel, W. 1801. Observations tending to investigate the Nature of the Sun. *Phil. Trans. R. Soc. Lond. A*, **91**, 265–318.
- Hines, C. O. 1974. Possible Mechanism for Production of Sun-Weather Correlations. *Journal of the Atmospheric Sciences*, **31**(2), 589–591.
- Holton, J. R. 2004. *An introduction to dynamic meteorology*. Fourth edn. London: Elsevier Academic Press.
- Holton, J. R., & Tan, H. C. 1980. The Influence of the Equatorial Quasi-Biennial Oscillation on the Global Circulation at 50 Mb. *Journal of the Atmospheric Sciences*, **37**(10), 2200–2208.
- Hoskins, B. J., & Simmons, A. J. 1975. Multilayer Spectral Model and Semi-Implicit Method. *Quarterly Journal of the Royal Meteorological Society*, **101**(429), 637–655.
- Hoyt, D. V., & Schatten, K. H. 1997. *The role of the sun in climate change*. Oxford University Press.
- Karoly, D. J., & Hoskins, B. J. 1982. 3 Dimensional Propagation of Planetary-Waves. *Journal of the Meteorological Society of Japan*, **60**(1), 109–123.
- Kodera, K. 2003. Solar influence on the spatial structure of the NAO during the winter 1900-1999. *Geophysical Research Letters*, **30**(4).
- Kodera, K. 2004. Solar influence on the Indian Ocean Monsoon through dynamical processes. *Geophysical Research Letters*, **31**(24).
- Kodera, K., & Kuroda, Y. 2002. Dynamical response to the solar cycle. *Journal of Geophysical Research-Atmospheres*, **107**(D24).

-
- Kodera, K., Yamazaki, K., Chiba, M., & Shibata, K. 1990. Downward Propagation of Upper Stratospheric Mean Zonal Wind Perturbation to the Troposphere. *Geophysical Research Letters*, **17**(9), 1263–1266.
- Kodera, K., Mukougawa, H., & Itoh, S. 2008. Tropospheric impact of reflected planetary waves from the stratosphere. *Geophysical Research Letters*, **35**(16).
- Kristjansson, J. E., & Kristiansen, J. 2000. Is there a cosmic ray signal in recent variations in global cloudiness and cloud radiative forcing? *Journal of Geophysical Research-Atmospheres*, **105**(D9), 11851–11863.
- Kristjansson, J. E., Staple, A., Kristiansen, J., & Kaas, E. 2002. A new look at possible connections between solar activity, clouds and climate. *Geophysical Research Letters*, **29**(23).
- Kristjansson, J. E., Kristiansen, J., & Kaas, E. 2004. Solar activity, cosmic rays, clouds and climate - an update. *Solar Variability and Climate Change*, **34**(2), 407–415.
- Kushner, P. J., & Polvani, L. M. 2004. Stratosphere-troposphere coupling in a relatively simple AGCM: The role of eddies. *Journal of Climate*, **17**(3), 629–639.
- Kushner, P. J., & Polvani, L. M. 2006. Stratosphere-troposphere coupling in a relatively simple AGCM: Impact of the seasonal cycle. *Journal of Climate*, **19**(21), 5721–5727.
- Labitzke, K. 1987. Sunspots, the Qbo, and the Stratospheric Temperature in the North Polar-Region. *Geophysical Research Letters*, **14**(5), 535–537.
- Labitzke, K. 2003. The global signal of the 11-year sunspot cycle in the atmosphere: When do we need the QBO? *Meteorologische Zeitschrift*, **12**(4), 209–216.

- Labitzke, K., & van Loon, H. 2000. The QBO effect on the solar signal in the global stratosphere in the winter of the Northern Hemisphere. *Journal of Atmospheric and Solar-Terrestrial Physics*, **62**(8), 621–628.
- Labitzke, K., Austin, J., Butchart, N., Knight, J., Takahashi, M., Nakamoto, M., Nagashima, T., Haigh, J., & Williams, V. 2002. The global signal of the 11-year solar cycle in the stratosphere: observations and models. *Journal of Atmospheric and Solar-Terrestrial Physics*, **64**(2), 203–210.
- Larkin, A., Haigh, J. D., & Djavidnia, S. 2000. The effect of solar UV irradiance variations on the Earth's atmosphere. *Space Science Reviews*, **94**(1-2), 199–214.
- Lean, J., & Rind, D. 2001. Earth's response to a variable sun. *Science*, **292**(5515), 234–236.
- Lean, J. L., Rottman, G. J., Kyle, H. L., Woods, T. N., Hickey, J. R., & Puga, L. C. 1997. Detection and parameterization of variations in solar mid- and near-ultraviolet radiation (200–400 nm). *Journal of Geophysical Research-Atmospheres*, **102**(D25), 29939–29956.
- Lee, S., Son, S. W., Grise, K., & Feldstein, S. B. 2007. A mechanism for the poleward propagation of zonal mean flow anomalies. *Journal of the Atmospheric Sciences*, **64**(3), 849–868.
- Leith, C. E. 1975. Climate Response and Fluctuation Dissipation. *Journal of the Atmospheric Sciences*, **32**(10), 2022–2026.
- Limpasuvan, V., Thompson, D. W. J., & Hartmann, D. L. 2004. The life cycle of the Northern Hemisphere sudden stratospheric warmings. *Journal of Climate*, **17**(13), 2584–2596.
- Lockwood, M. 2002. An evaluation of the correlation between open solar flux and total solar irradiance. *Astronomy & Astrophysics*, **382**(2), 678–687.

- Lockwood, M., & Fröhlich, C. 2007. Recent oppositely directed trends in solar climate forcings and the global mean surface air temperature. *Proceedings of the Royal Society A-Mathematical Physical and Engineering Sciences*, **463**, 2447–2460.
- Lorenz, D. J., & DeWeaver, E. T. 2007. Tropopause height and zonal wind response to global warming in the IPCC scenario integrations. *Journal of Geophysical Research-Atmospheres*, **112**(D10).
- Lorenz, D. J., & Hartmann, D. L. 2001. Eddy-zonal flow feedback in the Southern Hemisphere. *Journal of the Atmospheric Sciences*, **58**(21), 3312–3327.
- Lorenz, D. J., & Hartmann, D. L. 2003. Eddy-zonal flow feedback in the Northern Hemisphere winter. *Journal of Climate*, **16**(8), 1212–1227.
- Lu, H., Jarvis, M. J., Graf, H. F., Young, P. C., & Horne, R. B. 2007. Atmospheric temperature responses to solar irradiance and geomagnetic activity. *Journal of Geophysical Research-Atmospheres*, **112**(D11).
- Marsh, D. R., & Garcia, R. R. 2007. Attribution of decadal variability in lower-stratospheric tropical ozone. *Geophysical Research Letters*, **34**.
- Marsh, N., & Svensmark, H. 2000. Cosmic rays, clouds, and climate. *Space Science Reviews*, **94**(1-2), 215–230.
- Matsuno, T. 1970. Vertical Propagation of Stationary Planetary Waves in Winter Northern Hemisphere. *Journal of the Atmospheric Sciences*, **27**(6), 871–883.
- Matthes, K., Kodera, K., Haigh, J. D., Shindell, D. T., Shibata, K., Lange-matz, U., Rozanov, E., & Kuroda, Y. 2003. GRIPS Solar Experiments Intercomparison Project: Initial Results. *Papers in Meteorology and Geophysics*, **54**(2), 71–90.

- Matthes, K., Langematz, U., Gray, L. L., Kodera, K., & Labitzke, K. 2004. Improved 11-year solar signal in the Freie Universität Berlin climate middle atmosphere model (FUB-CMAM). *Journal of Geophysical Research-Atmospheres*, **109**(D6).
- Matthes, K., Kuroda, Y., Kodera, K., & Langematz, U. 2006. Transfer of the solar signal from the stratosphere to the troposphere: Northern winter. *Journal of Geophysical Research-Atmospheres*, **111**(D6).
- Meehl, G. A., Washington, W. M., Wigley, T. M. L., Arblaster, J. M., & Dai, A. 2003. Solar and greenhouse gas forcing and climate response in the twentieth century. *Journal of Climate*, **16**(3), 426–444.
- Ogurtsov, M. G., Nagovitsyn, Y. A., Kocharov, G. E., & Jungner, H. 2002. Long-period cycles of the Sun's activity recorded in direct solar data and proxies. *Solar Physics*, **211**(1-2), 371–394.
- Orlanski, I., & Gross, B. 2000. The life cycle of baroclinic eddies in a storm track environment. *Journal of the Atmospheric Sciences*, **57**(21), 3498–3513.
- Orszag, S. A. 1970. Transform Method for Calculation of Vector-Coupled Sums - Application to Spectral Form of Vorticity Equation. *Journal of the Atmospheric Sciences*, **27**(6), 890–895.
- Perlwitz, J., & Harnik, N. 2003. Observational evidence of a stratospheric influence on the troposphere by planetary wave reflection. *Journal of Climate*, **16**(18), 3011–3026.
- Perlwitz, J., & Harnik, N. 2004. Downward coupling between the stratosphere and troposphere: The relative roles of wave and zonal mean processes. *Journal of Climate*, **17**(24), 4902–4909.
- Piexoto, J. P., & Oort, A. H. 1992. *Physics of Climate*. New York: American Institute of Physics.

- Plumb, R. A., & Semeniuk, K. 2003. Downward migration of extratropical zonal wind anomalies. *Journal of Geophysical Research-Atmospheres*, **108**(D7).
- Polvani, L. M., & Kushner, P. J. 2002. Tropospheric response to stratospheric perturbations in a relatively simple general circulation model. *Geophysical Research Letters*, **29**(7).
- Ramaswamy, V., Chanin, M. L., Angell, J., Barnett, J., Gaffen, D., Gelman, M., Keckhut, P., Koshelkov, Y., Labitzke, K., Lin, J. J. R., O'Neill, A., Nash, J., Randel, W., Rood, R., Shine, K., Shiotani, M., & Swinbank, R. 2001. Stratospheric temperature trends: Observations and model simulations. *Reviews of Geophysics*, **39**(1), 71–122.
- Rind, D., Lonergan, P., Balachandran, N. K., & Shindell, D. 2002. 2 x CO₂ and solar variability influences on the troposphere through wave-mean flow interactions. *Journal of the Meteorological Society of Japan*, **80**(4B), 863–876.
- Ring, M. J., & Plumb, R. A. 2007. Forced annular mode patterns in a simple atmospheric general circulation model. *Journal of the Atmospheric Sciences*, **64**, 3611–3626.
- Ring, M. J., & Plumb, R. A. 2008. The Response of a Simplified GCM to Axisymmetric Forcings: Applicability of the Fluctuation-Dissipation Theorem. *Journal of the Atmospheric Sciences*, **65**(12), 3880–3898.
- Robinson, W. A. 2000. A baroclinic mechanism for the eddy feedback on the zonal index. *Journal of the Atmospheric Sciences*, **57**(3), 415–422.
- Ruzmaikin, A., & Feynman, J. 2002. Solar influence on a major mode of atmospheric variability. *Journal of Geophysical Research-Atmospheres*, **107**(D14).
- Salby, M., & Callaghan, P. 2004. Evidence of the solar cycle in the general circulation of the stratosphere. *Journal of Climate*, **17**(1), 34–46.

- Santer, B. D., Wehner, M. F., Wigley, T. M. L., Sausen, R., Meehl, G. A., Taylor, K. E., Ammann, C., Arblaster, J., Washington, W. M., Boyle, J. S., & Bruggemann, W. 2003. Contributions of anthropogenic and natural forcing to recent tropopause height changes. *Science*, **301**(5632), 479–483.
- Scafetta, N., & West, B. J. 2005. Estimated solar contribution to the global surface warming using the ACRIM TSI satellite composite. *Geophysical Research Letters*, **32**(18).
- Schmidt, H., & Brasseur, G. P. 2006. The response of the middle atmosphere to solar cycle forcing in the hamburg model of the neutral and ionized atmosphere. *Space Science Reviews*, **125**(1-4), 345–356.
- Scott, R. K., & Polvani, L. M. 2004. Stratospheric control of upward wave flux near the tropopause. *Geophysical Research Letters*, **31**(2).
- Shepherd, T. G. 2002. Issues in stratosphere-troposphere coupling. *Journal of the Meteorological Society of Japan*, **80**(4B), 769–792.
- Shindell, D., Rind, D., Balachandran, N., Lean, J., & Lonergan, P. 1999. Solar cycle variability, ozone, and climate. *Science*, **284**(5412), 305–308.
- Shindell, D. T., Schmidt, G. A., Mann, M. E., Rind, D., & Waple, A. 2001. Solar forcing of regional climate change during the maunder minimum. *Science*, **294**(5549), 2149–2152.
- Shindell, D. T., Faluvegi, G., Miller, R. L., Schmidt, G. A., Hansen, J. E., & Sun, S. 2006. Solar and anthropogenic forcing of tropical hydrology. *Geophysical Research Letters*, **33**(24).
- Sigmond, M., Siegmund, P. C., & Kelder, H. 2003. Analysis of the coupling between the stratospheric meridional wind and the surface level zonal wind during 1979-93 Northern Hemisphere extratropical winters. *Climate Dynamics*, **21**(2), 211–219.

-
- Simmons, A. J., & Burridge, D. M. 1981. An Energy and Angular-Momentum Conserving Vertical Finite-Difference Scheme and Hybrid Vertical-Coordinates. *Monthly Weather Review*, **109**(4), 758–766.
- Solomon, S., Qin, D., Manning, M, Chen, Z, Marquis, M., Averyt, K. B., Tignor, M., & Miller, H. L. 2007. *IPCC, 2007: Climate change 2007: The physical science basis. Contributions of working group 1 to the Fourth Assessment Report of the Intergovernmental Panel on Climate Change*. Report.
- Son, S. W., & Lee, S. 2006. Preferred modes of variability and their relationship with climate change. *Journal of Climate*, **19**(10), 2063–2075.
- Son, S. W., Polvani, L. M., Waugh, D. W., Akiyoshi, H., Garcia, R., Kinnison, D., Pawson, S., Rozanov, E., Shepherd, T. G., & Shibata, K. 2008a. The impact of stratospheric ozone recovery on the Southern Hemisphere westerly jet. *Science*, **320**(5882), 1486–1489.
- Son, S. W., Lee, S., Feldstein, S. B., & Hove, J. E. T. 2008b. Time scale and feedback of zonal-mean-flow variability. *Journal of the Atmospheric Sciences*, **65**(3), 935–952.
- Song, Y. C., & Robinson, W. A. 2004. Dynamical mechanisms for stratospheric influences on the troposphere. *Journal of the Atmospheric Sciences*, **61**(14), 1711–1725.
- Soukharev, B. E., & Hood, L. L. 2006. Solar cycle variation of stratospheric ozone: Multiple regression analysis of long-term satellite data sets and comparisons with models. *Journal of Geophysical Research-Atmospheres*, **111**(D20).
- Svensmark, H. 2007. Cosmoclimatology: a new theory emerges. *Astronomy & Geophysics*, **48**(1), 18–24.

-
- Svensmark, H., & FriisChristensen, E. 1997. Variation of cosmic ray flux and global cloud coverage - A missing link in solar-climate relationships. *Journal of Atmospheric and Solar-Terrestrial Physics*, **59**(11), 1225–1232.
- Thompson, D. W. J., & Solomon, S. 2002. Interpretation of recent Southern Hemisphere climate change. *Science*, **296**(5569), 895–899.
- Thompson, D. W. J., & Wallace, J. M. 2000. Annular modes in the extratropical circulation. Part I: Month-to-month variability. *Journal of Climate*, **13**(5), 1000–1016.
- Trenberth, K. 1984. Some effects of finite sample size and persistence on meteorological statistics. Part 1: Autocorrelations. *Monthly Weather Review*, **112**, 2359–2368.
- Tung, K. K., & Camp, C. D. 2008. Solar cycle warming at the Earth's surface in NCEP and ERA-40 data: A linear discriminant analysis. *Journal of Geophysical Research-Atmospheres*, **113**(D5).
- Vallis, G. K., Gerber, E. P., Kushner, P. J., & Cash, B. A. 2004. A mechanism and simple dynamical model of the North Atlantic Oscillation and annular modes. *Journal of the Atmospheric Sciences*, **61**(3), 264–280.
- van Loon, H., & Labitzke, K. 2000. The influence of the 11-year solar cycle on the stratosphere below 30 km: A review. *Space Science Reviews*, **94**(1-2), 259–278.
- van Loon, H., Meehl, G. A., & Arblaster, J. M. 2004. A decadal solar effect in the tropics in July-August. *Journal of Atmospheric and Solar-Terrestrial Physics*, **66**(18), 1767–1778.
- Welch, B. L. 1947. The generalization of 'students' problem when several different population variances are involved. *Biometrika*, **34**(1-2), 28–35.

-
- White, W. B. 2006. Response of tropical global ocean temperature to the Sun's quasi-decadal UV radiative forcing of the stratosphere. *Journal of Geophysical Research-Oceans*, **111**(C9).
- White, W. B., Lean, J., Cayan, D. R., & Dettinger, M. D. 1997. Response of global upper ocean temperature to changing solar irradiance. *Journal of Geophysical Research-Oceans*, **102**(C2), 3255–3266.
- White, W. B., Dettinger, M. D., & Cayan, D. R. 2003. Sources of global warming of the upper ocean on decadal period scales. *Journal of Geophysical Research-Oceans*, **108**(C8).
- Williams, G. P. 2006. Circulation sensitivity to tropopause height. *Journal of the Atmospheric Sciences*, **63**(7), 1954–1961.
- Wittman, M. A. H., Polvani, L. M., Scott, R. K., & Charlton, A. J. 2004. Stratospheric influence on baroclinic lifecycles and its connection to the Arctic Oscillation. *Geophysical Research Letters*, **31**(16).
- Wittman, M. A. H., Charlton, A. J., & Polvani, L. M. 2007. The effect of lower stratospheric shear on baroclinic instability. *Journal of the Atmospheric Sciences*, **64**(2), 479–496.
- Zhou, S. T., Miller, A. J., Wang, J., & Angell, J. K. 2002. Downward-propagating temperature anomalies in the preconditioned polar stratosphere. *Journal of Climate*, **15**(7), 781–792.